



University of Kentucky
UKnowledge

University of Kentucky Doctoral Dissertations

Graduate School

2006

A MASS SPECTROMETRY-BASED STUDY OF SERUM BUTYRYLCHOLINESTERASE INHIBITION FROM PESTICIDE EXPOSURE AND ORGANOPHOSPHATE PESTICIDE-INDUCED PROTEOME ALTERATION

Jinchun Sun

University of Kentucky, jsun2@uky.edu

[Right click to open a feedback form in a new tab to let us know how this document benefits you.](#)

Recommended Citation

Sun, Jinchun, "A MASS SPECTROMETRY-BASED STUDY OF SERUM BUTYRYLCHOLINESTERASE INHIBITION FROM PESTICIDE EXPOSURE AND ORGANOPHOSPHATE PESTICIDE-INDUCED PROTEOME ALTERATION" (2006). *University of Kentucky Doctoral Dissertations*. 290.

https://uknowledge.uky.edu/gradschool_diss/290

This Dissertation is brought to you for free and open access by the Graduate School at UKnowledge. It has been accepted for inclusion in University of Kentucky Doctoral Dissertations by an authorized administrator of UKnowledge. For more information, please contact UKnowledge@lsv.uky.edu.

ABSTRACT OF DISSERTATION

Jinchun Sun

The Graduate School
University of Kentucky
2006

A MASS SPECTROMETRY-BASED STUDY OF SERUM
BUTYRYLCHOLINESTERASE INHIBITION FROM PESTICIDE EXPOSURE
AND ORGANOPHOSPHATE PESTICIDE-INDUCED PROTEOME ALTERATION

ABSTRACT OF DISSERTATION

A dissertation submitted in partial fulfillment of the
requirements for the degree of Doctor of Philosophy in the
College of Arts and Sciences
at the University of Kentucky

By
Jinchun Sun

Lexington, Kentucky

Director: Dr. Bert C. Lynn, Professor of Chemistry

Lexington, Kentucky

2006

Copyright © Jinchun Sun 2006

ABSTRACT OF DISSERTATION

A MASS SPECTROMETRY-BASED STUDY OF SERUM BUTYRYLCHOLINESTERASE INHIBITION FROM PESTICIDE EXPOSURE AND ORGANOPHOSPHATE PESTICIDE-INDUCED PROTEOME ALTERATION

Pesticides including organophosphates (OPs) and carbamates (CBs) are widely used to control undesirable pests. These compounds are neurotoxic and inhibit hydrolysis of the neurotransmitter acetylcholine by acetylcholinesterase. Public health concerns have increased with the escalating usage of pesticides. Reliable monitoring programs are required to detect and quantify pesticide exposure, as well as to promote an understanding of their neurotoxic properties. In this dissertation, both the anticholinergic (Part I) toxicity and neurotoxicity in neuroblastoma cells (Part II) of pesticides were explored using mass spectrometry (MS). The high sensitivity and high-throughput of this technique renders it well-suited for proteomics analysis.

Part I describes the study of butyrylcholinesterase (BChE) inhibition resulting from OP and CB exposure. The main hypothesis of Part I is that the special modification of BChE can provide the origin and extent of pesticide exposure. A novel method for detection and quantification of pesticide exposure was designed using a proteomics approach and equine BChE (eBChE) as a model system. The methodology featured detection and analysis of phosphorylated or carbamylated peptides at the active site serine residue. The developed technique was successfully applied towards the study of human BChE (hBChE) inhibition *in vitro* and in serum samples. A specially designed affinity column enabled an isolation of BChE from serum. Enriched BChE was subjected to enzymatic digestion by a novel on-bead double digestion protocol. LC/MS/MS was employed to produce a calibration system for the analysis of hBChE inhibition, which was then applied towards quantification of the enzyme.

Part II describes a proteomic study of the neurotoxicity in neuroblastoma cells caused from chlorpyrifos (CPF), an organophosphate pesticide. The concerns of CPF exposure to pregnant women, infants and children are increasing due to developmentally neurotoxic effects of this chemical. The main hypothesis of Part II is that CPF can cause protein alterations and these altered proteins can be detected using proteomics. Systematic studies at subcellular levels evaluated proteome changes in SH-SY5Y cells exposed to CPF. Two-dimensional gel electrophoresis (2DE) was applied with MALDI-TOF-MS to analyze differential protein expression. Thirty seven common unique altered proteins were identified, which play important roles in metabolic pathway.

Key words: Proteomics, Mass Spectrometry, Pesticide, Butyrylcholinesterase, Chlorpyrifos, SH-SY5Y.

Jinchun Sun

January 26, 2006

A MASS SPECTROMETRY-BASED STUDY OF SERUM
BUTYRYLCHOLINESTERASE INHIBITION FROM PESTICIDE EXPOSURE
AND ORGANOPHOSPHATE PESTICIDE-INDUCED PROTEOME ALTERATION

By

Jinchun Sun

Dr. Bert C. Lynn

Director of Dissertation

Dr. Mark Meier

Director of Graduate Study

DISSERTATION

Jinchun Sun

The Graduate School
University of Kentucky
2006

A MASS SPECTROMETRY-BASED STUDY OF SERUM
BUTYRYLCHOLINESTERASE INHIBITION FROM PESTICIDE EXPOSURE
AND ORGANOPHOSPHATE PESTICIDE-INDUCED PROTEOME ALTERATION

DISSERTATION

A dissertation submitted in partial fulfillment of the
requirements for the degree of Doctor of Philosophy in the
College of Arts and Sciences
at the University of Kentucky

By
Jinchun Sun

Lexington, Kentucky

Director: Dr. Bert C. Lynn, Professor of Chemistry

Lexington, Kentucky

2006

Copyright © Jinchun Sun 2006

ACKNOWLEDGEMENTS

I would first like to express sincere thanks and gratitude to Dr. Bert Lynn for his guidance and support throughout this dissertation. He provided me with the wonderful opportunity to grow and succeed as a scientist. Dr. Lynn always inspires me with his high enthusiasm in research, and he himself sets up a good example. His patience and willingness to always help me will be remembered forever.

I would like to extend many thanks to Dr. Jack Goodman, manager of the University of Kentucky Mass Spectrometry Facility, whose technical expertise and knowledge made this achievement possible. It has been a pleasure knowing and working with him.

Dr. Mark Lovell, an Advisory Committee member, deserves many thanks for his help and providing priceless samples. His knowledge and dedication were very important to my project.

I would like to thank my advisory committee for their guidance and support throughout of this dissertation. Without their invaluable knowledge and encouragement, this achievement would not be possible.

Also, a great thanks to all my friends and co-workers in the mass spectrometry group. Thank you all for your support and for making my experience in the group a memorable one.

Lastly, I would like to thank my mother, father, and sisters who have always been there to support me. I thank them for all they have provided me – support, faith, confidence and patience – it all helped me get where I am today.

TABLE OF CONTENTS

Acknowledgement	iii
Table of contents.....	iv
List of Tables	x
List of Figures.....	xii
General Introduction	
Pesticide Background.....	1
Proteomics Background	4
Statement of Research.....	29
Part I. STUDY OF SERUM BUTYRYLCHOLINESTERASE INHIBITION FROM PESTICIDE EXPOSURE	
	31
CHAPTER ONE: INTRODUCTION	
Butyrylcholinesterase Background.....	32
Statement of Research.....	32
CHAPTER TWO: IDENTIFICATION AND QUANTIFICATION OF INHIBITED BUTYRYLCHOLINESTERASE AFTER EXPOSURE TO ORGANOPHOSPHATES AND CARBAMATES USING MALDI-TOF-MS	
	38
Introduction.....	38
Experimental	40
Materials.....	40
eBChE inhibition.....	41
eBChE activity	42
Trypsin digestion.....	42
MALDI-TOF-MS analysis	42
Determination of IC ₅₀ and IC ₁₀₀	43
Results.....	44

Discussion.....	62
Conclusions.....	66

CHAPTER THREE: QUANTIFICATION OF MULTIPLE PESTICIDE

EXPOSURE USING LC/MS/MS 68

Introduction.....	68
Experimental.....	70
Offline Peptide Separation	70
Instrument.....	71
Results and discussion	71
Conclusions.....	87

CHAPTER FOUR: DEVELOPMENT OF A PURIFICATION SCHEME FOR THE ANALYSIS OF HUMAN SERUM BUTYRYLCHOLINESTERASE 89

Introduction.....	89
Experimental.....	90
Materials	90
Preparations of affinity gels	91
Affinity chromatography.....	91
Evaluate affinity gels.....	91
Results and discussion	92
Conclusions.....	106

CHAPTER FIVE: ANALYSIS OF HUMAN BUTYRYLCHOLINESTERASE EXPOSED TO ORGANOPHOSPHATES AND CARBAMATES IN SERUM WITH A COMBINATION OF AFFINITY CHROMATOGRAPHY AND MASS SPECTROMETRY 107

Introduction.....	107
Experimental.....	109
Chemicals	109
Instruments	109

Double Digestion.....	110
Results.....	111
Discussion.....	128
Conclusions.....	133
CHAPTER SIX: CONCLUSIONS.....	135
Part II. A STUDY OF ORGANOPHOSPHATE PESTICIDE-INDUCED PROTEOME ALTERATIONS IN SH-SY5Y CELLS	137
CHAPTER ONE: INTRODUCTION	
Chlorpyrifos Background.....	138
SH-SY5Y Cell Line.....	140
Two-dimentional Electrophoresis with Immobilized pH Gradient.....	141
Database search MASCOT algorithm.....	142
Statement of Research.....	144
CHAPTER TWO: CHLORPYRIFOS INDUCED PROTEIN ALTERATIONS IN THE SH-SY5Y CELL LINE	145
Introduction.....	145
Experimental.....	147
Cell culture.....	147
Protein sample preparation.....	148
2D gel elctrophoresis.....	149
In-gel digestion.....	151
Mass spectrometry.....	151
Database search.....	152
Results.....	152
Discussion.....	164
Conclusions.....	175

CHAPTER THREE: CONCLUSIONS	176
GENERAL CONCLUSIONS	179
REFERENCES	184
VITA	192

LIST OF TABLES

Table 0-1	Some common UV-MALDI matrices.....	15
Table 1.2.1.	Masses of observed MH^+ (average mass) for the intact and modified active site peptide of eBChE treated with 1 μM inhibitor.....	48
Table 1-2-2.	Masses of observed MH^+ (average mass) ^b for the precursor ions and fragment ions from PSD analysis.....	53
Table 1-2-3.	Normalized intensity ratios (NIRs) of intact peptide, modified peptide, and relative activities of eBChE treated with methyl paraoxon at different concentrations.....	55
Table 1-2-4.	Normalized intensity ratios of intact peptide, modified peptide, and relative activities of eBChE treated with ethyl paraoxon at different concentrations.....	56
Table 1-2-5.	Normalized intensity ratios of intact peptide, modified peptide, and relative activities of eBChE treated with EPN oxon at different concentrations.....	57
Table 1-2-6.	Normalized intensity ratios of intact peptide, modified peptide, and relative activities of eBChE treated with carbaryl at different concentrations.....	58
Table 1-3-1.	The relative ratio of modified peptide peak area or intensity by ethyl paraoxon to the intact peptide peak area or intensity from the RIC LC/MS/MS and that from MALDI	78
Table 1-4-1.	hBChE activities of the diluted serum before and after incubation with beads.....	98
Table 1-4-2.	hBChE activities from direct absorbance measurement on beads.	99
Table 1-5-1.	Masses of observed MH^+ (average mass) for the intact and modified active site peptide of hBChE treated with 5 μM inhibitor..	116
Table 2-2-1.	Gradient program of IEF..	150
Table 2-2-2.	Experimental and theoretical ratios of proteins with relative errors for the first experimental set..	154

Table 2-2-3.	Experimental and theoretical ratios and their relative error for the second experimental set.....	155
Table 2-2-4.	Summary of down-regulated proteins after treatment of SH-SY5Y cells with 50 μ M CPF for 24 h compared with control.....	159
Table 2-2-5.	Summary of up-regulated proteins after treatment of SH-SY5Y cells with 50 μ M CPF for 24 h compared with control.....	160
Table 2-2-6.	Summary of additional down-regulated proteins after treatment of SH-SY5Y cells treated with 50 μ M CPF for 16 h compared with control.....	165
Table 2-2-7.	Summary of additional up-regulated proteins after treatment of SH-SY5Y cells with 50 μ M CPF for 16 h compared with control.....	166

LIST OF FIGURES

Figure 0-1.	Strategies for the analysis of protein mixture using mass spectrometry....	6
Figure 0-2.	Relationship between HETP and linear velocity.....	9
Figure 0-3.	Schematic representation of 2D gel electrophoresis.....	12
Figure 0-4.	Schematic representation of reflectron mode of MALDI-TOF-MS....	18
Figure 0-5.	Schematic representation of a typical ESI source.....	22
Figure 0-6.	Schematic representation of electrochemical process in ESI.....	23
Figure 0-7.	Quadrupole ion trap.....	25
Figure 0-8.	Stability diagram for a quadrupole ion trap.....	27
Figure 1-1-1.	The scheme of CHE inhibited by inhibitors.. ..	35
Figure 1-2-1.	Structure of pesticides.....	41
Figure 1-2-2.	MALDI-TOF-MS spectra of the tryptic digest of eBChE from (A) control and (B) ethyl paraoxon treated sample.....	45
Figure 1-2-2.	MALDI-TOF-MS spectra of the tryptic digest of methyl paraoxon (C) and EPN oxon (D) treated eBChE . ..	46
Figure 1-2-2.	MALDI-TOF-MS spectra of the tryptic digest of carbaryl treated eBChE (E).....	47
Figure 1-2-3.	PSD analysis of precursor ion with average mass at m/z 2294.3 (A), at m/z 2308.6 (B).....	50
Figure 1-2-3.	PSD analysis of precursor ion with average mass at m/z 2336.8 (C), at m/z 2368.3 (D).....	51
Figure 1-2-3.	PSD analysis of precursor ion with average mass at m/z 2257.2 (E).....	52
Figure 1-2-4.	Plots of the normalized intensity ratio to the [methyl paraoxon] (A), [ethyl paraoxon] (B).....	59
Figure 1-2-4.	Plots of the normalized intensity ratio to [EPN oxon] (C), and [carbaryl] (D).....	60
Figure 1-2-5.	Plots of relative activity to [OPs] (A) and [carbaryl] (B).....	61
Figure 1-3-1.	MS/MS of the alkyl-phosphorylated peptide by ethyl paraoxon.....	73
Figure 1-3-2.	MS/MS/MS of the alkyl-phosphorylated peptide by ethyl paraoxon....	74
Figure 1-3-3.	MS/MS of intact active site peptide.....	75

Figure 1-3-4.	MS/MS of the carbamylated peptide.....	77
Figure 1-3-5.	Representative MALDI-TOF-MS spectrum of the 15 th fraction separated with HPLC.....	80
Figure 1-3-6.	Reconstructed ion chromatogram (RIC) of the modified active site peptide after two offline HPLC fractionations.....	81
Figure 1-3-7.	Reconstructed ion chromatogram (RIC) of the modified active site peptide without offline fraction prior LC/MS analysis.....	83
Figure 1-3-8.	RIC of the modified active-site peptide with carbamate.....	84
Figure 1-3-9.	Reconstructed ion chromatograms (RIC) of common fragment ion (m/z 1091 ²⁺).....	86
Figure 1-4-1.	Activation of Sepharose by CNBr and subsequent coupling of ligand...94	
Figure 1-4-2.	IR spectra (KBr) of dried original beads.....	95
Figure 1-4-3.	IR spectrum (KBr) of dried CNBr-activated beads.....	96
Figure 1-4-4.	IR spectrum (KBr) of dried CH-Sepharose 4B beads.....	97
Figure 1-4-5.	(A) RIC of the selected peptide (MH^{2+} at m/z 1141 ²⁺), (B) Product ion spectrum of the selected peptide ion.....	101
Figure 1-4-6.	(A)RIC of the selected peptide (MH^{2+} at m/z 1464 ⁺²), (B) Product ion spectrum of the selected peptide ion	102
Figure 1-4-7.	(A)RIC of the selected peptide (MH^{2+} at m/z 1185 ⁺²), (B) Product ion spectrum of the selected peptide ion.....	104
Figure 1-4-8.	Representative MALDI-TOF-MS spectra of (A) control and (B) tryptic peptides of hBChE treated with carbaryl.....	105
Figure 1-5-1.	Schematic of the procedure for the analysis of hBChE inhibition in serum matrix.....	112
Figure 1-5-2.	MALDI-TOF-MS spectra of the digest of hBChE after double digestion from (A) control, (B) carbaryl treated sample.....	113
Figure 1-5-3.	MALDI-TOF-MS spectra of the digest of hBChE after double digestion from (A) by ethyl paraoxon, and (B) by EPN oxon.....	114
Figure 1-5-4.	MS/MS of the triply charged intact active site peptide ion (MH^{3+} at m/z 732.7 ³⁺).....	117
Figure 1-5-5.	MS/MS of the triply charged carbamylated peptide ion (MH^{3+}	

	751.7 ³⁺).....	118
Figure 1-5-6.	MS/MS of the triply charged phosphorylated peptide ions (MH ³⁺ at <i>m/z</i> 777.7 ³⁺ for ethyl paraoxon and 788.7 ³⁺ for EPN oxon).....	119
Figure 1-5-7.	MS/MS/MS of the phosphorylated peptide ions.....	120
Figure 1-5-8.	Plots of intensity ratios vs carbaryl concentrations trypsin digestion (A) double digestion (B) from MALDI analysis.....	122
Figure 1-5-9.	Plots of peak area ratios vs concentration of pesticides (A) for carbaryl, (B) for ethyl paraoxon.....	123
Figure 1-5-10.	Plots of ratio of peak areas vs EPN oxon concentrations.....	124
Figure 1-5-11.	RIC of intact and modified peptide (A) carbaryl (B) ethyl paraoxon....	126
Figure 1-5-12.	RIC of intact peptide and modified peptide by EPN oxon.....	127
Figure 1-5-13.	RIC of carbamylated (A), phosphorylated peptide by ethyl paraoxon (B), and phosphorylated peptide by EPN oxon (C).....	129
Figure 2-1-1.	Photograph of a Bio-Rad isoelectric focusing chamber and focusing tray.....	143
Figure 2-2-1.	Viability of SH-SY5Y cells exposed to vehicle alone (control), chlorpyrifos (CPF) for 24 h.....	156
Figure 2-2-2.	A typical example of a gel image region that contains proteome feature up-regulation (A, B).....	157
Figure 2-2-2.	(C)The normalized optical densities of spots 1, 2, and 3.....	158
Figure 2-2-3.	2D sodium dodecyl sulfate polyacrylamide gel electrophoresis (SDS PAGE) analysis. The down-regulated proteins are labeled on the control gels (A).....	161
Figure 2-2-3.	2D sodium dodecyl sulfate polyacrylamide gel electrophoresis (SDS PAGE) analysis The up-regulated proteins are labeled on the treated sample gel (B).....	162
Figure 2-2-4.	Summary for the modes of action of CPF-induced altered proteins.....	173
Figure 2-2-5.	Distribution of the identified proteins.....	174

LIST OF FILES

JinchunSunThes.pdf 9,620 KB

GENERAL INTRODUCTION

PESTICIDE BACKGROUND

Pesticides are biologically active by design and intentionally dispersed into the environment. They are extensively used in the world to destroy or control undesired pests, including insects, weeds, bacteria or other organisms. A prominent group of cholinesterase inhibitors includes two different kinds of pesticides, organophosphate (OP) and carbamate (CB), which were investigated in this dissertation. The following describes their properties, metabolism, and mode of action.

Properties

Forty one different kinds of OPs are registered for use in the United States. They are normally esters, amides, or thiol derivatives of phosphoric, phosphonic, phosphorothioic, or phosphonothioic acids. Although there are various structures of OPs, they share a common basic structure $(R_1)(R_2)(X)P=(S \text{ or } O)$. All OPs contain a central phosphorus atom with a double bond to either sulfur or oxygen. R_1 and R_2 groups are usually simple alkyl or aryl groups, both of which may be either bonded directly to the phosphorus, or linked via $-O-$, or $-S-$. A leaving group X is specific to the individual OP, which can be any one of a wide variety of substituted and branched aliphatic, aromatic, or heterocyclic groups linked to phosphorus via a bond (usually $-O-$ or $-S-$). In order to be useful, these OP compounds must be reasonably stable at a neutral pH. Many OPs are formulated as high concentration in oil, or in a water-miscible solvent, and they are slightly soluble in water and have a high oil-water partition coefficient and low vapor pressure. As such, OPs are applied either directly or after dispersion in water to reach target organisms. All the OPs can be degraded by hydrolysis, yielding water-soluble products that are believed to be non-toxic at all practical concentrations.

More than 50 carbamates are known as N-substituted esters of carbamic acid. Their general structure is $R_1NHC(O)OR_2$, in which R_2 is an aromatic and/or aliphatic moieties. Three main classes of CBs are known: (i) carbamate insecticides (R_1 is a methyl group); (ii) carbamate herbicides (R_1 is an aromatic moiety); and (iii) carbamate fungicides (R_1 is a

benzimidazole moiety). Carbamate ester derivatives are crystalline solids of low vapor pressure with variable, but usually low, water solubility. They are moderately soluble in solvents such as benzene, toluene, xylene, and chloroform. In general, they are poorly soluble in nonpolar organic solvents such as petroleum but highly soluble in polar organic solvents like ethanol. CBs can be hydrolyzed by alkali. The instability in alkali is of use for decontamination and clean-up.

Metabolism

The metabolic fate of OPs and CBs is basically the same in insects, and animals. Animals take in OPs and CBs through the skin, inhalation, or gastrointestinal tract. Metabolism of OPs occurs primarily by oxidation, hydrolysis by esterases, and by transfer of portions of the molecule to glutathione. Oxidation of OPs may result in more or less toxic products. Phosphorothioates generally require oxidative metabolism to produce the proximal toxin, which exerts their acute effects. The rates of hydrolysis of OPs by esterases mostly are faster in mammals than insects. Therefore, mammals are often more efficient in their detoxification processes. In most cases, the products from the glutathione transferase reactions are of low toxicity. Hydrolytic and transferase reaction affect both the thioates and their oxons. Numerous conjugation reactions follow primary metabolic processes, and elimination of the phosphorus-containing residue may be via the urine and feces.

CBs are metabolically transformed by a variety of chemical reactions, including oxidation and enzymatic hydrolysis by enzyme, into more water soluble molecules with increased polar properties. Oxidative products are more or less toxic and are cholinesterase inhibitors. CBs are hydrolyzed either spontaneously or by esterases, yielding as final products, an amine, carbon dioxide, and an alcohol or phenol. Most mammals have more efficiency in hydrolytic enzymes than insects and, therefore, are often more efficient their detoxification processes. The conversion to conjugated compounds of the hydroxyl products produced from the primary metabolic processes is an important reaction that leads to the water-soluble compounds, which can be eliminated via urine and feces.

Mode of action

OPs and CBs exert their acute effects in both insects and mammals by inhibiting acetylcholinesterase (AChE) in the nervous system with subsequent accumulation of toxic levels of acetylcholine (ACh), which is a neurotransmitter. In many cases, the organophosphorylated enzyme is fairly stable, so that recovery from intoxication may be very slow. However, the carbamylated enzyme is unstable, and the regeneration of AChE is relatively rapid compared with that of a phosphorylated enzyme. Thus, carbamate pesticides are less dangerous with regard to human exposure than OPs. The ratio between the dose required to cause death and the dose required to produce minimum symptoms of poisoning is substantially larger for CBs than for OPs.

With the introduction of the organophosphate pesticides (OPs) and carbamates (CBs) into American agriculture, interest in their chemistry, mode of action, and toxicity has increased. Many articles and books have been published concerning the inhibitory action of pesticides on AChE. The inhibitory action of OPs and CBs on AChE appears to be largely responsible for their toxicity toward invertebrates and vertebrates. The action of pesticides may be purely anticholinergic; however, several researchers discovered that some of the OPs chlorpyrifos (CPF) for example are more than cholinergic agonist.

In this dissertation, both the anticholinergic properties (Part I) and neurotoxicity in neuroblastoma cells (Part II) of CPF were studied using proteomics approaches and mass spectrometry (MS). In the last decade, the sensitivity of MS has improved by several orders of magnitude (1). Because of the high sensitivity, selectivity and its high-throughput operations, MS has become an increasingly reliable technique for protein identification. Two new mass spectrometric techniques, electrospray ionization (ESI) and matrix-assisted laser desorption/ionization (MALDI), have dramatically extended protein analysis. These two types of mass spectrometry work in different ways and produce different, but complementary, information. Both MALDI and LC/MS were applied in this dissertation and will be discussed later.

PROTEOMICS BACKGROUND

Marc Wilkins and colleagues first mentioned “proteomics” and “proteome” to mirror “genomics” and “genome” in the early 1990s. Proteomics is the protein complement of the organism’s genome (2). Three developments changed the biological landscape and formed the foundation of the new biology. The first was the growth of the gene database, expressed sequence tag (EST), and protein sequence databases during the 1990s. The genome-sequencing projects yielded complete genomic sequences of bacteria, yeast, nematodes, and drosophila, and culminated recently in the complete sequence of the human genome in the late 1990s. The second key development was the introduction of browser-based bioinformatics tools to extract information from the gene databases. Searching an entire genome for specific nucleic acid or protein sequences in seconds is possible. The third key development is the oligonucleotide microarray. The array contains a series of gene-specific oligonucleotides or cDNA sequences on a slide or a chip.

Although gene microarrays offer a global view of the expression of many or all genes in a cell, it can not predict the levels of the corresponding proteins in a cell. In addition, mRNA levels tell us nothing about the functions of the corresponding proteins, whose activities and functions are subject to many posttranslational modifications. Consequently, many proteins are present in many forms. The detection and differentiation between multiple protein isoforms add an analytical challenge of proteomics.

To address these concerns, scientific researchers recently started to focus on elucidating genomic sequence to total protein analysis, giving rise to a new scientific discipline called “proteomics” (3, 4). Proteomics requires analytical tools to detect and quantify proteins in their different isoforms. Currently two methods, “top-down” and “bottom-up”, are performed for proteomics analysis. Both techniques rely on mass spectrometry (MS) for the protein analysis. However, only “bottom-up” proteomics is described and used in this dissertation.

Bottom-up Proteomics

A proteomics approach currently drawing the most attention is that of bottom-up proteomics. The approach collects protein information from the analysis of peptides

generated from proteolytic digests and can be carried out via two basic strategies. The first strategy of proteomics approaches (Figure 0-1 A) is known as the peptide mass finger-printing scheme by combination of two dimensional gel electrophoresis (2D gel) with mass spectrometry. The protein mixture can be resolved by 2D gel in high resolution, and proteins can be identified using MS in high sensitivity. A typical protocol of this approach begins with 2D gel electrophoresis, where protein mixtures are separated by charge (pI) in the first dimension and then separated orthogonally by size (MW) in the second dimension. Resolved proteins are visualized by staining proteins with Coomassie Blue, SYPRO Ruby, or Silver staining. After analysis of the 2D gel image with software e.g. PDQuest (Bio-Rad), proteins of interest are excised and subjected to in-gel digestion. The digests are further analyzed to generate mass spectra by MALDI-TOF-MS. The experimental peptide masses are then compared to the theoretical ones from the *insilico* digestion of the protein database to identify the protein of interest.

A second proteomic approach is by peptide fragmentation (Figure 0-1B). The approach starts to convert a protein or protein mixture into peptides by protease digestion (Figure 0-1 B). Generated peptides are then resolved by different types of chromatography columns, and each peptide is subjected to MS/MS analysis to produce unique peptide fragmentations. Through electrospray ionization (ESI), peptides in the HPLC effluent are directly introduced into the mass analyzer, such as ion trap or triple quadrupole, allowing on-line MS/MS analysis. The experimental MS/MS spectrum of each peptide is compared with the theoretical MS/MS spectra to elucidate its amino acid sequence using modern protein database search algorithms. Thus, the parent protein of interest is identified.

Bottom-up Proteomics Tools

As described in the previous section, the growth of proteomics is dependent on the development of mass spectrometry and the ability to rapidly obtain accurate masses of proteins and peptides. A typical proteomics experiment is divided into three main classes: protein preparation and analysis, mass spectrometry, and bioinformatics. A variety of instrumentation is required to resolve protein/peptide mixtures and introduce them to the analyzer for analysis. After an analysis using mass spectrometry, bioinformatics tools are

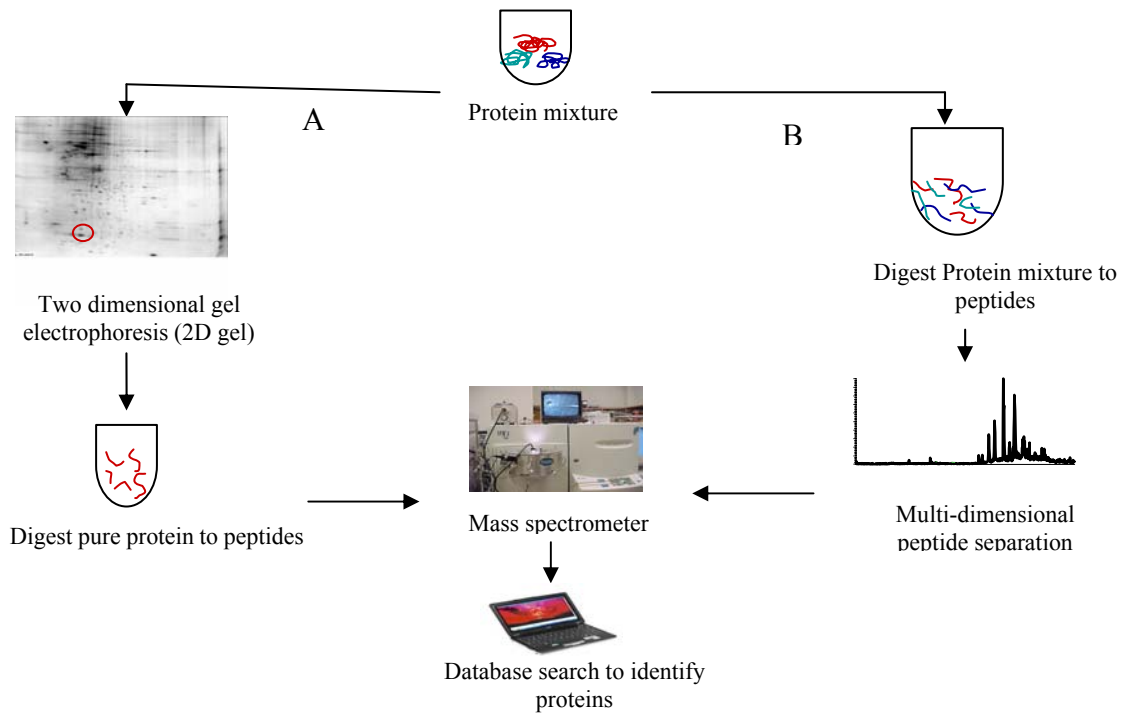


Figure 0-1. Strategies for the analysis of protein mixture using mass spectrometry. (A) Protein mixtures can be resolved by 2D gel electrophoresis. The protein of interest is picked, digested, and analyzed by mass spectrometry. (B) The entire protein mixture is digested, separated by multi-dimensional chromatography, analyzed by tandem MS, and identified by database search.

then applied to identify proteins of interest by searching protein databases. This section will describe some important tools used in this dissertation. These tools include HPLC, two dimensional gel electrophoresis (2DE), MALDI-TOF-MS, ESI, and quadrupole ion trap mass analyzer.

High-pressure Liquid Chromatography

High-pressure liquid chromatography (HPLC) separation/ electrospray ionization (ESI) mass spectrometric detection has been an important tool in proteomics since the last ten years (5, 6). HPLC performs separation by pumping the mobile phase through a column at high pressure to increase the separation performance. Furthermore, the diversity of stationary phases and separation modes increases HPLC resolving power. The major HPLC separation modes used in peptide separation and the characteristics that dictate separation are listed as follows.

- Reversed phase (RP): hydrophobicity
- Strong cation exchange: net positive charge
- Strong anion exchange: net negative charge
- Affinity: interaction with specific functional groups

However, RP-HPLC is usually chosen for resolving a mixture of peptides. The stationary phase of RP-HPLC is non-polar, and the mobile phase is a polar solvent. A typical stationary phase of the reversed phase (RP) chromatography consists of silica based packings or the other supports covalently bound with n-alkyl chains. For example, C-8 signifies an octyl chain and C-18 an octadecyl ligand in the matrix. A typical mobile phase is a mixture of water or buffer with polar solvents such as methanol, acetonitrile, or tetrahydrofuran.

The more hydrophobic the matrix, the greater is the tendency of the column to retain hydrophobic moieties. There are three competing explanations for retention in reverse phase chromatography: the hydrophobic theory, partitioning, and adsorption. However, a complete theory of retention mechanism of reversed-phase chromatography must include both partitioning and adsorption(7). The theory of Jaroniec (8) treats the retention mechanism as a mixture of partitioning and displacement. The partitioning model can explain how peptide mixtures can be resolved in RP-HPLC. Based on this theory, an

equilibrium exists when peptides partition between the stationary phase and the liquid mobile phase. Peptides migrate in and out of the stationary phase along with the mobile phase. However, the equilibrium can be shifted toward the mobile phase by increasing the organic component of the solvent. Peptides in a mixture are separated based on their hydrophobicity using a gradient mobile phase of increasing organic component.

The separation of a peptide mixture into its individual components takes place in the chromatography column. In order to understand the mechanism of retention and selectivity and thus be in a position to exercise some control over the chromatography system, it is necessary to know the theory of chromatography. Next, the theory of chromatography, especially of the hydrodynamics of chromatography will be covered.

The quality of a separation is measured by the plate count N , which is related to the height equivalent to a theoretical plate (HETP). HETP is described by the equation:

$$h = \frac{d\sigma^2}{dL} \quad (0.1)$$

Where L is the column length, σ is the standard deviation of a Gaussian distributed chromatographic peak. Generally, if HETP is plotted against a linear velocity, a curved relationship with a minimum of the HETP will be obtained (Figure 0-2). Among all the equations describing the dependence of the HETP on linear velocity, the van Deemter equation (9) is conceptually the simplest. It is assumed that the overall spreading of a peak is the result of a number of individual, non-interacting, random processes that, taken together, account for the total peak dispersion. Since these contributions are independent of each other, HETP is simply described by adding them up:

$$H = A + \frac{B}{u} + Cu \quad (0.2)$$

Where u is the velocity; A , velocity-independent, is a function of the size and distribution of the inter-particle channels and other non-uniformities in the packed bed; B , describing the molecular diffusion in the axial direction, is inversely proportional to the linear velocity; C , containing all terms related to mass transfer, is directly proportional to the linear velocity.

The A term of the van Deemter equation is expressed as

$$A = \lambda_i d_p \quad (0.3)$$

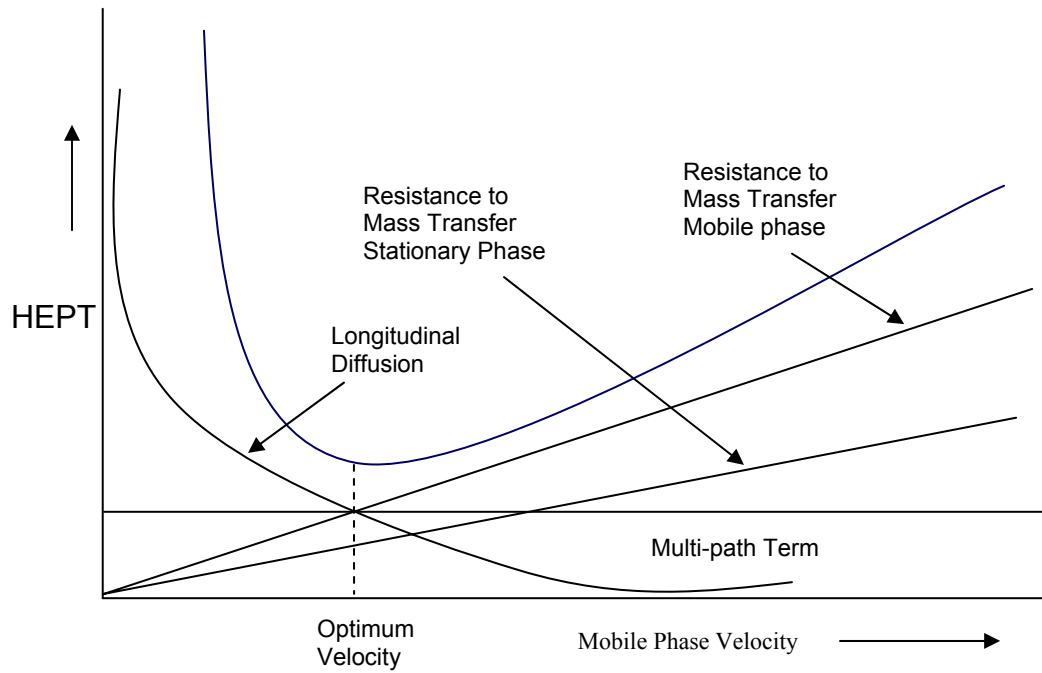


Figure 0-2. Relationship between HETP and linear velocity. The curve has a minimum and the right-hand branch increases usually practically linearly with the linear velocity.

Where λ_i stands for the factor of the packed bed, which is between 1.5 and 2, d_p is the particle diameter. The A term is proportional to the particle size and can be influenced by the column packing technique.

The B term of the van Deemter equation is described as

$$B = 2\gamma \frac{D_M}{u} \quad (0.4)$$

The coefficient γ is the obstruction factor, which depends on the amount and the nature of the “obstruction” that is in the way of free movement of the molecule. The factor γ is usually between 0.5 and 1. D_M is the diffusion coefficient in the mobile phase, assuming that the diffusion coefficient in the pores is the same as that in the interstitial mobile phase.

Now, let us look at the term of the van Deemter equation that describes all the phenomena resulting in an increase in HETP with increasing linear velocity. This term includes the mass transfer from the center of the moving mobile phase to the surface of the particle (mobile-phase mass transfer), through the stagnant mobile phase in the pores to the stationary phase on the internal surface of the packing (mobile-phase mass transfer resistance to the stagnant mobile phase), and the interaction kinetics with the stationary phase (stationary-phase mass transfer). Although these contribute to the resistance to mass transfer, a rough estimation is made for the coefficient on the mass-transfer term in a packed bed with porous particles in the practical range as

$$C = c \frac{d_p^2}{D_M} u \quad (0.5)$$

Where the coefficient c is between 0.1 and 0.3 in most practical cases; d_p is the particle diameter; D_M is the diffusion coefficient in the mobile phase.

The whole van Deemter equation is described as follows, including all the coefficients used to estimate the HETP for a normal packed bed of porous particles:

$$H = 1.5d_p + \frac{D_M}{u} + \frac{1}{6} \frac{d_p^2}{D_M} u \quad (0.6)$$

The plate count of a column can be estimated using this equation assuming that the diffusion coefficient is known. Figure 0-2 shows a curve with a minimum, which means that there is an optimum mobile phase velocity at which the column will give the minimum

HETP, and consequently, a maximum efficiency. In practice, this usually means that reducing the flow rate of a column will increase the efficiency, and thus, the resolution. In doing so, however, it also will increase the analysis time. In addition, there is a limit to velocity procedure, as reducing the column flow rate so that the mobile phase velocity falls below the optimum will result in an increase in the HETP, and thus, a decrease in column efficiency.

It is seen that equation (0.6) is explicit and would permit the design of a column to have the particular efficiency required for a specified analysis. Based on this theory, designed columns, packed in laboratory, were applied in this dissertation. ESI requires low liquid flow rate and, thus, very small diameter HPLC columns. Currently, microflow ($\mu\text{l}/\text{min}$) and nanoflow (nl/min) HPLC have already been developed (10). Packed capillary columns range in inner diameter (I.D.) from 50-500 μm with 15 to 30 cm in length. The required flow range (e.g. 100 nl/min to 5 $\mu\text{l}/\text{min}$) for a packed capillary column with conventional HPLC pump can be obtained by using a flow splitter prior to the injector. In addition to the compatibility with direct mass spectrometry, microflow and nanoflow HPLC also provide an advantage of smaller sample volumes and increased sensitivity.

Two-dimensional Gel Electrophoresis

Two-dimensional gel electrophoresis (2D gel) is still the best method for simultaneously resolving highly complex protein mixtures. In brief, 2D gels resolve proteins in the first dimension by charge (pI) and in the second dimension by molecular weight (MW) (Figure 0-3).

The introduction of immobilized pH gradients (IPG) for the isoelectric focusing step (IEF), has greatly improved the reproducibility of 2D gel electrophoresis (11). IPGs are based on the principle that the pH gradient is generated by a limited number of well-defined chemicals, which are co-polymerized with the acrylamide matrix. IPGs allow the generation of pH gradients of any desired range between pH 3 and 12. The first dimension of 2D gel electrophoresis, isoelectric focusing (IEF), is performed in individual IPG gel strips 5 mm wide. Prior to IEF, the IPG strip is hydrated with protein mixture in sample hydration buffer (containing chaotropic reagent and ampholytes), and proteins are slowly loaded into the strip under voltage prior to isoelectric focusing. After 12 hours of

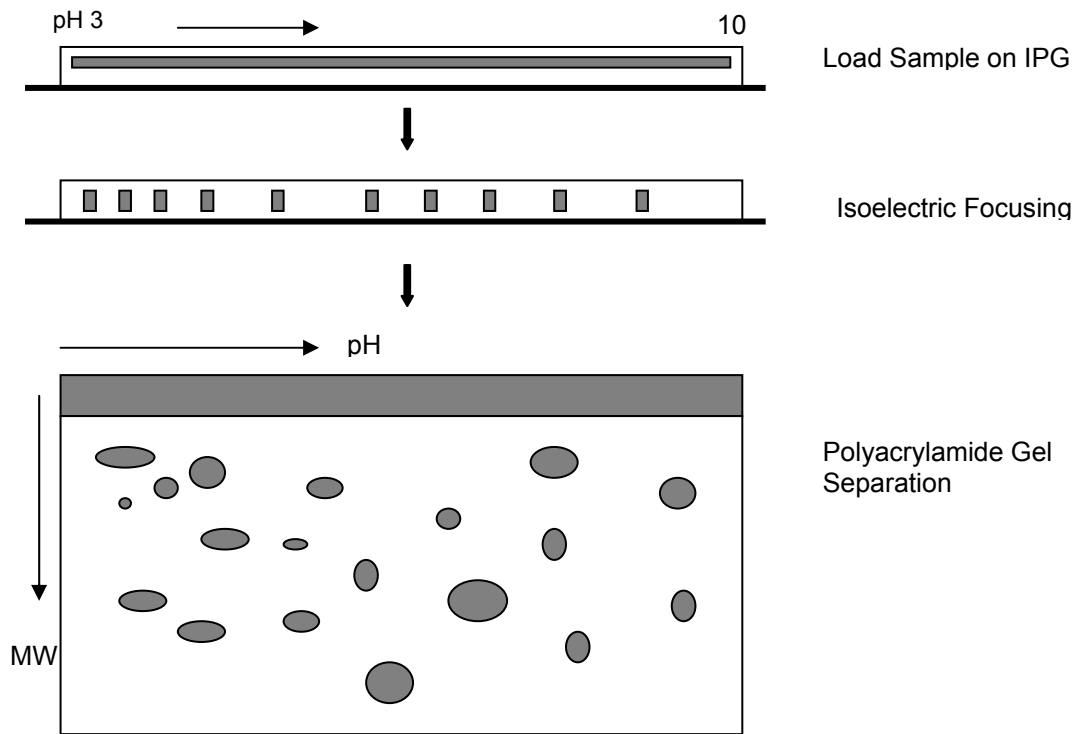


Figure 0-3. Schematic representation of 2D gel electrophoresis.

loading time, the voltage is then increased to achieve focusing. With the presence of a pH gradient in the IEF technique, a protein will migrate to the position in the gradient where its charge is zero. Proteins with a positive net charge will migrate toward the cathode until it meets its pI. Similarly, proteins with a negative net charge will migrate toward the anode until it meets its pI. IEF is performed under high voltages (> 1000 V) until the proteins have reached their final position in the pH gradient.

After the focusing step, the strip is then treated with equilibration buffers containing a thiol reductant and denaturing reagent (i.e. SDS) followed by loading it on the second dimensional gel, polyacrylamide gel electrophoresis (PAGE). In this situation, the IPG strip with the focused proteins is like a 'stacking gel' in a 1D SDS gel electrophoresis. The proteins are then separated on the SDS-PAGE on the basis of their size in the same manner as the 1D gel electrophoresis. Gels are run at constant current until the blue dye front line reaches the bottom of the gel. After termination of the second dimension run (PAGE), it is necessary to immobilize the resolved proteins in the gel with a fixing solution. TCA (20%) or methanolic or ethanolic acetic acid are widely used as fixatives. Proteins can be visualized by several staining methods – silver staining, fluorescent staining, colloidal Coomassie Blue G-250 staining, and Coomassie R-250 staining. The protein of interest can be digested with proteolytic enzymes, such as trypsin. The digest is then subjected to MALDI-TOF-MS or ESI-MS analysis.

MALDI-TOF-MS

MALDI Source

For purposes of proteomics, data on peptide masses is obtained by matrix-assisted laser desorption ionization-time of flight (MALDI-TOF), whereas MALDI refers to a method of ionization, and TOF refers to the mass analyzer. The question of how to obtain good data requires us to understand how a MALDI-TOF instrument works. It is easiest to start with the MALDI source for understanding the principle of MALDI-TOF instruments. The production of ions depends on the selection of laser and matrix.

Lasers and Matrix

There are different kinds of lasers, including ultraviolet (UV) and infrared (IR) lasers. Because of their ease of use and low price, UV lasers are the most common.

Nitrogen lasers ($\lambda = 337 \text{ nm}$) and Nd : YAG ($\lambda = 266$ or 355 nm) are used, among which nitrogen lasers are considered standard. IR lasers include Er : YAG lasers ($\lambda = 2.94 \text{ }\mu\text{m}$) and CO₂ lasers ($\lambda = 10.6 \text{ }\mu\text{m}$). The production of ion current depends on the total energy in the laser pulse at a given wavelength. The pulse widths of lasers vary from a few tens of nanoseconds to a few hundred microseconds. Big molecular ions are generally observed at slightly higher laser power. However, high energy causes extensive fragmentation and lower mass resolution. It is important to set up a suitable laser pulse power, which starts desorption of the matrix, to obtain a high quality mass spectrum.

High quality mass spectra also depend on the matrix selection. A good matrix must have the following properties: strong absorbance at the laser wavelength, low molecular weight, stability in high vacuum condition, and low chemical reactivity. After investigating numerous matrix candidates, only a few have been proven as good matrices (Table 0-1). Table 0-1 lists some common matrices and their applications in the compounds analysis.

Principle of MALDI

Matrix-assisted laser desorption/ionization is achieved in two steps. In the first step, the analyte is mixed with a chemical matrix solution containing small organic molecules, which absorb light at a certain wavelength. The most popular matrix compounds are α -cyano-4-hydroxycinnamic acid (CHCA), 2,5-dihydroxybenzoic acid (DHB), and 3,5-dimethoxy-4-hydroxycinnamic acid (sinapinic acid). A dried-droplet method is the most frequently used on-target preparation. The protocol for producing a dried droplet sample has several simple steps. First, make a saturated solution of the matrix chemical and mix with sufficient peptide for a final concentration of 1-10 mM. Second, place a droplet (0.5-2 μl) of the former solution on the sample target of the mass spectrometer. Dry the droplet at room temperature or through blowing room-temperature air over the droplet to dry the spot. The result is a "solid solution" deposit of analyte-mixed matrix crystals, where the analyte molecules are distributed in the matrix and separated from each other.

The second step involves irradiation of the solid solution by an intense pulse of laser light. The laser energy can be adjusted to ionize different samples. The matrix chemicals absorb photons from a laser beam, which induces rapid heating of the crystals.

Table 0-1. Some common UV-MALDI matrices.

Matrix	Applications
α -Cyano-4-hydroxycinnamic acid	Peptides, proteins, organic compounds
3,5-Dimethoxy-4-hydroxycinnamic acid	Higher mass biopolymers
2,5-Dihydroxybenzoic acid	Peptides, proteins, carbohydrates
3-Hydroxypicolinic acid	Oligonucleotides
Trihydroxyacetophenone	Oligonucleotides, peptides
5-chlorosalicylic acid	Water-insoluble polymers

Such rapid heating causes localized sublimation of matrix crystals and dispersion of the matrix into the gas phase. During this process, the matrix serves to reduce sample damage from the laser pulse by absorbing most of the incident energy. At the same time, the matrix also plays important roles in the energy transfer from the laser to analyte. Ionization reactions can occur at any time during this process. However, it is still not fully understood how the ions are originally produced in MALDI. Chemical and physical ionization pathways for MALDI include gas-phase photonization, excited-state proton transfer, ion-molecule reactions, desorption of preformed ions, etc. It is most widely accepted that the ion formation mechanism involves gas-phase proton transfer in the expanding cloud with photonized matrix molecules. Both positive and negative ions can be formed during ionization process based on the nature of the sample. Usually, each peptide molecule accepts one proton from the matrix as it enters into the gas phase to form a single-charged ion. Because of the pulse property of laser desorption, a time-of-flight analyzer is chosen as a detector. The ions formed in the MALDI source are then extracted and directed into the TOF mass analyzer.

TOF Analyzer

The first linear time-of-flight (TOF) was developed in 1946 by Stephens (12). After ions are expelled from the source in bundles produced by laser desorption, they are accelerated by a high potential field. Ions with different mass-to-charge ratios have the same kinetic energy, but with different velocities resulting in different flight time through a field free drift tube. Mass-to-charge ratios are determined by the flight time in the drift tube between the source and the detector. When an ion leaves the ion source, its kinetic energy is described as:

$$\frac{mv^2}{2} = zeV_s \quad (0.7)$$

Where m and z are the mass and charge of the ion, v is the velocity of the ion, V_s is the acceleration voltage.

The time needed to pass through the drift-tube (distance is d):

$$t = \frac{d}{v} \quad (0.8)$$

Replacing v with the former equation (0.7), it gives a new equation as following:

$$t^2 = \frac{m}{z} \left(\frac{d^2}{2V_s e} \right) \quad (0.9)$$

This equation shows that the lower the m/z ratio, the faster it will reach the detector. The typical length of flight tube is 1-2 m, and acceleration voltage of at least 20 kV for keeping the sensitivity high.

Due to variations in the velocities of ions of the same m/z , the resolution of linear mode is poor. Mass resolution is affected by the following factors: the length of the ion formation pulse (time distribution), where the ions are formed (space distribution), and initial kinetic energy of the ions (kinetic energy distribution). A technique called “pulse ion extraction” was first developed by Wiley and McLaren in the 1950s (13). A time delay between ion formation and extraction is used to reduce the kinetic energy distribution of ions with the same m/z ratio. The process of delayed pulses extraction has two simple steps. First, ions produced in the source are allowed to expand into a field-free region. Second, a voltage pulse is applied to extract the ions outside the source after a certain delay (hundreds of nanoseconds to several microseconds).

In the delayed pulse extraction mode, ions initially separate according to their kinetic energy in the field-free region. For ions with the same m/z ratio, those with more kinetic energy move further toward the detector than those with less energy. Then the extraction pulse is applied after a certain delay time, which transmits more energy to the ions that remained for a longer time in the source. Thus, the ions with initially less energy receive more kinetic energy. Thus, ions with the same m/z ratios are energy focused.

Reflectron mode of TOF analyzer was used in this dissertation (Figure 0-4). The reflectron field is composed of a series of grids and ring electrodes, which was first proposed by Mamyrin (14). It acts as an ion mirror by reflecting the ions and sending them back through the flight tube. The higher resolution in the reflectron mode is obtained by a reflecting field at the end of the flight tube equipped with higher potential and the same polarity as the accelerating voltage. Ions with the same m/z value but different velocities are time-focused with the reflector. Indeed, ions with more kinetic energy will penetrate the reflectron more deeply and will spend more time in reflectron. Thus, they reach the detector at the same time as those with slower velocity.

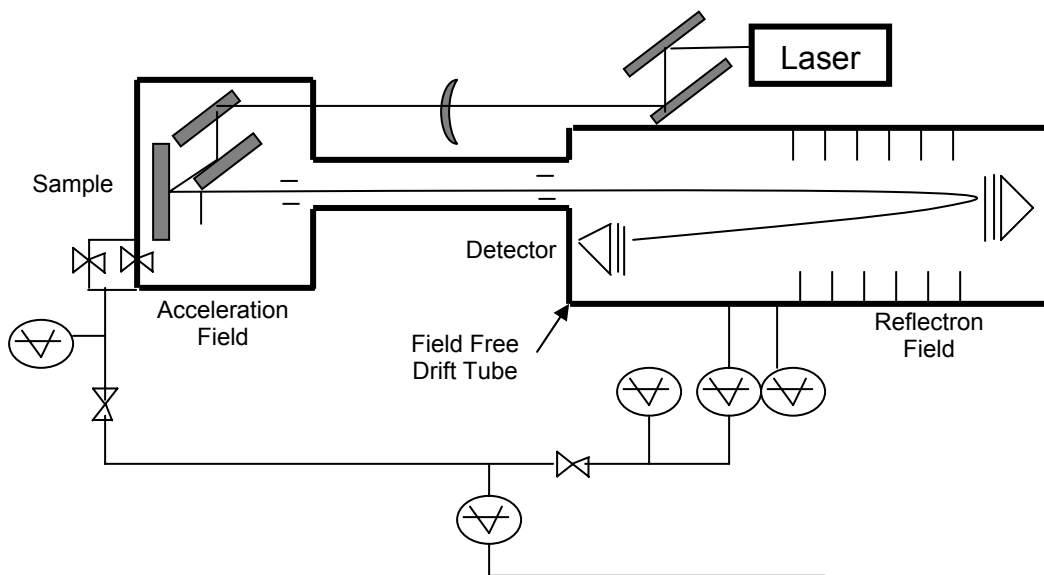


Figure 0-4. Schematic representation of reflectron mode of MALDI-TOF-MS.

If two ions with the same m/z ratio but with different energies: one with kinetic energy E_k and another one with kinetic energy E_k' , we define the ratio of two kinetic energies as

$$\frac{E_k'}{E_k} = a^2 \quad (0.10)$$

So, the ratio of the velocity of two ions can be obtained

$$\frac{V_{is}'}{V_{is}} = a \quad (0.11)$$

Thus, the ratio of the time of these two ions in the field-free flight is

$$t' = t/a \quad (0.12)$$

And the ratio of the time of these two ions in the reflectron is

$$\frac{t_r'}{t_r} = a \quad (0.13)$$

The total flight time (including flight time in field-free tube and reflectron field) for these two ions are

$$t_{TOT} = t + t_r, \text{ and } t_{TOT}' = t' + t_r' = t/a + at_r \quad (0.14) (0.15)$$

When $a > 1$, ions with high kinetic energy take less time to pass through the field-free tube, but will spend longer time inside the reflectron field. Thus, the variations of the flight times compensate each other. A good compensation will yield the same total flight time for all ions with the same m/z ratios but with different kinetic energy, which requires the proper values for reflectron field strength, acceleration voltage, and the length of the field-free flight tube.

Post Source Decay (PSD)

The term post-source decay refers to the fragmentation of molecular ions, which occurs after ion acceleration field and prior to detection region. PSD analysis is an extension of MALDI-TOF-MS, which allows one to observe and identify structural information of precursor ions. The precursor ion can be selected by applying electrodes after the source on the ion path before entering into the field free tube. Ions can be deflected by applying potential. Turning off this potential for a short time allows the selected ions to pass through. After leaving the ion source, all ions have the same nominal kinetic energy,

most of them are unfragmented precursor ions and they already acquired internal energy by various mechanisms. During their flight through the field-free drift region they have a long time available for post source decay into product ions. These product ions still have basically the same velocity as their precursor ions, but have a much lower kinetic energy because of their lower mass. The kinetic energy of the product ions is a measure of their mass. The kinetic energy of fragment products is described as:

$$E_{kf} = E_{kp} \frac{m_f}{m_p} \quad (0.16)$$

Where E_{kf} and E_{kp} are kinetic energy of fragment and precursor ions respectively, m_f and m_p are the mass of the fragment and precursor ions.

Thus, the penetration depth of fragments in the reflectron is:

$$x_f = x_p \frac{m_f}{m_p} \quad (0.17)$$

Where x_f and x_p are the penetration depth of fragment and precursor in the reflectron.

Hence, the flight time of the fragment in the reflectron is:

$$t_{rf} = t_{rp} \frac{m_f}{m_p} \quad (0.18)$$

This equation shows that the fragment ions take shorter time in the reflectron than the precursor. Measurement of the flight times of fragment ions corresponding to a particular precursor ion makes it possible to get the sequence information of this ion.

Although PSD is not the best MS technique to obtain peptide sequencing, it was successfully used to identify the phosphorylated peptide in this dissertation.

LC/MS Instrument

Electrospray Ionization

The success of electrospray ionization (ESI) started when Fenn and coworkers showed that multiply charged ions were obtained from proteins (15). Proteins in multiple charged forms are detected with the instruments whose mass range is limited to as low as 2000 Da. Later on, the use of ESI extended not only to analyze polymers or biopolymers, but also to analyze small polar molecules. ESI is widely used throughout the biochemical

field, since it is easily coupled with high performance liquid chromatography (HPLC), micro-HPLC and capillary electrophoresis. A lot of researchers discussed electrospray principles and its biological applications(16-18). Based on the understanding of their theories, the following describes the principle of electrospray.

An electrospray is produced by applying a strong electric field(19-22), which is obtained by the use of a potential difference of 3-6 kV between a capillary and its counter-electrode located at the entrance to the mass spectrometer 0.3-2 cm away. When a flow in stream containing sample is pumped through this narrow-bore capillary with high potential, the resulting high field induces a charge accumulation at the liquid surface located at the end of the capillary, which will break into droplets with multiple charges (Figure 0-5). Gas at a low flow rate is applied coaxially to disperse the spray into a mist of very fine, charged droplets. The 'onset voltage' to form a spray depends on the solvent, the surface tension of which is different for different solvents. As this voltage is applied, the shape of the drop changes (Figure 0-6), and the surface tension is broken. During this time, charge separation of ions occurs in solution as negative ions migrate to the needle surface and positive ions move toward to the counter electrode. As the solvent contained in the droplets evaporates, the droplets shrink to the point where the repelling coulombic forces reach the Rayleigh instability limit, thereby causing their division. These droplets continue to be divided, and they become smaller and smaller. This process of droplet desolvation and fissions continues until all solvent is completely removed and only ions in gas phase remain.

A unique characteristic of ESI is the production of multiply charged ions for big molecules such as proteins and peptides. These multiply charged ions are either in positive-ion mode, or negative-ion mode, and also cover a range of charge states. On average, one charge is added per 1000 Da in mass. Many peptides have multiple proton accepting sites, resulting in singly charged or multiply charged ions in solution. Because tryptic peptides have lysine or arginine residues at their C-termini as well as N-terminal amino groups, and both of them can be protonated in acidic solutions, they normally have double charges. Obtaining multiply charged ions is an especially convenient feature, since ESI can analyze high-molecular-weight molecules using an analyzer with a weak nominal mass limit, such as a quadrupole mass filter.

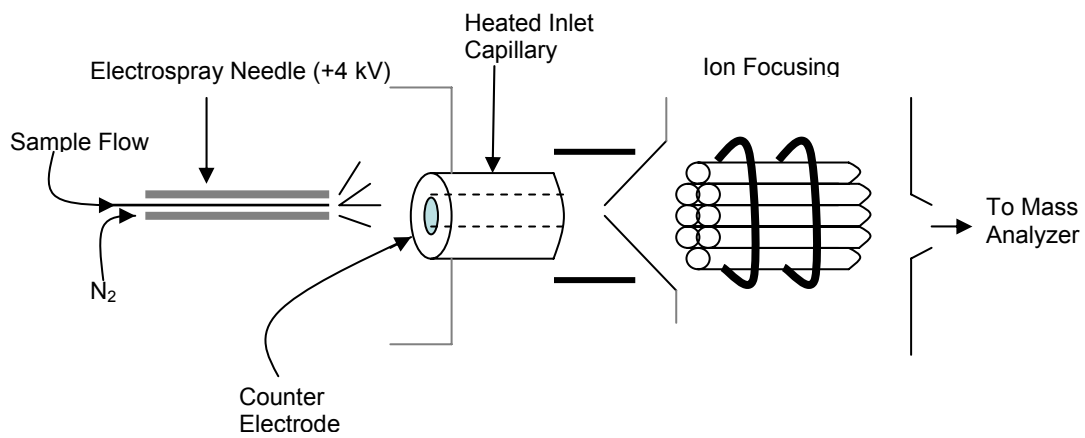


Figure 0-5. Schematic representation of a typical ESI source.

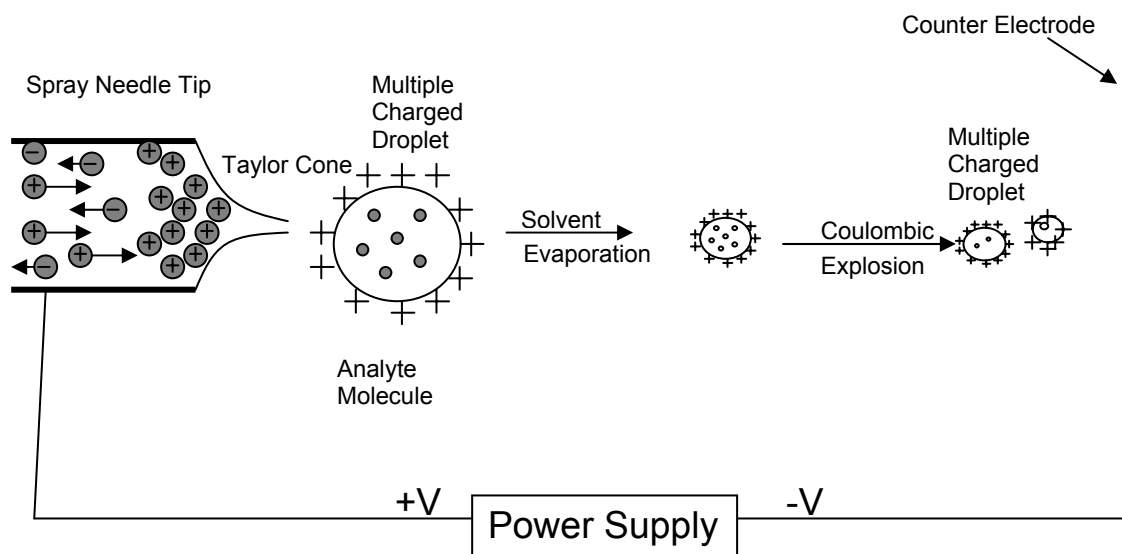


Figure 0-6. Schematic representation of electrochemical process in ESI.

The Quadrupole Ion Trap

In 1960, Paul and Steinwedel (23) (24) invented the ion trap, which was further developed to a useful mass spectrometer by Stafford et al. (25). An ion trap is comprised of three hyperbolic electrodes: the ring electrode, the entrance endcap electrode and the exit endcap electrode. Both endcap electrodes have small holes in the center through which the ions can enter/exit. The ring electrode is located halfway between the two endcap electrodes. Paul and Steinwedel proposed that this ion trap could be used as a mass spectrometer by applying a resonant frequency on the endcap to expel the ions along z .

Stable trajectory of ions at a given masse can be located by the mathematic analysis through the Mathieu equation. In the trap, the motion of ions is in three dimensions, x , y , and z , which is under the influence of the applied potentials on the ring electrode. However, because the ion trap is cylindrical symmetry $x^2 + y^2 = r^2$, two coordinates, z and r , are used to describe the motion of the trapped ions (Figure 0-7).

The equations of the movement of ions inside the trap are described as followed:

$$\frac{d^2z}{dt^2} - \frac{4Ze}{m(r_0^2 + 2z_0^2)}(U - V \cos \omega t)z = 0 \quad (0.19)$$

$$\frac{d^2r}{dt^2} - \frac{2Ze}{m(r_0^2 + 2z_0^2)}(U - V \cos \omega t)r = 0 \quad (0.20)$$

Where ω is the angular frequency (in rad s^{-1}) $= 2\pi\nu$, ν is the frequency of the radio frequency (RF) on the ring electrode, U is the direct potential and V is the amplitude of the RF voltage, r_0 is the distance between the center of the ion trap and the ring electrode, Z is used for the number of charges, r and z are the distance between the ring and endcap electrodes, respectively.

The following equation was established in 1866 by Mathieu in order to describe the propagation of waves in membranes:

$$\frac{d^2u}{d\xi^2} + (a_u - 2q_u \cos 2\xi)u = 0 \quad (0.21)$$

Where u stands for either z or r . Comparing the preceding equations with this Mathieu

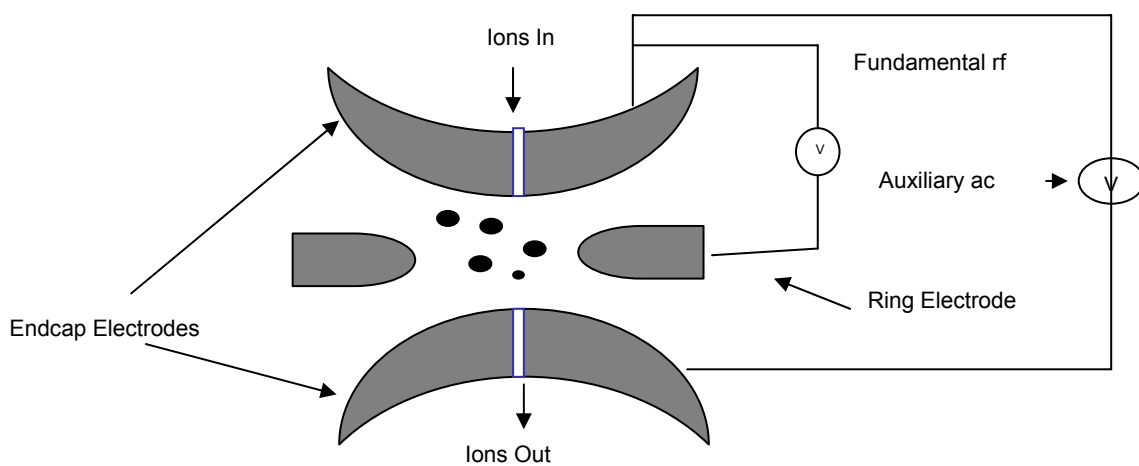
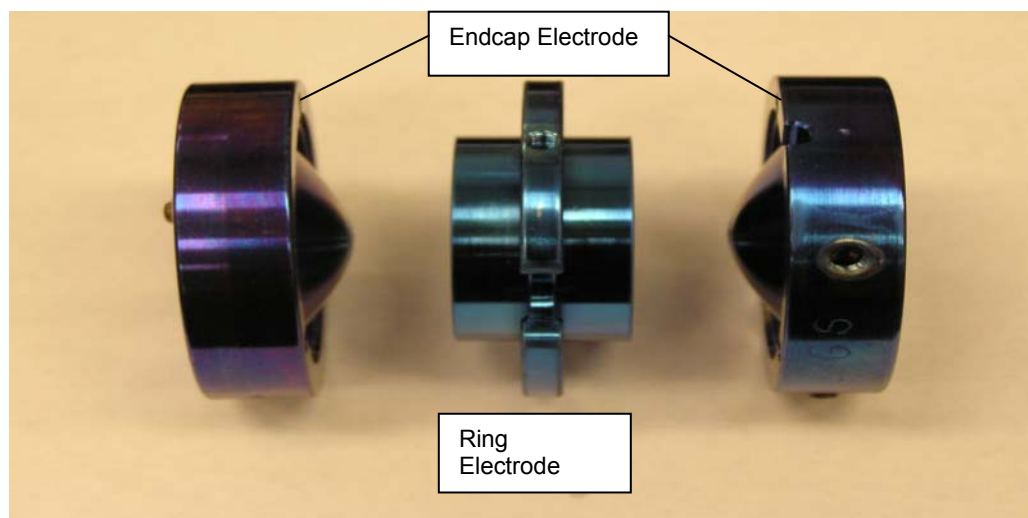


Figure 0-7. Quadrupole ion trap. (A) Photograph of disassembled ion trap. (B) Schematic representation of an ion trap MS instrument.

equation, the following changes of variables allow the equation of motion to be depicted in the form of Mathieu equation:

$$\xi = \frac{\omega t}{2}, \quad a_u = a_z = -a_r = \frac{-16ZeU}{m(r_0^2 + 2z_0^2)\omega^2} \quad (0.22)$$

$$q_u = q_z = -q_r = \frac{8ZeV}{m(r_0^2 + 2z_0^2)\omega^2} \quad (0.23)$$

As long as r and z both are less than r_0 and z_0 , ions are trapped in the ion trap with a stable trajectory. A function $e^{(\alpha+i\beta)}$ is needed to integrate the Mathieu equation by the Floquet and Fourier method. The stable trajectories of ions requires both $\alpha = 0$ and $0 < \beta_u < 1$. The parameter β_u can be obtained from q_u and a_u parameters of the Mathieu equation. A simpler approximate equation of β_u is as following for q_u is less than 0.4.

$$\beta_u = [a_u + (q_u^2 / 2)]^{1/2} \quad (0.24)$$

Because β_u can be calculated from q_u and a_u , and also based on the limitation of β_u for a stable trajectory, a , q values inside the limited values of β_u for a stable trajectory are displayed in Figure 0-8. Based on the expression of equation (0.23), q_z will increase if V increases and will decrease if m increases assuming the other parameters (including r_0, z_0 and ω) are constant. If V is increased, the q_z value of all the ions will become bigger. When $q_z = 0.908$, β is equal to 1, the ion has reached its stability limit. This ion will have an unstable trajectory if the V is slightly increased, and will be ejected from the trap in the z direction, which allows the ions present in the trap to be analyzed. Thus, a mass spectrum is generated by sequentially ejecting fragment ions from low mass to high mass by scanning amplitudes of the fundamental rf potential that sequentially makes the ion trajectories unstable; 50% of the ejected ions will reach the detector.

Ions can also be ejected from the trap by applying a *supplementary potential* on the endcap electrodes. This technique is called as “*resonance ejection*”, which allows ejection to occur at voltage lower than those required for ejection at $q_z = 0.908$. *Resonance* is caused by matching the frequency of the *supplementary potential* to the *secular frequency* (f_z) of the ion, which is determined by the values of β_z and the frequency of the fundamental rf.

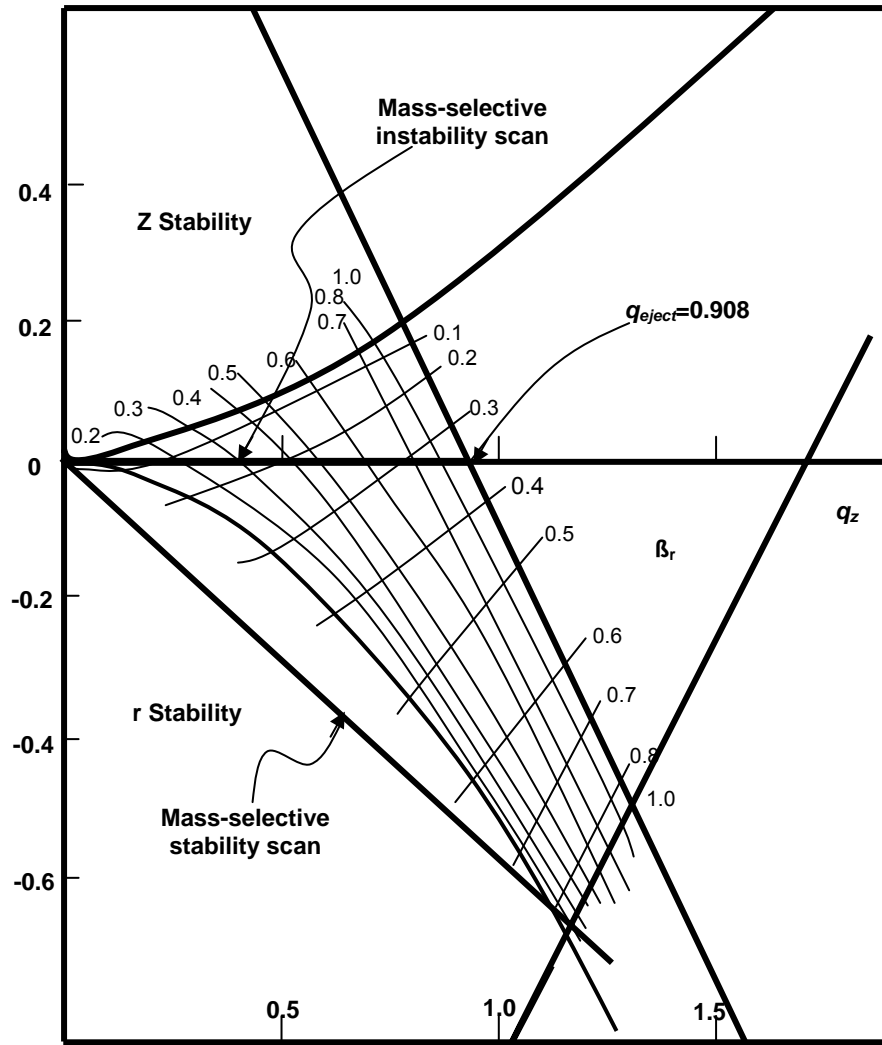


Figure 0-8. Stability diagram for a quadrupole ion trap. The value at $\beta_u=1$ along the q_z axis is $q_z = 0.908(26)$.

$$f_z = \beta_z \nu / 2 \quad (0.25)$$

where f_z is secular frequency, ν is the frequency of the fundamental rf.

If the frequency of the *supplementary potential* is at f_z , the ion will come in resonance and the amplitude of its oscillations will increase along the z -axis. If the applied amplitude is sufficient, the oscillations of the ion will be large enough to be ejected from the trap in z direction. When resonance ejection is used and the amplitude of the voltage is ramped from low to high amplitudes, all the ions are sequentially ejected from the trap and detected. It is also used to isolate ions in the trap by combination of forward and reverse resonance ejection ramps.

After the production of ions, they are focused through a skimmer and two RF-only octapoles. A gating lens is used to manipulate the number of the injected ions to an acceptable limit with a reasonable resolution and sensitivity. A positive potential is used for positive ions. However, during injection of ions, a negative potential is used to draw ions into ion trap. A gating time can be calculated in order to inject the selected number of ions, which will not overfill the trap and produce a space-charge effect. After the injection of ions in the trap, they encounter helium to remove excess energy by collision. The pressure of helium in the ion trap is around 1×10^{-3} torr. Ions can be further analyzed according to their masses by scanning the fundamental rf voltage on the ring or combination with additional rf voltage to the endcaps as described before.

In some circumstance, it may be desirable to obtain structure information of a particular ionized molecule subjecting it to MS/MS fragmentation. The special isolation of an ion with a particular m/z in the ion trap prior to the ion dissociation event is required for tandem mass analysis. There are several ways to perform tandem mass spectrometry in an ion trap. The general sequence of operation is described as follows.

First, ions with a particular mass-to-charge ratio were isolated through expelling all other ions from ion trap. This approach can be obtained in several ways. One approach for isolation of a precursor ion is by selecting the precursor ion at the apex of the stability diagram. This is accomplished through the use of a dc potential to the ring electrode in addition to the preexisting fundamental rf. The ion of interest is brought to the apex of the stability diagram (Figure 0-9) by a combination of dc and rf potentials. All other ions will be ejected from ion trap at q_z less than 0.908. Another approach to isolate a precursor ion is

by the use of a supplemental potential to the endcaps through resonance ejection of all ions except for the selected one.

Secondly, a precursor ion isolated in an ion trap is then subjected to fragmentation into product ions. This fragmentation is improved by excitation of the selected ions through the application of a low-amplitude ac resonance signal across the endcap electrodes, which causes the ion kinetic energies to increase. These excited ions are then subjected to dissociate due to many collisions with the helium damping gas.

Finally, tandem mass spectrum is obtained by one of the scanning methods: stability limit or with the assistance of resonance ejection as described before.

Perhaps the biggest strength of the ion trap technique lies in the multiple stages of mass spectrometry. Up to 12 stages of tandem mass (MS^{12}) have been performed using an ion trap, which greatly increase the structural information for a given molecule. Product ions can also be further isolated and dissociated to provide MS^n mass spectra using this technique. MS^n is obtained by retaining the fragment ions from MS/MS and further acquiring another round of fragmentation. MS^n analysis is useful to yield highly detailed information in certain cases. For example, a dominant doubly charged fragment ion corresponds to the loss of the modification group from the interesting alkyl-phosphorylated peptide, which makes it impossible to localize the modification site. So, MS^3 is further applied to determine the amino acid sequence, and localize the phosphorylation site.

STATEMENT OF RESEARCH

As mentioned before, the actions of pesticides on the organisms include anticholinergic mode and neurotoxic mode. Both of the properties of pesticides are investigated in this dissertation. The remainder of this dissertation is divided into two parts: anticholinergic study of pesticides (Part I), and toxic study of CPF in neuroblastoma cells (Part II).

Anticholinergic Study of Pesticides

The first part of this dissertation studied the butyrylcholinesterase (BChE) inhibition resulting from OPs and CBs. Three steps were included in this project. First of

all, a new methodology was developed for the detection and quantification of pesticide exposure using MALDI-TOF and eBChE as a model system (Chapter 2 of Part I). The methodology was based on the analysis of pesticide-inhibited BChE, particularly based on the detection of modified active site peptide produced from trypsin digests of the enzyme. Although MALDI method was proven to be useful for the analysis of single pesticide exposure, the lower response of phosphorylated peptide in MALDI and the suppression of the modified peptides in a peptide mixture make this method limited for the analysis of multiple pesticide exposure. In the second stage, an *in vitro* investigation was designed to examine the relative quantification of each pesticide exposure, and to identify the types of pesticide using LC/MS/MS and eBChE as a model system (Part I, Chapter 3). This LC/MS/MS technique was successfully applied to analyze a mixture of the phosphorylated peptides *in vitro*, and the precursor ions were monitored by a common fragment ion. Finally, the developed technique was applied to investigate hBChE inhibition *in vitro* and in serum samples (Part I, Chapter 4 and 5). Chapter 4 of Part I focused on the method development for synthesizing the affinity column, which enabled the isolation of BChE from the serum. The performance characteristics of the synthesized affinity beads were evaluated. Chapter 5 described the application of the developed method (LC/MS/MS method) towards the analysis of hBChE inhibition in the serum sample. A calibration system was constructed for the analysis of hBChE inhibition, which was then applied towards the quantification of the enzyme present in the serum. A novel on-bead double digestion protocol was investigated. The reliability of this double digestion was also evaluated.

Neurotoxic study of CPF

The second part of this dissertation studied the neurotoxic properties of CPF, an organophosphate. Systematic studies at subcellular levels were designed to evaluate proteome changes in SH-SY5Y cells exposed to CPF. Two-dimensional gel electrophoresis (2DE) was applied with MALDI-TOF-MS to analyze differential protein expression. Results proved our hypothesis as described in Part II, Chapter 2.

PART I. STUDY OF SERUM BUTYRYLCHOLINESTERASE INHIBITION FROM
PESTICIDE EXPOSURE

CHAPTER ONE

INTRODUCTION OF PART I

BUTYRYLCHOLINESTERASE BACKGROUND

Dale predicted the existence of cholinesterase in 1914 (27). However, until 1932, the term 'cholinesterase' (CHE) was used to name an enzyme from a horse serum (28) by Stedman et al. The identification of CHE was based on the ability to hydrolyze acetylcholine (ACh) in horse serum, which was distinct from the other esterases known at the time. Stedman et al. were the first to use conventional rate studies to measure ACh hydrolysis catalyzed by the enzyme. They also observed that horse serum BChE hydrolyzes butyrylcholine more rapidly than ACh, which is one of the criteria to distinguish BChE from AChE. In 1950, Sturge and Whittaker proposed the terms "aceto-cholinesterase" for AChE and "butyro-cholinesterase" for plasma CHE. These terms were later changed to acetylcholinesterase (AChE) and butyrylcholinesterase (BChE). BChE is restricted as the class of CHE present in plasma, which is distinguished from AChE present in nerve system or red blood cells.

Properties of hBChE

Ninety-five percent of hBChE is a water soluble globular tetrameric G-4 form, the subunits of which are connected by two disulfide bonds (29). The G-4 form of hBChE has four identical subunits. The molecular weight of each subunit is 340,000, and it contains 574 amino acids and 9 carbohydrate chains (about 23.9% of the subunit) (30). The remaining 5% of hBChE occurs as monomers and dimers. The concentration of BChE in human serum is 5 mg/l. Human serum only contains BChE, no AChE. However, human red blood cells contain AChE, but no BChE. The resulting concentration of BChE in whole blood is 36 nM taking into account that the packed red cells take up 40% of the volume of blood. BChE is a non-specific enzyme, which can hydrolyze a variety of esters, including butylthiocholine, butyrylcholine, propionylthiocholine, propionylcholine, acetylthiocholine, acetylcholine, heroin, and aspirin, among others. Another characteristic

of plasma BChE is its relative high stability. BChE can be stored at -70°C and have little effect on the activity after being frozen and thawed several times. Furthermore, plasma BChE can be stored for several years at -20°C without loss of activity (31). Therefore, outdated blood from blood banks is recommended for large studies, for example, BChE purification from serum.

BChE in Diagnosis of Pesticide Poisoning

Organophosphorous compounds (OPs) and carbamates (CBs) are extensively used as insecticides, fungicides and herbicides. The chemicals exert their toxic action by their ability to inhibit AChE, which plays an important role in the catalyzing the release and removal of acetylcholine at the neuromuscular junction. Diagnosis of poisoning by OPs and CBs is made on the basis of clinical symptoms and laboratory measurement of cholinesterase, including AChE and BChE, activity. However, serum BChE is the most sensitive enzyme for poisoning measurement. Plasma BChE activity decreases are separated into several inhibition levels. These levels are 20-50%, 80-90% and over 90%, which correspond to mild, moderate and severe poisoning, respectively. It has to be emphasized that the percentage decreases in enzyme activity are only guidelines and are not absolute indicators of the degree of poisoning. The severity of the symptoms can not be judged through the BChE activity decreases (32). As such, the assessment of clinical severity must be based on clinical symptoms, and the measurement of serum cholinesterase activity.

Protective Role of BChE

Although no physiological function has been assigned to BChE, it plays an important role in the protection against pesticides (33, 34). BChE reacts with a variety of anticholinesterase poisons stoichiometrically. Poisons hydrolyzed by BChE are unable to inhibit AChE, and in this way BChE guards against toxicity. The protective role of BChE is demonstrated by the finding that pesticide applicators can have reduced BChE activity with no clinical signs of poisoning. When the dose of pesticide is low so that only BChE activity but not AChE activity is reduced, there is no threat to health. For instance, if only BChE activity is reduced, even up to 70% decrease of a preexposure value, there is no

health threat (35). The protective role of BChE against pesticides can also be demonstrated by injecting purified BChE into the animals before they were treated with nerve agents. Pretreatment with BChE increased survival and alleviated post-exposure symptoms, which was proven by an *in vivo* animal study of mice and rats treated with the nerve agents. In further experiments (36), monkeys were injected with 503 nmols BChE, and then exposed to 2 times the LD₅₀ of soman. Results showed that BChE was far more effective than the conventional treatment with pralidoxime (2-PAM).

Inhibition of BChE by Pesticides

In 1973, Hart and O'Brien (37) proposed an original description of the cholinesterase (including AChE and BChE) inhibition process. The inhibition process includes two steps: equilibrium of the OP compound with the active site of CHE and a phosphorylation reaction by forming a covalent bond between the phosphorus of the OP compound and the oxygen of the hydroxyl group of serine at the active site. In general, CHE (EH) combines with pesticides (PX) resulting in an enzyme-pesticide complex (EHPX) that is converted to an inhibited enzyme (EP) and a leaving group (HX) (Figure 1-1-1). If the inhibited enzyme is caused by OPs, an aging reaction could happen by further removing an alkyl group from the covalently bound OP, leaving a very stable OP-enzyme derivative. BChE inhibited by OPs can be regenerated by some nucleophilic agents, such as pralidoxime (2-PAM), if the agent is used within a few hours of poisoning, before the OP-enzyme complex has had time to age. The esterase inhibited by CBs spontaneously reactivates by hydrolytic de-carbamylation, a process similar to that which happens with their natural substrates, such as acetylcholine (38, 39), but much slower.

Purification of Plasma Cholinesterase

Although BChE was discovered by Stedman et al. in 1932 (28), it was not sequenced until 1986 due to the difficulty of purification from plasma (40). Svensmark mentioned in 1965 that the molecular properties of BChE had not been studied extensively at that time mainly because of the lack of the pure enzyme (41).

Many efforts have been made to purify BChE and AChE from a few sources such as pig parotid glands (42), dog pancreas (43), and human liver (44). However, most efforts

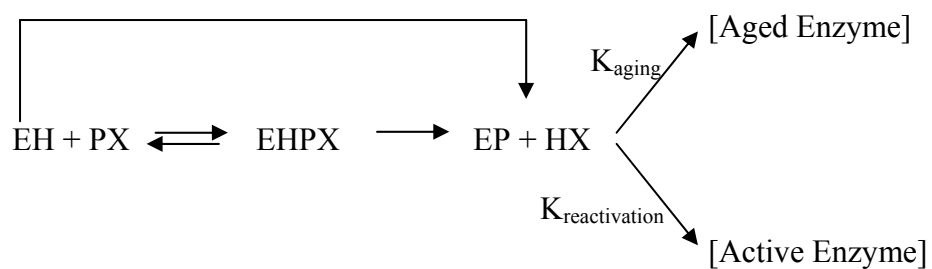


Figure 1-1-1. The scheme of CHE inhibition. Where EH is CHE (including AChE and BChE), PX is pesticide, EHPX is a reversible enzyme-pesticide complex and EP is the modified enzyme. Aged enzyme is the phosphorylated enzyme with the loss of the alkyl group from EP.

have been put on the purification of the BChE and AChE from horse and human plasma. The purification of BChE has proven to be difficult due to several factors: i) the large size and the complex structure of BChE make it difficult to purify, ii) the low concentration of BChE in plasma (about 3 to 5 mg/l) and the complex protein composition of plasma make the purification of plasma BChE more difficult. The following describes a history of the BChE purification development.

In the early history of BChE purification, the first step in most of the horse plasma BChE purification was 33% saturation with $(\text{NH}_4)_2\text{SO}_4$, giving a two-fold purification. Later, the key step in the most successful procedures for purifying horse serum CHE was the acidification of $(\text{NH}_4)_2\text{SO}_4$ serum fractions proposed by Strelitz, which gave a seven-fold purification (45). The Strelitz method was not widely used to purify hBChE from plasma because of the less stable property of hBChE than eBChE in solution at low pH value (46).

Another significant purification development was the introduction of DEAE cellulose column chromatography in the purification procedure by Connel and Shaw (47). BChE is bound to the DEAE cellulose at pH 4.2, while most of the serum proteins are washed off. The BChE is then eluted with 0.2 M NaCl resulting in a 45-fold purification and 53% yield.

The most significant improvement of the purification methods with the high efficiency and capacity is the use of affinity gels to supply the amount of pure enzyme needed for structural study. Affinity gels were originally made for the purification of AChE, particular for electric eel AChE. P-phenyl-trimethylammonium (PTA) gel was one of the first gels developed by Kalderon et al (48). However, PTA-gels were proven to be ineffective for purifying serum BChE. In 1972, a highly effective methylacridinium (MAC) affinity gels were introduced by Dudai et al (49). The potential of MAC gels for purifying serum BChE was reported by Blanchet et al (50). A 26 ml bed volume column of MAC gels was used to purify BChE from 20 ml horse serum, resulting in 2176-fold purification and 115% yield after a second passage. Although purification of BChE was improved using MAC, the wide usage of this affinity gel was hindered because of its difficult synthesis.

Finally, procainamide affinity gel was used to simplify the purification procedure into a two-step process introduced by Lockridge and La Du (51). Procainamide gel was relatively easy to synthesize compared with MAC gel. The synthesis procedure of the procainamide gel is briefly described as follows, the same procedure is also used in this dissertation. Sepharose 4B was activated with cyanogen-bromide and then coupled with 6-aminohexanoic acid to make CH-Sepharose 4B, which was further coupled to the procainamide through a carbodiimide reaction at room temperature for 24 h (52). Procainamide gel was effectively used in the first step of a large-scale purification procedure.

These affinity gels are far more effective than commonly used ion exchange gels, such as DEAE. The selectivity of these affinity gels is based on the interaction of the ligands with the active sites of BChE. The specificity of the affinity gels makes them widely applicable for the enzyme purification. Although the affinity gels are very effective, it is worth noting that they must still be supplemented by earlier techniques to obtain pure enzyme.

RESEARCH STATEMENT

This chapter provided a general background of BChE, including properties, physical function, pesticide inhibition mechanism, and the purification history of plasma BChE. Chapter 2 includes a method development for detection and quantification of BChE inhibition using MALDI-TOF-MS. Chapter 3 describes how to analyze a mixture of the phosphorylated peptides *in vitro* using LC/MS/MS. Chapter 4 focuses on the method development for BChE isolation from human serum. The specific character of the affinity column was evaluated. Finally, Chapter 5 presents the application of the developed method towards the human serum by combination affinity chromatography with MS.

CHAPTER TWO

IDENTIFICATION AND QUANTIFICATION OF INHIBITED BUTYRYLCHOLINESTERASE AFTER EXPOSURE TO ORGANOPHOSPHATES AND CARBAMATES USING MALDI-TOF-MS

INTRODUCTION

The potential for civilian exposure to cholinesterase inhibitors is greater today than anytime in history. In addition to exposure to cholinesterase inhibiting pesticides, today the threat of chemical warfare (CW) terrorism raises the stakes. Several recent events such as the 1988 slaughter of Kurds in Iraq (53) and the 1995 Tokyo Subway Attack (54) point to a need for accurate and sensitive methods to monitor exposure to CW agents and pesticides. Identification of the type of cholinesterase inhibitor (CW or pesticides) is critical for deciding an appropriate treatment. We developed a new method for detection, quantification, and categorization of cholinesterase inhibitors using two types of pesticides, a proteomics approach and MALDI-TOF-MS. Our technique is based on the analysis of the inhibited active-site peptide produced from trypsin digestion of BChE. Our *in vitro* studies indicate that the type of pesticides can be determined by the mass difference between the inhibited and intact active-site peptide. In this chapter, we evaluated all phosphyl and carbamyl adducts on the active site serine of BChE from commercial organophosphates (OPs) and carbamates (CBs). Although we did not investigate CW agents in this study, information about their presence can be deduced from mass differences using the same approach.

BChE present in serum is of toxicological and pharmacological importance. Although no physiological function has been assigned to BChE, it plays a key role in ester detoxification. Pesticides such as OPs and CBs inhibit AChE, which plays an important role in removing the neurotransmitter acetylcholine at the synapses. Because BChE is highly reactive with pesticides, it sacrificially protects AChE against pesticides. Therefore, serum BChE activity measurement is the most sensitive way to detect pesticide exposure.

To determine pesticide exposure, U.S. Environmental Protection Agency (USEPA)

scientists proposed a blood esterase monitoring program for pesticide exposure (55) based on the measurement of red blood cell AChE and plasma BChE activity. The most conventional method for detection of pesticide exposure is based on the measurement of BChE activity by the Ellman method (56). However, the Ellman method has several drawbacks. First, the percentage decrease in BChE activity is only a guideline and it is not accurate to determine the degree of poisoning (32). Second, the source of cholinesterase inhibition can not be determined by detection of the decline of BChE activity using the Ellman method. This is because the decline of the enzyme activity can be caused from a number of ailments such as liver disease, anemia, acute infections, cardiac failure, and renal disease. Furthermore, since BChE is a nonspecific enzyme, many chemicals can influence activity measurement such as aspirin, which will influence the accuracy of activity measurement.

In addition to the Ellman method, Polhuijs et al. (57) developed a technique to monitor exposure to pesticides based on the analysis of pesticide inhibited BChE. In brief, the method is based on the reactivation of the inhibited enzyme with fluoride ions producing a phosphofluoridate. Identification and quantification of phosphofluoridate by GC/MS can be related to the BChE inhibition. This Polhuijs method requires a sophisticated chemical technique, and it is time consuming. The major limitation of the Polhuijs method from *in vivo* analysis is that the aged enzyme cannot be analyzed, because the aged enzyme blocks the reactivation reaction with fluoride ions. Doorn et al. (58, 59) used MALDI-TOF-MS to detect the inhibited peptide from a tryptic digest of AChE in order to study the mechanism of AChE inhibition with OPs. In addition, Fidder et al. (60) developed a procedure for detection of nerve agent exposure using LC/MS. This analysis is based on the detection of phosphorylated nonapeptides obtained after pepsin digestion of hBChE. Since pepsin is a nonspecific protease, reproducible pepsin digestion was difficult to achieve, thus limiting the universal application of this approach.

We developed a new method for detection and quantification of the inhibited BChE after *in vitro* pesticide exposure using MALDI-TOF-MS. In this initial study, eBChE was selected because this enzyme is commercially available. Three OPs, methyl paraoxon, ethyl paraoxon and EPN oxon, represented all possible types of phosphoryl group found in commercial OPs. Carbaryl was selected to represent the N-methyl carbamates in common

commerce. Oxons were used in this *in vitro* study to represent OPs. OPs require Phase I metabolic biotransformation to become active inhibitors. By selecting oxons, no further metabolism was required to facilitate the *in vitro* study. OPs and CB inhibit BChE by forming a covalent bond with the active site serine by attaching a phosphoryl or carbamyl group resulting in inhibited enzyme. The modified peptide was generated by trypsin digestion of this inhibited eBChE. Using our new improved method, the category of pesticides was identified. The degree of poisoning was also determined based on the intensity of the modified peak and that of the intact active site peak from mass spectrometric analysis. Furthermore, these results demonstrate that our newly developed method is more sensitive than the Ellman method.

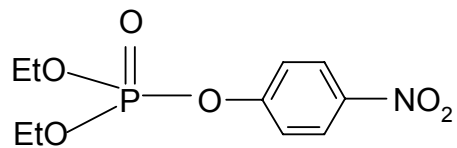
EXPERIMENTAL

Chemicals

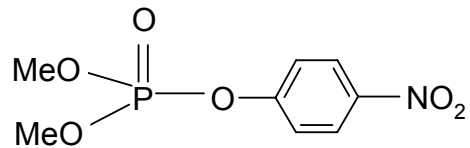
All the OPs (EPN, methyl paraoxon, and ethyl paraoxon) and carbaryl (Figure 1-2-1) were purchased from Chem Service, Inc (West Chester, PA). Chemical purity of these inhibitors were >99% as assessed by the supplier. eBChE (610 units/mg solid, 50% protein of solid), butyrylthiocholine iodide (BTCh), 5, 5'-dithiobis-(2-nitrobenzoic acid) (DTNB) were purchased from Sigma Chemical Co. (ST. Louis, MO). Sequencing grade modified porcine trypsin was purchased from Promega Corporation (Madison, WI). EPN oxon (Figure 1-2-1) was oxidized from EPN (61). In brief, a 2 mM EPN solution in acetonitrile was mixed with the same volume of 40 mM bromine solution in acetonitrile. The resulting solution was mixed for one minute. After the reaction, the solution was dried by Speed Vacuum concentrator to remove the excess bromine and the residue dissolved in 500 μ l methanol prior to analysis. The chemical purity of EPN oxon was >99% as assessed by GC/MS.

eBChE Inhibition

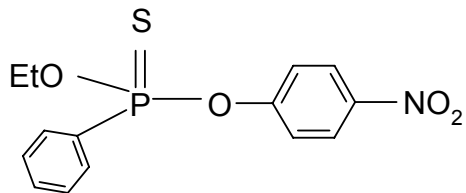
eBChE (265 units) was dissolved in 400 μ l 50 mM ammonium bicarbonate buffer, and incubated with OPs (dissolved in methanol) for 1 h, and with carbaryl for



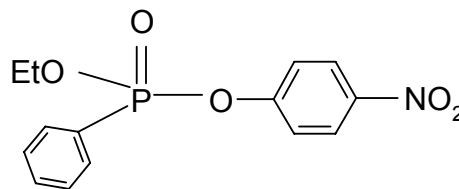
Ethyl paraoxon



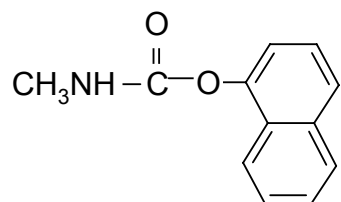
Methyl paraoxon



EPN



EPN oxon



Carbaryl

Figure 1-2-1. Structure of pesticides.

30 min at 37°C. The final concentration of methanol was less than 0.05% (v/v) and did not significantly affect enzyme activity.

eBChE Activity

A modified Ellman assay (56) was used to measure the eBChE activity. BTCh (4 μ l of 0.25 M) and DTNB (16 μ l of 0.02 M) were added to 1 ml phosphate buffer (50 mM, pH=8), and the resulting solution was used as a baseline for the later measurements. Then, an aliquot of inhibited eBChE or control was added in the same cuvet. The absorbance of the solution was measured at 412 nm for the first 10 min of the reaction. Plotting absorbance vs time, a straight line was obtained ($R=0.99$). The slope of the line was calculated from three parallel measurements, and the mean value of the slopes from triplicate analysis was used in all calculations. Raw data were converted to the relative activity (percent) of the control.

Trypsin Digestion

Acetonitrile was added as a mild protein denaturant (62) to each sample in order to increase trypsin activity, at a final concentration of 40% (v/v). The digestion was performed in a 60 mM NH_4HCO_3 buffer with a ratio of 20:1 eBChE to trypsin and incubated at 40 °C overnight. Formic acid was used to terminate the reaction.

MALDI-TOF-MS Analysis

The matrix solution was 10 mg/ml α -cyano-4-hydroxycinnamic acid in 50% (v/v) acetonitrile / 50% (v/v) aqueous 0.1% (v/v) trifluoroacetic acid. Sample preparation for the MALDI experiment involved addition of 1 μ l of 1 mM diammonium citrate solution to 1 μ l analyte and 1 μ l matrix solutions. The mixture (1 μ l) was then applied to the MALDI Massive target (Bruker, Billerica, MA). Samples were allowed to air dry and crystallize before the target was loaded into the mass spectrometer. An Autoflex MALDI-TOF (Bruker, Billerica, MA) mass spectrometer was used for all analysis. Standard instrument parameters for peptide analysis were used. All spectra resulted from an average of 300 laser shots. A standard peptide mixture consisting of angiotensin II and vasopressin was used to provide an external mass calibration. The trypsin autolysis product m/z 842.51 was

used for an internal mass calibration. The identity of an OP or CB adduct was confirmed by analyzing the post source decay (PSD) MALDI-TOF mass spectra of modified active site peptides. The time ion selector was set for the modified peptide and the ion selector window was ± 1 % of the m/z value of the precursor ions. Mirror voltage acceleration voltage of 20 kV, 16 kV, 13.11 kV and 10.61 kV were used to obtain the PSD spectrum.

Determination of IC₅₀ and IC₁₀₀

The relative activity (the percentage activity of eBChE inhibited by the pesticides relative to the control), and the intensity ratios (the intensity of the modified or intact active site peptide to the native reference peptide at m/z 2222.5) were reported based on the triplicate analysis. Normalized intensity ratios (NIRs) were obtained through dividing the intensity ratios of intact peptide or modified peptide by the total intensity of all peptide signals that contains the active site serine, and these NIRs were further used for data analysis. All data were analyzed using Microsoft Office Excel 2003 (Redmond, WA).

Determination of IC₅₀s

Two linear regression lines were obtained by plotting the NIR of the intact peptide vs concentration of OPs and the NIR of the modified peptide vs concentration of OPs. IC₅₀ from MALDI method was calculated from the intercept of these two regression lines. Determination of IC₅₀ for methyl paraoxon is different from the other OPs, because the aged peptide (further removal of the alky group from phosphate group) contribution required an additional regression line. The IC₅₀ for methyl paraoxon was determined when the NIR of the intact active site peptide equals to the sum of NIR of the inhibited and the aged peptide.

IC₅₀s were also obtained for the Ellman method by plotting relative activity vs concentration of OP. IC₅₀ values were determined from the regression line equations assuming a relative activity of 50 %.

IC₅₀s for carbaryl from MALDI and the Ellman method were calculated using the same approach as OPs. A linear relationship of NIR or relative activity with logarithmic concentration of carbaryl (plot not shown) was used for the calculation.

Determination of IC₁₀₀s

IC₁₀₀s for OPs from MALDI and Ellman method were determined by extrapolating lines of NIR of intact peptide and relative activity to the x-axis. IC₁₀₀s were determined from this x-intercept. IC₁₀₀ for carbaryl was determined using the same approach and linear regression lines of NIR or relative activity with logarithmic concentration of carbaryl.

RESULTS

MALDI-TOF-MS Analysis

Mass spectra were collected for the control and pesticide-treated samples. Figure 1-2-2 shows MALDI-TOF-MS spectra for the control and eBChE treated with OPs and carbaryl. The modified peptides were determined by comparing the mass spectra before and after treatment. For example, the modified peptide by ethyl paraoxon at an average mass 2336.1 was determined by comparing the mass spectra before (Figure 1-2-2 A) and after treatment (Figure 1-2-2 B). This modified active site peptide peak appeared in the mass spectrum for the pesticide-treated sample but not for the control sample. However, peaks with an average mass corresponding to the intact active site peptide (average mass 2200.1) appeared in both control and treated sample with 1 μ M ethyl paraoxon. A peak at m/z 2222.1 was also observed in both control and treated sample, which was used as native reference peptide in this study.

The same method was also performed to determine modified peptides from methyl paraoxon, EPN oxon and carbaryl. Peaks with average masses corresponding to the modified and intact active peptides were observed in mass spectra of tryptic digests of OP and CB inhibited eBChE (Figure 1-2-2). Table 1-2-1 summarizes the observed MH⁺ peaks at average mass corresponding to the intact and modified active site peptide of eBChE treated with 1 μ M of individual pesticide. MH⁺ (Table 1-2-1) were the average masses of the modified or the intact peptide containing the catalytic serine by the tryptic digestion.

Modified groups were determined based on the mass differences (Table 1-2-1) between the modified peptide and the intact active site peptide. For example, the mass difference (Table 1-2-1) between the modified peptide at m/z 2336.5 and the intact active peptide at m/z 2200.5 was 136 Da for ethyl paraoxon. This mass difference takes into

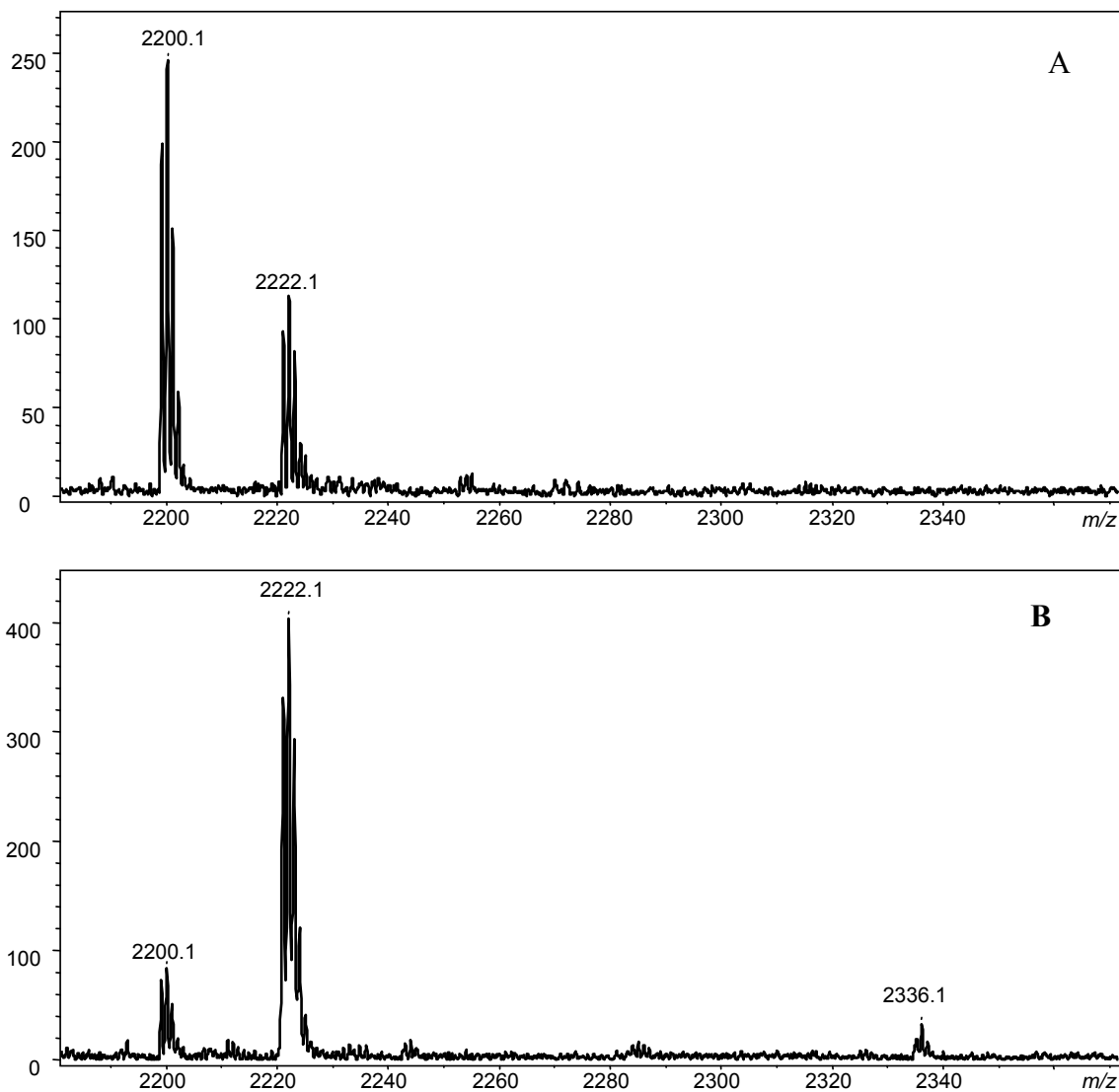


Figure 1-2-2. MALDI-TOF-MS spectra of the tryptic digest of eBChE from (A) control and (B) treated sample by ethyl paraoxon. Peaks with average masses at m/z 2200.1 demonstrate the presence of unmodified active site peptide. Peak at m/z 2336.1 (B) corresponds to the modified active site peptide with O,O-diethyl phosphorylated group.

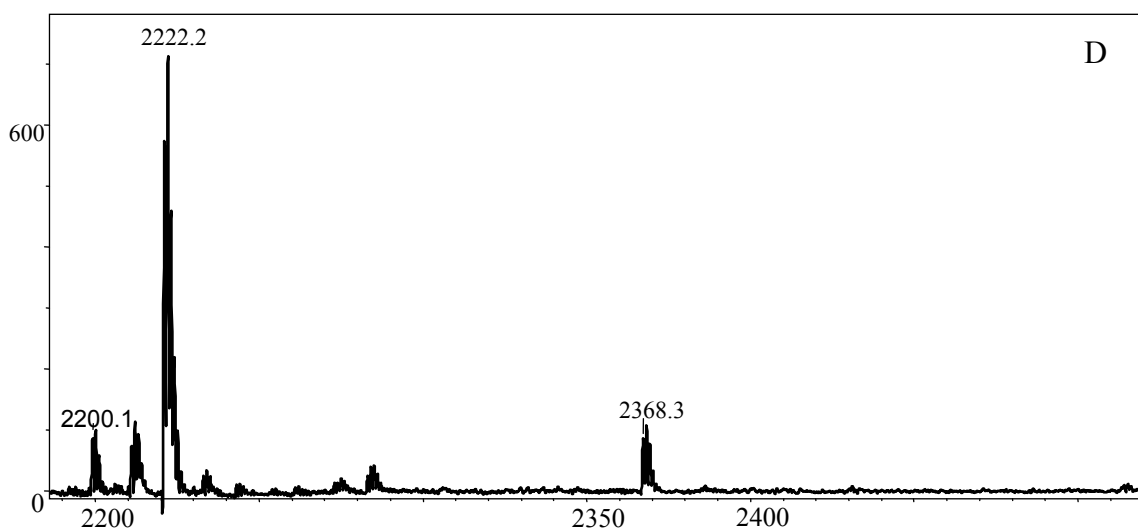
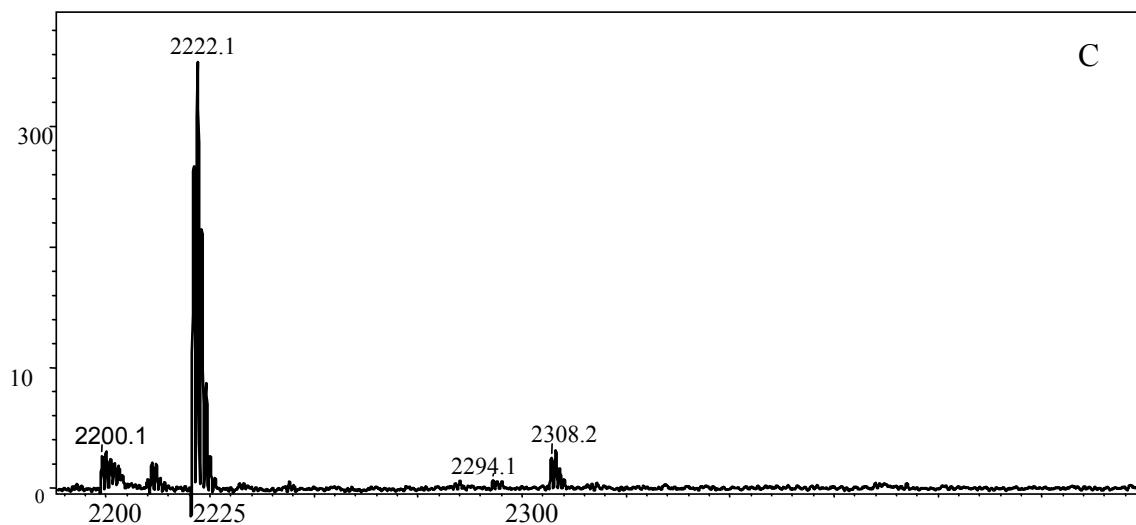


Figure 1-2-2. MALDI-TOF-MS spectra of the tryptic digest of methyl paraoxon (C) and EPN oxon (D) treated eBChE, respectively. Peaks at m/z 2294.1 and 2308.2 (C) represent the modified peptide with O-methyl phosphorylated group, and O,O-dimethyl phosphate respectively. Peak at m/z 2368.3 (D) is the modified peptide with O-ethyl phenyl phosphate.

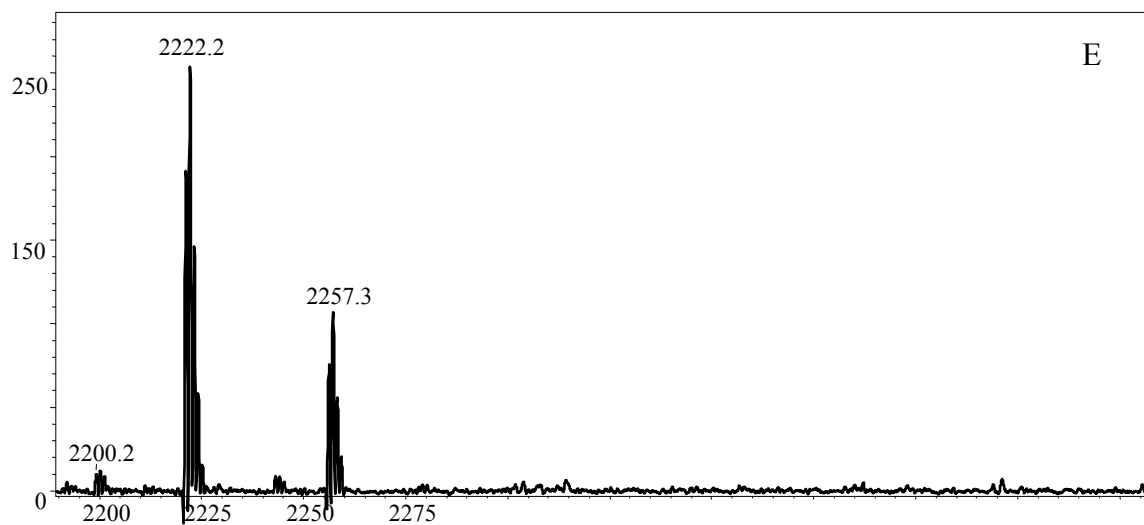


Figure 1-2-2. MALDI-TOF-MS spectra of the tryptic digest of eBChE (E) treated sample by carbaryl. Peak at m/z 2257.3 (E) is the modified peptide with carbamylate group.

Table 1-2-1. Masses of observed MH^+ (average mass)^b for the intact and modified active site peptide of eBChE treated with 1 μ M inhibitor

Pesticide	Intact (<i>m/z</i>)	Inhibited (<i>m/z</i>)	Δm^a (Da)	Modified with group	aged	Δm^a (Da)	Modified with group
Methyl paraoxon	2200.5	2308.5	108	$\begin{array}{l} \text{CH}_3\text{O} \backslash \\ \text{CH}_3\text{O} \text{---} \text{P}=\text{O} \end{array}$	2293.5	93	$\begin{array}{l} \text{CH}_3\text{O} \backslash \\ \text{---O---} \text{P}=\text{O} \end{array}$
Ethyl paraoxon	2200.5	2336.5	136	$\begin{array}{l} \text{CH}_3\text{CH}_2\text{O} \backslash \\ \text{CH}_3\text{CH}_2\text{O} \text{---} \text{P}=\text{O} \end{array}$	-----	----	-----
EPN oxon	2200.5	2368.5	168	$\begin{array}{l} \text{CH}_3\text{CH}_2\text{O} \backslash \\ \text{C}_6\text{H}_5 \text{---} \text{P}=\text{O} \end{array}$	-----	----	-----
Carbaryl	2200.5	2257.5	57	$\text{O}=\text{C}-\text{NHCH}_3$	-----	----	-----

^a Difference in mass between the modified and the intact active site peak. All these mass differences are taking account of the proton loss on the catalytic serine during the phosphorylation reaction.

^b The average mass of the modified or the intact peptide containing the catalytic serine by the tryptic digestion.

account the proton loss on the catalytic serine during the phosphorylation reaction. Based on this mass difference, the modified group was deduced as O,O-diethyl phosphate. Using the same approach, two modified groups were determined for methyl paraoxon as O-methyl phosphate and O,O-dimethyl phosphate, which correspond to the modified peptides at m/z 2293.5 and 2308.5, respectively. Similarly, the modified group for EPN oxon was O-ethyl phenyl phosphate. The corresponding modified peptide was observed at m/z 2368.5. The modified group for carbaryl was the carbamate group that was observed at m/z 2257.5.

Post Source Decay (PSD) Analysis

To further confirm the phosphorylated and carbamylated peptide, PSD analysis in MALDI-TOF-MS was used. All of PSD analyses of modified peptide ions are shown in Figure 1-2-3, which correspond to the modified active site peptides with phosphate or carbamate generated from tryptic digests of eBChE treated with OPs or CB. The timed ion selector of MALDI was set for a series of precursors with average masses. These precursors were at m/z 2293.5 and 2308 (aged and inhibited peptide by methyl paraoxon) (Figure 1-2-3 A and B), at m/z 2336 (inhibited peptide by ethyl paraoxon) (Figure 1-2-3 C), at m/z 2368 (inhibited peptide by EPN oxon) (Figure 1-2-3 D), and at m/z 2257 (inhibited peptide by carbaryl) (Figure 1-2-3 E). In PSD analysis, a common fragment ion at m/z 2182.1 was observed for all of the precursor ions (Figure 1-2-3). The fragment ion at 2182.1 was formed by elimination on serine to form the homoalanine residue. However, precursor ion at m/z 2293.5 had an additional fragment ion at m/z 2199.5 (Figure 1-2-3 A), which was formed by removal of the phosphate group from the catalytic serine.

Lost neutral fragments were deduced from the mass differences between the precursor ions and fragment ions (Table 1-2-2). The fragment ions at m/z 2199 and m/z 2182.1 were generated by the loss of CH_3OPO_2 (94 Da) and $\text{CH}_3\text{OP}(\text{O})(\text{OH})_2$ (112 Da), respectively, from the precursor ion at m/z 2294 corresponding to O-methyl phosphorylated peptide. Similarly, the fragment ions at m/z 2182.1 of precursor ions at m/z 2308, 2336, 2368, and 2257, were generated by the neutral loss of $(\text{CH}_3\text{O})_2\text{P}(\text{O})\text{OH}$ (126 Da), $(\text{CH}_3\text{CH}_2\text{O})_2\text{P}(\text{O})\text{OH}$ (154 Da), $(\text{CH}_3\text{CH}_2\text{O})\text{P}(\text{O})(\text{OH})(\text{C}_6\text{H}_5)$ (186 Da) and $\text{CH}_3\text{NHC}(\text{O})\text{OH}$ (75 Da) from their precursor ions, respectively.

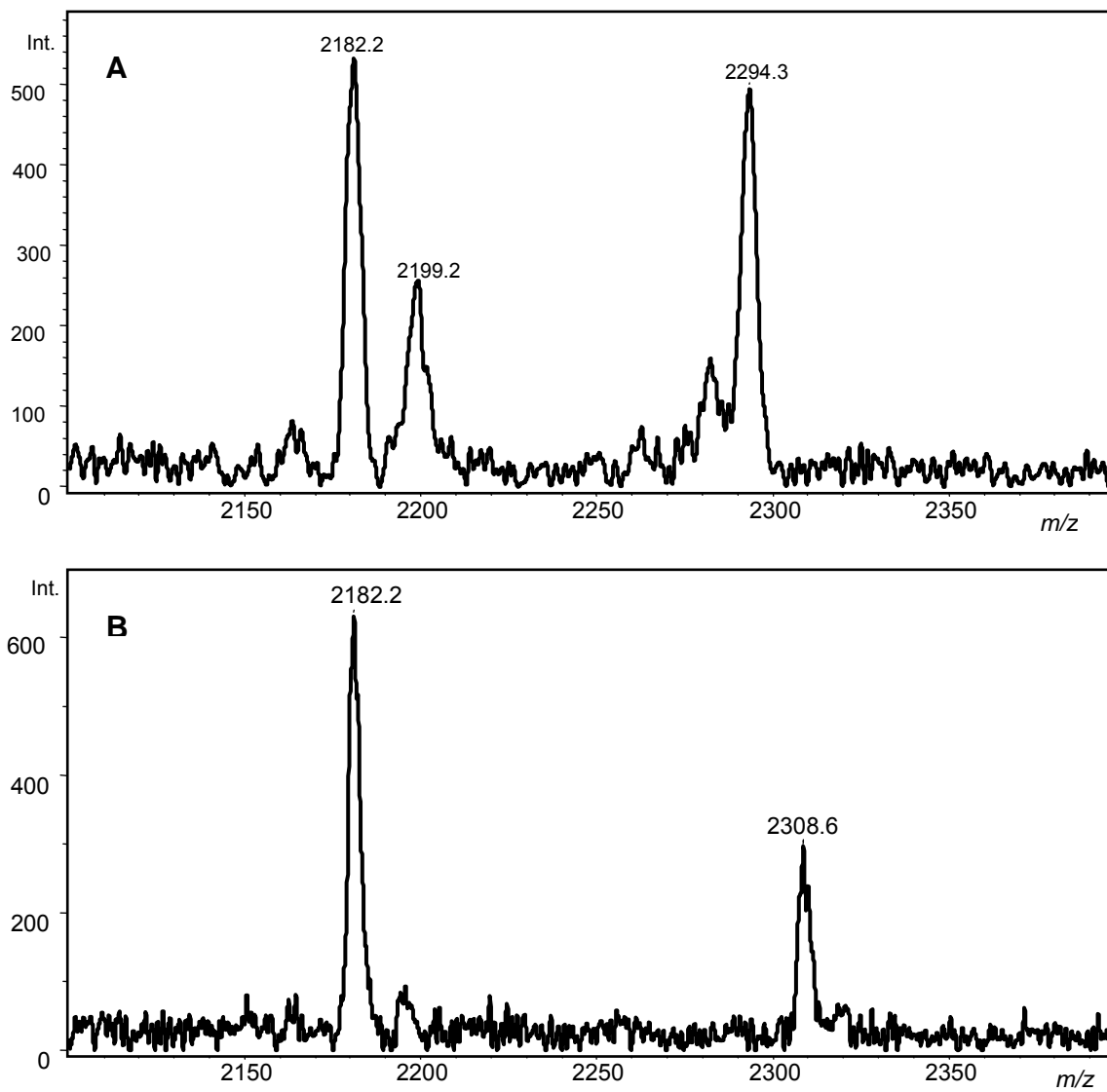


Figure 1-2-3. PSD analysis of precursor ion with average mass at m/z 2294.3 represents the aged peptide with O-methyl phosphate by methyl paraoxon (A), at m/z 2308.6 is inhibited peptide with O,O-dimethyl phosphate group (B).

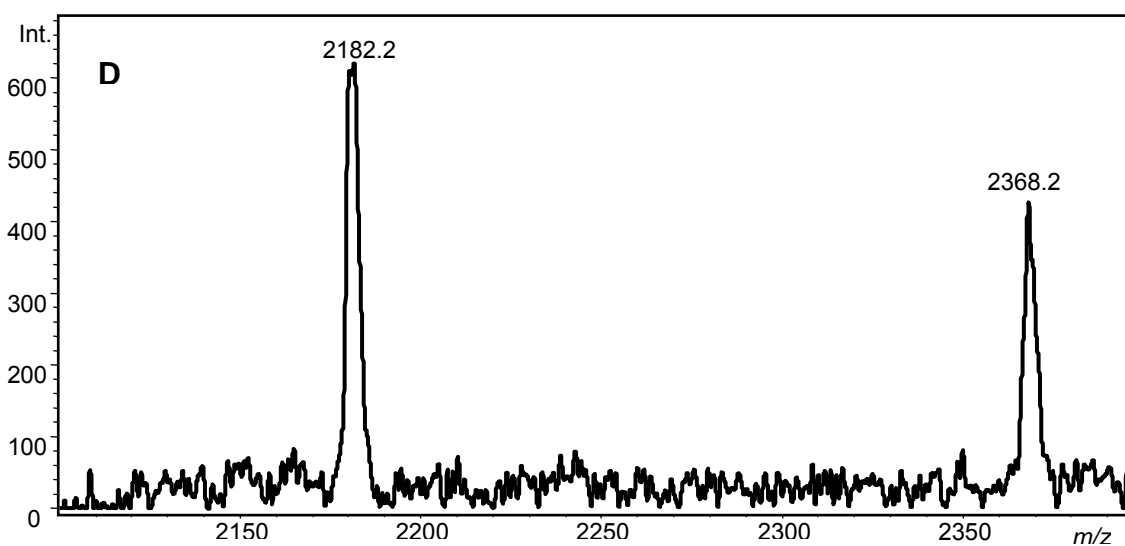
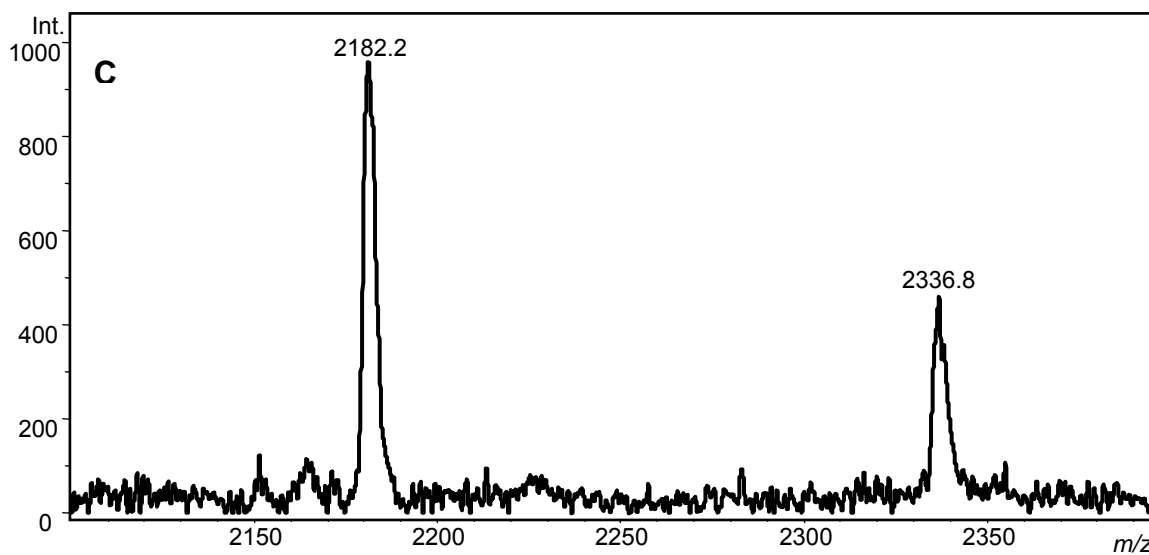


Figure 1-2-3. PSD analysis of precursor ion with average mass at m/z 2336.8 corresponds to the modified active site peptide with O,O-diethyl phosphorylated group generated from the tryptic digest of eBChE treated with ethyl paraoxon (C), peptide at m/z 2368.3 is with O-ethyl phenyl phosphate from EPN oxon (D).

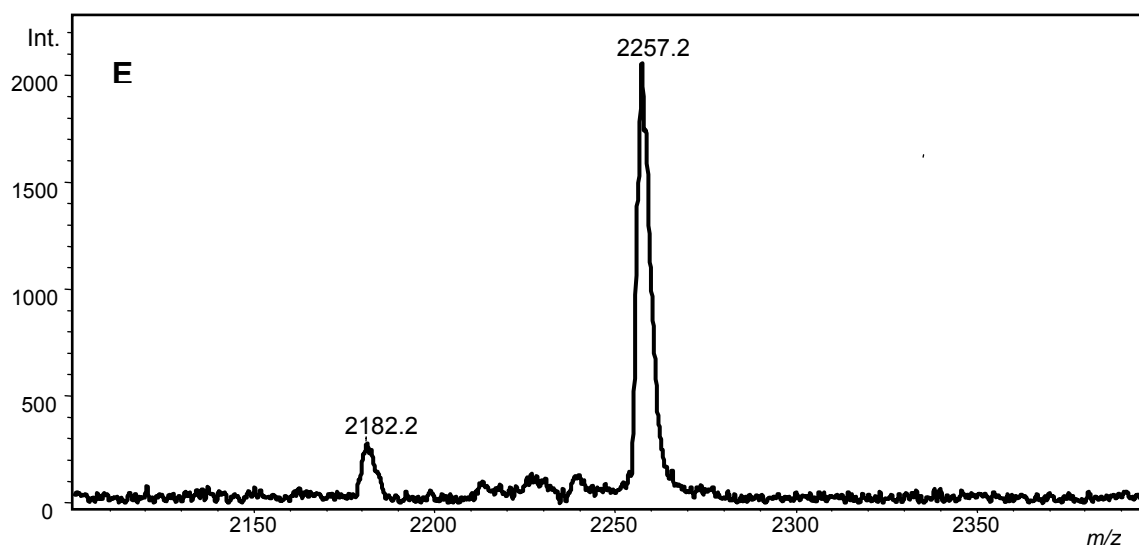


Figure 1-2-3. PSD analysis of precursor ion with average mass at m/z 2257.2 corresponds to the modified active site peptide with carbamylated group (E).

Table 1-2-2. Masses of observed MH^+ (average mass)^a for the precursor ions and fragment ions from PSD analysis.

Pesticide	Precursor	Fragment		Loss of the Adduct	Fragment		Loss of the Adduct
		Ion 1	Δm		Ion 2	Δm	
Methyl paraoxon	2293.5	2182.1	112	$\begin{array}{c} \text{CH}_3\text{O} \diagdown \\ \text{HO} \diagup \text{P}=\text{O} \\ \text{HO} \end{array}$	2199.2	94	$\begin{array}{c} \text{CH}_3\text{O} \diagdown \\ \text{O} \diagup \text{P}=\text{O} \end{array}$
	2308.5	2182.1	126	$\begin{array}{c} \text{CH}_3\text{O} \diagdown \\ \text{CH}_3\text{O} \diagup \text{P}=\text{O} \\ \text{HO} \end{array}$	----- ^b	--- ^b	----- ^b
Ethyl paraoxon	2336.5	2182.1	154	$\begin{array}{c} \text{CH}_3\text{CH}_2\text{O} \diagdown \\ \text{CH}_3\text{CH}_2\text{O} \diagup \text{P}=\text{O} \\ \text{HO} \end{array}$	----- ^b	--- ^b	----- ^b
EPN oxon	2368.5	2182.1	186	$\begin{array}{c} \text{CH}_3\text{CH}_2\text{O} \diagdown \\ \text{C}_6\text{H}_5 \diagup \text{P}=\text{O} \\ \text{HO} \end{array}$	----- ^b	--- ^b	----- ^b
Carbaryl	2257.1	2182.1	75	$\begin{array}{c} \text{NHCH}_3 \\ \text{O}=\text{C} \diagdown \\ \text{OH} \end{array}$	----- ^b	--- ^b	----- ^b

^a The average mass of the modified or the intact peptide containing the catalytic serine obtained from the tryptic digestion.

^b No fragment 2 was found.

IC₅₀ and IC₁₀₀ Values

The relative activities and the normalized intensity ratios (NIR) were reported (Table 1-2-3, 1-2-4, 1-2-5, and 1-2-6) based on the triplicate parallel analysis after the inhibition of eBChE by pesticides. Graphs of NIR vs concentration of pesticides were plotted according to these reported data. Plots of NIR vs concentration of OPs and carbaryl are shown in Figure 1-2-4. A linear relationship between the NIR of the modified peptide and intact peptide with the concentration of [OP] was observed for all three OPs. For the Ellman method, linear relationships between the relative activity and the concentration of OP were observed for all three OPs (Figure 1-2-5). While for CB, both methods produced a non-linear relationship between the NIR or relative activity and the concentration of carbaryl (Figure 1-2-4 D and Figure 1-2-5 B). To obtain IC₅₀ (the concentration required for producing 50% BChE inhibition) and IC₁₀₀ (the concentration required for producing 100% BChE inhibition) data, the NIR or relative activity was plotted against the logarithm of concentration of carbaryl (plot not shown).

IC₅₀s and IC₁₀₀s of EPN oxon for both methods were determined from Figure 1-2-4 and Figure 1-2-5 (see Experimental section). The same approach was also applied to determine IC₅₀s and IC₁₀₀s of the other pesticides. IC₅₀s from this study were 1.30 ± 0.08 , 0.90 ± 0.05 , 1.19 ± 0.01 , 3.57 ± 0.03 μM , and corresponding IC₁₀₀s were 2.72 ± 0.09 , 1.75 ± 0.06 , 2.48 ± 0.01 , and 17.3 ± 0.03 μM for methyl paraoxon, ethyl paraoxon, EPN oxon and carbaryl, respectively. To compare results from our new method, IC₅₀s and IC₁₀₀s from the Ellman method were also obtained. The IC₅₀s from the Ellman method were 1.10 ± 0.97 , 0.79 ± 0.69 , 0.97 ± 0.27 , 4.9 ± 0.1 μM , and IC₁₀₀s were 2.41 ± 0.80 , 1.54 ± 0.86 , 2.20 ± 0.31 , and 23.6 ± 0.11 μM for methyl paraoxon, ethyl paraoxon, EPN oxon, and carbaryl, respectively. IC₅₀ and IC₁₀₀ for carbaryl from both methods were determined from the linear regression between NIR or relative activity and logarithm of concentration of carbaryl (plots not shown).

The IC₅₀ value of carbaryl was larger than those of OPs, which means eBChE is the least sensitive to carbaryl compared to OPs. These data were consistent with the facts provided by the supplier that carbaryl is a significant less potent inhibitor of eBChE (LD₅₀ of carbaryl 500 mg/kg; methyl paraoxon 3 mg/kg; and ethyl paraoxon 2 mg/kg).

Table 1-2-3. Normalized intensity ratios (NIRs) of intact peptide, modified peptide, and relative activities of eBChE treated with methyl paraoxon at different concentrations

Concentration (μM)	NIRs of Intact Peptide (m/z 2200.1)	NIRs of Aged Peptide (m/z 2294.1)	NIRs of Inhibited Peptide (m/z 2308.1)	Relative Activity (%)
0.00	1.00 ± 0	N/A	N/A	100 ± 0
0.10	0.97 ± 0.02	0 ± 0.01	0.03 ± 0.01	96.6 ± 2.5
0.20	0.87 ± 0.03	0.04 ± 0.01	0.08 ± 0.01	95.3 ± 3.1
0.50	0.73 ± 0.05	0.10 ± 0.01	0.16 ± 0.02	54.2 ± 7.5
1.00	0.52 ± 0.08	0.11 ± 0.03	0.37 ± 0.02	49.6 ± 1.0
1.80	0.38 ± 0.07	0.13 ± 0.01	0.48 ± 0.05	23.0 ± 1.5

Table 1-2-4. Normalized intensity ratios (NIRs) of intact peptide, modified peptide, and relative activities of eBChE treated with ethyl paraoxon at different concentrations

Concentration (μM)	NIRs of Intact Peptide (m/z 2200.2)	NIRs of Inhibited Peptide (m/z 2336.1)	Relative Activity (%)
0	1.00 ± 0	N/A	100 ± 0
0.1	0.97 ± 0.01	0.03 ± 0.01	100 ± 3.5
0.2	0.78 ± 0.05	0.22 ± 0.05	82.3 ± 2.5
0.5	0.83 ± 0.06	0.17 ± 0.02	71.6 ± 3.0
0.8	0.67 ± 0.05	0.33 ± 0.05	53.7 ± 1.5
1	0.56 ± 0	0.44 ± 0.02	35.9 ± 2.5
1.5	N/A	1.00 ± 0.05	0.65 ± 0.5

Table 1-2-5. Normalized intensity ratios (NIRs) of intact peptide, modified peptide, and relative activities of eBChE treated with EPN oxon at different concentrations

Concentration (μM)	NIRs of Intact Peptide (m/z 2200.1)	NIRs of Inhibited Peptide (m/z 2368.1)	Relative Activity (%)
0	1.00 ± 0	N/A	100 ± 0
0.2	0.93 ± 0.02	0.07 ± 0.01	100 ± 3.5
0.5	0.76 ± 0.01	0.24 ± 0.02	71.2 ± 2.5
0.7	0.64 ± 0.03	0.36 ± 0.03	50.3 ± 2.0
1	0.49 ± 0.05	0.51 ± 0.04	32.5 ± 5.0
2	0.23 ± 0.01	0.77 ± 0.02	1.76 ± 1.5
2.5	N/A	1.00 ± 0.02	0.649 ± 0.5

Table 1-2-6. Normalized intensity ratios of intact peptide, modified peptide, and relative activities of eBChE treated with carbaryl at different concentrations

Concentration (μM)	NIRs of Intact Peptide (m/z 2200.1)	NIRs of Inhibited Peptide (m/z 2257.1)	Relative Activity (%)
1	0.84 ± 0.02	0.16 ± 0.02	95 ± 1.5
1.5	0.75 ± 0.03	0.25 ± 0.03	90 ± 1.0
2.5	0.68 ± 0.05	0.32 ± 0	81 ± 1.5
3	0.58 ± 0.06	0.42 ± 0.04	73 ± 2.0
4	0.50 ± 0.05	0.50 ± 0.03	50 ± 3.2
5	0.42 ± 0.06	0.58 ± 0.05	40 ± 4.0
8	0.23 ± 0.03	0.77 ± 0.02	33 ± 1.0
10	0.13 ± 0.01	0.87 ± 0.05	27 ± 1.2
15	0.03 ± 0.01	0.97 ± 0.03	18 ± 1.4

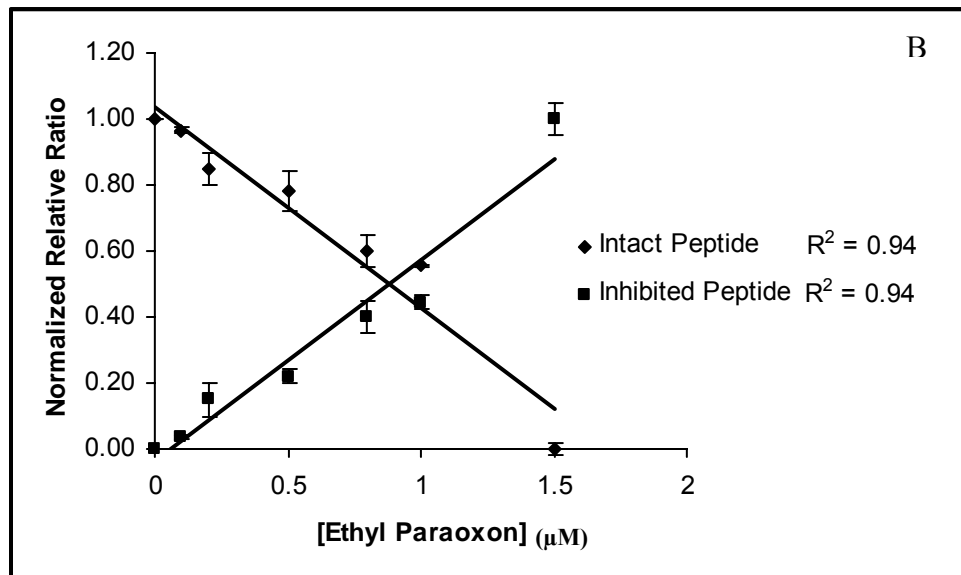
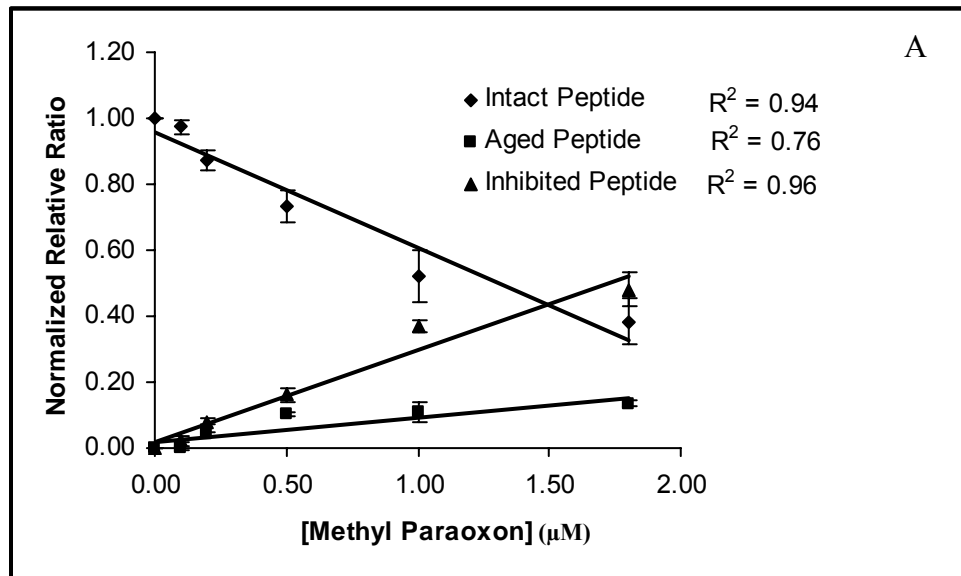


Figure 1-2-4. Plots of the normalized intensity ratio to the [methyl paraoxon] (A), [ethyl paraoxon] (B).

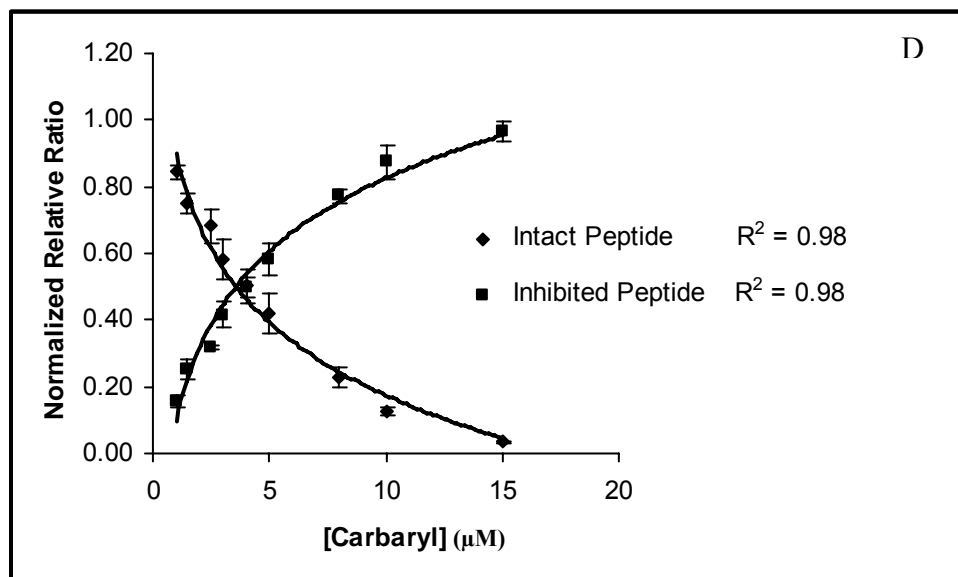
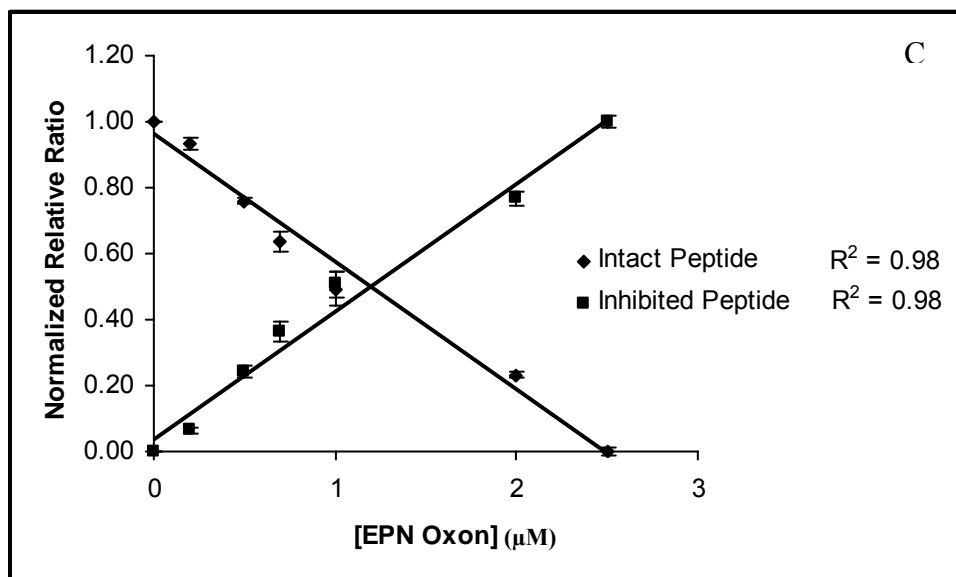


Figure 1-2-4. Plots of the normalized intensity ratio to [EPN oxon] (C), and [carbaryl] (D). The intensity ratio is the intensity of the modified or the intact active site peptide relative to that of the native reference peptide (average $m/z=2222.5$). The intensity ratios of all peptides containing catalytic serine were added to obtain a sum value. The normalized intensity ratios (NIRs) were obtained by dividing the intensity ratios of intact peptide and modified peptide with the sum value. The IC_{100S} were determined from the points by extrapolation of linear-regression to x-axis. Results are expressed as mean \pm SD ($n=3$).

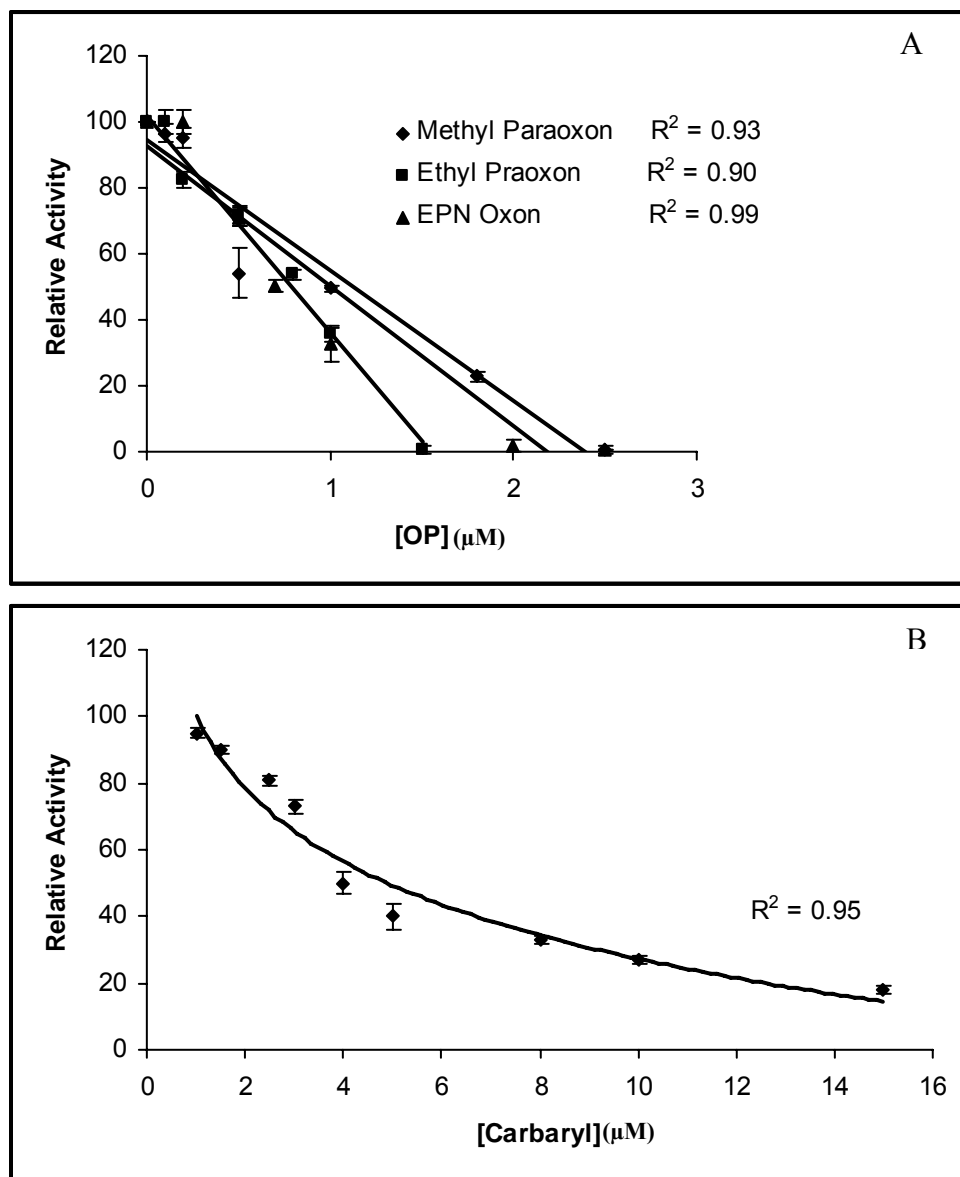


Figure 1-2-5. Plots of relative activity vs [OPs] (A) and [carbaryl] (B). Results are expressed as mean \pm SD (n=3).

DISCUSSION

The goal of this work was to develop an improved method for the detection of OP and CB exposure using a proteomic approaches and MALDI-TOF-MS. The advantage of this approach is that both the origin and the extent of the exposure to pesticide can be determined. This method is based on the analysis of the inhibited BChE, particularly based on the detection of active site peptide of BChE from tryptic digests. The amino acid sequence of the tryptic peptide containing active site serine from eBChE is SVTLFGESAGAASVSLHLLSPR (calculated MH^+ at m/z 2200.5), where the catalytic serine is underlined.

eBChE was separately incubated with each of the four pesticides studied in this chapter. The resulting inhibited eBChE was digested with trypsin and peptide containing active site serine was identified by MALDI-TOF-MS. Modified peptides were identified by comparing the MALDI mass spectra before and after treatment, and further confirmed by PSD analysis. During the modified peptide identification processes, we observed that the aged peptide was detected only from methyl paraoxon treated eBChE (Table 1-2-1). Usually, the rate of an aging reaction of a cholinesterase (ChE) inhibitor has an inverse relationship with the rate of spontaneous reactivation (63). Since the esterase inhibited by CBs undergoes fast reactivation by hydrolytic decarbamylation compared with OPs, it is understandable that no aged peptide was detected for carbaryl. In addition to this, the aging reaction also depends on the nature of the substituents on the phosphorus atom attached to the active site residue of the enzyme. Mason *et al* (64) reported that the order of the aging reaction rate for the alkyl phosphate substituents is dimethoxy > methoxy-phenyl = diethoxy, which is consistent with our observation. O'Brien also reported that the rate of aging of dialkylphosphorylated AChE is dimethoxy > diisoproxy > diethoxy (65). Our findings that aged peptide was detected only for methyl paraoxon agree with the previous observations (64) that dimethoxy phosphorylated BChE by methyl paraoxon aged faster than BChE modified by both EPN oxon and ethyl paraoxon.

When eBChE was treated with methyl paraoxon at concentrations lower than 0.1 μ M, only modified peptide at m/z 2308.1 was observed and no aged peptide showed in the MALDI spectrum. This is because that the aged peptide with $(CH_3O)OP(O)$ moiety had a

negative charge and a peptide in anionic form exhibited low ionization efficiency in MALDI experiment (66). As such, the detection of the aged peptide was limited using MALDI-MS, although ammonium citrate greatly improved the detection signal of the phosphorylated peptides. Another possible explanation is that the peptide inhibited by phosphorylation is very stable, thus the further aging reaction is unlikely to occur. We suggest that the former explanation is correct.

In the PSD analysis, one common fragment ion at m/z 2182.1 was observed as a dominant fragment ion for each inhibited peptide (Table 1-2-2). A likely explanation is that the phosphate elimination occurs at a higher rate than skeletal bond cleavage. The available internal energy content of the ions is used to eliminate phosphate groups instead of producing a series of the sequence related fragment ions. The observations were consistent with those from the previous studies of a triphosphorylated peptide by MALDI (67) and a pentaphosphorylated peptide using LC/MS (68). Another interesting phenomenon was that it was more preferable to lose the alkyl phosphoric acid than the phosphate group from the precursor ions during fragmentation pathway. When internal energy of the precursor ion was high, the process was prone to lose the alkyl phosphoric acid, which produced a fragment ion with lower energy. As such, the fragment ion at 2182.1 was exclusively observed as the dominant product ion. This observation was consistent with Annan and Carr's results (67), which have shown that singly phosphorylated peptides mainly lose H_3PO_4 with a relative minor loss of HPO_3 . Although the subjects of our study were alkyl phosphorylated peptides, the same results were observed.

After the modified peptides were detected, the extent of the inhibition was determined based on the normalized intensity ratios of modified peptides to the reference peptide and intact peptide to the reference peptide. A peptide (average MH^+ m/z 2222.5) generated from a tryptic digest of eBChE (amino acid sequence: AILQSGSSNAPWAVTSLYEAR) was used as the native reference peptide. It is known that the quantification of analyte using MALDI can be disturbed by some external influences, such as the crystal forms of matrix on target, the laser power used for collecting the mass spectra, and the different response of analytes for MALDI. Therefore, the native reference peptide at m/z 2222.5 was used to minimize or control for these influences. This tryptic peptide has no missed cleavage, no modified amino acid and the similar response to

MALDI as the intact active site peptide (average MH^+ m/z 2200.5). All these properties for this peptide satisfied the criteria for an ideal native reference peptide as proposed by Ruse et al.(69). The relative intensity ratios between the peptide of the intact active site or the modified peptide and the native reference peptide reflect the extent of the pesticide exposure.

Comparison of IC₅₀s and IC₁₀₀s from MALDI Method and from Ellman Method

The normalized relative intensity ratios were reported and plotted as a function of the concentrations of pesticides based on the mass spectra collected from the tryptic digests of inhibited eBChE. Figure 1-2-4 shows plots of the NIR vs EPN oxon concentration and NIR vs carbaryl concentration. IC₅₀s from MALDI method were obtained from the plots based on the recorded data (Table 1-2-2, 1-2-3, 1-2-4, and 1-2-5) for each OP (see details in Experimental section). The IC₅₀s were $1.30 \pm 0.08 \mu\text{M}$ for methyl paraoxon, $0.90 \pm 0.05 \mu\text{M}$ for ethyl paraoxon, and $1.19 \pm 0.01 \mu\text{M}$ for EPN oxon. These results were compared with the IC₅₀s obtained from the Ellman method, which were 1.10 ± 0.97 , 0.79 ± 0.69 , and $0.97 \pm 0.27 \mu\text{M}$ for methyl paraoxon, ethyl paraoxon, and EPN oxon, respectively. IC₁₀₀s of the OPs were determined graphically from linear regressions by extrapolation of linear-regression fits to the points on the x-axis (see details in Experimental section). The IC₁₀₀s from our method were $2.72 \pm 0.09 \mu\text{M}$ for methyl paraoxon, $1.75 \pm 0.06 \mu\text{M}$ for ethyl paraoxon, and $2.48 \pm 0.01 \mu\text{M}$ for EPN oxon. In order to compare the results from the MALDI method with the Ellman method, the plot of linear regression of the relative activity and the concentration of OPs were shown in Figure 1-2-5A. The IC₁₀₀s from the relative activity were also determined graphically from Figure 1-2-5A using the same method as those from NIR. From the Ellman method, IC₁₀₀s were $2.41 \pm 0.80 \mu\text{M}$ for methyl paraoxon, $1.54 \pm 0.86 \mu\text{M}$ ethyl paraoxon and $2.20 \pm 0.31 \mu\text{M}$ for EPN oxon, respectively, which were very close to the values obtained by our method.

An interesting phenomenon was observed that all the IC₅₀s and IC₁₀₀s of OPs were higher from the MALDI method than those from the Ellman method. The possible explanation is that the response of the modified peptides was lower than that of the intact active site peptide and resulting in the higher measured IC₅₀s and IC₁₀₀s. This observation is consistent with the study of Liao *et al.* (70), who have reported that the

desorption/ionization efficiencies for phosphopeptides in MALDI-MS are about one order of magnitude lower than for their non-phosphorylated form. This lower response of the phosphorylated peptides in MALDI possibly results from the high negative electron density of oxygen attached on phosphorus atom, which will cause a partial negative charge on the phosphate group.

Similarly, the IC_{50} and IC_{100} of carbaryl from our method were determined from the linear-regression relationship of NIR vs logarithm of carbaryl concentration, which were 3.57 ± 0.03 and 17.3 ± 0.03 μM , respectively. In order to compare the results from the MALDI method with those from the Ellman method, the relative activities were reported and plotted as a function of the carbaryl concentration (Figure 1-2-5B). IC_{50} and IC_{100} of carbaryl from the Ellman method were determined as 4.9 ± 0.10 and 23.6 ± 0.11 μM from this linear relationship between the relative activity and logarithm of concentration of carbaryl.

In contrast, the results from carbaryl were different from that of OPs. For both methods, NIR or relative activity had nonlinear relationships with concentration of carbaryl, while for OPs, a linear relationship was obtained for both NIR and relative activity. This non-linearity was due to the different CB inhibition mechanism. ChE inhibition occurs via the formation of enzyme-inhibitor complex followed by carbamylation or phosphorylation of the active site and release of the leaving group. The aging reaction, resulting in the non-reversible enzyme, may occur after the inhibition reaction for OPs. No reactivation will happen for the phosphorylated enzyme. However, a spontaneous reactivation of carbamylated enzyme will happen very quickly for CBs. The different carbaryl inhibition mechanism resulted in the linear regression of NIR or relative activity versus logarithm of concentration of carbaryl. This result was in agreement with the study of Rao et al. (71), except that they plotted the linear regression of relative inhibition versus \log [carbaryl].

In contrast to OPs, IC_{50} and IC_{100} of carbaryl from the Ellman method based on the measurement of eBChE activity were greater than those from the MALDI method. The response to MALDI for the carbamylated active-site peptide was higher than that of the phosphorylated peptide. Although ammonium citrate greatly increased the response of phosphorylated peptides as reported by Rao et al. (71), the ionization efficiency of

phosphorylated peptides were still not competitive with that of the intact peptide. Since carbaryl inhibits eBChE in a noncompetitive pattern, the natural substrate can competitively displace the carbamate group from the enzyme-inhibitor complex and result in a greater measured activity. In addition, free thiols produced from DTNB in the Ellman reagents may help decarbamylation of inhibited enzyme and eventually helps to reactivate the carbamylated enzyme during the measurement of eBChE activity. Therefore, the measured enzyme activity was greater than the actual value. Competition with the phosphate group will not happen for the phosphorylated enzyme, because the phosphorylated eBChE is so stable that natural substrate cannot reactivate this inhibited enzyme.

From all the above mentioned results, we can conclude that our newly developed method can detect and quantify pesticide exposure and IC_{50} s and IC_{100} s from the MALDI method are comparable with those from the Ellman method. This method is not only useful for the detection and quantification of eBChE exposure to OPs, but also useful for exposure to CBs, despite their spontaneous reactivation.

CONCLUSION

In conclusion, a new method was developed to provide unambiguous identification of the modified active-site peptide produced from tryptic digest of eBChE using MALDI-TOF-MS. Furthermore, this method can be applicable to quantify pesticide exposure using the linear relationship between the modified peptide intensity with OP concentration or logarithmic carbaryl concentration. The Ellman measurement of eBChE activity is limited for pesticide exposures at inhibition levels less than 20%. However, the reported method can provide information on eBChE inhibition levels as low as 5%. This assay was also suitable for the analysis of carbaryl inhibited eBChE, although carbamylated enzyme has higher spontaneous reactivation.

Although CW agents were not investigated in this chapter, the analysis of the chemical exposures can be examined using the same methodology. For example, if eBChE is exposed to soman, a CW agent, the eBChE will be inhibited. The digest will be subjected

to the MALDI analysis after the inhibited eBChE is hydrolyzed by trypsin. The inhibited active site peptide should be observed at m/z 2280.3 in MALDI mass spectrum. The mass difference between the modified peptide at m/z 2280.3 and the intact peptide at m/z 2200.1 is unique to soman. The identification of the soman inhibited peptide could be confirmed by PSD analysis. Furthermore, the extent of the soman exposure could be determined by the relative intensity ratios of the modified and intact active-site peptides.

The broad use of pesticides in every day life and the increasing threat of terrorism of chemical war agents have raised the chances of multiple pesticide exposure. Because of the limitation of using MALDI to analyze complex peptide mixtures, a novel methodology is required for the analysis of multiple pesticide exposure. Chapter 3 will cover an *in vitro* study for the analysis of a mixture of phosphorylated peptides using LC/MS/MS techniques.

CHAPTER THREE

ANALYSIS OF MULTIPLE PESTICIDE EXPOSURE USING LC/MS/MS

INTRODUCTION

The potential for multiple-pesticide exposure, either sequentially or concurrently, is greater today than anytime in history, due to the extensive use of pesticides. With the onset of the Gulf War Syndrome (72), the issue of multiple chemical exposures poses an ever increasing military and civilian threat. The rising public healthcare concerns over multiple chemical exposures require more sensitive and reliable methods to monitor multiple-chemical exposure. However, about 95% of all chemical studies were performed on individual chemicals(73). In this study, a novel methodology was developed to analyze multiple chemical exposures using LC/MS/MS techniques. An *in vitro* investigation was designed to examine the relative quantification of each pesticide exposure, and to identify the types of pesticide using eBChE as a model system. Although we did not examine chemical warfare (CW) agents in this study, investigation of BChE inhibition resulting from pesticides can provide insight into human exposure to these classes of compounds.

As described in Chapter 2, the analysis of inhibited BChE was used to monitor pesticide exposure (57, 60). In our previous work (Chapter 2), we successfully identified and quantified the modified (phosphorylated or carbamylated) active site peptide generated from tryptic digests of inhibited eBChE using MALDI-MS. In this chapter, we continued to investigate the analysis of a mixture of phosphorylated active site peptides after multiple-pesticide exposure using LC/MS/MS.

In the last decade, mass spectrometry has emerged as an increasingly viable technique for the analysis of protein modifications, such as phosphorylation. Although both electrospray ionization mass spectrometry (ESI-MS) and matrix-assisted laser desorption ionization-mass spectrometry (MALDI-MS) have been used quite successfully for phosphoprotein analysis (74), ESI-MS offers a better choice for investigations with

more complex phosphoprotein mixtures because of online separation capabilities. Chapter 2 described the successful identification of phosphorylated peptides by MALDI-MS, through comparisons of the peptide maps before and after treatment. However, a noteworthy limitation of the MALDI approach is observed in the low desorption/ionization efficiency of phosphorylated peptides. This lower response was established by comparing MALDI data with results from LC/MS/MS investigations. In addition, a further worsening of the detection signal for these analytes arises due to ion suppression in the presence of the other peptides. Therefore, investigations of a mixture of OP-modified active site peptides were much more challenging using MALDI methodology. A further limitation of the MALDI technique stems from the difficulty in obtaining sequence information of the phosphoprotein under study. Although the modified peptide was confirmed by post-source-decay (PSD) MALDI-MS analysis, it was not possible to obtain sequence information. Since loss of the phosphate moiety was the dominant fragmentation pathway and the yield of the other fragments was low, the collection and interpretation of sequence information from PSD mass spectra was difficult. It was evident that the MALDI methodology described here was not suitable for multiple pesticide exposure analyses.

In this chapter, three OPs, methyl paraoxon, ethyl paraoxon, and EPN oxon, were used to inhibit eBChE, separately. Subsequently, the inhibited enzyme was digested with trypsin. The same amount of tryptic digests was mixed, and the resulting mixture was further analyzed using LC/MS due to its online separation capability. However, the phosphorylated peptide separation and the quality of their product spectra were still not good enough for the analysis. This is because the other abundant peptides in the mixture suppress the peptide ions of interest. Some situations make the phosphorylated peptide analysis even worse, such as coelution of four phosphorylated peptides as well as the other peptides and relatively long duty cycles (time for MS full scan and subsequent MS/MS). Therefore, an LC/MS/MS technique for the analysis of the phosphorylated peptide ions during on-line analysis, was applied for the investigation of the mixture. The ions of interest can be isolated and fragmented in the ion trap even in the presence of the other abundant peptides using LC/MS/MS techniques. The isolation ability of LC/MS/MS technology was evaluated by comparing the ion chromatogram (IC) of one kind of phosphorylated peptide enriched from the offline fractionated sample with that from the

un-fractionated sample. Results demonstrated that this LC/MS/MS technique was a powerful tool for the analysis of the phosphorylated peptide mixture. Results clearly showed that this method was applicable for the measurement of the relative abundance of each individual phosphorylated peptide in a complex peptide mixture. Furthermore, the phosphorylation and carbamylation sites were localized from LC/MS³ and LC/MS/MS analysis, respectively.

EXPERIMENTAL

Chemicals and Reagents

All the chemicals, and enzymes, including their purity and grade, are the same as those described in Experimental Section of Part I, Chapter 2.

eBChE Inhibition

The same eBChE inhibition protocol was used as described in Experimental Section of Part I, Chapter 2.

Trypsin FDigestion

The same trypsin digestion protocol was used as described in Experimental Section of Part I, Chapter 2.

Offline Peptide Separation

A tryptic digest of eBChE (200 μ l, 184 μ g) was injected onto the C18 reversed phase column (2.1 mm x 25 cm, 3 μ m). Peptide separation was done by a linear gradient elution that started with 95% (v/v) solvent A [water + 0.1% trifluoroacetic acid] and 5% solvent B [acetonitrile + 0.1% trifluoroacetic acid] using a flow rate of 0.25 ml/min. Phosphorylated peptides were enriched by HPLC separation. For the first separation, the concentration of solvent B was increased to 95% (v/v) in 30 min, then kept at this concentration for 5 min. Fractions containing modified active site peptide were collected and concentrated using a Speed Vacuum concentrator. The residue was dissolved in 20 μ l

of solvent A and subjected to the second offline separation. For the second separation the concentration of solvent B was increased to 85% over 50 min and then to 95% over 1 min, and kept this concentration for 2 min. Peaks were detected at 214 nm. Each peak was manually collected in 1 ml vials.

Instrument

MALDI-TOF-MS Analysis

The sample preparation, target spotting technique and parameters of the instrument were the same as described in the Experimental Section of Part I, Chapter 2.

LC-MS Analysis

A tryptic digest of eBChE (9 μ L, about 19 pmol) was injected into the capillary column. Separations were performed with an HP 1100 HPLC modified with a custom splitter to deliver mobile phase at 4 μ L/min to a custom C18 capillary column (300 μ m id x 15 cm, packed in-house with Macrosphere 300 \AA 5 μ m C18 (Alltech Associates, Deerfield, IL)). A linear gradient was used to elute peptides from the capillary column that started with 95% (v/v) solvent A [water + 0.1% formic acid] and 5% solvent B [acetonitrile + 0.1% formic acid] using a flow rate of 0.2 ml/min. The concentration of solvent B was increased to 20% over 8 min and then to 90% over 25 min, and kept at this concentration for 8 min. The heated capillary temperature of the mass spectrometer was 175 $^{\circ}$ C. The number of microscans was 5 and the scan range was from 150 Da to 2000 Da. The acquisition time was 45 min. For LC/MS/MS technique, the isolation width was 5 Da (m/z), normalized collision energy was 35%, activation Q was 0.25 and the activation time was 30 ms.

RESULTS AND DISCUSSION

Sequence Information of Phosphorylated Peptides

In order to confirm the identity of the phosphorylated peptides, LC/MS/MS was applied to obtain the amino acid sequence information. A representative LC/MS/MS of the phosphorylated peptide (calculated MH^{2+} at m/z 1168 $^{2+}$) by ethyl paraoxon is shown in Figure 1-3-1. As shown in Figure 1-3-1, a dominant fragment ion at m/z 1091 $^{2+}$ was

observed corresponding to the loss of the alkyl phosphate group $\text{HOP(O)(OCH}_2\text{CH}_3)_2$. The low intensity of the other fragment ions made it impossible to obtain the fragmentation information of the phosphorylated peptide ions. A similar phenomenon was observed in the MS/MS spectra of the other three phosphorylated peptides (data not shown), where the dominant product ion was at m/z 1091²⁺. The common fragment ion corresponded to the neutral fragment loss of the alkyl phosphoric acid from the phosphorylated ions. As such, the alkyl-phosphorylated peptides were differentiated by the neutral fragment loss.

In order to acquire sequence information of the phosphorylated peptide ions, MS/MS of the dominant product ion was obtained. Figure 1-3-2 shows the MS/MS of 1091²⁺, which was the common daughter ion for all of the phosphorylated peptides. A high quality tandem mass spectrum was obtained for the common product ions (Figure 1-3-2). The sequence of the active site peptide of eBChE digested by trypsin is known to be SVTLFGESAGAASVSLHLLSPR (calculated MH^+ at m/z 2200.5, numbered 1 to 22 from right to left), where the active site serine is underlined (75). The MS/MS spectrum of the intact active site peptide is also reported (Figure 1-3-3). It is known that fragmentation of peptides usually occurs at the peptide bonds to produce a series of fragment ions, where ions containing an N-terminal are “b” ions and ions containing an C-terminal are “y” ions. Most fragment ions were observed as y-ions in the tandem mass spectra of both intact peptide and the common product ion of phosphorylated active site peptides (Figure 1-3-2 and Figure 1-3-3). By comparing the tandem mass spectra of Figure 1-3-2 and Figure 1-3-3, an identical set of unphosphorylated fragment ions corresponding to y14 - y3 was observed. Mass shifts with 18 Da were observed for y15 Δ - y19 Δ ions (Figure 1-3-2) compared with those y ions from the intact peptide. This mass shift was due to the elimination of alkyl phosphoric acid on the catalytic serine resulting in a homoalanine residue. All the fragmentation information confirmed that the precursor ion at m/z 1168²⁺ was the phosphorylated peptide. Furthermore, the modified group can be deduced based on the mass difference (77 Da) between the precursor ion and fragment ion. The lost fragment should be 2 times that of the mass difference due to the doubly charged precursor and product ions. As such, the modified group was identified as O,O-diethyl phosphate (154 Da). The other phosphorylated peptides can be determined using the same approach. In addition, the phosphorylation site was also localized as serine at position 15.

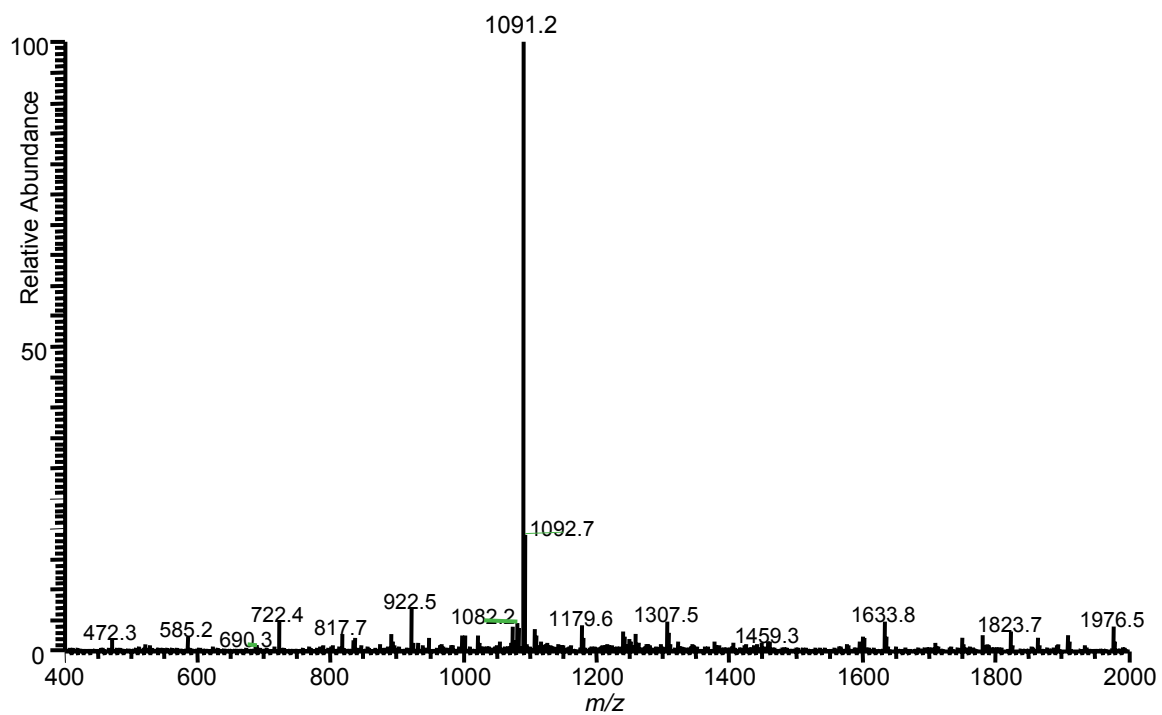


Figure 1-3-1. MS/MS of the alkyl-phosphorylated peptide by ethyl paraoxon. The doubly charged precursor ion at m/z 1168²⁺ was selected for collision-induced dissociation. The dominant fragment ion was doubly charged ion at m/z 1091²⁺ corresponding to the loss of the O,O-ethyl phosphoric acid from the precursor ion.

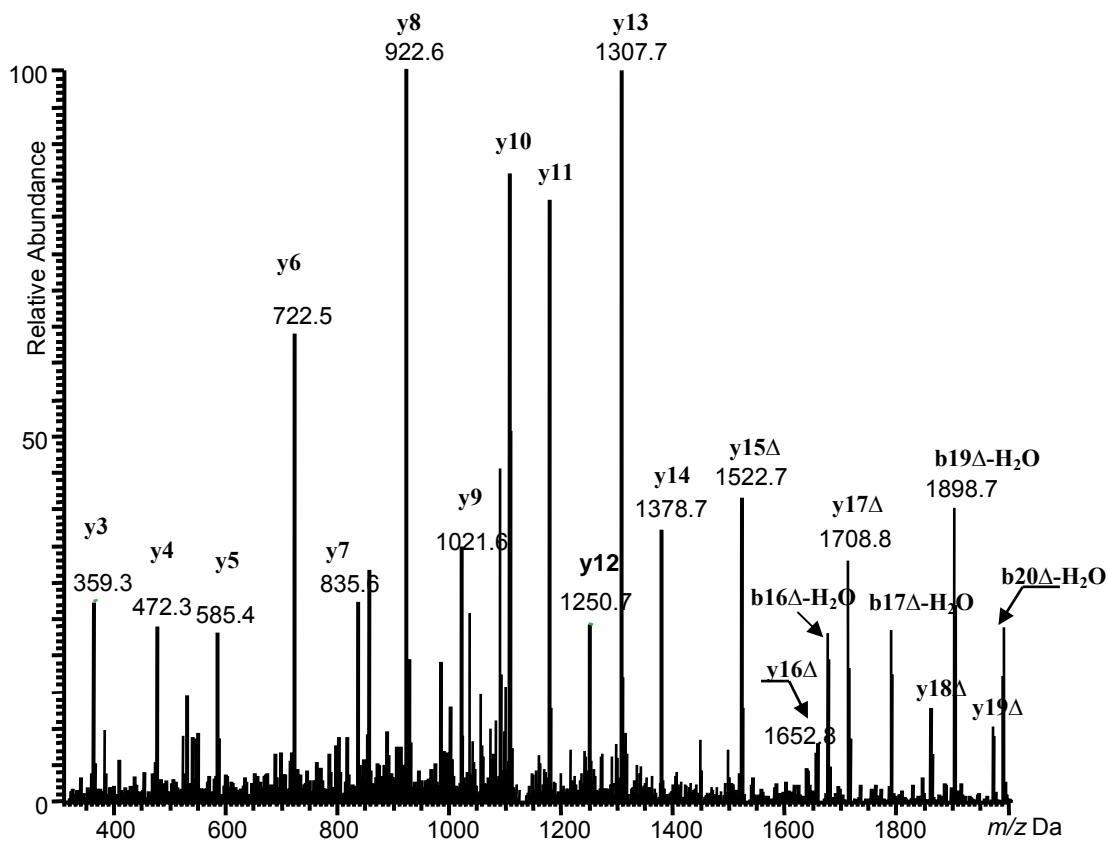


Figure 1-3-2. MS/MS/MS of the alkyl-phosphorylated peptide by ethyl paraoxon. The doubly charged product ion at m/z 1091²⁺ was selected for collision-induced dissociation. Product ions with neutral loss of the alkyl phosphoric acid are indicted by Δ.

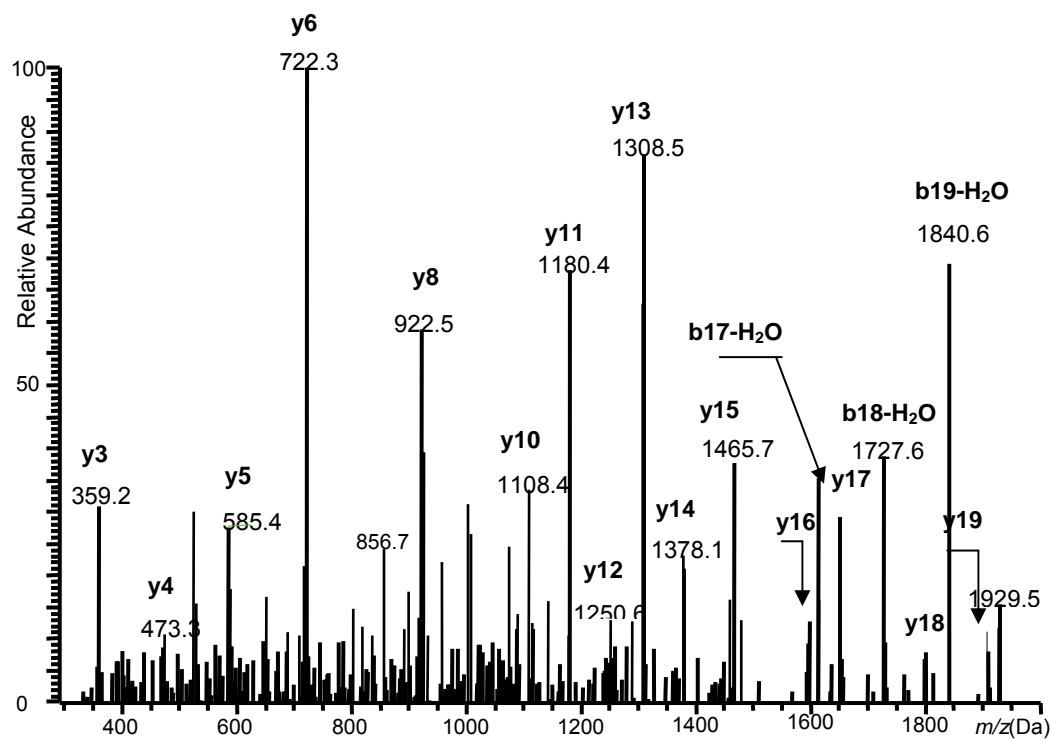


Figure 1-3-3. MS/MS of intact active site peptide. The doubly charged precursor ion at m/z 1100²⁺ was selected for collision-induced dissociation. The amino acid sequence of the intact active site peptide is SVTLFGESSAGAASVSLHLLSPR (calculated MH²⁺ at m/z 1100²⁺, the active site serine is underlined, and numbered as 1 to 22 from right to left).

Identification of the Carbamylated Peptide

The MS/MS spectrum of the doubly charged precursor ion at m/z 1129²⁺ was also obtained (Figure 1-3-4). The pattern of tandem MS for the carbamylated peptide was different from those of phosphorylated peptides. Although the doubly charged ion at m/z 1091²⁺, due to the loss of the carbamylated group, was also observed, it was not the dominant fragmentation ion. Enough fragmentation information was collected to identify the doubly charged precursor ion at m/z 1129²⁺ from the tandem mass spectrum. Comparing the product mass spectra of the carbamylated peptide and the intact peptide, an identical set of unmodified fragment ions corresponding to y14-y3 was observed. Mass shifts with 57 Da, due to the attached carbamylated-group (57 Da) on the active site serine residue, were observed for y15 Δ -y19 Δ ions (Figure 1-3-4). It was evident that the precursor ion at m/z 1129²⁺ was the carbamylated peptide, and the carbamylation site was identified as serine at the position 15 from the LC/MS/MS analysis.

Comparison of Sensitivity of MALDI and LC/MS/MS

In Chapter 2, we successfully detected and quantified inhibited eBChE resulting from OP and CB exposure using MALDI-TOF-MS methodology. In order to compare the detection sensitivity of the MALDI-TOF-MS method and the LC/MS method, the tryptic digests of eBChE treated by ethyl paraoxon at different concentrations were used. Table 1-3-1 lists the peak area ratios (peak area of phosphorylated peptide to that of intact peptide) from LC/MS analysis and the intensity ratios (intensity of the phosphorylated peptide to that of the intact peptide) from MALDI-MS at different concentrations of ethyl paraoxon (0, 0.05, 0.5, 1.0, and 1.5 μ M).

The peak area ratios from the LC/MS method were higher than the intensity ratio from the MALDI-MS method for the same tryptic digest. This is because the low response of phosphorylated peptides detected by MALDI. The poor detection signal of the phosphorylated peptide by the MALDI method resulted from the electron withdrawing property of the phosphate group on the modified peptide. The low response of phosphorylated peptides was also due to the suppression effects in the presence of the other peptides from the tryptic digest of eBChE. In contrast, the online separation of LC/MS/MS

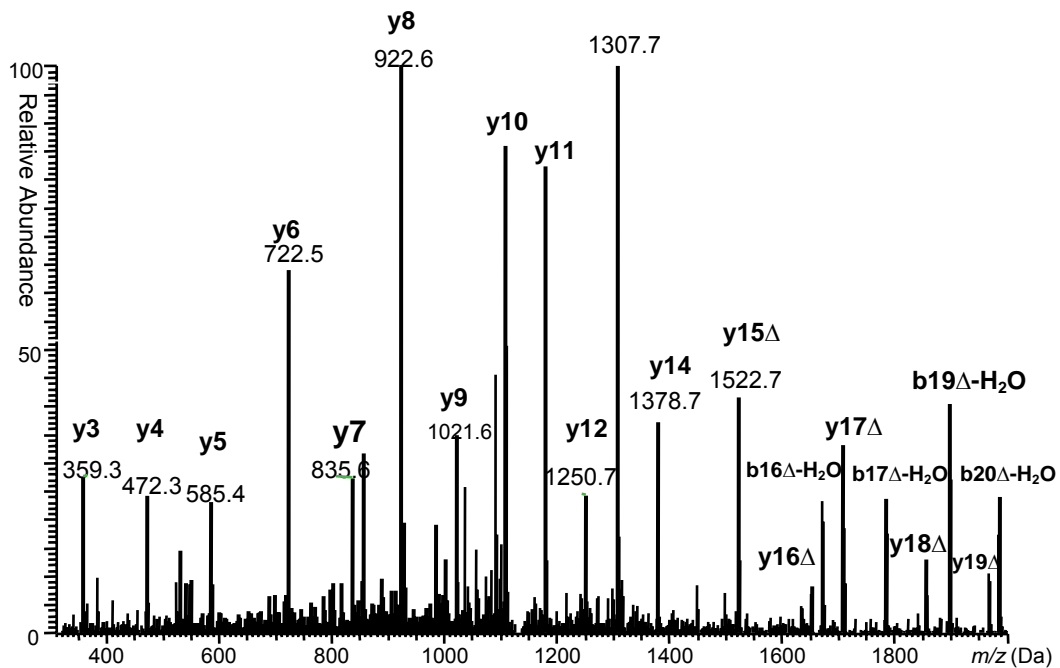


Figure 1-3-4. MS/MS of the carbamylated peptide. The doubly charged precursor ion at m/z 1129²⁺ was selected for collision-induced dissociation. Fragment ions with the attached carbamate on the serine are indicated by Δ .

Table 1-3-1. The relative ratio of modified peptide peak area or intensity by ethyl paraoxon to the intact peptide peak area or intensity from the RIC^a LC/MS/MS and that from MALDI.

Concentration of ethyl paraoxon (μM)	$I_{2336.2}/I_{2200.2}$ ^b from MALDI	$I_{2336.2}/I_{2200.2}$ ^c from RIC of LC/MS/MS
0.05	0	0.47
0.5	0.20	1.72
1	0.79	3.02
1.5	∞	35.06

^a: RIC stands for reconstructed ion chromatogram;

^b: the data from the previous work (Chapter 2);

^c: the relative ratio of the modified peak (at m/z 2336.2) area by ethyl paraoxon to that of the intact peptide (at m/z 2200.2).

method decreased the complexity of the peptide mixture, and increased the response for each individual peptide accordingly. Furthermore, the CID of the selected ion for the LC/MS analysis dramatically increased the interest-peptide response. The data (Table 1-3-1) clearly showed that the LC/MS/MS method was more sensitive than MALDI method. For instance, no phosphorylated peptide was detected from the sample treated with 0.05 μM ethyl paraoxon, and no intact peptide was identified when the concentration of ethyl paraoxon was at 1.5 μM using the MALDI method. However, both the modified peptide and the intact peptide were detected at 0.1 μM and 1.5 μM ethyl paraoxon using the LC/MS/MS method.

MALDI and LC/MS/MS Analysis for Offline-fractionated Peptides

In order to reduce the complexity of the peptide mixture and enrich the phosphorylated peptide, a tryptic digest of ethyl paraoxon inhibited eBChE was fractionated by offline HPLC with UV detector (see Experimental section). Every peak was manually collected as a different fraction using UV detector at 214 nm. After two offline separations, the MALDI spectrum of every fraction was obtained to determine which fractions contained the modified peptide. The modified peptide at m/z 2336.2 was identified all the fractions from 13th to 18th. Only the 15th fraction was analyzed using LC/MS/MS. Figure 1-3-5 shows the MALDI mass spectrum of the 15th fraction separated from the tryptic digest of the eBChE inhibited by ethyl paraoxon (see Experimental section). Although most of the small peptides were removed from the mixture, the modified peptide at m/z 2336.2 was observed in the 15th fraction as well as the other peptides. The modified peptide ion with a double charge at m/z 1168²⁺ was selected, specially isolated and fragmented using the LC/MS/MS technique. Figure 1-3-6 shows the ion chromatogram (IC) of LC/MS/MS of the precursor ion at m/z 1168²⁺. The phosphorylated peptide was monitored by its dominant doubly charged fragment ion at m/z 1091²⁺ (lower panel of Figure 1-3-6), which corresponded to the neutral loss of $(\text{CH}_3\text{CH}_2\text{O})_2\text{P}(\text{O})(\text{OH})$ from the precursor ion. A typical Gaussian-shaped peak at retention time 26.50 min was observed. The peak area was related to the amount of the phosphorylated peptide present in the mixture.

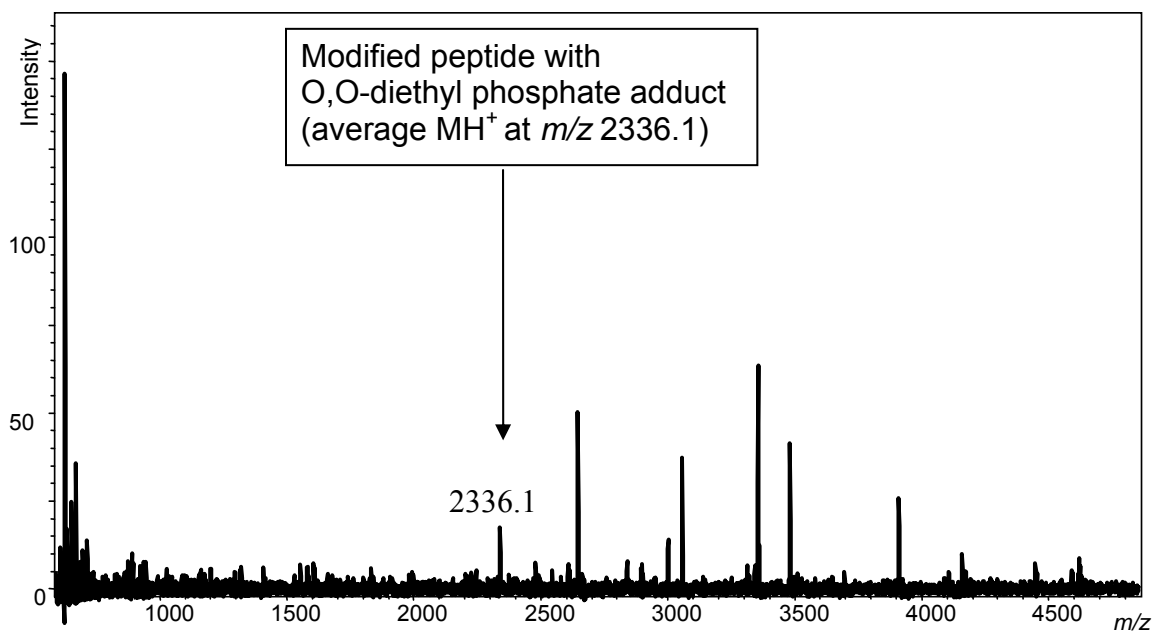


Figure 1-3-5. Representative MALDI-TOF-MS spectrum of the 15th fraction separated by HPLC containing the modified peptide with O,O- diethyl phosphate group from the tryptic digest of eBChE treated with ethyl paraoxon. The modified peptide is labeled with an arrow.

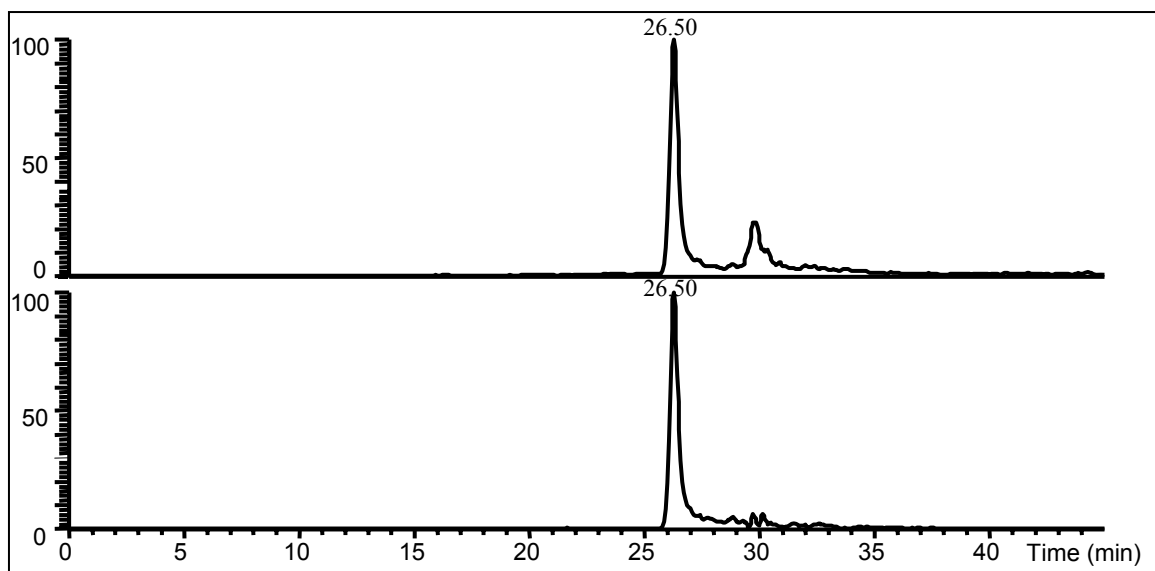


Figure 1-3-6. Reconstructed ion chromatogram (RIC) of the modified active site peptide after two offline HPLC fractionations. RIC of the doubly charged precursor ions at m/z 1168²⁺ is shown in the upper panel. RIC of the fragment ion at m/z 1091²⁺, which corresponds to the loss of the alkyl phosphoric acid HOP(O)(OCH₂CH₃)₂ and is used to monitor the phosphorylated peptide, is shown in the lower panel.

LC/MS/MS Analysis for Unfractionated Phosphorylated-peptides

From the above discussion, LC/MS/MS was capable of analyzing the enriched phosphorylated-peptide after two offline separations. At this stage, we were curious to determine whether or not the assay could be used for the isolation of the phosphorylated peptide from the un-fractionated peptide mixture. Figure 1-3-7 shows the RIC of 1168²⁺ from the un-fractionated tryptic digest of inhibited eBChE resulting from ethyl paraoxon exposure. LC/MS/MS techniques were performed to analyze particular ions of interest. The fragment ion at m/z 1091²⁺ was used to monitor the precursor ion. A sharp and narrow peak, corresponding to the precursor ion m/z 1168²⁺ at retention time 26.55 min, was observed.

By comparing the results from the fractionated (Figure 1-3-6) and un-fractionated (Figure 1-3-7) digests of the inhibited eBChE by ethyl paraoxon, the RIC of the modified peptide from the fractionated sample was found to not be better than that of the unfractionated one. A side shoulder peak of the RIC for the phosphorylated peptide from the fractionated sample, which was a peptide with the same m/z as that of the interest-peptide. The disadvantages of the fractionated methodology were its time consuming nature and the low sample recovery. All the results clearly showed that the LC/MS/MS technique was a powerful tool for the isolation of the phosphorylated peptide ions without offline separation before analysis.

LC/MS/MS for Un-fractionated Carbamylated- peptides

The carbamylated peptide was baseline-isolated from un-fractionated tryptic digests of the carbamylated eBChE (Figure 1-3-8) using LC/MS/MS analysis. The fragment ion at m/z 1091²⁺ was also used to monitor the carbamylated peptide ion. Because the fragment ion was not the dominant ion in the product mass spectrum, the peak area of the fragment ion at 1091²⁺ was much less than that of the precursor ion (Figure 1-3-8). Although the LC/MS/MS method was applicable for the isolation of carbamylated peptide, the amount of the carbamylated ions can not be monitored by the fragment ion at m/z 1091²⁺.

Relative Quantification of the Phosphorylated Peptides

One kind of phosphorylated peptide was successfully analyzed using LC/MS/MS method without any offline fractionation prior analysis. We were curious to find out

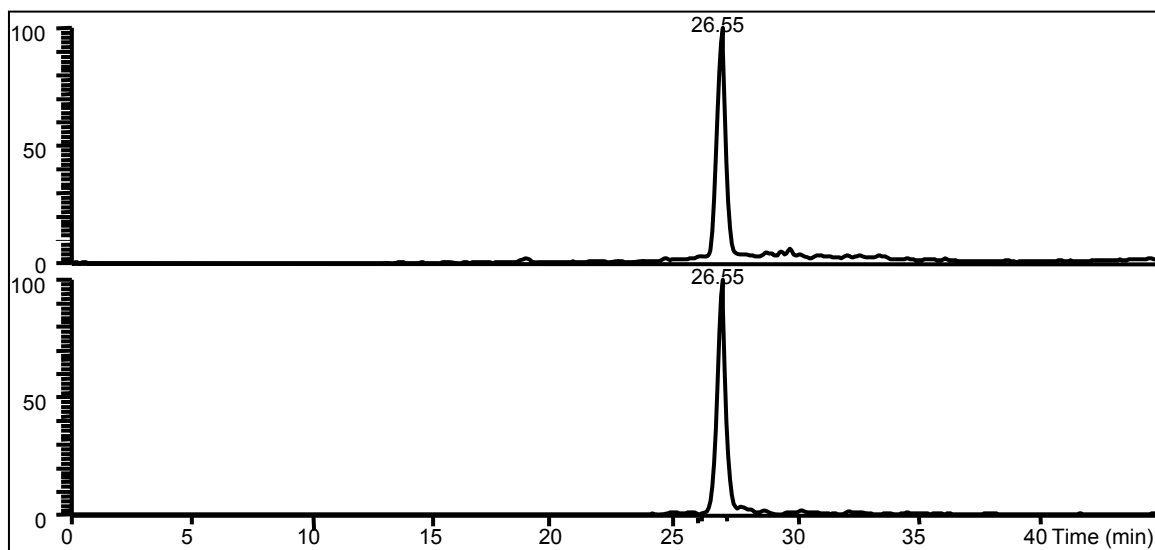


Figure 1-3-7. Ion chromatogram (IC) of the modified active site peptide without offline fraction prior to LC/MS analysis. The modified peptide with O,O-diethyl phosphate adduct (MH^{2+} at m/z 1168 $^{2+}$) is shown in the upper panel and the fragment ion at m/z 1091 $^{2+}$ with the loss of the alkyl phosphoric acid $HOP(O)(OCH_2CH_3)_2$ is shown in the lower panel.

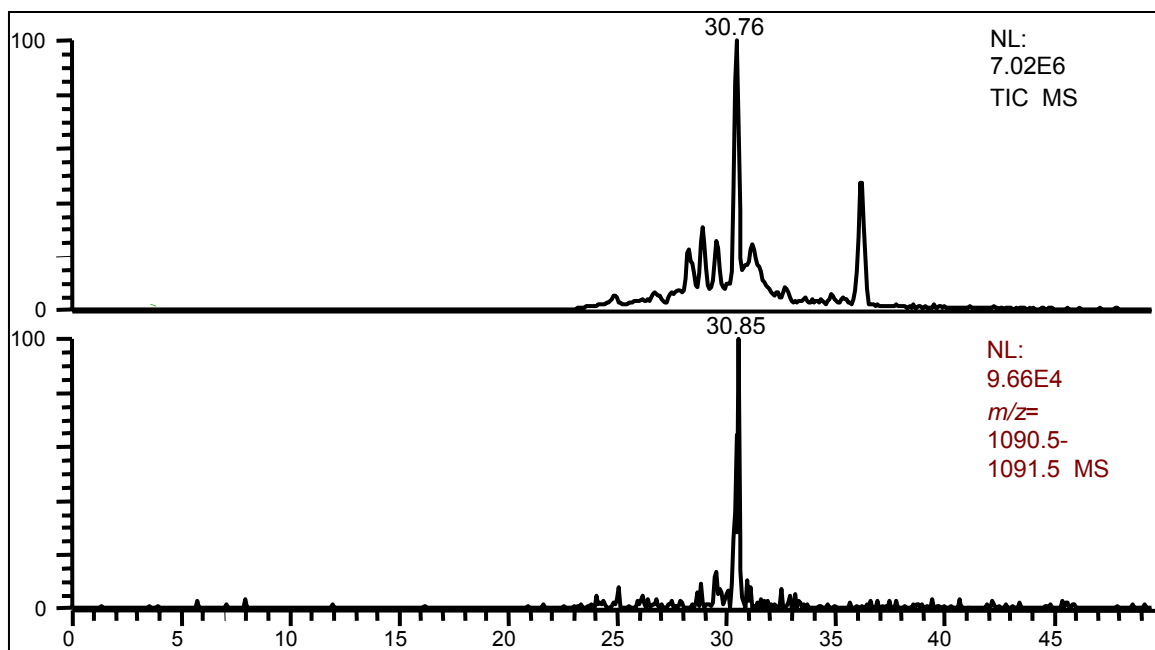


Figure 1-3-8. IC of the modified active-site peptide with carbamate group (MH^{2+} at m/z 1129 $^{2+}$) in the upper panel and RIC of the fragment ion 1091 $^{2+}$ with the loss of the carbamate group $CH_3NHC(O)OH$ in the lower panel.

whether the same assay could be used for the analysis of a mixture of phosphorylated peptides. eBChE was inhibited with 1.2 μM methyl paraoxon, 0.5 μM ethyl paraoxon, and 0.2 μM EPN oxon, separately. Each of these three treated samples was subsequently digested with trypsin, respectively. The same amount of the tryptic digest (0.9 $\mu\text{g}/\mu\text{l}$) of the inhibited BChE by methyl, ethyl and EPN oxon were mixed, and analyzed with LC/MS/MS technique.

As described in Chapter 2, inhibited peptides resulting from methyl paraoxon exposure were detected as phosphorylated peptides with O-methyl phosphate (calculated MH^+ at m/z 2294.5) and O, O-dimethyl phosphate (calculated MH^+ at m/z 2308.5). The inhibited peptide from ethyl paraoxon was identified with O,O-diethyl phosphate (calculated MH^+ at m/z 2336.5). Similarly, the inhibited peptide from EPN oxon was detected with O-ethyl phenyl phosphate (calculated MH^+ at m/z 2368.5). All the above results were obtained using MALDI-TOF-MS technique (Chapter 2).

Phosphorylated peptides were further confirmed through the sequence information using LC/MS/MS analysis (Figure 1-3-1 and Figure 1-3-2). Collision induced dissociation (CID) of the phosphorylated peptides ions were specially selected to isolate and fragment in the ion trap. If only data dependent acquisition for the CID of the four precursor ions was used, the phosphorylated peptide by EPN oxon was always omitted (data not shown). Data dependent acquisition is set up to analyze the most abundant ions each time. Because the four phosphorylated peptides eluted from the capillary column during a short time interval (2.23 minutes for elution of all the four selected ions, Figure 1-3-9) and the suppression from the other abundant ions, not all of the ions of interest can be analyzed. A time segment LC/MS/MS technique was used to solve the problem, which was referred that the mass spectrometer was set up to analyze one kind of precursor ion during a certain time period and ignore all the other peptides. Using the time-segmented LC/MS/MS technique, the phosphorylated peptides from the mixture of the tryptic digests of eBChE were baseline separated (Figure 1-3-9).

As described before, all phosphorylated peptides had a similar product mass spectrum. Only one dominant fragment ion at m/z 1091²⁺ was observed, which corresponded to the loss of the alkyl phosphoric acid (neutral fragment) from the precursor ions. As such, the phosphorylated peptides were deduced by the neutral fragment ion from

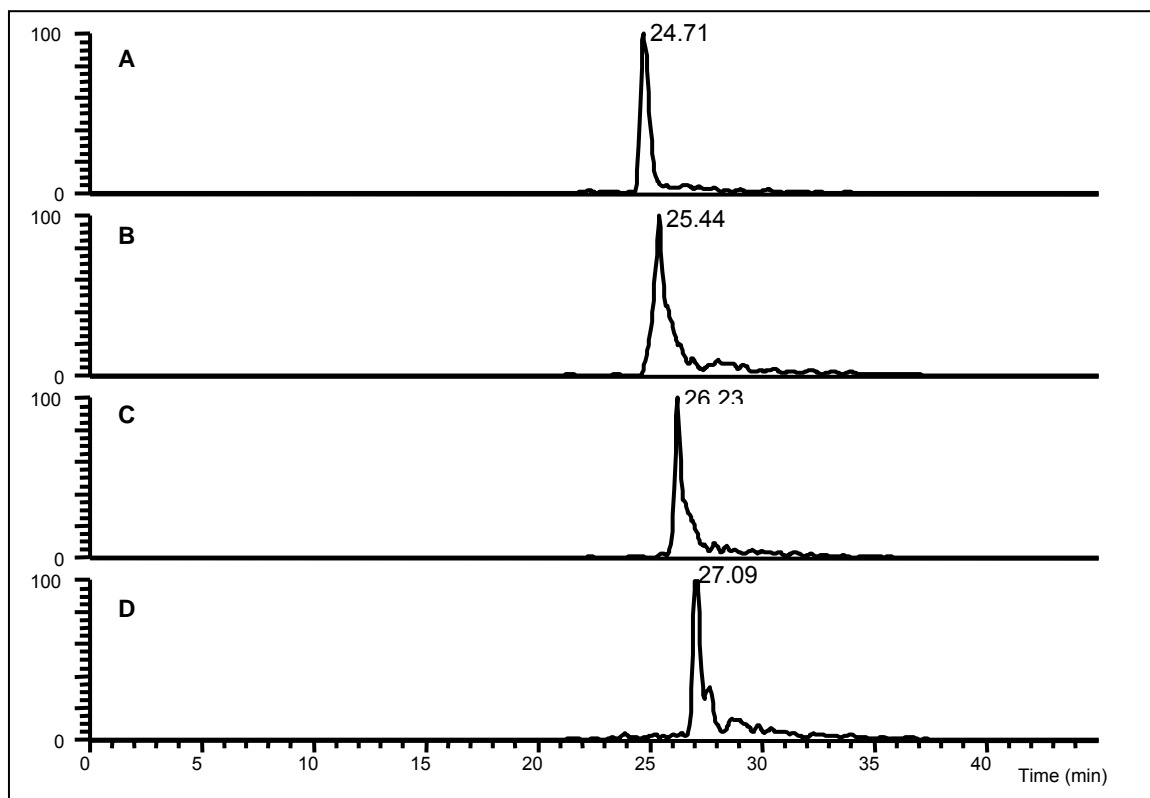


Figure 1-3-9. Ion chromatograms (IC) of common fragment ion (m/z 1091²⁺). Precursor ions were determined by the neutral loss fragments. Panel A is with neutral loss fragment 112 Da, corresponding to $\text{CH}_3\text{OP}(\text{O})(\text{OH})_2$ (112 Da), from the precursor ion MH^{2+} at m/z 1147²⁺ modified by methyl paraoxon; panel B is with neutral loss fragment 126 Da, corresponding to $(\text{CH}_3\text{O})_2\text{P}(\text{O})\text{OH}$ (126 Da), from the precursor ion MH^{2+} at m/z 1155²⁺ modified by methyl paraoxon; panel C is with neutral loss fragment 154 Da, corresponding to $(\text{CH}_3\text{CH}_2\text{O})_2\text{P}(\text{O})(\text{OH})_2$ (154 Da), from the precursor ion MH^{2+} at m/z 1168²⁺ modified by ethyl paraoxon; panel D is with neutral loss fragment 186 Da, corresponding to $(\text{CH}_3\text{CH}_2\text{O})(\text{C}_6\text{H}_5)\text{P}(\text{O})(\text{OH})_2$ (186 Da), from the precursor ion MH^{2+} at m/z 1184²⁺ modified by EPN oxon.

the precursor ions. For instance, the neutral loss-fragment in panel A (Figure 1-3-9) was 56, which was the mass difference between the doubly charged precursor ion and the doubly charged fragment ion at 1091²⁺. The precursor ion was then deduced as 1147²⁺ corresponding to the modified peptide with O-methyl phosphate (112 Da). Using the same approach, all the precursor ions for panel B, C, and D (Figure 1-3-9) were deduced based on the neutral loss of O,O- dimethyl phosphoric acid (126 Da), O,O-diethyl phosphoric acid (154 Da), and O-ethyl phenyl phosphoric acid (186 Da), respectively.

The stoichiometries of the phosphorylated peptides were obtained by comparing the integrated peak intensities. An assumption was made that all the alkyl phosphorylated peptides ionized at the same efficiencies in electrospray source. The integrated peak area of the various phosphorylated peptide indicated the extent of exposure to each OP. The relative ratio of the integrated peak intensities was AA1147 : AA1155 : AA1168 : AA1184 = 2.5 : 4.3 : 2.7 : 1 (AA is the area of the peak). The AA1147 was then added with AA1155 to obtain a total value, which demonstrated the total exposure to methyl paraoxon. As such, the relative ratio was methyl paraoxon : ethyl paraoxon : EPN oxon = 6.8 : 2.7 : 1. This indicated that eBChE was exposed to methyl paraoxon 6.8 times more than EPN oxon, and 2.7 times more than ethyl paraoxon. The result of this method was consistent with the actual incubation concentration ratios, which was methyl paraoxon : ethyl paraoxon : EPN oxon = 1.2:05:0.2 = 6.0 : 2.5 : 1. The relative standard error was 8% between the detected value and the actual value. Such difference was caused by the different inhibition efficiency of OPs. Based on the results from our previous work (Chapter 2), the inhibitory ability of methyl paraoxon was lower than that of ethyl paraoxon and EPN oxon. The lower inhibition efficiency produced less inhibited peptides, which corresponded to the extent of pesticide exposure by methyl paraoxon. It has to be emphasized that the quantification was not absolute, because no internal standard was used. However, a relative quantification was obtained, and was consistent with the actual pesticide concentrations.

CONCLUSION

A new methodology was developed here to provide identification and baseline separation of a mixture of phosphorylated active site peptides using LC/MS/MS. The

LC/MS/MS methodology was more sensitive due to its online separation, which reduced the complexity of the peptide mixture. Using the methodology, no offline separation was needed before the analysis, which avoided the sample loss during the preparation procedure. The methodology was successfully used in the analysis of single pesticide exposure. In this study, a common dominant fragment ion at m/z 1091²⁺ was observed in tandem mass spectra of all phosphorylated peptides, and was used to monitor the precursor ions. The phosphorylated peptides were differentiated by the neutral loss from the precursor ions. The common fragment ion at m/z 1091²⁺ was further fragmented to acquire the sequence information and modification site of the phosphorylated peptides. LC/MS/MS was a powerful technique for obtaining sequence information and for localizing the phosphorylation site of the modified peptides. The methodology was also successfully applied for the analysis of d peptide modified by carbaryl. Finally, the time segment of LC/MS/MS analysis of the selected ions was a great tool for baseline separation, detection, identification, and quantification of the phosphorylated active site peptides in a single analysis run.

The application of the LC/MS/MS methodology for the analysis of multiple pesticide exposure to human will be the subjects of future experiments. A purification method for the isolation of BChE from human serum is a challenge. Chapter 4 describes how to solve this problem.

CHAPTER FOUR

DEVELOPMENT OF A PURIFICATION SCHEME FOR THE ANALYSIS OF HUMAN SERUM BUTYRYLCHOLINESTERASE

INTRODUCTION

BChE has been notoriously difficult to purify. Although it was discovered in 1932 as an enzyme that hydrolyzes esters (76), hBChE was not sequenced until 1986(40) due to the lack of adequate amounts of pure enzyme. The relatively low concentration of plasma BChE (3-5 mg/l), and the complex protein compositions in serum make BChE purification difficult. Affinity gels are widely used in the purification procedure due to their relatively specific characters. In this work, affinity gels were synthesized in laboratory to enable hBChE isolation from serum.

The invention of affinity gels was a milestone in the BChE purification history, which has been applied for more than 35 years. Before the application of affinity gels, a conventional purification method was employed for the BChE isolation. This method was based on the use of an ammonium sulfate fraction at neutral and acid pH (45, 76). A drawback of this method is poor purification and yield. Furthermore, the method is not suitable hBChE purification, because the enzyme is not stable at low pH. A big improvement in the esterase purification occurred in 1970. Affinity gels were used for the BChE purification, which were originally developed for the purification of AChE by Kalderon (77). Until 1978, affinity gels with procainamide ligands, which totally changed the BChE purification history, were first introduced in a small-scale purification of hBChE by Lockridge & La Du (51). The use of the procainamide affinity gels enabled the production of high purity and high yield BChE from serum.

Ralston et al. (52) applied two large-scale methods for the purification of horse and human serum BChE using procainamide gels. In brief, the procainamide-Sepharose 4B gels were used to treat large volumes of serum followed by the elution of BChE. The eluted fractions containing BChE were then subjected to ion-exchange chromatography on DEAE-Sephadex, and the bound BChE was eluted with choline chloride gradient. The

eluted fractions containing BChE were further purified with preparative polyacrylamide-gel electrophoresis. This assay needs a large amount of sample, which was not available in this dissertation.

This chapter describes a procedure for synthesizing procainamide-affinity gels. The ability of the synthesized affinity gels to isolate hBChE was also evaluated and compared with that of the normal Sepharose 4B column. Laboratory-synthesized affinity gels were also applied for the analysis of the serum hBChE. In order to analyze hBChE present in serum, a new strategy was developed in this chapter. An on-bead digestion protocol was developed in the study. The new assay was based on the combination of affinity chromatography with LC/MS. In brief, affinity beads synthesized in our laboratory were used to isolate BChE from serum. The enriched BChE bound on the affinity beads was further subjected to trypsin digestion. The tryptic digest was subsequently analyzed using LC/MS/MS. Collision induced dissociation (CID) was applied to analyze peptide of interest generated from a tryptic digest of hBChE. Our results clearly demonstrated that procainamide-Sepharose 4B was a powerful tool for the isolation of both intact and inhibited BChE from human serum.

EXPERIMENTAL

Materials

Frozen human serum was obtained from cognitively normal control subjects through the neuropathology core of the University of Kentucky Alzheimer's Disease Center (ADC), Lexington, KY, using UK Institutional Review Board (IRB) approved protocols. The serum was diluted to 10 times the original volume with 0.10 M NaCl / 50 mM-sodium phosphate buffer, pH 8.0. Butyrylthiocholine iodide (BTCh), 5, 5'-dithiobis-(2-nitrobenzoic acid) (DTNB), procainamide hydrochloride, 1-(3-dimethyl-aminopropyl)-3-ethylcarbodi-imide hydrochloride (EDC), CNBr and 6-aminohexanoic acid were purchased from Sigma Chemical Co. (ST. Louis, MO). Sequencing grade modified porcine trypsin was purchased from Promega Corporation (Madison, WI).

Preparation of Affinity Gels

Procainamide-Sepharose 4B affinity gel was synthesized in three steps as described by Cuatrecasas and Anfinsen (78). The washed and settled Sepharose-4B beads (10 ml) were activated with 2.5 g CNBr for 30 min at pH 11 to produce CNBr-activated beads. After reaction, 1 mg beads were washed with acetone and dried by Speed Vacuum concentrator. IR spectra (KBr) of dried beads were determined. 6-Aminohexanoic acid, 0.1416 g dissolved in 8 ml 0.2 M Na₂CO₃ buffer pH 9.29, was added to the washed CNBr-activated beads and gently stirred at 4 °C overnight. As such, CH-Sepharose 4B was produced, and IR spectra (KBr) of 1 mg such dried beads were obtained. CH-Sepharose 4B beads (5 ml) were re-suspended in 5 ml 1M HCl pH 4.5. Procainamide (2.72 g) dissolved in 5 ml 1M HCl pH 4.5 was added to the former suspension. EDC was added dropwise as an aqueous solution to a final concentration of 0.1 M. The mixture was rotated overnight at room temperature. The total amount of procainamide bound to beads was determined through measuring the free procainamide in the washing solutions based on the extinction coefficient of 16,900 M⁻¹ cm⁻¹ at 278 nm.

Affinity Isolation

Settled affinity gels (27 µl) were incubated in diluted serum, 100 µl serum diluted to 1 ml with 0.10 M NaCl / 50 mM-sodium phosphate buffer, pH 8.0, for 4 h at 4 °C. After incubation with serum, beads were washed with 10 ml buffer A (20 mM phosphate, 1 mM EDTA, pH 6.9), followed by 10 ml of 0.10 M NaCl in buffer A, further washed with 10 ml 0.15 M NaCl in buffer A, and finally equilibrated with 5 ml 25 mM NH₄HCO₃.

Evaluation of Affinity Gels

The same bead incubation procedure was used as described above. BChE activities of the diluted serum before and after incubation with affinity beads (modified beads) or original beads (unmodified beads) were detected and compared.

hBChE Activity

The same procedure was used to measure hBChE activity in diluted serum as described in Experimental Section of Part I, Chapter 2.

The procedure for direct measurement of the bound hBChE activity on beads is as follows. Beads suspended in solution of 50% glycerol in water (v/v) were used for the enzyme activity measurement. The absorbance of the suspended bead solution with a mixture of BTCh (1mM) and DTNB (0.32 mM), was measured at 412 nm for the first 10 min of the reaction. Raw data were converted to the relative activity (percent) of the diluted serum before the incubation with beads.

On-bead Digestion

Affinity beads with bound proteins were incubated in 10 μ l trypsin (0.01 μ g / μ l in 25 mM NH_4HCO_3 buffer) overnight at 37 °C. The supernatants with peptides from tryptic digestion were separated from the beads, and were ready for mass spectrometric analysis.

LC-MS Analysis

HPLC separation program, C18 capillary column, and parameters of the mass spectrometer were the same as described in the Experimental Section of Part I, Chapter 3.

MALDI-TOF-MS Analysis

The sample preparation, target spotting technique and parameters of the mass spectrometer were the same as described in the Experimental Section of Part I, Chapter 2.

RESULTS AND DISCUSSION

Preparation of Affinity Beads

IR was used to confirm the first two reactions of the affinity gel synthesis (reaction of Step 1 and 2 shown in Figure 1-4-1). Beads (1 mg) after each reaction were washed with acetone and dried by Speed Vacuum concentrator. IR spectra (KBr) of dried beads were recorded (Figure 1-4-2 to 1-4-4). The following peaks, shown in the IR of CNBr-activated beads (Figure 1-4-3), but absent in the original beads (Figure 1-4-2), were: 2593.6 cm^{-1}

(C≡N), 1735 cm⁻¹ (C=N). This observation was consistent with previous study (63), that confirmed the formation of C≡N and C=N bond on the Sepharose 4B beads. The peak at 2593.6 cm⁻¹ (C≡N) shown in the IR of CNBr-activated beads (Figure 1-4-2), was absent in that of CH-Sepharose 4B beads (Figure 1-4-4). As shown in Figure 1-4-4, a peak at 3400 cm⁻¹ in the IR of CH-Sepharose 4B beads suggested the –COOH groups bound on beads, which indicated that the 6-aminohexanoic acid was attached to the CNBr-activated beads.

The total amount of procainamide bound to beads was determined through measuring the unbound procainamide in the washing solutions based on the extinction coefficient of 16,900 M⁻¹ cm⁻¹ at 278 nm. The yield of the affinity gels was of 12.7 μmol procainamide / ml of the swollen beads.

Evaluation of Affinity Isolation

Equal volume of settled affinity beads (synthesized in laboratory) and original beads were incubated in the same diluted serum. hBChE activity was measured (see Experimental section) at 412 nm. Slopes of the line resulting from the plot of absorbance vs time, were obtained. Table 1-4-1 summarized all of the slopes indicating hBChE activities from the diluted serums before and after incubation with affinity beads and original beads. Three parallel experiments were performed. After incubation with affinity beads, the percentage of hBChE left in solution was 18.1 %. However, the percentage of the remaining BChE in solution after incubation with non-modified beads was 87.8 %. Results from preliminary experiments indicated that the binding of hBChE to procainamide-Sepharose 4B beads was 6.7 times more than that to the original beads.

The specific character of the affinity beads can also be confirmed by direct measurement of the bound BChE activity on beads. Beads suspended in solution of 50% glycerol in water (v/v) were used for the enzyme activity measurement. Table 1-4-2 lists the slopes from three parallel experiments. The percentage of hBChE bound to procainamide-Sepharose 4B gels was 55.7 ± 4.7 %. However, only 1.93 ± 2.5 % was detected for the original beads. This result showed that hBChE bound to the affinity gels was about 29 times more than that bound to the original beads.

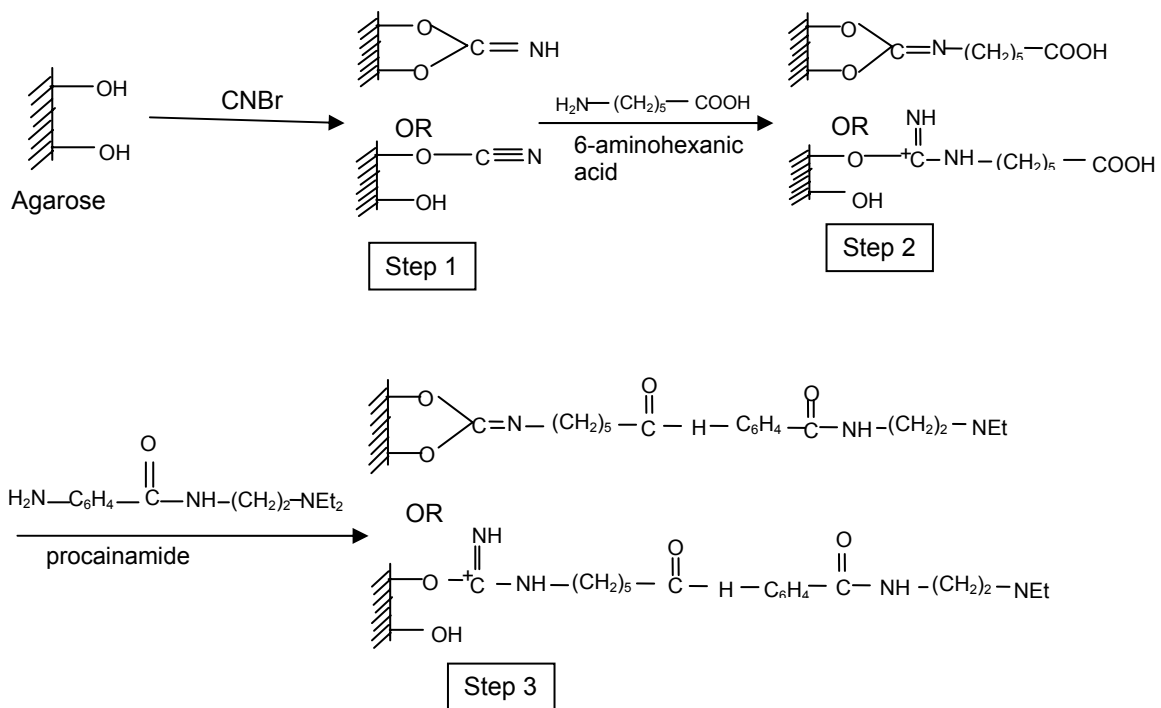


Figure 1-4-1. Activation of Sepharose by CNBr and subsequent coupling of ligand.

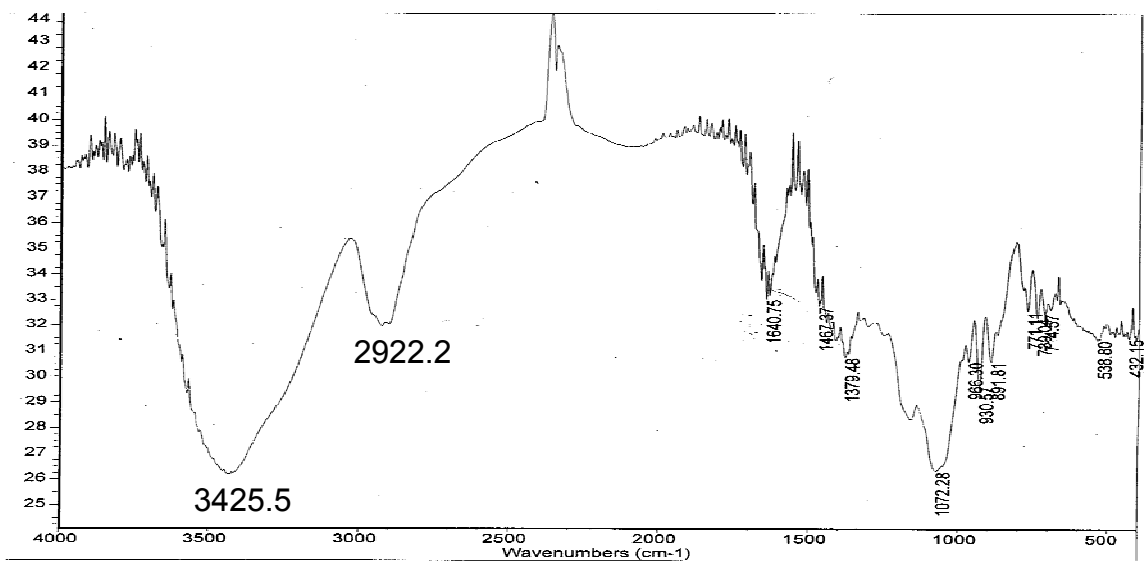


Figure 1-4-2. IR spectrum (KBr) of dried original beads (unmodified beads).

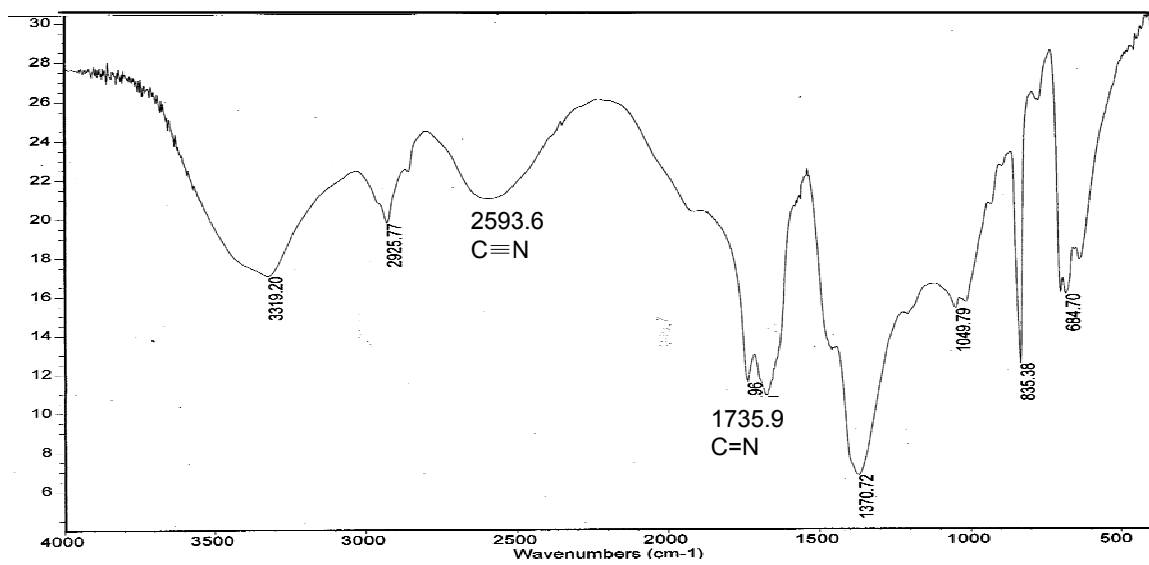


Figure 1-4-3. IR spectrum (KBr) of dried CNBr-activated beads.

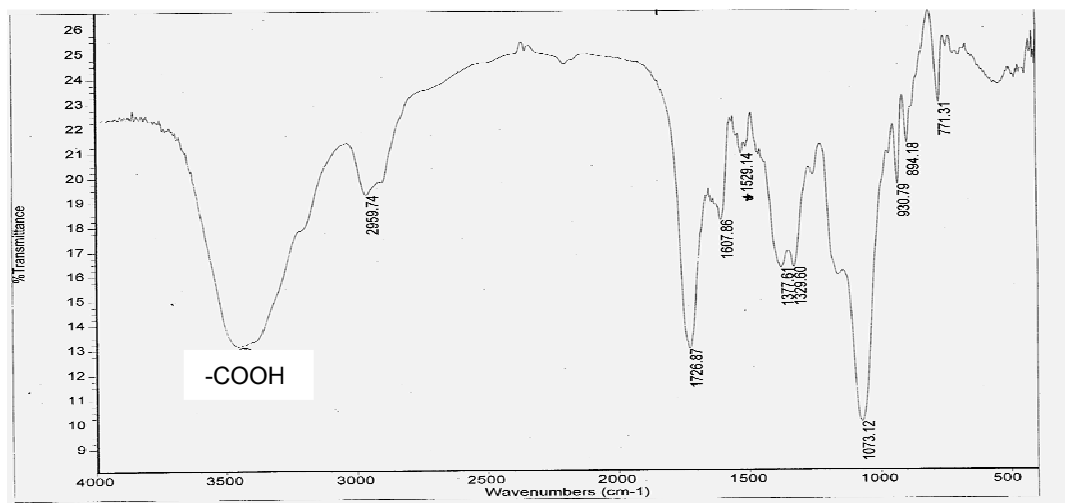


Figure 1-4-4. IR spectrum (KBr) of dried CH-Sepharose 4B beads.

Table 1-4-1. hBChE activities of the diluted serum before and after incubation with beads.

Exp.	Slope before incubation	Slope after incubation with affinity beads	% left after incubation with affinity beads	Slope after incubation with original beads	% left after incubation with original beads
1	0.2590	0.0406	15.7	0.19245	84.3
2	0.2059	0.036	17.5	0.19945	96.9
3	0.2224	0.04675	21.0	0.18305	82.3
		Ave. \pm SD	18.1 \pm 2.7	Ave. \pm SD	87.8 \pm 7.9

Table 1-4-2. hBChE activities from direct absorbance measurement on beads.

Exp.	Slope before incubation	Slope on affinity beads	% hBChE on affinity beads	Slope on original beads	% hBChE on original beads
1	0.2590	0.1307	50.4	0.013	4.9
2	0.2059	0.1219	59.2	0.001	0.5
3	0.2224	0.1276	57.4	0.001	0.4
		Ave. \pm SD	55.7 \pm 4.7	Ave. \pm SD	1.9 \pm 1.5

The big difference between the two measurements was because the light was diffracted by the suspended beads during the absorbance measurements. We suggested that the activity measurement in solution was more reliable than the measurement direct on beads. Despite the difference, both measurements proved that affinity beads (synthesized in laboratory) were able to enrich hBChE from the serum.

LC/MS/MS Analysis

The procainamide-Sepharose 4B gels facilitated the enrichment of hBChE in the presence of the other serum proteins. However, the high concentration of albumin and immunoglobulins in the serum increased the amount of nonspecific binding to the affinity beads, and increased the number of proteins subjected to proteolytic digestion. Consequently, a much more complex peptide mixture, generated from these non-specific binding proteins, made it more difficult to detect the peptide of interest from hBChE. In order to reduce non-specific binding of serum proteins, high concentrations of salt were used to wash the affinity beads (see Experimental Section).

After the stringent washing steps, the entire isolated protein complex was digested with trypsin while still bound on the affinity beads. The resulting digest was then subjected to LC/MS/MS analysis. The presence of hBChE was confirmed by the collision-induced dissociation (CID) of a selected ion MH^+ at m/z 2282.5⁺, which represents a tryptic peptide of hBChE. The sequence of the ion was AILQSGSFNAPWAVTSLYEAR (calculated average mass 2281.2). So, doubly charged ions at m/z 1141²⁺ were isolated and fragmented in the ion trap with the presence of other abundant peptides. Figure 1-4-5 shows the IC of 1141²⁺ from a trypsin digest of hBChE and the tandem mass spectrum of this selected peptide using the LC/MS/MS method.

The presence of hBChE on beads was also confirmed by the detection of the tryptic active-site peptide at m/z 2928.5, the sequence of which was SVTLFGESSAGAASVSLHLLSPGSHSLFTR (the catalytic serine is underlined). Figure 1-4-6 shows the RIC and tandem mass spectrum of 1464²⁺ from on-bead tryptic digest of hBChE using LC/MS/MS method. The poor MS/MS spectrum of the selected ion was because it was out of mass detection limit of the ion trap, which was less than 2000 Da.

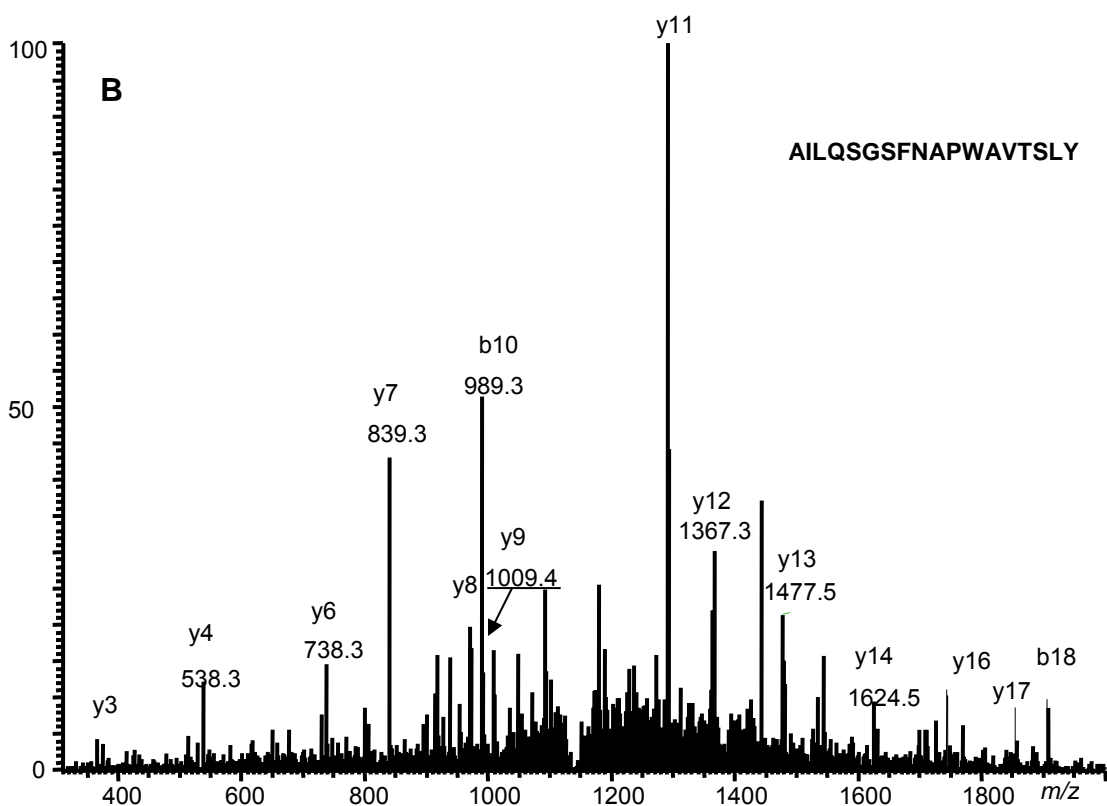
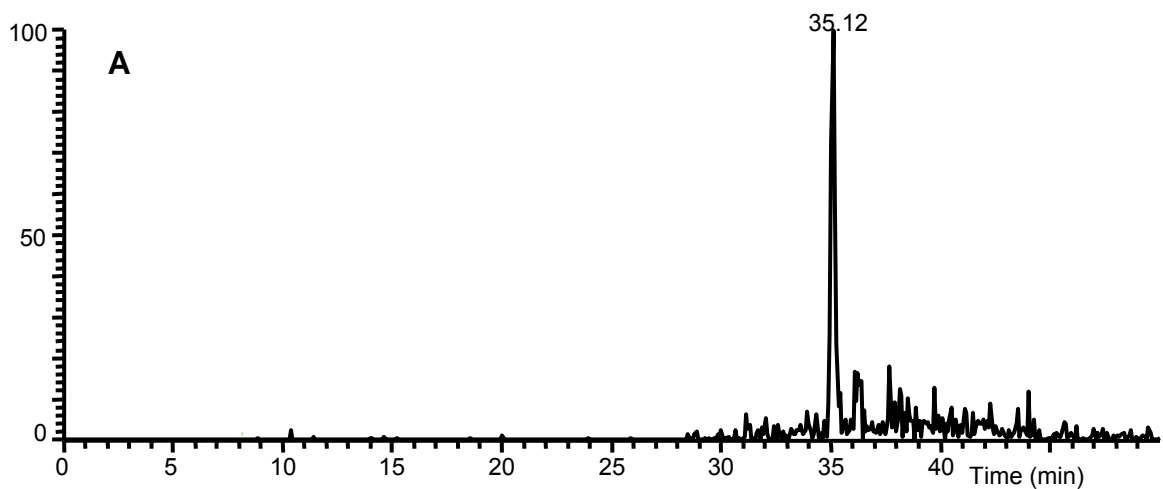


Figure 1-4-5. (A) RIC of the selected peptide (MH^{2+} at m/z 1141 $^{2+}$) for collision-induced dissociation of LC/MS/MS analysis from tryptic digest of hBChE. (B) Product ion spectrum of the selected peptide ion, the sequence of which was AILQSGSFNAPWAVTSLY^{EAR}.

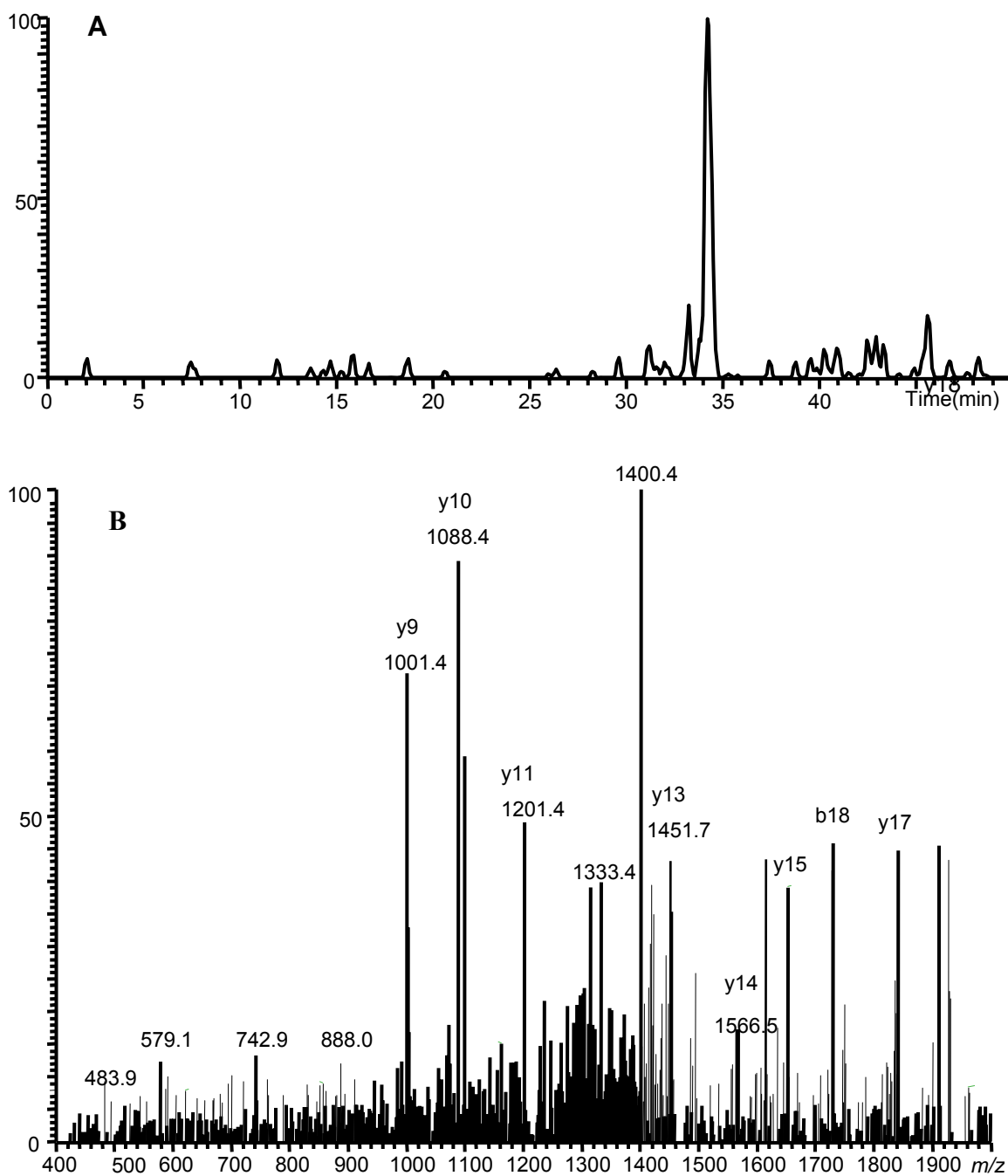


Figure 1-4-6. (A) RIC of the selected peptide (MH^{2+} at m/z 1464 $^{+2}$) for collision-induced dissociation of LC/MS/MS analysis from tryptic digest of hBChE. (B) Product ion spectrum of the selected singly charged peptide, the sequence of which was SVTLFGESAGAAASVSLHLLSPGSHSLFTR (the catalytic serine is underlined).

In order to prove that procainamide-Sepharose 4B beads are able to isolate inhibited BChE, eBChE was used. Since an ion trap cannot detect ions higher than 2000 Da, it is unsuitable to detect the inhibited active site peptide by ethyl paraoxon (calculated MH^+ at m/z 3096⁺) from a tryptic digest of hBChE. The modified peptide by ethyl paraoxon (calculated MH^+ m/z 2368⁺) generated from a tryptic digest of eBChE is much smaller than that from hBChE (calculated MH^+ at m/z 3096⁺). Therefore, the inhibited eBChE by ethyl paraoxon was used to evaluate the enrichment ability of the inhibited enzyme. Figure 1-4-7 shows the RIC and MS/MS of this selected ion at m/z 1185²⁺ from a tryptic on-bead digest of inhibited eBChE. The results clearly showed that procainamide-Sepharose 4B beads were able to isolate inhibited eBChE.

From the above discussion, tandem mass spectrum of the active site peptide generated from the tryptic digest of eBChE was better than that from hBChE. Two reasons are responsible for this phenomenon. First, the tryptic active-site peptide (calculated MH^+ at m/z 2200.5) from eBChE is smaller than that (calculated MH^+ at m/z 2928.5) from hBChE. Furthermore, the performance of procainamide-Sepharose 4B gels at retaining BChE from native human serum is worse than that from eBChE (52).

MALDI-TOF-MS analysis

The enrichment of the active and inhibited hBChE for procainamide-Sepharose 4B beads was also proved by MALDI-TOF-MS analysis. Figure 1-4-8 A shows the MALDI spectrum of the tryptic on-bead digest of the enriched hBChE. After serum was incubated with carbaryl, the inhibited hBChE was enriched on the affinity beads. Then, the isolated hBChE bound on the beads was subjected to trypsin digestion. The resulting tryptic digest was analyzed using MALDI-TOF-MS technique. The peak at m/z 2985.5 corresponded to the modified active site peptide with carbamate group $CH_3NHC(O)$ (Figure 1-4-8B). Although there is no detection mass limit for MALDI-TOF, low responses of both the active site peptide and the modified active site peptide of hBChE were observed. The suppression of the peptide of interest, resulting from the presence of the other peptides, was responsible for the low detection signal. Despite the low detection response, data shown here demonstrate that procainamide-Sepharose 4B gels were able to isolate the intact hBChE, as well as to isolate the inhibited hBChE.

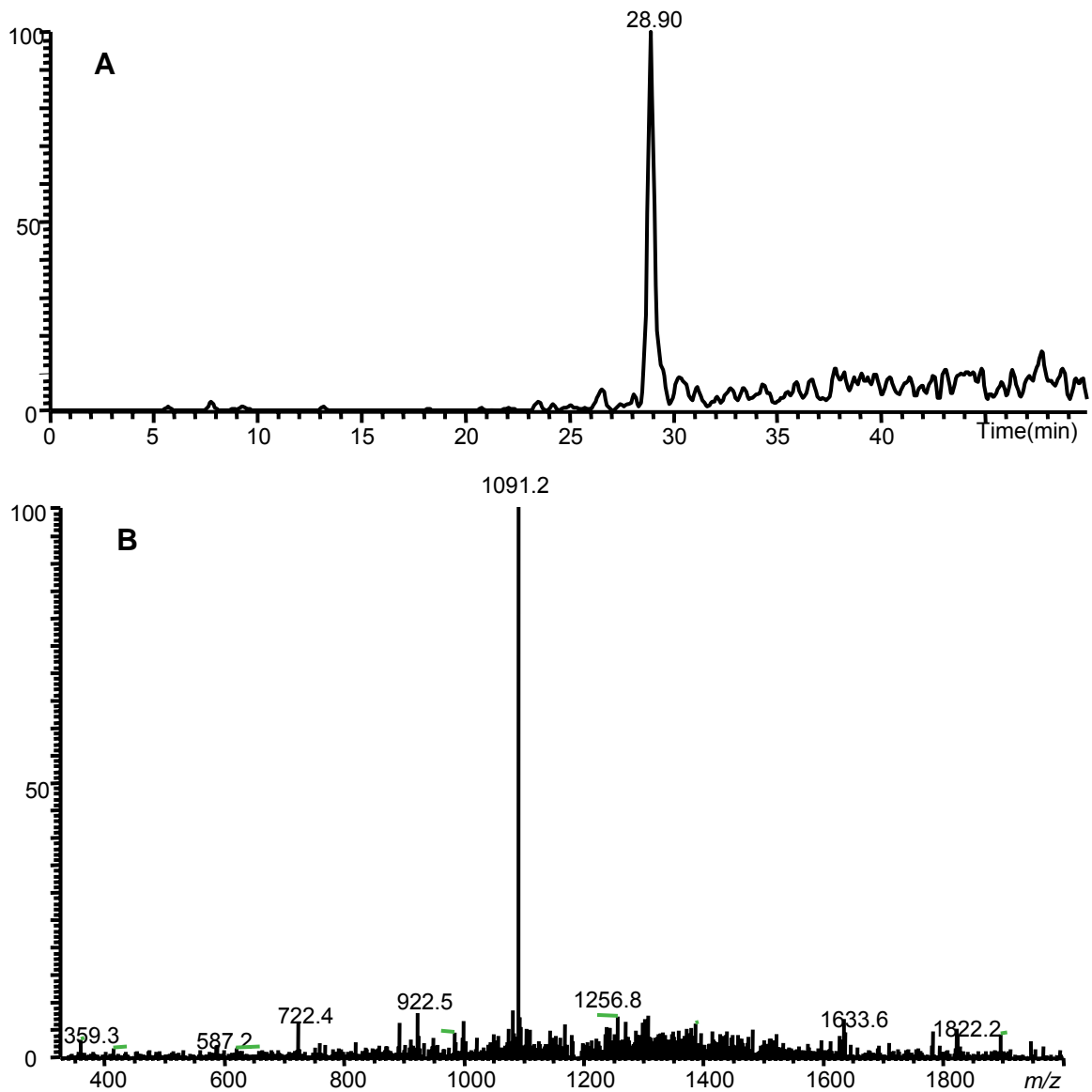


Figure 1-4-7. (A) IC of the selected peptide (MH^{2+} at m/z 1185 $^{2+}$) for collision-induced dissociation of LC/MS/MS analysis from tryptic digest of eBChE. (B) Product ion spectrum of the selected singly charged peptide, where 1091 $^{2+}$ corresponds to the inhibited peptide with loss of O-ethyl phenyl phosphoric acid.

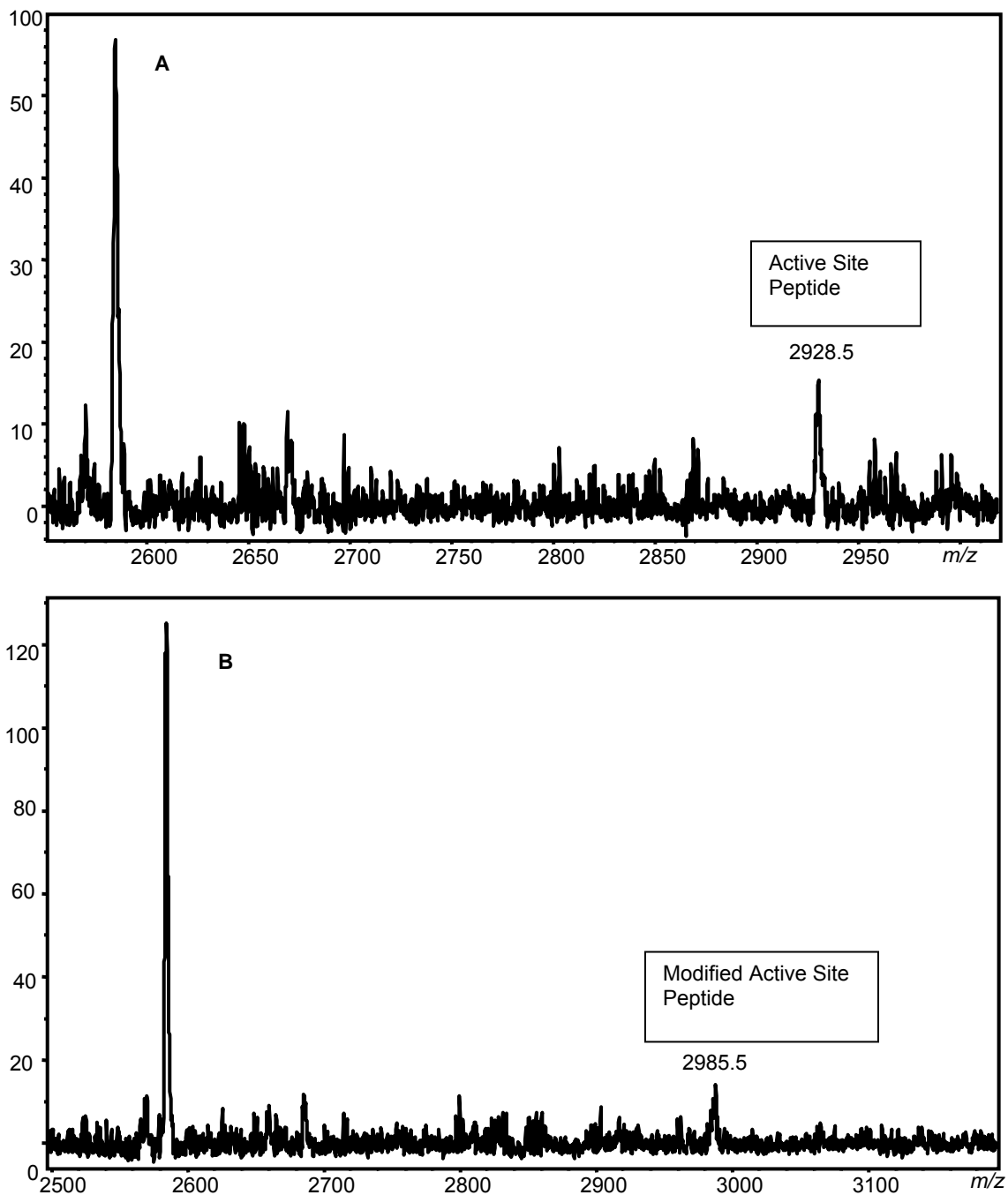


Figure 1-4-8. Representative MALDI-TOF-MS spectra of control (A) and tryptic digests of hBChE treated with carbaryl (B). Labeled peaks with average mass correspond to the presence of unmodified and modified active site peptides. The peak at m/z 2985.5 corresponds to the active site peptide modified with carbamylation group ($\text{CH}_3\text{NHC}(\text{O})$).

CONCLUSION

Affinity beads were successfully synthesized in the laboratory. The specific character of the affinity beads was proven by the hBChE activity measurement in the diluted human serum before and after incubation with affinity beads. Results demonstrated that the procainamide-Sepharose 4B beads enriched BChE at least 6.7 times more than the original beads. The specific enrichment for both intact and inhibited BChE was proven by both LC/MS/MS and MALDI-TOF-MS analysis. Our results confirmed that procainamide-Sepharose 4B was a powerful technique for isolation of both intact and inhibited BChE from human serum. The phosphorylated and carbamylated peptides were successfully detected, which indicated that the developed method was not only useful for the analysis of OP exposure, but also useful for the analysis of CB exposure. The developed method was based on the combination of the affinity chromatography and mass spectrometry. Furthermore, the detection of tryptic active site peptide of both hBChE and eBChE indicated that the on-bead digestion protocol worked efficiently.

Although the developed method was successfully applied to the detection of a small amount of BChE in human serum, the detection signal was much less than expected for both LC/MS/MS and MALDI-TOF-MS techniques. A noteworthy limitation of MALDI as described in Chapter 5, LC/MS/MS is a better choice for the hBChE analysis in human serum. However, a low detection signal was observed for LC/MS/MS techniques in this Chapter, because the tryptic active-site peptide was out of the detection mass range of the ion trap. A new digestion method is required to produce a suitable size of peptide containing the active-site serine of hBChE, which will be the next step in the analysis of hBChE inhibition in real sample, as described in Chapter 5.

CHAPTER FIVE

ANALYSIS OF HUMAN BUTYRYLCHOLINESTERASE EXPOSED TO ORGANOPHOSPHATES AND CARBAMATES IN SERUM WITH A COMBINATION OF AFFINITY CHROMATOGRAPHY AND MASS SPECTROMETRY

INTRODUCTION

There is an increasing concern over the extensive use of pesticides, such as OPs and CBs, in the agricultural and other industries. The concern is based on the fact that OPs and CBs cause the inhibition of key synaptic enzymes, including AChE. Some OPs are in the form of chemical warfare (CW) agents, two of which, sarin and VX, were involved in the 1995 Tokyo subway terrorist attack (79). With the increasing terrorism and the escalating use of CW agents in the battlefield like the Iran-Iraq conflict, the healthcare systems for both military and civilians require a sensitive and reliable monitoring program for detection of pesticide exposure. While most OPs and CBs are not extremely neurotoxic, investigation of their cholinesterase inhibition can provide insight into human exposure to these classes of compounds. In this chapter, a method is described for the identification and quantification of OP and CB exposure in serum, with a combination of affinity chromatography and LC/MS/MS.

The interest in hBChE as a bioscavenger of OPs and CBs is increasing because of the extensive use of these chemicals. The rising concern in hBChE study is also because chemical warfare (CW) agents (80) are used by terrorists based on their properties of the mass destruction and low costs. OPs (including CW agents) and CBs exert their inhibitory action by forming a covalent bond with the active site serine of BChE in a highly reactive mode. Therefore, the cholinesterase inhibitors scavenged by BChE are unavailable for further reaction with AChE, which is present in the nervous system and is much more important than BChE. Although its true physiological function remains undetermined, BChE is of pharmacological and toxicological importance. A major clinical application of inhibited plasma BChE analysis is to detect OP and CB exposure.

Fidder et al. (60) published a method for the analysis of human serum samples from the victims in the 1995 Tokyo subway terrorism. The Fidder method is based on the detection of nonapeptides obtained from pepsin digests of hBChE. Pepsin is known as a nonspecific protease, which cleaves proteins more or less randomly. The use of Fidder method is limited due to the poor reproducible pepsin digestion. In addition, synthesized phosphorylated peptide is used for the quantification of inhibited hBChE. The radioactive-phosphorylated peptide is synthesized using F-moc chemistry, which is time consuming, requires a lot of chemical techniques, and needs a specialist for handling the radioactive reagents. Furthermore, isolation of hBChE from serum involves multiple steps: elution of proteins from the procainamide affinity column followed by heating the fractions containing hBChE; digest filtered proteins on the filter; wash of peptides from filters, and concentration of digested solution before LC/MS/MS analysis. It is known that this multi-step procedure results in a low recovery due to lose of analyte during processing.

In this chapter, a novel improved procedure was developed for the analysis of hBChE inhibition that has overcome all of the limitations of the Fidder method. Although our method was also based on the analysis of the modified active site peptide of the inhibited hBChE using electrospray tandem mass spectrometry, the improved methodology provided higher sensitivity and reproducibility than the Fidder method. We developed a new digestion method called 'double digestion', which incorporated a trypsin digestion followed by a protease V8 digestion. A compatible size of the active site peptide with LC/MS/MS was produced from the double digestion, which gave a reproducible digest. The sequence of the intact active site peptide generated from double digestion is SAGAASVSLHLLSPGSHSLFTR (average mass 2195.2), where the active site serine is underlined. Results clearly show that double digestion works as efficiently as trypsin digestion. An on-bead digestion was also developed here to minimize the analyte loss during the sample preparation. In addition, a calibration system was constructed based on the detection of modified active site peptides *in vitro* using LC/MS/MS technique. The developed calibration system was applied to analyze the hBChE inhibition in serum sample. Furthermore, results demonstrated that the improved methodology was applicable for the detection and quantification of multiple pesticide exposure.

EXPERIMENTAL

Chemicals

Highly purified hBChE (EC 3.1.1.8) was a kind gift of Dr. Oksana Lockridge, University of Nebraska Medical Center (Nebraska, USA). This hBChE was provided as 2790 units/ml buffer (10 mM potassium phosphate, 0.15 M NaCl, 0.02% sodium azide). Slide-A-Lyzer Dialysis Cassettes purchased from Pierce (Rockford, IL) were used to remove salts from the former solution. The desalted hBChE solution was collected and dried by Speed Vacuum concentrator, and the residue was dissolved in ammonium bicarbonate buffer (pH=7.8). The concentration of hBChE was determined by the enzyme activity measurement. Frozen human serum was obtained from cognitively normal control subjects through the neuropathology core of the University of Kentucky Alzheimer's Disease Center (ADC), Lexington, KY, using UK Institutional Review Board (IRB) approved protocols. The serum was diluted to 10 times the original serum volume with 0.10 M NaCl/50 mM-sodium phosphate buffer, pH 8.0. Butyrylthiocholine iodide (BTCh), 5,5'-dithiobis-(2-nitrobenzoic acid) (DTNB) EPN, ethyl paraoxon and carbaryl were used as described in Experimental Section of Part I, Chapter 2. Sequencing grade modified porcine trypsin was purchased from Promega Corporation (Madison, WI). Sequencing grade protease V8 from *Staphylococcus aureus* V8 was purchased from Roche (Indianapolis, IN). The synthesized procainamide affinity beads (Chapter 4) were used for the study in this chapter.

Instrumentation

Electrospray LC/MS/MS Analysis

All mass spectrometric experiments were conducted on a mass spectrometer (Finnigan LCQ) equipped with a standard electrospray interface. Digested hBChE (5 μ l, about 2 μ g) was injected into a capillary column. HPLC separation program, C18 capillary column, and parameters of the mass spectrometer were the same as described in the Experimental Section of Part I, Chapter 3.

MALDI-TOF-MS Analysis

The sample preparation, target spotting technique and parameters of the mass spectrometer were the same as described in the Experimental Section of Part I, Chapter 2.

hBChE Inhibition

hBChE (316 units) was dissolved in 1ml 50 mM ammonium bicarbonate buffer (pH=7.8), and incubated with OPs or carbaryl (dissolved in methanol) at 37 °C for 1 h or 30 min, respectively. The final concentration of methanol was less than 0.05% (v/v) and did not significantly affect enzyme activity.

hBChE Activity

hBChE activity was measured using the Ellman assay (56). Briefly, the absorbance of the solution, containing hBChE with a mixture of BTCh (1 mM) and DTNB (0.32 mM), was measured at 412 nm for the first 10 min of the reaction.

Double Digestion

Tryptic digestion was performed in 40% ACN with a 20:1 excess of hBChE to trypsin. hBChE (10 µl of 316 units/ml solution) was subjected to trypsin digestion for each experiment. The digest was performed in a 50 mM ammonium bicarbonate buffer (pH=7.8) at 37 °C overnight. Half of the tryptic digest was terminated by formic acid and analyzed using MALDI-TOF-MS. The remaining 5 µl of hBChE solution continued to be incubated with a 20:1 excess of hBChE to protease V8 for 24 h at 25 °C. Formic acid was used to terminate the double digestion. The resulting digest was analyzed using MALDI-TOF-MS and LC/MS/MS techniques.

Procedure for Analysis of hBChE Inhibition in Serum

A schematic of the procedure for analysis of hBChE inhibition is shown in Figure 1-5-1. In brief, 100 µl of serum sample was incubated with carbaryl for 30 min as described by Rao et al. (71)), or with OPs for 1 h as described by Doorn et al. (58, 59). After reaction, the serum sample was diluted with 1000 µl of 0.1 M NaCl in 50 mM phosphate buffer (pH 8) to reduce the non-specific protein binding on the affinity beads. The settled affinity beads (50 µl) were incubated with the diluted serum sample for 4 h at 4 °C to ensure complete reaction of hBChE with procainamide-Sepharose 4B beads as described by Ralston et al. (52). After incubation, the diluted serum solution was removed, and affinity beads were washed with 10 ml buffer A (20 mM phosphate, 1 mM EDTA, pH 6.9), followed by 10 ml 0.10 M NaCl in buffer A, and further washed with 10 ml 0.15 M NaCl in

buffer A, and finally equilibrated with 5 ml 25 mM NH_4HCO_3 (pH 7.8). After the washing solution was removed, the remaining affinity beads with bound proteins were incubated with 10 μl of 0.01 $\mu\text{g} / \mu\text{l}$ trypsin in 25 mM NH_4HCO_3 for 24 h at 37 °C. Sequentially, 0.13 μg protease V8 was added and incubated for 24 h at 25 °C. Supernatants with peptides from double digestion were separated from beads, and were ready for mass spectrometric analysis.

RESULTS

Identification of the Modified Peptides from Double Digestion

MALDI mass spectra for both the control and the treated sample were obtained. The modified peptides in the digests of inhibited hBChE, after double digestion, were determined by comparing the mass spectra before and after treatment. Figure 1-5-2 and Figure 1-5-3 show the mass spectra of a control sample and a sample treated by OPs and carbaryl. The peak at m/z 2253.2 was identified as a carbamylated peptide, since it is present in the mass spectrum of the treated sample (Figure 1-5-2 B), but absent in the control sample (Figure 1-5-2 A). However, peaks at m/z 2196.2 corresponding to the intact active site peptide appear in both control and treated sample.

Modified peptides by ethyl paraoxon (Figure 1-5-3 A) and EPN oxon (Figure 1-5-3 B) were also determined using the same approach. Peaks with average masses, which correspond to the modified and intact active peptides, were observed in mass spectra generated from the digest of the inhibited hBChE after double digestion. Table 1-5-1 summarizes the observed peaks with average masses of MH^+ , corresponding to the intact and modified active site peptide of hBChE treated with 5 μM pesticides. Modified groups were determined based on the mass differences (Table 1-5-1) between the modified peptide and the intact active site peptide. For instance, the modified group for carbaryl was determined as carbamate ($\text{O}=\text{C}-\text{NHCH}_3$, 58 Da), which is based on the mass difference of the modified peptide (average m/z at 2253.2) and intact active site peptide (average m/z at 2196.2). This mass difference takes into account the proton loss on the catalytic serine during the carbamylation reaction. Using the same approach, the modified group from ethyl paraoxon was determined as O,O-diethyl phosphate, which corresponded to the

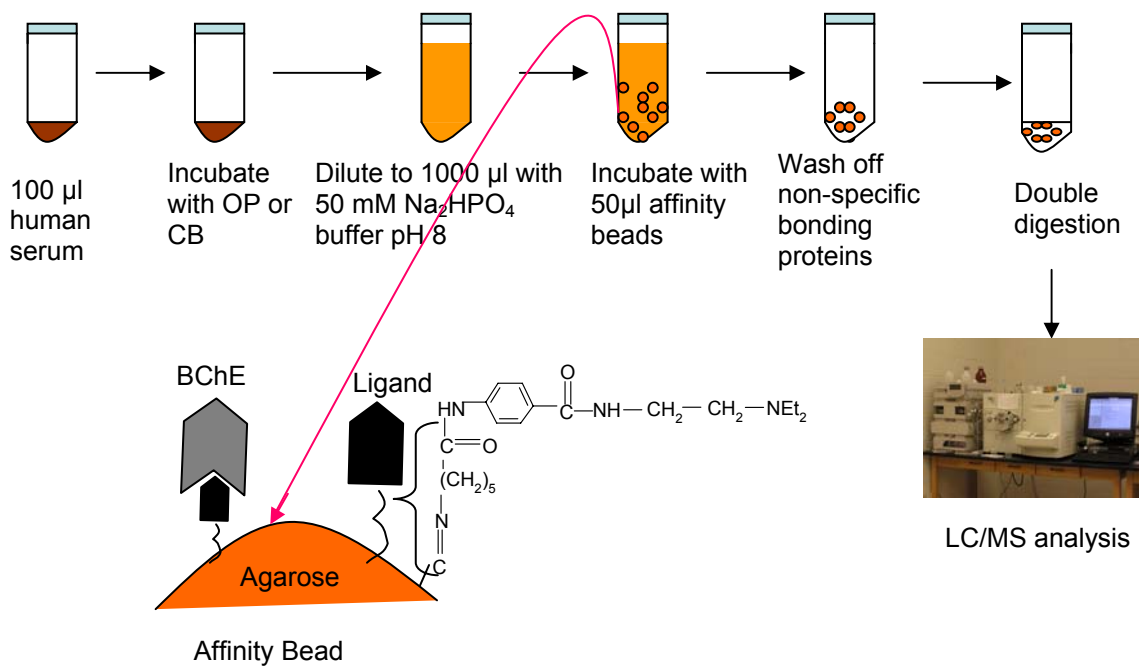


Figure 1-5-1. Schematic of the procedure for the analysis of hBChE inhibition in serum matrix.

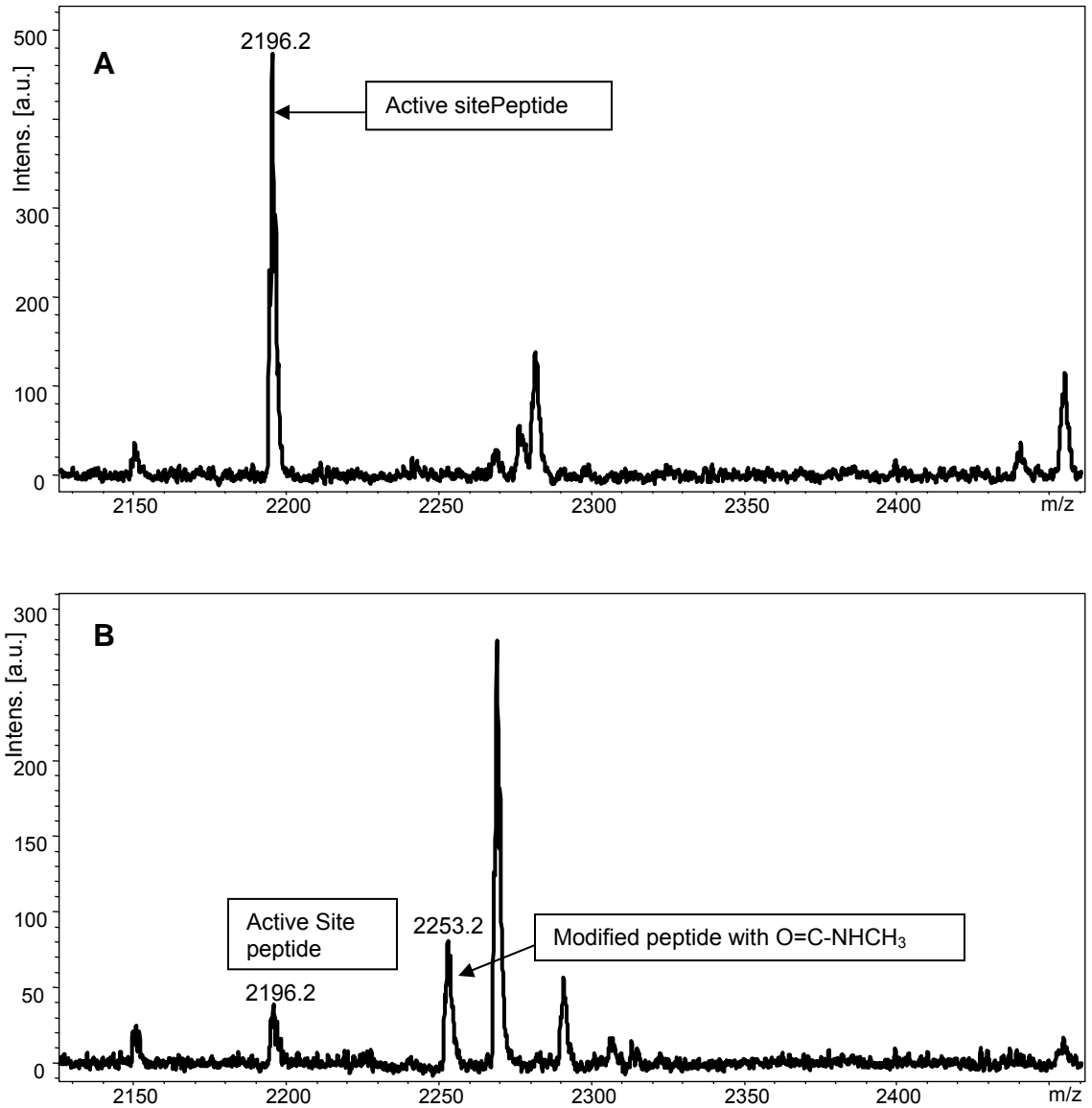


Figure 1-5-2. MALDI-TOF-MS spectra of the digest of hBChE after double digestion control (A), carbamyl treated sample (B). Peak at m/z 2253.2 corresponds to the modified active site peptide with carbamylated group.

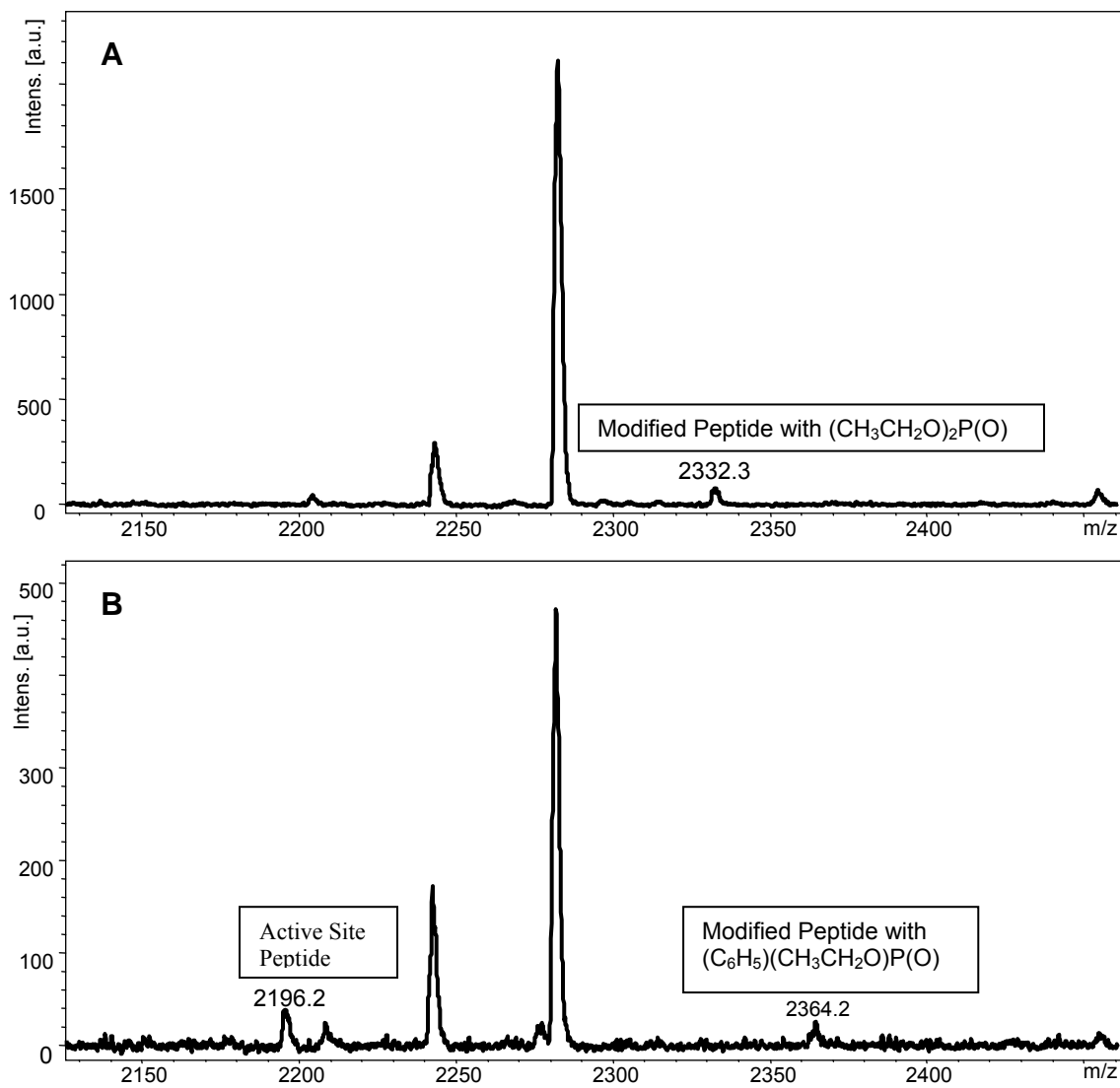


Figure 1-5-3. MALDI-TOF-MS spectra of the hBChE digest after double digestion, which was inhibited by ethyl paraoxon (A), by EPN oxon (B). Labeled peaks display the average masses of peptides. Peaks at m/z 2332.3, and 2364.2 correspond to the modified active site peptide with O,O-diethyl phosphate, and O-ethyl phenyl phosphate, respectively.

modified peptide at m/z 2332.5. Similarly, the modified group from EPN oxon was identified as O-ethyl phenyl phosphate, which corresponded to the modified peptide at m/z 2364.2.

LC/MS/MS Analysis to Identify the Amino Acid Sequence of Modified Peptides

MS/MS was used to further confirm intact peptide and modified peptides generated from the digests of inhibited hBChE after double digestion. The amino acid sequence of carbamylated peptide was identified as (S-carbamate)AGAASVSLHLLSPGSHSLFTR using MS/MS (MH^{3+} at m/z 751.7³⁺ Figure 1-5-5). An identical set of y ions were observed in the tandem mass spectrum of the carbamylated peptide (Figure 1-5-5) with that of the intact peptide (Figure 1-5-4). However, b ions had 57 Da mass shifts, because they contained the active site serine with an attached carbamylated group. All the information confirmed that the triply charged precursor ion MH^{3+} at m/z 751.7³⁺ was the carbamylated peptide.

The tandem mass spectrum of phosphorylated peptides is shown in Figure 1-5-6. Although precursor ions of phosphorylated peptides were different (MH^{3+} at m/z 777.7³⁺ for ethyl paraoxon, and at m/z 788.7³⁺ for EPN oxon), they had the same tandem mass spectrum. Only one fragment ion at m/z 726.8³⁺ dominated in the MS/MS spectra of the phosphorylated peptides (Figure 1-5-6). The common fragment ion was produced by a neutral loss at the active site serine resulting in a homoalanine residue. Therefore, the phosphorylated precursor ions can be identified by the neutral loss.

In order to know the amino acid sequence of the phosphorylated peptides, the tandem mass spectrum of the product ion at m/z 726.8³⁺ was also obtained (Figure 1-5-7). All the y-ions (Figure 1-5-7) were the same as those in the tandem mass spectrum of the intact peptide (Figure 1-5-4). However, b-ions had 18 Da mass shift for singly charged ions and 9 Da mass shift for doubly charged ions, because b-ions contained active site serine. Results clearly showed that precursor ions MH^{3+} at m/z 777.7³⁺ and 788.7³⁺ were phosphorylated peptides, which corresponded to O,O-diethyl phosphorylated peptide and O-ethyl phenyl phosphorylated peptide, respectively.

Table 1-5-1. Masses of observed MH⁺ (average mass)^a for the intact and modified active site peptide of hBChE treated with 5 μM inhibitor.

Pesticide	intact	inhibited	Δm ^b	Modified with group
Carbaryl	2196.2	2253.3	57	O=C-NHCH ₃
Ethyl paraoxon	2196.2	2332.5	136	$\begin{array}{c} \text{CH}_3\text{CH}_2\text{O} \\ \text{CH}_3\text{CH}_2\text{O} \end{array} \text{P}=\text{O}$
EPN oxon	2196.2	2364.2	168	$\begin{array}{c} \text{CH}_3\text{CH}_2\text{O} \\ \text{C}_6\text{H}_5 \end{array} \text{P}=\text{O}$

^a The average mass of the modified or the intact peptide containing the catalytic serine after double digestion.

^b Difference in mass between the modified and the intact active site peak. All these mass differences takes into account the proton loss from the catalytic serine during the phosphorylation reaction.

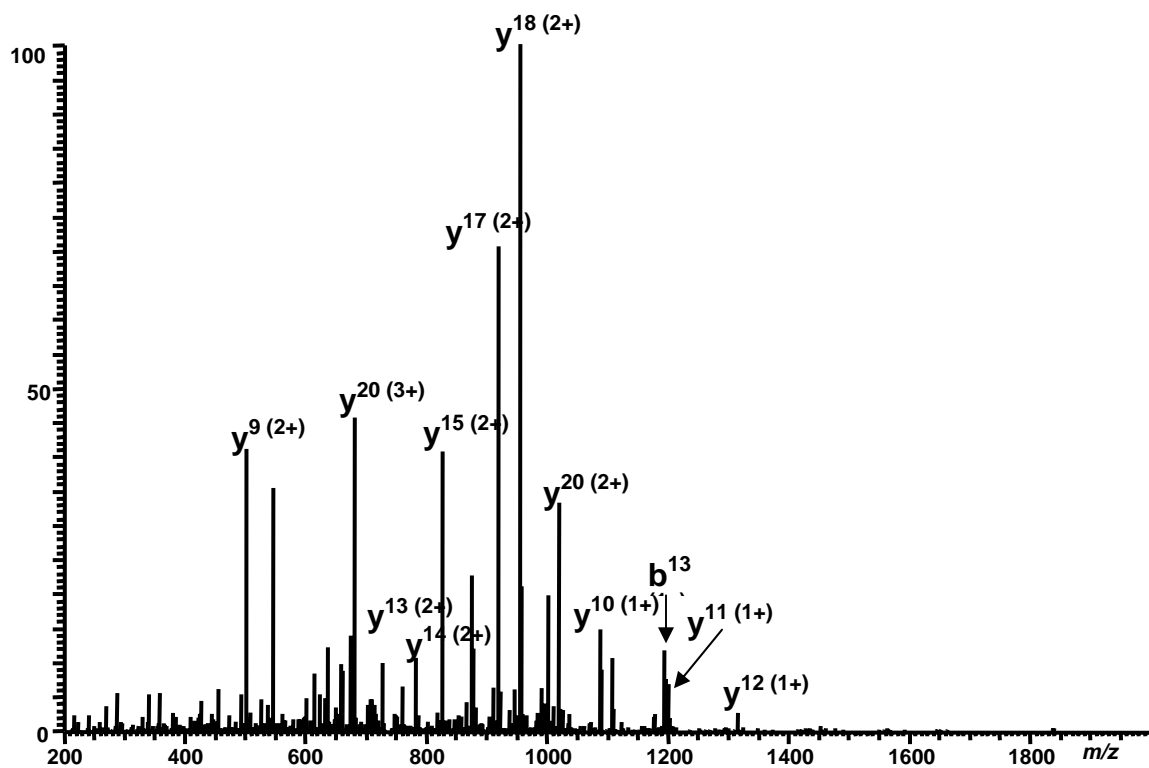


Figure 1-5-4. MS/MS of the triply charged intact active site peptide ion (MH^{3+} at m/z 732.7 $^{3+}$). The amino acid sequence of the intact active site peptide is SAGAASVSLHLLSPGSHSLFTR (numbered from right to left), where the catalytic serine is underlined.

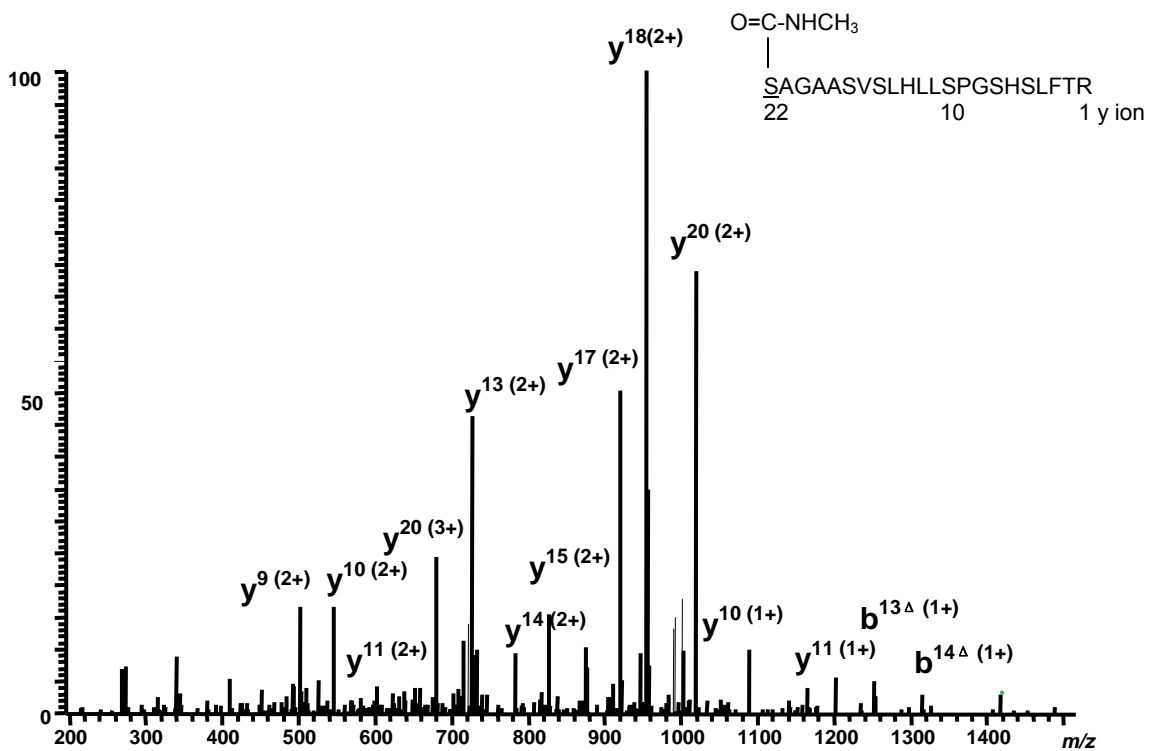


Figure 1-5-5. MS/MS of the triply charged carbamylated peptide ion (MH^{3+} at m/z 751.7 $^{3+}$). Carbamylated peptide is identified by the mass shifts of b-ions, which contain active site residue serine.

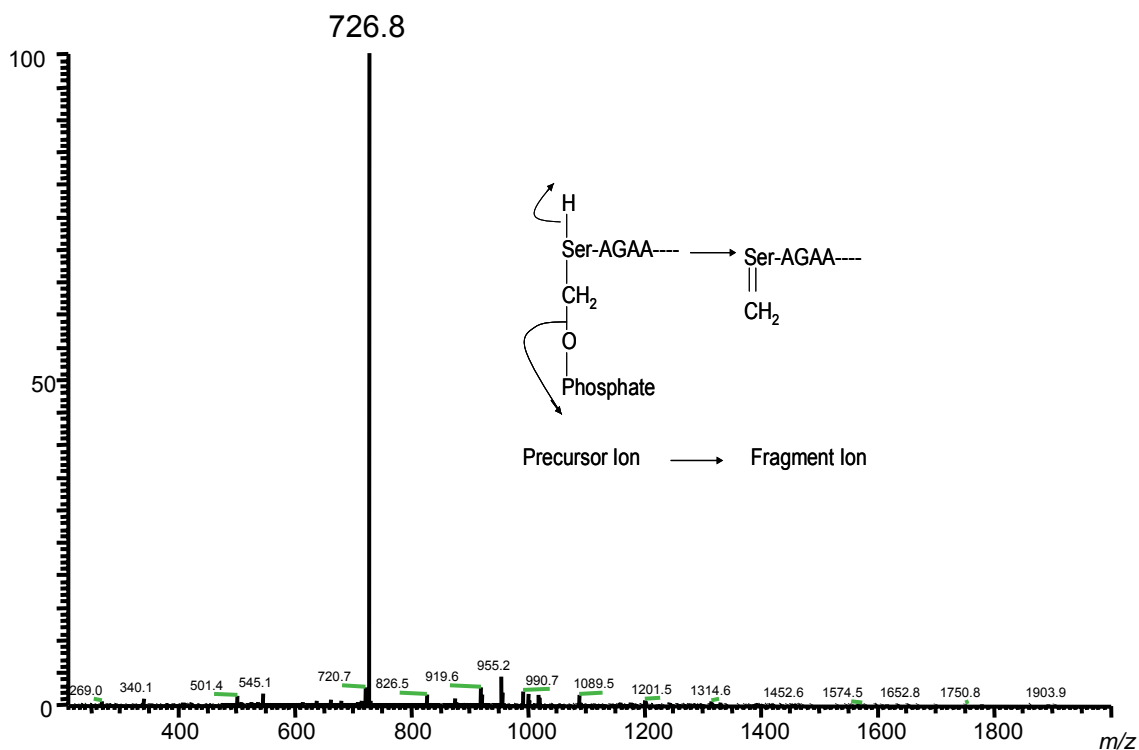


Figure 1-5-6. MS/MS of the triply charged phosphorylated peptide ions (MH^{3+} at m/z 777.7³⁺ for ethyl paraoxon and 788.7³⁺ for EPN oxon). The dominant fragment ion MH^{3+} at m/z 726.8³⁺ corresponds to the precursor ions with the loss of alky phosphoric acid. Phosphorylated peptides can be differentiated by the neutral loss from the precursor ions.

Evaluation Double Digestion using MALDI

The inhibited hBChE by carbaryl was digested with trypsin. Half of the tryptic digest of hBChE was subjected to MALDI-TOF-MS analysis. The remaining tryptic-digested hBChE was subsequently incubated with protease V8 for 24 h at 25 °C. The resulting digest was then analyzed using MALDI-TOF-MS. The intensities of both intact and carbamylated peptides were obtained from the MALDI analysis (data not shown). The total intensity of active site peptides was obtained by adding the intensity of the intact peptide and that of the modified peptide. The relative intensity ratio was the intensity of intact peptide or modified peptide divided by the total intensity. Based on these reported data, graphs of relative intensity ratio vs carbaryl concentrations were plotted for both of the hBChE digests from trypsin digestion and from double digestion (Figure 1-5-8). IC_{50} s (concentration required for 50% hBChE inhibition) and IC_{100} s (concentration required for complete hBChE inhibition) were determined from these plots (Figure 1-5-8). From trypsin digestion, IC_{50} and IC_{100} were determined as 21.00 μ M and 41.84 μ M, respectively (Figure 1-5-8 A). These values were very close to the IC_{50} and IC_{100} from double digestion, which were 20.19 and 40.60 μ M, respectively (Figure 1-5-8 B). In addition, the slopes for the intact peptide and the modified peptide were the same for both digestion methods. Therefore, it is evident that double digestion had high efficiency and reproducibility as single trypsin digestion.

Calibration System Construction using LC/MS/MS

Every digest of hBChE treated by CB and OPs, generated from double digestion, was analyzed using LC/MS/MS methodology. Peak areas of intact peptides and modified peptides were obtained from LC/MS/MS analysis (data not shown). The total peak area was calculated by adding the peak area of the intact peptide and that of the modified peptide. The relative area ratios were the peak area of intact peptide or modified peptide divided by the total peak area. Based on these reported data, the relative area ratios vs CB or OP concentrations were plotted (Figure 1-5-9 and Figure 1-5-10). A linear relationship between the relative area ratio and the pesticide concentration was observed. A calibration system for carbaryl, ethyl paraoxon, and EPN oxon was developed.

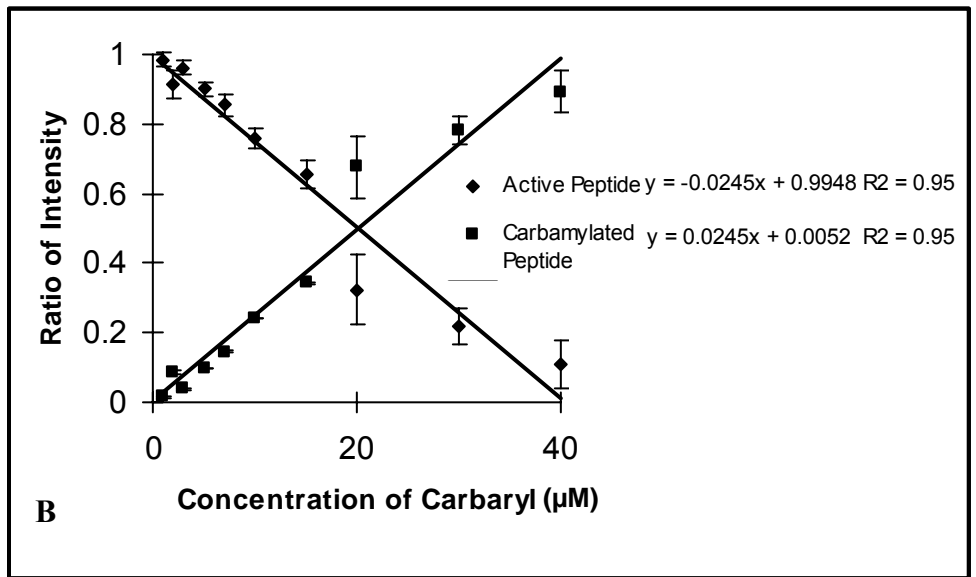
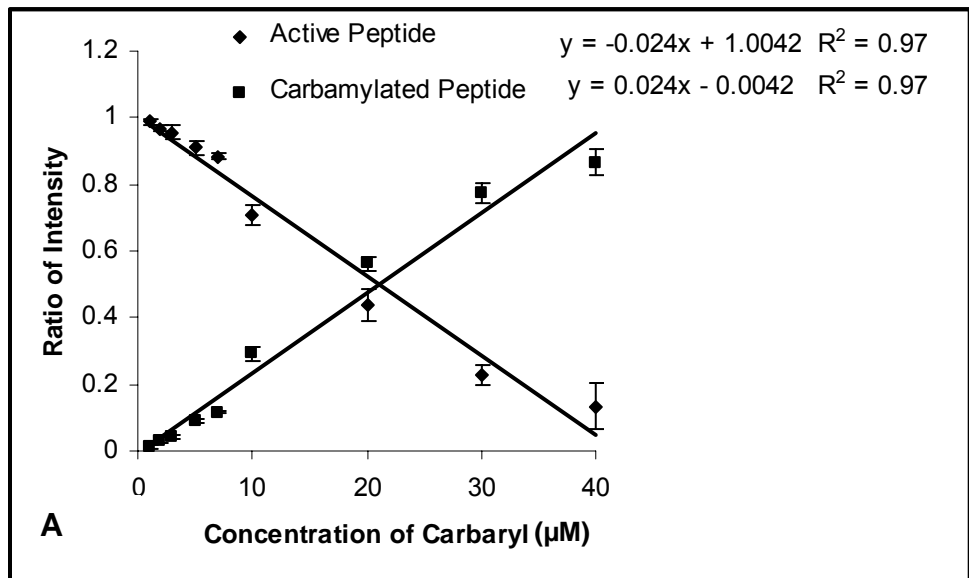


Figure 1-5-8. Plots of intensity ratios vs carbaryl concentrations (µM). Plots for trypsin digestion (A), and for double digestion (B) are from MALDI analysis.

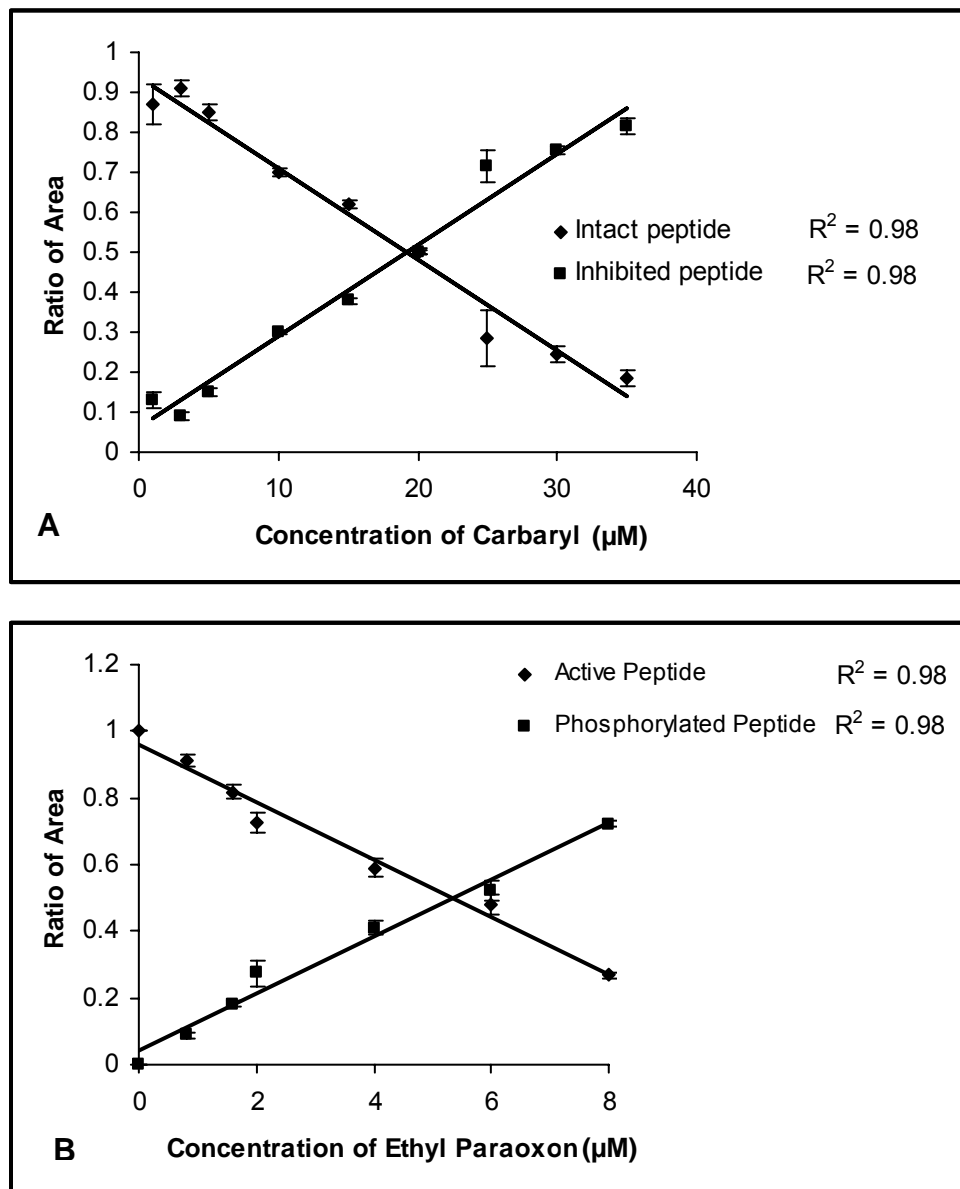


Figure 1-5-9. Plots of peak area ratios vs pesticide concentrations using LC/MS/MS. Calibration curves are for carbaryl (A) and for ethyl paraoxon (B).

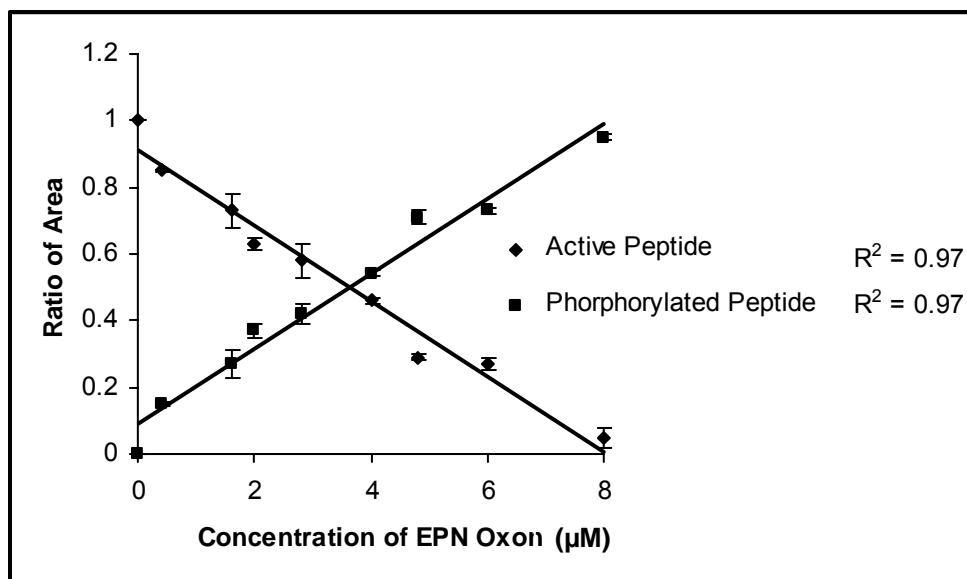


Figure 1-5-10. Plots of peak area ratios vs EPN oxon concentrations using LC/MS/MS.

Analysis of Single Pesticide Exposure

Serum was incubated with 0.2 μM carbaryl for 30 min, and with 0.1 μM ethyl paraoxon for 1h, separately. hBChE was then enriched on the affinity beads. The affinity beads with bound proteins were subjected to double digestion (see Experimental section). The resulting digests of the isolated hBChE were analyzed using LC/MS/MS technique. Triplicate analysis was performed as described above. Three triply charged precursor ions were selectively analyzed in the ion trap. Precursor ions MH^{3+} were at m/z 732.7³⁺ for intact active site peptide, 751.7³⁺ for carbamylated peptide, and 777.7³⁺ for phosphorylated peptide by ethyl paraoxon. Five main fragment ions, at m/z 680.1³⁺, 726.7²⁺, 919.7²⁺, 955.3²⁺, 1019.3²⁺, were used to monitor the precursor ions of intact active site peptide and carbamylated peptide (Figure 1-5-4 and Figure 1-5-5). A dominant fragment ion at m/z 726.8³⁺ was used to monitor the phosphorylated peptide (precursor ion) by ethyl paraoxon (Figure 1-5-6). Figure 1-5-11 demonstrates the RIC of the intact and modified active site peptides in one of the three analyses using LC/MS/MS technique. The concentrations of carbaryl and ethyl paraoxon were determined from the constructed calibration system based on the average relative area ratios of triplicate analysis. The detected concentration was $12.3 \pm 0.1 \mu\text{M}$ for carbaryl, and $6.26 \pm 0.4 \mu\text{M}$ for ethyl paraoxon from the calibration curves (Figure 1-5-11 A and B). Because hBChE concentration for calibration curves was 75 times higher than that in the serum sample, the detected concentrations needed to be normalized. The normalized concentration was $0.16 \pm 0.01 \mu\text{M}$ for carbaryl, and $0.08 \pm 0.01 \mu\text{M}$ for ethyl paraoxon, which were very close to the actual incubation concentration.

The assay was successfully performed for the analysis of pesticide exposure at a high level inhibition. We questioned the lowest limit of hBChE inhibition could be detected using the assay. To determine this, serum was incubated with EPN oxon, resulting in 5 % hBChE inhibition. The extent of hBChE inhibition was confirmed by the enzyme activity measurement (data not shown). hBChE was isolated, digested, and analyzed using affinity chromatography and LC/MS/MS techniques. Figure 1-5-12 shows the RIC of precursor ions at m/z 732.7³⁺ and 788.7³⁺ for intact peptide and modified peptide, respectively. The relative peak area ratio was 5 % for the modified peptide, which indicated that 5 % of hBChE inhibited. This result was consistent with the hBChE activity measurement.

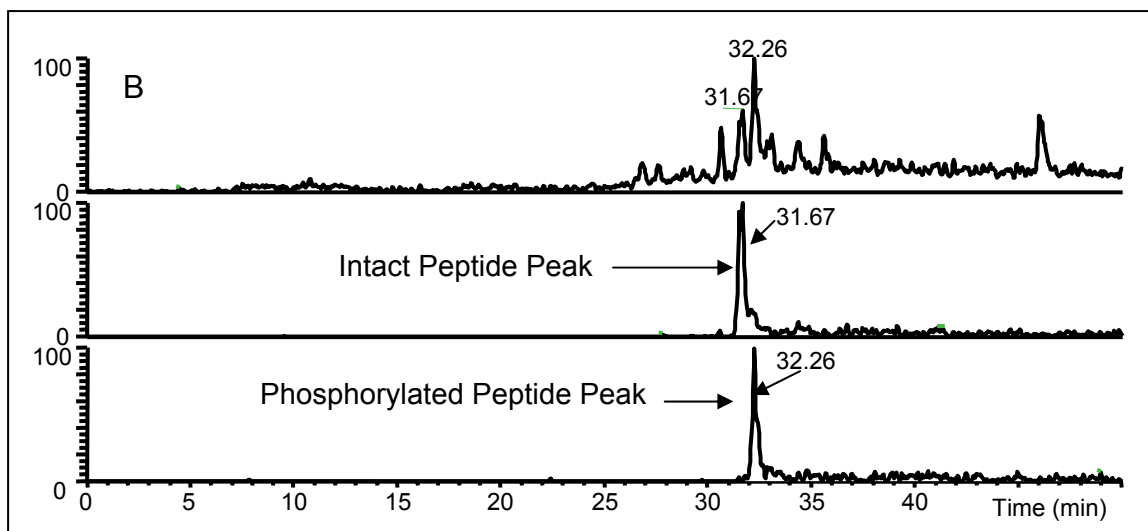
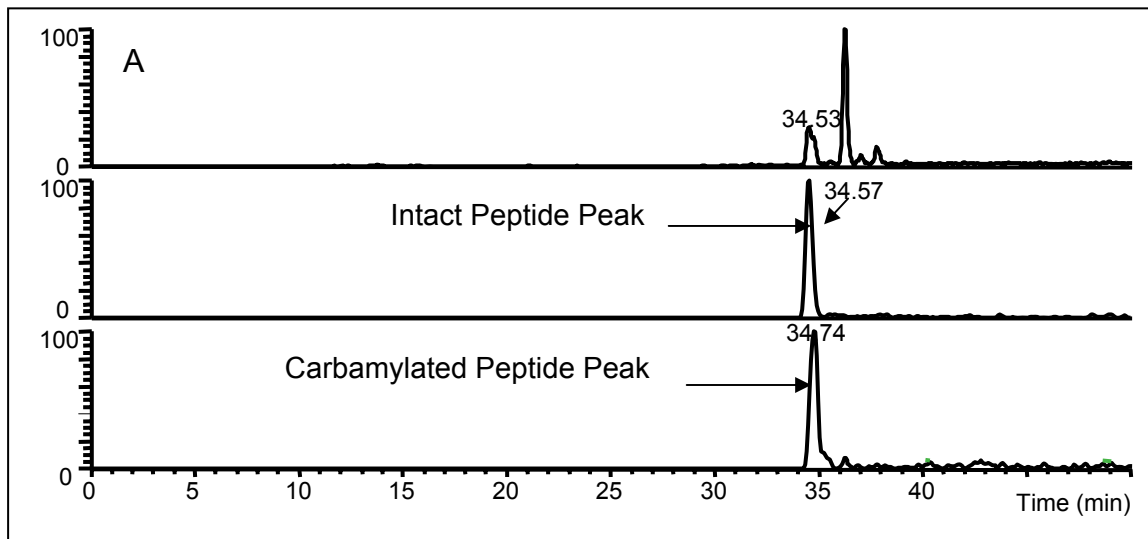


Figure 1-5-11. IC of intact and modified peptides. Representative of one set of results from three parallel experiments after serum treated with 0.2 μM carbaryl (A), and 0.1 μM ethyl paraoxon (B). Five main fragment ions at m/z 680.1²⁺, 726.7²⁺, 919.7²⁺, 955.3²⁺, 1019.3²⁺ were used to monitor intact active site peptide and carbamylated peptide, and the dominant fragment ion at m/z 726.8³⁺ was used to monitor the phosphorylated peptide by ethyl paraoxon.

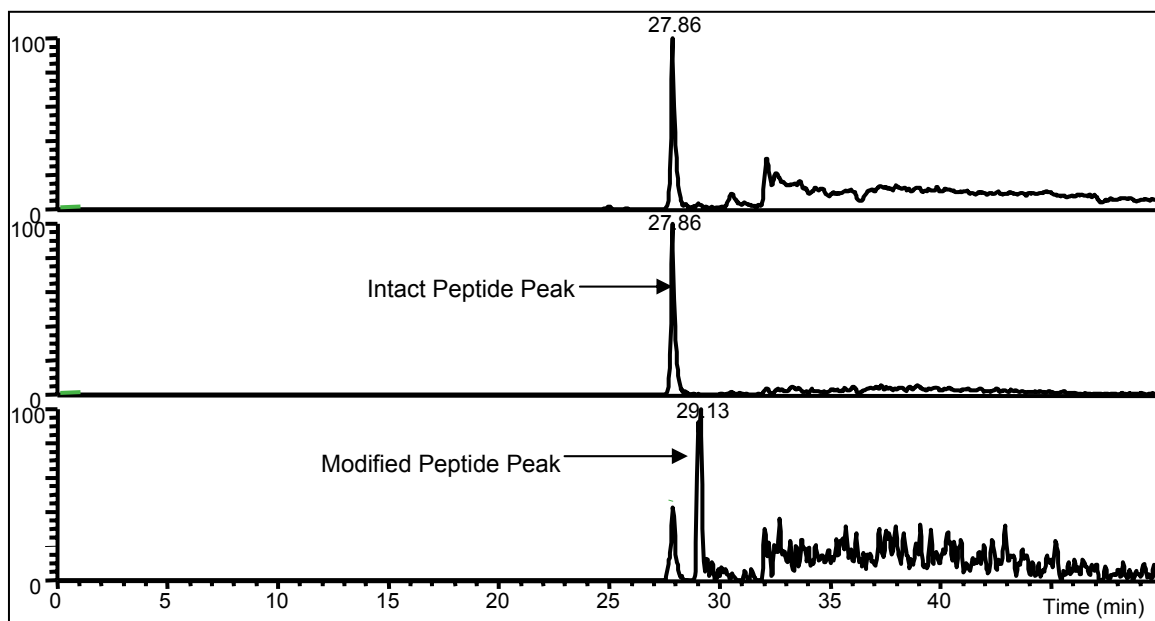


Figure 1-5-12. IC of intact peptide (MH^+ at m/z 732.7³⁺) and modified peptide (MH^+ at m/z 788.7³⁺) by EPN oxon. The intact peptide was monitored by 5 main fragment ions at m/z 680.1²⁺, 726.7²⁺, 919.7²⁺, 955.3²⁺, 1019.3²⁺. Modified peptides were monitored by the dominant fragment ion at m/z 726.8³⁺ corresponding to the phosphorylated peptide ion with neutral loss of O-ethyl phenyl phosphoric acid.

Analysis of Multiple Pesticide Exposure

From the abovementioned results, the assay was useful for the analysis of single pesticide exposure, even at low level exposure down to 5% hBChE inhibition. We were curious to find out whether the same assay could be used for the detection of multiple pesticide exposure. Serum was incubated with 0.27 μM carbaryl for 30 min, 0.07 μM ethyl paraoxon for 1h, and 0.05 μM EPN oxon for 1h, respectively. These concentrations were chosen, because each pesticide inhibited 50 % of serum BChE at their corresponding concentrations (proven by the enzyme activity measurement, data not shown). Equal volume of diluted serum after reaction was mixed. The mixture was incubated with affinity beads for 4 h. After incubation, affinity beads with enriched hBChE were washed, and subsequently digested with trypsin and protease V8. The digests were analyzed using the LC/MS/MS (Figure 1-5-13) method. Peaks of the carbamylated peptide (MH^{3+} at m/z 752³⁺), and two phosphorylated peptides (MH^{3+} at m/z 778³⁺ for ethyl paraoxon, MH^{3+} m/z 788³⁺ for EPN oxon) were baseline separated in a single analysis run. Phosphorylated peptides were determined by the mass differences (neutral loss) between the common fragment ion and precursor ions. Peak areas of these modified peptides indicated their relative abundance present in serum. The relative area ratios were AA752 : AA778 : AA788 = 0.90 : 1.1 : 0.99, where AA is peak area.

DISCUSSION

The goal of this study was to develop an improved methodology to detect and quantify hBChE inhibition after OP and CB exposure in serum matrix. The developed methodology was based on the combination of affinity chromatography with LC/MS/MS analysis, which greatly improved the reproducibility and sensitivity compared with the Fidler method. It also provided a critical evidence for an asserted exposure to pesticides.

Several digestion methods with different proteolytic enzymes were investigated. The active site peptide of hBChE from tryptic digests is at m/z 2928.5, which is out of the detection mass range of the ion trap analyzer, which is less than 2000 Da. Therefore, a new digestion method was required to produce a suitable size of active site peptides. Pepsin and chymotrypsin were applied to digest hBChE alone or in combination with trypsin

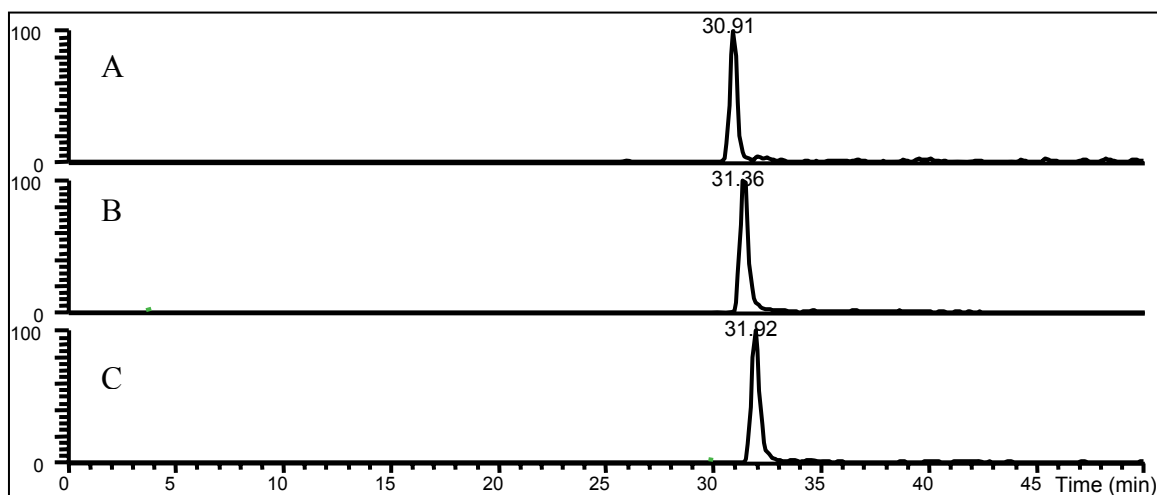


Figure 1-5-13. RIC of carbamylated peptide (MH^{3+} at m/z 752³⁺) from carbaryl (A), phosphorylated peptide (MH^{3+} at m/z 778³⁺) from ethyl paraoxon (B), and phosphorylated peptide (MH^{3+} at m/z 788³⁺) from EPN oxon (C). Five main fragment ions m/z 680.1³⁺, 726.7²⁺, 919.7²⁺, 955.3²⁺, and 1019.3²⁺ were used to monitor precursor ion at MH^{3+} 752³⁺ (A), common dominant fragment ions at m/z 726.8²⁺ were used to monitor precursor ion MH^{3+} at 778³⁺ (B), and at 788³⁺ (C).

digestion (data not shown). Unfortunately, no peptide containing the active site serine was detected due to the non-specific properties of the two proteolytic enzymes.

A double digestion was successfully developed, which greatly improved the digestion reproducibility. Two specific proteolytic enzymes, trypsin and protease V8, were used sequentially. After double digestion, the intact active site peptide, carbamylated peptide, and phosphorylated peptide were identified by MALDI analysis and further confirmed by LC/MS/MS analysis. The amino acid sequence of the intact peptide generated from double digestion is SAGAASVSLHLLSPGSHSLFTR, where the catalytic serine is underlined. Only one peptide, containing the active site serine residue, was observed from the untreated hBChE digests, which was much better than the pepsin digestion developed by Fidder et al. (60). In the Fidder study, several peptides containing the active site serine were observed.

Double digestion was evaluated by comparing calibration curves of the inhibited hBChE by carbaryl from trypsin digestion with that from double digestion using MALDI-TOF-MS (Figure 1-5-8). Slopes of the calibration curves from trypsin digestion were the same as those from the double digestion. In addition, IC_{50} s and IC_{100} s from the two calibration curves were very close to each other, the relative standard error was within 5%. The result indicated that double digestion worked as well as single digestion by trypsin. After the evaluation of double digestion, a calibration system of the double digested peptides was required for the analysis of pesticide exposure.

Calibration systems were constructed for both OPs and CB based on the analysis of hBChE inhibition *in vitro* using LC/MS methodology. From the LC/MS analysis, relative peak area ratios of the intact peptide and modified peptide were obtained and plotted against OP and CB concentrations. A linear relationship between peak area ratios and pesticide concentrations was observed. IC_{50} s determined from the calibration curves for ethyl paraoxon and EPN oxon were $5.35 \pm 0.04 \mu\text{M}$ and $3.66 \pm 0.06 \mu\text{M}$, respectively. After normalizing the detected concentration of hBChE to the same concentration in serum, the normalized IC_{50} s were $0.07 \mu\text{M}$ and $0.05 \mu\text{M}$ for ethyl paraoxon and EPN oxon, respectively. These normalized IC_{50} s were consistent with those from the study by Misser *et al.* (81) and Johnson *et al.* (82). Misser group (81) reported that IC_{50} of ethyl paraoxon is

71 ± 7 nM. The average IC₅₀ of EPN oxon is 51 nM based on the reported data by Johnson group (82) that IC₅₀s for L-EPN oxon and D-EPN oxon are 66 and 36 nM.

An interesting phenomenon was observed for the calibration curve of carbaryl, which demonstrated a linear relationship between the modified peak area ratios and carbaryl concentrations in this study. In contrast, a linear relationship was detected between NIRs of modified peptide vs logarithmic carbaryl concentration for the eBChE study (Chapter 1). This observation may result from differences between hBChE and eBChE. Although eBChE has a 90.1% identity with the hBChE sequence, the amino acid composition at active site of eBChE is significantly different from hBChE. As we described before, the tryptic active site peptide for eBChE is at *m/z* 2200 while for hBChE is at *m/z* 2928. The different amino acid sequence at active site of BChE may cause a different reaction mechanism with inhibitors. As such, the observation of the linear relationship between the modified peptide and carbaryl concentration for eBChE is different from that of hBChE.

A purification procedure needs to be developed before application of the assay to analyze hBChE inhibition in serum. Procainamide-Sepharose 4B affinity beads were synthesized in laboratory. As described in Chapter 4, the yield of the affinity bead was of 12.7 μmol procainamide / ml of beads. The yield was high enough for isolation of hBChE from serum due to the low concentration of enzyme (3-5 mg/l). Results from Chapter 4 also clearly showed that the synthesized affinity beads could enrich hBChE from serum matrix.

Procainamide-Sepharose 4B affinity chromatography ideally facilitated the enrichment and separation of hBChE from the rest of serum proteins. However, since the concentrations of proteins like albumin and immunoglobulins surpass that of hBChE by several orders of magnitude, the non-specific binding of these proteins on the affinity beads can not be omitted. Although LC/MS/MS is useful in isolating ions of interest, it is still unlikely to analyze one kind of ions in the presence of other high-abundant ions (several orders more than the ions of interest). Therefore, a more stringent washing procedure (with a buffer containing high concentration of salt) was applied to minimize nonspecific binding proteins on the affinity beads. Care must be taken here, because the high salt-concentration buffer can also wash off hBChE from affinity beads resulting in a low yield of isolated analyte. In addition to the stringent washing steps, incubation of

affinity beads in the diluted serum solution with 0.1 M NaCl buffer also helped to reduce the non-specific proteins bound to beads.

In order to increase the recovery efficiency, the affinity-chromatography/on-bead digestion approach, performed in a single microtube, was applied in the study of hBChE inhibition in serum. The common conventional affinity chromatography requires elution of proteins from the column to isolate hBChE from serum followed by concentrating the fractions containing hBChE. More experimental steps are required to further purify the former fractions, such as filtration, resulting in more proteins or peptides loss. Since hBChE concentration in the serum is low and sample is limited, an on-bead digestion was developed in this chapter. The on-bead digestion approach reduced analysis time and the number of experimental steps, which resulted in minimizing the proteins loss and decreasing the possibility of inducing sample contamination during the preparation process.

From the abovementioned results, a calibration system was already constructed, and a purification procedure was successfully developed. At this stage, results demonstrated that the assay was ready for the analysis of hBChE inhibition in serum samples. Serum was exposed to 0.2 μM carbaryl and 0.1 μM ethyl paraoxon, separately. To reveal the application of the assay, the treated serum was analyzed. The average normalized detected concentration from triplicate analysis was 0.16 ± 0.01 μM for carbaryl and 0.08 ± 0.01 μM for ethyl paraoxon. The relative standard error was 20% for both analyses, which was much better compared with at least 50 % detection error based on the recovery value using the Fidler's method. The lower detection value was caused from the low recovery of the inhibited hBChE during the purification procedure. The binding ability of the inhibited hBChE on affinity beads was less favorable than the intact hBChE, since the modification group (including carbamylated and alkyl phosphorylated group) at the active site blocks the interactions with ligands on the beads.

The detection limit of pesticide exposure was also investigated using the assay developed in this chapter. Serum was incubated with EPN oxon, which caused 5 % hBChE inhibition based on the enzyme activity measurement. From the three parallel experiments, the average relative peak area ratio of the modified peptide was 5 % using LC/MS/MS method. Although the peak of modified peptide was absolutely detected, the signal was

very weak at such a low inhibition level. No further investigation of a lower inhibition level was performed.

At this stage, the assay was successfully applied to detect hBChE inhibition after single pesticide exposure, even at low inhibition level of 5%. Since the chances of multiple pesticide exposure are much more than single pesticide exposure in the daily life, we were curious to find out whether the same methodology is useful for the investigation of multiple pesticide exposure. The assay was applied for the detection of hBChE inhibition after exposed to multiple pesticides. The carbamylated peptide and phosphorylated peptides were baseline separated in a single analysis run. The relative abundances of these modified peptides, which were related to the extent of exposure to individual pesticide, were estimated by the peak area ratios. In this study, the peak area ratio (AA752 : AA778 : AA788 = 0.90 : 1.1 : 0.99) was consistent with the original ratio (1:1:1). The detected relative amount of carbamylated peptide was lower than the expected value because the reactivation of the carbamylated enzyme occurred during the incubation time with affinity beads.

CONCLUSION

An improved novel methodology has been developed for the detection and quantification hBChE inhibition in serum by combination of affinity chromatography and LC/MS/MS analysis. A novel double digestion was initially developed in this chapter, which made it possible to analyze hBChE inhibition using LC/MS methods. Results clearly showed that the double digestion method worked as efficiently as single trypsin digestion. In addition, a novel on-bead double digestion protocol was investigated, which eliminated the number of experimental steps, reduced the protein loss during sample preparation. The on-bead digestion greatly improved the sample recovery resulting in high detection sensitivity and elevated accuracy. The developed methodology was successfully used in the analysis of both single pesticide exposure and multiple pesticide exposure in serum.

The improved assay was applied for the analysis of single pesticide exposure in serum sample. The detected values were within 20% relative standard error, which was

much better than the Fidler's method. The detection limit of the assay for the pesticide analysis was also determined at hBChE inhibition level as low as 5 %. For the analysis of multiple pesticide exposure, all the modified peptides were baseline separated, and the extent of exposure to each pesticide was estimated by the individual peak area. Results from the assay were consistent with the predicted values. Furthermore, carbamylated peptides were differentiated from phosphorylated peptides based on the different pattern of tandem mass spectra. Phosphorylated peptides were determined based on the mass differences (neutral loss) between the common fragment ion and precursor ions. Therefore, the types of pesticides and the extent of pesticide exposure to serum can be determined using the developed methodology. Because of its high sensitivity, good reproducibility and reliability, it is promising to apply the assay in clinical diagnosis in the near future.

Following the onset of the Gulf War Syndrome (72), the issue of multiple chemical exposures poses an ever increasing military and civilian threat. Although analysis of the hBChE exposed to chemical warfare (CW) agents was not investigated, the types and extent of CW agent exposure should be detected and quantified using the same assay. However, an unpredicted exposure, like the 1995 Tokyo Subway Attack (79), requires a quick investigation from forensic analysis. How to apply the method in field is a challenge for all mass spectrometry specialists. This will be the subject for the future research.

CHAPTER SIX

CONCLUSIONS

With the introduction of the organophosphate pesticides (OPs) and carbamates (CBs) into American agriculture, there has been considerable interest in their chemistry, mode of action, and toxicity. From the public health perspective, a reliable monitoring program is required to detect and quantify pesticide exposure. The U.S. Environmental Protection Agency (USEPA) scientists proposed a blood esterase monitoring program for pesticide exposure in 1991, which is based on the measurement of red cell blood AChE and plasma BChE activity. However, because of the intrinsic drawbacks of these existing monitoring methods, such as non-specificity, a novel and reliable method is required to detect the source of inhibition, and quantify the extent of pesticide exposure.

Because of their high sensitivity, tolerance of protein mixtures and high-throughput, MALDI-TOF-MS and LC/MS/MS were used to detect and quantify OP and CB exposure in this dissertation. OPs and CBs inhibit BChE by forming a covalent bond with the active site serine by attaching a phospholite or carbamylate group. The developed methodology is based on the analysis of inhibited BChE *in vitro* and in serum. As such, quantification of inhibited BChE can serve as a measurement of pesticide exposure.

A MALDI-TOF-MS methodology was designed for the sensitive detection and accurate quantification of pesticide exposure. eBChE was chosen as a model system to develop the methodology, because it is commercially available. The degree of poisoning was determined by the intensity ratios of the modified peptide and the intact active site peptide. The types of pesticides can also be determined by the mass difference between the modified peptide and the intact active site peptide. Although the MALDI methodology was successfully applied for the analysis of single pesticide exposure, it is limited for analysis of multiple pesticide exposure. So, a methodology involving LC/MS/MS istechniques was further investigated, because LC/MS/MS has more benefits, such as high sensitivity, lower limit of detection (LOD) and simultaneous analysis of multiple pesticide exposure. For *In vitro* study, the LC/MS/MS methodology was successfully applied for the analysis of a mixture of the phosphorylated peptides generated from tryptic digests of the inhibited eBChE. LC/MS/MS was proven as a great tool for separation, detection, identification,

quantification, and categorization of phosphorylated peptide mixture in a single analysis run.

Application of the developed LC/MS/MS methodology for measuring pesticide exposure *in vitro* and in human serum clearly demonstrated the power of MS-based methods in pesticide analysis. Results provided critical evidence for the trace exposure to OPs and CB as low as 5 % hBChE inhibition in serum, which the traditional Ellman method can not. A novel double digestion was firstly developed in this study, which made the assay feasible to analyze hBChE inhibition using LC/MS methodology. In addition, a novel on-bead double digestion protocol with high recovery was developed, which reduced the experimental steps and minimized the analyte loss during the sample preparation. The developed methodology, by combination of affinity chromatography and mass spectrometry, greatly improved the sensitivity, reproducibility and accuracy in the hBChE inhibition analysis. The reliability of the developed methodology was proved by the successful use in the analyses of both the single pesticide exposure and the multiple pesticide exposure in serum. Results from the developed methodology were consistent with the predicted values.

The methodology developed here was very well-suited for detecting and quantifying the pesticide analysis. This study reveals a promising future of the proteomics approach and mass spectrometry for the analysis of pesticide exposure due to their high sensitivity and high reliability. However, LC/MS/MS methodology is not the only technique for measuring pesticide exposure. The combined use of all methods is valuable, both in diagnosis of poisoning and in determination of exposure. The other methods, such as determination of urinary metabolites using GC/MS, can also provide an indication of exposure. Unfortunately, it is not possible to relate the concentration of urinary metabolites to the level of intoxication. LC/MS/MS techniques are some of the best analytical tools for pesticide analysis providing high sensitivity and analysis of multiple pesticide exposure in a single analysis run. As with any poisoning, the best mode of action is treatment, which relies on the identity and quantification of toxin exposure. Detection, diagnosis and treatment at early exposure and at low level are the key ingredients to save victim lives.

PART II. A STUDY OF ORGANOPHOSPHATE PESTICIDE-INDUCED PROTEOME
ALTERATION IN SH-SY5Y CELLS

CHAPTER ONE

INTRODUCTION

CHLORPYRIFOS BACKGROUND

Chlorpyrifos (CPF) is an organophosphate pesticide, widely used to control a variety of pests including fire ants, turf and ornamental plant insects, mosquitoes, cockroaches, and termites. It is also used as a soil insecticide, in seed treatment, and applied to dormant and foliar plants. An estimated average of 21 million pounds active ingredient of CPF was used on 20 million acres of U.S. crops per year from 1987 through 1989. The domestic use of CPF has been curtailed by U.S. regulatory provisions (83) because of its adverse neurological consequences, particularly in situations of fetal and childhood pesticide exposure. Nevertheless, CPF remains a widely used pesticide, and will continue to be so for the foreseeable future. As such, the mode of action and toxicity of CPF has generated considerable interest.

Mode of Action of Cholinesterase Inhibition

The mechanism of esterase inhibition by CPF is similar to that observed in other OPs. OPs exert their acute effects in both insects and mammals by inhibiting AChE in the nervous system. As described in Part I, Chapter 1, CHE combines with inhibitors (OPs or CBs) to form a Michaelis complex, followed by phosphorylation at the active site serine of CHE with the loss of the X (leaving group of OPs). Two possible pathways can follow this reaction. Reactivation may occur spontaneously at a rate dependent on the effect of the attached group at the active site serine. Alternately, an “aging” reaction can occur, which involves the cleavage of an R-O-P-bond with the subsequent loss of R (alkyl group on the phosphorus), resulting in the formation of a charged mono-substituted phosphoric acid residue on the enzyme. Once the “aging” reaction has occurred, the enzyme will never be reactivated.

AChE functions to terminate neurotransmission by hydrolyzing acetylcholine (Ach), a neurotransmitter produced at cholinergic nerve endings in response to nervous stimuli. Inhibited AChE causes an accumulation of acetylcholine (Ach) (84), thus prolonging the action of Ach. If CPF is administered to developing organisms at high concentration levels to cause systemic toxicity, a cholinergic hyperstimulation is observed. As shall be shown in the following paragraphs, anticholinergic toxicity is just part of CPF action.

Developmental Neurotoxicity

The fact that CPF may cause neurobehavioral damage during brain development is becoming a major biomedical and social concern (85). As described below, CPF has additional effects on brain development that may be overshadowed by its cholinergic component. A variety of studies have clearly indicated that CPF has adverse effects on brain development more than cholinesterase inhibition. Recent findings indicate that potential exposures to pregnant women and children above the “No Observable Adverse Effect Level” show that children are at higher risks of later behavior deficits (86). Animal studies also confirm that exposure of neonates to CPF result higher risks than adults (71). The LD50 values of CPF for neonates are about an order of magnitude lower than that for adults.

Roy et al (87) describe an alternate experiment to show CPF action on neural development. Rat embryo cultures were treated with CPF for 48 h at a concentration an order of magnitude below that found in human meconium (88) at the neural tube stage of development. The authors found mitotic abnormalities and apoptosis in the developing brain. However, it should be noted that choline acetyltransferase, the enzyme responsible for Ach biosynthesis, is not detectable at the neural tube stage of development. As such, Ach is not available at this stage. So, inhibition of cholinesterase by CPF would not produce cholinergic stimulation. It is evident that the consequence of CPF action is not linked to anticholinergic toxicity.

Other studies (89, 90) have further confirmed that alternate mechanisms might play important roles in CPF action on the developing brain. It has been hypothesized that prenatal CPF exposure, at concentrations below the threshold for detectable cholinesterase inhibition without systemic toxicity, induces later-appearing deficits. This hypothesis has been directly tested using *in vivo* and *in vitro* models of postnatal CPF exposure. One-day-old rats were treated with CPF (91), and acute inhibition of DNA synthesis was observed in areas with low cholinergic innervations (cerebellum), as well as in regions with cholinergically enriched zones (brainstem and forebrain). These results were different from that for nicotinic (AChE inhibitor) treatment - only DNA synthesis had clearly been altered at expected regions with high cholinergic enrichment. Another study was conducted to test the hypothesis in a much more direct way. A certain amount of CPF was injected directly into brain, which skipped the activation process to CPF oxon, and the same observation as CPF *in vivo* study was obtained. All these results show that CPF affects DNA synthesis by an initial,

noncholinergic mode of action. CPF exposure at a concentration insufficient to produce systemic toxicity, not only causes DNA synthesis inhibition, but also affects other biological processes, including deficits in the number of neural cells (92), suppression of gene expression and reduction of macromolecular constituents (important in cell differentiation) (79, 93), abnormalities of synaptic function, and resulting in abnormally behavioral performance (79, 94).

In vitro experiments further showed that CPF causes developmental neurotoxicity through alternate mechanisms than those involved in cholinesterase inhibition. For example, when undifferentiated PC12 cells were treated with CPF at low level concentrations without causing detectable CHE inhibition, DNA synthesis suppression was observed (95). Other similar studies (96) also found potent inhibition of neurite outgrowth. These studies were unrelated to cholinesterase inhibition.

Although many investigations have been undertaken to understand the noncholinergic mechanisms in the developmental neurotoxicity of CPF, the actual mechanisms remain elusive and complicated. To this day, no systematic studies at the subcellular, molecular levels have been undertaken to evaluate proteome changes in neuronal cell line cultures exposed to CPF at low concentrations. In order to study the toxicity caused by CPF in neuroblastoma cells, and as a result of the low levels of choline acetyltransferase, the SH-SY5Y was chosen as a model for this work.

SH-SY5Y CELL LINE

The neuroblastoma cell line SH-SY5Y (SK-N-SH-SY5Y), which was subcloned from human neuroblastoma SK-N-SH, is a nearly diploid dopaminergic neuronal cell line with high levels of dopamine β -hydroxylase (a key enzyme in adrenergic neurotransmitter synthesis). SK-N-SH was established in 1970 from the bone marrow biopsy of a 4-year-old girl with metastatic neuroblastoma, and consists of two cell types with the neuroblast phenotype being predominant. When SH-SY5Y cells are grown in 15% fetal calf serum, they have neuroblast-like properties in their undifferentiated state. Treatment with dibutyryl cyclic AMP or nerve growth factor (NGF) results in morphological and physiological differentiation (84). SH-SY5Y cell lines have low levels of choline acetyltransferase, which makes them a good candidate

for neurotoxicity studies. The SH-SY5Y cell line is a convenient resource for research on neuronal cell biology *in vitro*.

TWO-DIMENSIONAL ELECTROPHORESIS WITH IMMOBILIZED PH GRADIENTS

Two-dimensional gel electrophoresis (2D gel) was developed by O'Farrell in 1975 (97). Proteins are separated based on their intrinsic charges (pI) by isoelectric focusing (IEF) in the first dimension and followed by molecular weight (MW) based separations with SDS-PAGE in the second dimension. 2D gels can resolve complex mixtures of proteins and simultaneously analyze hundreds or even thousands of proteins. After the introduction of immobilized pH gradients (IPG) for IEF, the reproducibility of 2D gel data greatly improved (11). The pH gradients of IPGs are prepared by a limited number (6-8) of well defined chemicals (the 'immobilines'). These chemicals are co-polymerized with the acrylamide matrix, which enhances the reproducibility of 2D gels. Due to the high reproducibility and high loading capacity of IPG strips, 2D gel electrophoresis has become the core technology of proteome analysis in combination with either matrix-assisted laser desorption / ionization-time of flight - mass spectrometry (MALDI-TOF-MS) or electrospray mass spectrometry (ESI-MS).

Prior to IEF, IPG dry strips are rehydrated with sample solution containing 8 M urea, 0.5–2% (non-ionic or zwitterionic) detergent, 0.2% dithiothreitol (DTT) and 0.2% carrier ampholytes. The rehydrated strips are then placed onto the cooling plate of an electro-focusing chamber (Figure 2-1-1). A program, including desired rehydration time, voltage gradient, and temperature, is set for IEF running condition. After IEF, IPG strips are incubated with equilibration buffers containing dithiothreitol (DTT) for 10 min in the first step. They continue to be equilibrated in the buffer containing iodoacetamide for 10 min in the second step. After equilibration, the IPG gel strip is placed on the top of a pre-cast polyacrylamide gel (PAGE) and overlaid with agarose solution. After termination of the second dimension run (SDS-PAGE), it is necessary to immobilize the resolved proteins in the gel with fixing solution. Twenty percent TCA, methanolic or ethanolic of acetic acid are extensively used as fixatives. Proteins can be visualized by several staining methods – silver staining, fluorescent staining, colloidal coomassie blue G-250, and Coomassie R-250 staining. Both fluorescent

staining (laboratory synthesized ruthenium reagents) and Colloidal Coomassie blue G-250 staining were used in this project, as both approaches afford high sensitivity and MS compatibility. Gel images were then captured with the VersaDoc Imaging system (Bio-Rad), and quantitatively analyzed by PDQuest software (Bio-Rad). All protein spots with a relative quantitative difference equal to or greater than a 2-fold change were excised and further analyzed by MALDI-TOF-MS, following tryptic in-gel digestion. Finally, these proteins were identified by database searching with the MASCOT algorithm.

DATABASE SEARCH USING MASCOT ALGORITHM

Several algorithms have been used to identify proteins by searching an appropriate database using peptide mass-fingerprinting mass spectra or tandem mass spectrometry (MS/MS) data. Currently, MASCOT (98) and SEQUEST (15) algorithms for database searching are the most popular in proteomics. Only MASCOT was used in this dissertation, so a brief overview of this algorithm will be discussed.

The scoring algorithm of MASCOT is based on probability with a number of additional advantages: i) it is simple to judge whether a result is significant or not, ii) different types of matching (peptide masses or MS/MS fragment ion masses) can easily be combined into a single search, iii) it is feasible to compare scores from different searches and different databases, iv) searching parameters can be readily optimized.

MOWSE Score

The MOWSE scoring algorithm was first described in 1993 by Pappin et al. (99). Based on this algorithm, experimental data are first compared with the calculated peptide masses for each protein in the sequence database. Each calculated value within a user-defined mass tolerance of an experimental value is taken as a match. Molecular weight, pI values, and sources for the intact protein can be used as pre-filters.

A statistical weighting factor is empirically assigned to each individual peptide match instead of counting the number of matching peptides. All matching fragments contribute to the final score for every database entry scanned.



Figure 2-1-1. Photograph of a Bio-Rad isoelectric focusing chamber and focusing tray.

A frequency factor matrix, **F**, is created. Each row in **F** represents an interval of 100 Da in peptide molecular weight, and each column is an interval of 10 kDa in intact protein molecular weight. The cells therefore contain the number of times that a particular fragment molecular weight occurred in a protein. It is similar for each protein in the database. Each cell value is divided by the total number of peptides in each 10 kDa protein interval to obtain cell frequency values. These frequency values are further divided by the largest cell value for each 10 kDa column to get the MORSE factor matrix **M**.

The matrix of weighting factors is described as follows:

$$m_{i,j} = \frac{f_{i,j}}{\left| f_{i,j} \right|_{\max \text{ in column } j}} \quad (2.1.1)$$

The MOWSE search program is based on these distribution frequency values for each cleavage reagent. For each matching peptide, a score is assigned by looking up the appropriate normalized distribution frequency value. When there are several matching peptides in any one target protein, the total frequency value equals the product of the distribution frequency for each peptide. Consideration of the average protein molecular weight as 50 kDa, the final score for each entry is calculated as follows:

$$S_{core} = \frac{50,000}{M_{prot} \times \prod m_{i,j}} \quad (2.1.2)$$

where M_{prot} is the molecular weight of the entry and $\prod m_{i,j}$ is the product of distribution factors for all the matching peptides between the experimental data and peptides calculated from the database.

STATEMENT OF RESEARCH

This part of the dissertation describes the first time systematic investigation of the CPF-induced toxicity at subcellular levels using SH-SY5Y as a model system. The hypothesis of this study is that changes in protein expression underlie neuronal anomalies associated with CPF exposure. After SH-SY5Y cell lines were treated with CPF, proteins from this cell line were collected and analyzed by 2DE-PAGE and MALDI-TOF-MS. Results clearly demonstrated that CPF has significant effects on cell process.

CHAPTER TWO

CHLORPYRIFOS-INDUCED PROTEIN ALTERATIONS IN THE SH-SY5Y CELL LINE

INTRODUCTION

Most children in the US have been exposed to chlorpyrifos (CPF), an organophosphate pesticide. In recent years, there has been heightened concern about exposure of pregnant women, infants and children to CPF in view of its developmental neurotoxic effects. Despite recent curtailment of its domestic use in US (U.S. Environmental Protection Agency 2000), CPF remains one of the most widely used pesticides in the world. Unfortunately, to date, no systematic studies at the subcellular level have been undertaken to evaluate CPF-induced proteome changes in neurons. In this chapter, investigation of whole proteome alterations induced by CPF is described. CPF concentrations at levels below the threshold for symptoms of systemic toxicity were studied using the SH-SY5Y cell line as a model system. The combination of two-dimensional gel electrophoresis (2DE) with matrix-assisted laser desorption/ionization-time of flight- mass spectrometry (MALDI-TOF-MS) was applied to take a closer look at protein alterations induced by exposure to this pesticide.

CPF is primarily recognized for its ability to induce physiological toxicity in humans and animals via acetylcholinesterase (AChE) inhibition. However, a variety of studies showed that CPF has additional effects besides cholinesterase inhibition. Levin et al. studied rats subjected to prenatal (90) and postnatal (94) exposure to CPF and evaluated their behavioral performance in adolescence and adulthood. The results showed that both prenatal and postnatal exposure to CPF induced long-term changes in cognitive performance. Other animal studies also confirmed that exposure of neonates to CPF subjected to higher risks than adults (71). The LD50 values of CPF for neonates are about an order of magnitude lower than that for adults. At the cellular level, S.J. Garcia *et al.* suggested that CPF had shifting targets, initially impairing neuronal development

(gestational days (GD) 17-20), and then influencing glia (postnatal days (PN 11-14). These findings were the result of examinations of neuroprotein markers (89) using biochemical techniques, such as western blot.

Studies both *in vivo* and *in vitro* confirm that CPF at sublethal levels can compromise cellular processes involved in brain development (100). However, the actual mechanism for CPF perturbation in neuronal development at the molecular level is complicated and remains unclear. All these studies show that CPF can influence neuronal development by targeting a diverse range of events including cell proliferation, migration, differentiation, neuritogenesis, synaptogenesis and synaptic function. Long-term irreversible consequences can happen by perturbing these processes (46). The perturbing processes are through adverse effects on the structure and function of the nervous system. Until now, no systematic studies at the molecular level have been undertaken to investigate these influences on neuronal development as initiated by CPF.

In this chapter, a description of the first systematic study of CPF-induced adverse effect on cell process at the molecular level is provided. We hypothesized that changes in protein expression underlie neuronal anomalies associated with CPF exposure. The SH-SY5Y neuroblastoma cell line was used as a model system due to the low level of choline acetyltransferase (the enzyme responsible for acetylcholine biosynthesis). Through a combination of 2DE and MALDI-TOF-MS, the whole proteome in SH-SY5Y cells was examined to identify altered proteins resulting from CPF exposure. The reproducibility of 2DE was also evaluated in this chapter. The differential proteins (which showed 2-fold change between the control and treated sample, based on the optical density measurement) were detected. Altered proteins were identified by comparing the experimental mass spectra with theoretical mass spectra from the *insilico* digestion of the protein database. The results clearly demonstrated that altered protein expressions induced by CPF exposure were linked to developmental damage observed in neuroblastoma cells.

EXPERIMENTAL

Materials

Isoelectric pH gradient (IPG) strips (5 mm wide, 7 cm or 18 cm long, pH 3-10 linear gradient), urea, Tris (electrophoresis grade), TEMED (electrophoresis purity reagent), acrylamide, heavy mineral oil, and a 2-D Starter kit were obtained from Bio-Rad (Hercules, CA). Dithiothreitol (DTT, electrophoresis grade), iodoacetamide (electrophoresis grade), ammonium bicarbonate, and SDS were all obtained from Sigma (St. Louis, MO). For protein staining of gels, fluorescent ruthenium reagents (lab synthesized); colloidal Coomassie Blue (J.T. Baker Chemical Co., Philipsburg, N.J.) were employed. Glacial acetic acid (ACS grade, EM Science, Gibbstown, N.J.), and methanol (HPLC grade, Fisher Scientific, Fair Lawn, NJ) were employed. For MALDI analysis of peptides, α -cyano-4-hydroxycinnamic acid (HCCA) matrix was purchased from Sigma (St. Louis, MO) and used without further purification. Trifluoroacetic acid employed in the extraction of peptides from de-stained gel spots was obtained from Fisher Scientific (Fair lawn, NJ). High-purity water ($18.2 \text{ M}\Omega \text{ cm}^{-1}$) was prepared using a water purification system (Nanopure II, Barnstead, Van Nuys, CA) and was employed for all protocols in this study.

Cell Culture

SY5Y neuroblastoma cells were grown to 75% confluence in 75 cm^2 flasks in Dulbecco modified essential medium (Omon) supplemented with 55 mM glucose, 26 mM NaHCO_3 , 16 mM KCl, 1.36 mM pyruvic acid, 10 mg/mL gentamicin sulfate, and 10% clarified bovine serum (pH 7.2). Cells were incubated at 37°C in 94% air/6% CO_2 . Cultures were split 1:3 every 2-3 days using 0.25% trypsin/0.03% EDTA. When cells reached confluence, they were switched to Locke's medium containing 154 mM NaCl, 56 mM KCl, 2.3 mM CaCl_2 , 1.0 mM MgCl_2 , 3.6 mM NaHCO_3 , 10 mM glucose, 5 mM HEPES (pH 7.2) with 10 mg/l gentamicin sulfate. Control cells were treated with dimethylsulfoxide (DMSO) only and treated with CPF at $50 \mu\text{M}$ in 1% DMSO.

Cell Viability Assay

Cells were plated in 96 well culture plates and treated with CPF. After treatment, cell viability was assayed by the addition of 10 μ l of 1 mg/ml 3-(4,5-dimethylthiazol-2-yl)-2,5-diphenyltetrazolium bromide (MTT)/well (100 μ l Locke medium) and incubated for the last hour of treatment. After removal of the media, the formazan crystals produced from MTT by mitochondrial enzymes in active cells were dissolved in 100 μ l DMSO. Formazan absorbance was measured at 620 nm using a multi-well plate reader. The mean value of 8 parallel experiments for cell viability was used. Raw data were converted to the relative percentage of control absorbance, and expressed as the mean \pm SEM % control absorbance.

Preparation of Cell Lysate for 2DE-PAGE

After the culture was switched to Locke's medium, treatment was initiated with 50 μ M CPF in 1% DMSO for 16 h or 24 h. After treatment, cultures were washed with phosphate buffered saline (PBS) pH 7.4, and cells were scraped into 3 ml PBS and pelleted by centrifugation at 800 x *g* for 10 min. The pellet was re-suspended in 200 μ L distilled/deionized water and homogenized using a micro-Dounce homogenizer. Protein content of this cell lysate was determined using a Pierce BCA kit.

Protein Sample Preparation

Following sonication for 20 minutes, 350 μ g aliquots of protein lysate were evaporated to dryness and subjected to 2D gel electrophoresis. The protein was then solubilized in rehydration buffer (8 M urea, 2 % CHAPS, 50 mM dithiothreitol (DTT), 0.2% (w/v) Bio-lyte 3/10 ampholytes and a trace of Bromophenol Blue). The protein solution was ready for Isoelectric focusing experiments.

2D Gel Electrophoresis Validation

In order to evaluate 2DE reproducibility, four proteins were used in this study. The used proteins were bovine serum albumin (BSA), ovalbumin (Ova), carbonic anhydrase (CA), and soybean trypsin inhibitor (STI). Each protein (0.1 μ g) was mixed, and then

solubilized in sample preparation buffer containing 0.5 M Tris-HCl pH 6.8, glycerol, SDS and 0.1% bromophenol blue. The resulting solution was loaded onto strips (5 mm wide, 7 cm long, pH 3-10 linear gradient). A second experimental set was designed for the evaluation of 2DE reproducibility, in which 0.1 µg of Ova, CA and STI, and 0.2 µg BSA were mixed. As described above, three parallel experiments were performed for statistical analysis. The optical density (OD) of each spot was normalized based on the percentage of the total valid spots on the 2D gel using PDQuest software.

2D Gel Electrophoresis

An aliquot of 350 µg of protein lysate from SY5Y cells was dissolved in 350 µl rehydration buffer. The solution was then added to an IPG strip (5 mm wide, 18 cm long, pH 3-10 linear gradient) (Bio-Rad). Following rehydration for 24 h, strips were subjected to isoelectric focusing (IEF) at 20°C. Table 2-2-1 lists the gradient program used for the experiment. Total focusing time was 23 h. After IEF was complete, strips were removed from the Protean IEF (Bio-Rad) cell. They were then equilibrated with 6 ml buffer A (6 M Urea, 2% SDS, 0.375 M Tris-HCl pH 8.8, 20% glycerol) containing an additional 0.12 mg DTT for 15 minutes in the first step. Subsequently, strips were incubated with buffer A containing 0.15 mg iodoacetamide for 15 minutes in the second step. Strips were removed from equilibration solution and placed on the top of pre-cast SDS gel (1 mm thick, 20 cm x 20 cm and 8%-16% linear acrylamide gradient). The strips were sealed into position with 0.5% low melting point agarose in 25 mM Tris, 192 mM glycine, 0.1% SDS, and a trace of bromophenol blue. Gels were run at a constant current 16 mA/ gel for 30 min, then 24 mA/ gel until the blue dye front line reached the bottom of the gel.

SDS gels were fixed in 30% EtOH/10% acetic acid overnight, then washed with 20% EtOH four times over 2 h. Gels were finally stained with lab-synthesized fluorescent ruthenium reagent (50 µl in 250 ml 20% EtOH) overnight. Gels were scanned using VersaDoc Imaging system (Bio-Rad) and 2D gel images were analyzed with PDQuest software (Bio-Rad).

In-Gel Digestion

Protein spots of interest were excised manually from the gel, and then placed into micro well plates. A Proteomeer dP robot (Bruker) was used for the in-gel digestion. The

Table 2-2-1. Gradient program of IEF.

	Voltage (V)	Time (h)
Step 1	300	5
Step 2	1000	1
Step 3	2500	1
Step 4	5000	16

digestion program was set up as follows: i) gel pieces were washed with 50 mM NH_4HCO_3 followed by washes with 25 mM NH_4HCO_3 in 50% acetonitrile for three cycles (10 min/cycle), then gel pieces were dried with acetonitrile for 5 min; ii) trypsin solution (10 μl , 6.7 $\mu\text{g}/\text{ml}$) was added to each well and incubated with the gel pieces for 30 min at 20 °C and for 4 h at 50 °C; iv) the supernatant containing peptides was recovered for MS analysis.

Mass spectrometry

A drying thin layer strategy was used to spot an affinity Anchorchip with a matrix solution of 10 mg/ml α -cyano-4-hydroxycinnamic acid in 0.2% TFA/acetone (1:9 by volume). Tryptic digests (4 μl) were loaded onto each matrix spot and allowed to desorb on the target for 10 min. The residue of sample solution was removed from the target followed by washing the spot with 0.1% TFA. An Autoflex MALDI-TOF mass spectrometer (Bruker) was used to obtain mass spectra. Analysis in the reflectron mode was accomplished with 19 kV accelerating potential and a lens voltage of 20 kV. Each spectrum was obtained from an average 300 laser shots. A standard peptide mixture consisting of angiotensin II and vasopressin was used to provide an external mass calibration. A trypsin autoproteolysis product m/z 842.5 was used for an internal mass calibration.

Database search

Proteins were identified by searching the National Center for Biotechnology Information (NCBI) database or Sprot using the MASCOT algorithm. The search parameters allowed for the oxidation of methionine. Mass accuracy at 150 ppm was used for the database search. Peptides were excluded if their masses corresponded to those for porcine trypsin, human keratins or other irrelevant proteins.

RESULTS

Cell Viability

Cell viability was investigated for CPF at a series of concentrations: 10, 25, 50, 100, 250, 500 and 1000 μM (Figure 2-2-1). These concentrations were investigated to find a suitable exposure level for the study of CPF-induced toxicity in SH-SY5Y cells. Results were calculated for each treated sample as the percentages of control sample based on the measurement of formazan absorbance (related to cell viability). Cell viability (as a percentage of control cells) was expressed as the mean \pm SEM % from eight parallel experiments. Statistical analysis was carried out using ANOVA with Dunnett's *post hoc* test for the cell viability of individual samples using commercially available ABSTAT software. The outcome from these statistical analysis showed that concentrations of CPF greater than 250 μM caused a significant ($p < 0.05$) decrease in cell viability. No significant change was observed in cell viability when the CPF incubation concentration was between 10 to 100 μM . CPF at 50 μM was chosen, because no systematic toxicity would happen at this concentration.

Evaluation of 2D Gel Reproducibility

BSA, Ova, CA and STI were used to evaluate 2D gel reproducibility. In the first set of experiments, 0.1 μg of each protein was used to do small format 2D gel experiments. All the OD values of the spots were normalized based on the percentage of the total valid spots on the 2D gel analyzed with PDQuest software. Table 2-2-2 lists the experimental values of proteins along with expected percentages. The relative standard errors for BSA, Ova, CA, and STI were 3.5 %, 3.0 %, 0.9 %, and 4.2 %, respectively. For the second set of experiments, 0.1 μg of Ova, CA and STI, along with 0.2 μg of BSA were used in small format 2 D gel analyses. Table 2-2-3 lists the experimental ratios of proteins along with expected values for the second experimental set. The relative errors for BSA, Ova, CA, and STI were 3.09, 1.17, 3.97, and 6.65%, respectively.

All the relative errors were within 10%. The results clearly showed that 2D gel is a reliable method for protein quantification and therefore well suited for the investigations present here.

Proteome Analysis of SH-SY5Y Cells

In this study, approximately 350 μg of total protein was loaded for each gel. Proteins were separated on an isoelectric focusing strip (18 cm long, pH 3-10 from left to right) in the first dimension, and resolved by linear gradient (8-16%) SDS-PAGE in the second dimension. The gels with separated proteins were stained with a lab-synthesized fluorescent ruthenium reagent. A typical set of 2D SDS gels for the treated (50 μM CPF for 24 h) and control sample is shown in Figure 2-2-2. Three independent assays are represented. Figure 2-2-2 illustrates a typical example of a gel image region containing up-regulated proteins in treated sample. The normalized optical densities of spots 1, 2 and 3 were plotted in Figure 2-2-2 C.

Table 2-2-4, and Table 2-2-5 present an overview of the CPF-induced down-, and up-regulated proteins that could be identified in one or more of the three experiments (Figure 2-2-3 refers to experiment set 2) using MS. Both tables list the National Center for Biotechnology Information (NCBI) accession numbers, the positions on the gels of Figure 2-2-3, and the calculated molecular masses of the identified proteins. Figure 2-2-3 identifies the spots corresponding to the identified proteins in experiment set 2 on the 2D gels of the sample from control and treated SY5Y cells. A total of 37 unique proteins from 56 spots were identified, out of which 16 proteins from 26 ± 4 spots were down-regulated, and 21 proteins from 30 ± 3 spots were up-regulated (mean \pm SD for three experiments). Spot count differences between experiments likely arise due to inter-individual differences in the protein spot patterns. Altered proteins were categorized as chaperone proteins, cytoskeletal proteins, enzymes, redox enzymes etc.

Table 2-2-2. Experimental and theoretical ratios of proteins with relative standard errors for the first experimental set.

Protein	Exp. #1	Exp. #2	Exp. #3	Avg. $(\bar{x} \pm s)$	Expected	Relative error (%)
BSA	0.91	0.95	1.04	0.97±0.06	1.00	3.00
Ova	1.07	1.01	0.84	0.97±0.12	1.00	3.00
CA	0.93	0.99	1.05	0.99±0.06	1.00	1.00
STI	0.97	0.92	1.24	1.04±0.17	1.00	4.00

Table 2-2-3. Experimental and theoretical ratios and their relative standard error for the second experimental set.

Protein	Exp. #1	Exp. #2	Exp. #3	Avg. ($\bar{x} \pm s$)	Expected Value.	Relative error (%)
BSA	1.78	1.72	1.80	1.77±0.04	1.71	3.09
Ova	0.87	0.85	0.82	0.85±0.03	0.86	1.17
CA	0.85	0.84	0.78	0.82±0.04	0.86	3.97
STI	0.81	0.79	0.80	0.80±0.01	0.86	6.65

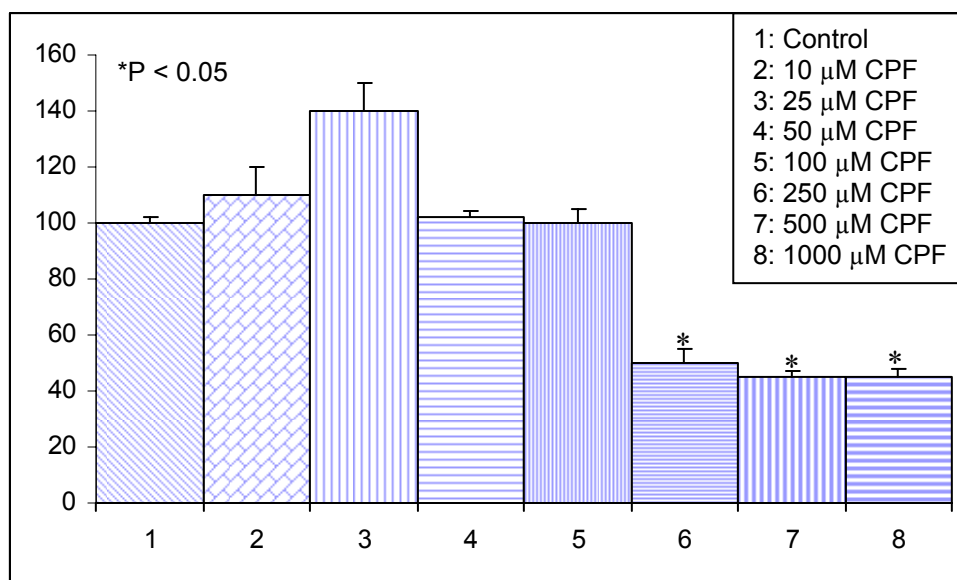


Figure 2-2-1. Viability of SH-SY5Y cells exposed to vehicle alone (control), 10, 25, 50, 100, 250, 500, and 1000 μM chlorpyrifos (CPF) for 24 h. Concentrations greater than 250 μM caused a statistically significant ($p < 0.05$) decrease in cell viability.

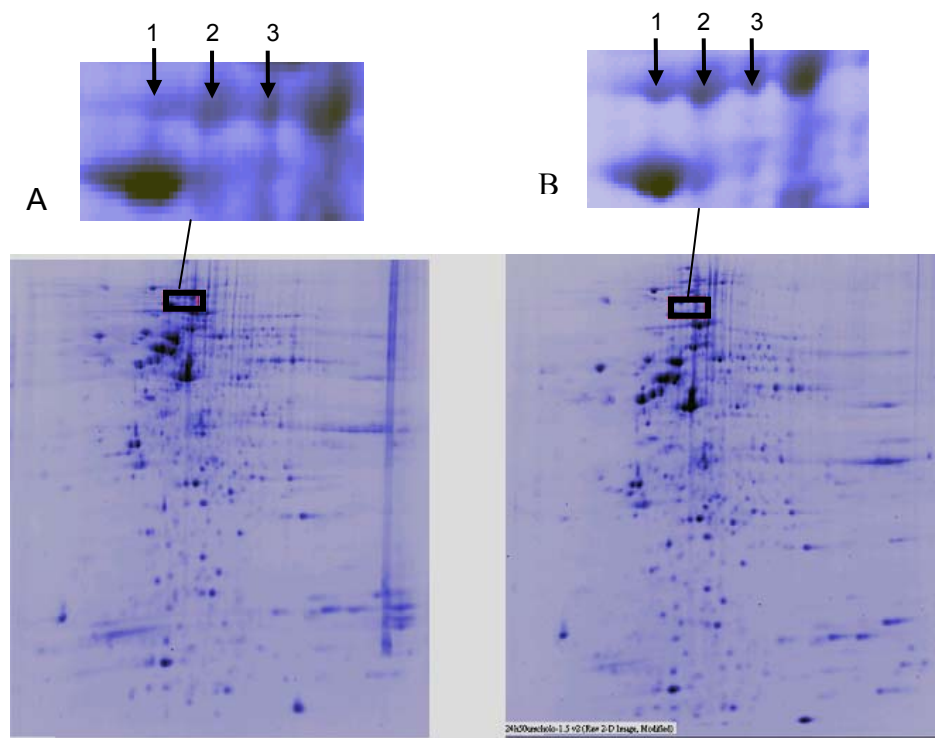


Figure 2-2-2. A typical example of gel image regions contain up-regulated proteins in the sample from the SY5Y cells treated with 50 μ M CPF for 24 h. Gel images for the control sample (A), and for the sample treated with 50 μ M CPF for 24 h (B). The experiment shown is representative of three trials.

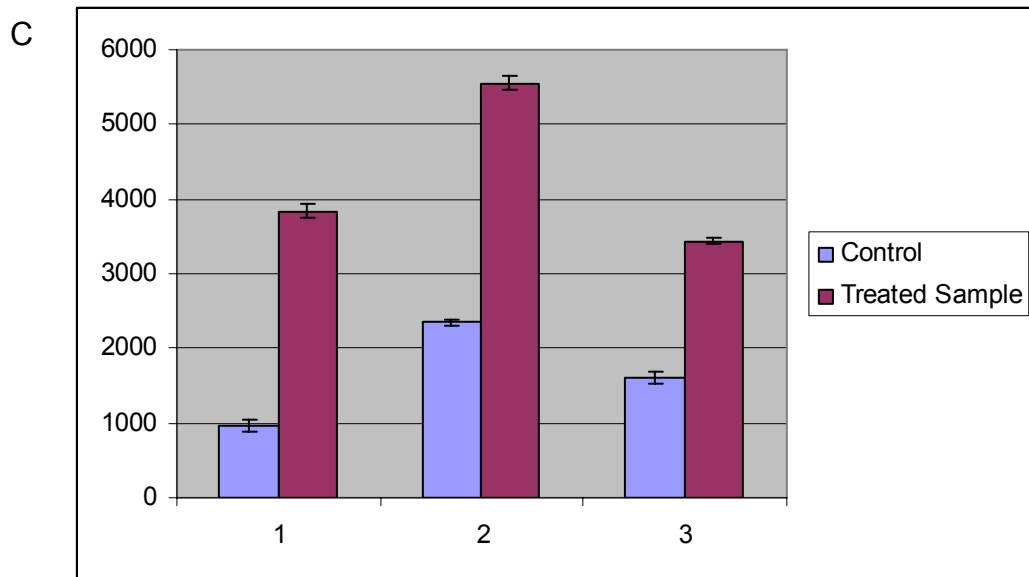


Figure 2-2-2. The normalized optical densities of spots 1, 2, and 3.

Table 2-2-4. Summary of down-regulated proteins in SH-SY5Y cells treated with 50 μ M CPF for 24 h compared with control samples.

Protein	NCBI Accession no.	Spot no.	Molecular mass (KDa)	Morwse Score	Coverage (%)
Chaperone Proteins					
HSP90-alpha	172222	1, 2	80	118	22
HSP70	5729877	4,17	70	279	38
HSP27	662841	26	22	121	14
Enzymes					
ATP synthase, H ⁺ transporting	32189394	6	56	96	30
Enolase1, alpha	4503571	15	47	117	32
Thioredoxin peroxidase B, chain A	9955007	9	21	61	14
Glyceraldehyde-3-phosphate dehydrogenase	31645	3	36	54	12
Mitochondrial short-chain enoyl-coenzyme A hydratase 1	433413	12	31	97	19
Cytoskeletal Proteins					
Actin, beta	15277503	23, 7,14	40	104	22
Ubiquilin	24659706	5	62	96	30
Tubulin	14389309	8,16,21	49	103	29
Vimentin	2119204	13,24	54	147	28
Other Proteins					
Histone family	4504259	18,19,20,22	14	75	30
Heterogeneous nuclear ribonucleoprotein C isoform b	4758544	10	32	62	14
CGI-150 protein	16198390	11	33	73	14
R33729-1	3513302	25	16	57	24

Table 2-2-5. Summary of the up-regulated proteins in SH-SY5Y cells treated with 50 μ M CPF for 24 h compared with control samples.

Protein	NCBI Accession no.	Molecular mass (KDa)	Spot no.	Morwse Score	Coverage (%)
Chaperone Proteins					
HSP90	72222	83	2,3,4	190	40
HSP gp96 precursor	15010550	90	12,15	168	29
HSP70	16507237	72	16	100	19
BIP protein	6470150	71	17	170	30
HSP70 protein isoform 1	5729877	71	18,22	85	10
T complex protein 1	135538	60	9	91	18
Chaperonin containing TCP 1	5453603	57	10	77	18
TATA binding protein interacting protein 49Kda	4506753	50	27	112	13
Enzymes					
Propyl 4-hydroxylase	20070125	57	23	56	6
Glucose-6-phosphate dehydrogenase	26224790	55	20	88	10
Protein disulfide isomerase- related	1710248	46	11	62	14
Enolase 1	4503571	47	21	218	36
Regulatory domain of human PP2a	4558258	65	24	84	15
Cytoskeletal Proteins					
Tubulin, beta	2119276	49	19	96	24
Vimentin	2119204	53	13,14	248	44
Profilin 1	4826898	15	7, 5	83	15
Cofilin 1	5031635	18	25	70	22
Similar to tubulin , beta 5	12804891	38	26	103	17
Other Proteins					
Neuro-endocrine specific protein VGF	17136078	67	1	65	11
GDP dissociation inhibitor 1	4503971	51	6	104	32
Human mitochondrial single-stranded DNA binding protein	148790	15	8	59	11
H2B histone family	4504259	14	28	92	41
Eukaryotic translation initiation factor 3 (fragment)	23503064	36	29	130	33
Annexin V	999926	36	30	101	17

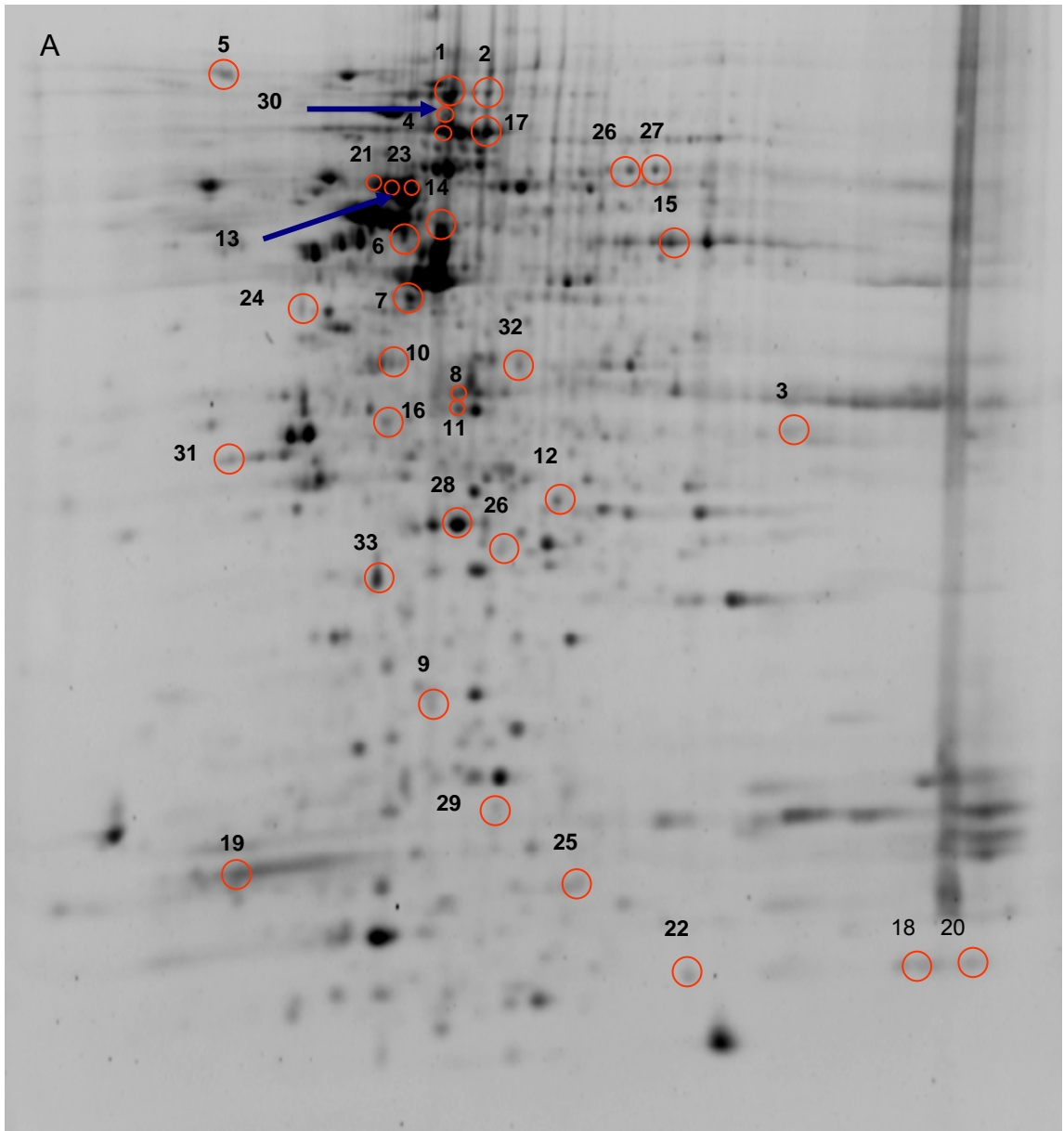


Figure 2-2-3. (A) 2D sodium dodecyl sulfate polyacrylamide gel electrophoresis (SDS-PAGE) of 350 μg total protein from the control SH-SY5Y cells. Proteins were separated on an isoelectric focusing strip (pH 3-10 from left to right) in the first dimension and by linear gradient (8-16%) SDS-PAGE in the second dimension. A lab-synthesized fluorescent ruthenium reagent was used to stain. The down-regulated proteins (Table 2-2-4 and Table 2-2-6) are labeled on the control (A) gels.

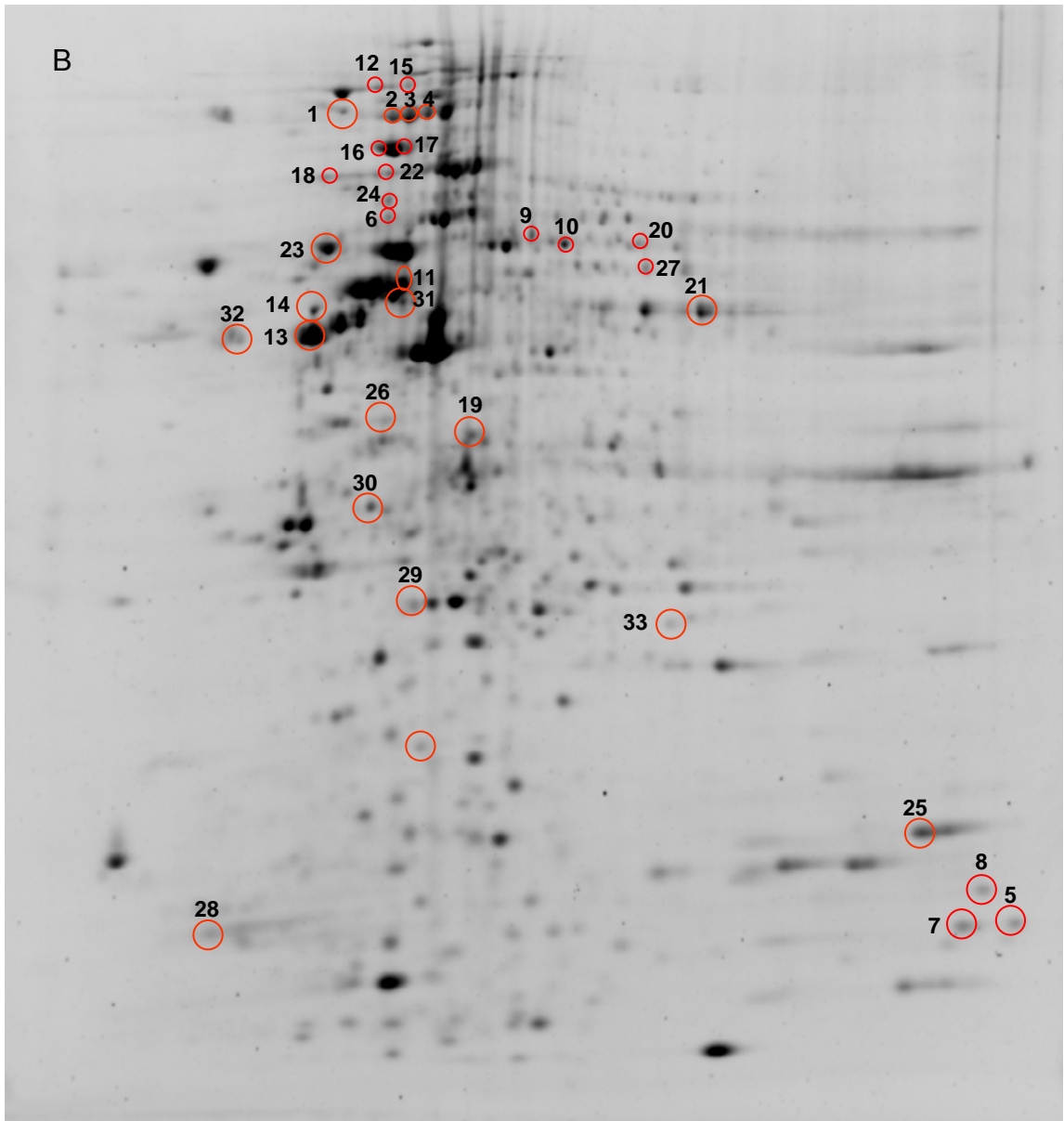


Figure 2-2-3. (B) 2D sodium dodecyl sulfate polyacrylamide gel electrophoresis (SDS-PAGE) of 350 μ g total protein from the SH-SY5Y cells treated with 50 μ M CPF. Proteins were separated on an isoelectric focusing strip (pH 3-10 from left to right) in the first dimension and by linear gradient (8-16%) SDS-PAGE in the second dimension. A lab-synthesized fluorescent ruthenium reagent was used to stain. The up-regulated proteins (Table 2-2-5 and Table 2-2-7) are labeled on the treated sample gel.

Among the altered proteins, some correspond to different isoforms of the same protein. Such isoforms aligned as a horizontal row of several spots on the 2D gel, with different pI values and the same molecular weight, and likely resulted from posttranslational modifications. In particular, HSP 90 was identified in 3 spots (Figure 2-2-1) as an up-regulated protein. A similar pattern was observed for enolase with the spots numbered as 15 in Figure 2-2-3 A and 21 in Figure 2-2-3 B. From amino acid composition of the enolase, the expected pI is 7.01, however the actual pIs for these two isoforms are about 5.8 and 6.6. The isoform at spot 15 in Figure 2-2-3 A (pI 5.8) was detected as down-regulated a protein, but the other isoform at spot 21 in Figure 2-2-3 B (pI 6.6) was detected as an up-regulated protein. A similar situation was also observed for other proteins like heat shock proteins, actin proteins, and tubulin proteins.

Proteome analysis of SH-SY5Y cells treated with 50 μ M CPF for 16h

The previous discussion explored proteome alterations of SH-SY5Y cells after treatment with 50 μ M CPF for 24 h. At this stage, we were curious to find out what proteome changes would occur after exposure to CPF for a shorter period of time. In order to study time-dependent proteome changes of SH-SY5Y cells caused by CPF, a separate proteome analysis was undertaken following exposure to 50 μ M CPF for 16 h. The resolved protein spots on gels, which showed a 2-fold change in concentration between control and treated sample based on OD density measurement, were digested by trypsin. The tryptic digests were further analyzed by MALDI-TOF-MS. The proteins were then identified by searching the Spot database using the MASCOT algorithm.

Table 2-2-6 and Table 2-2-7 present an overview of the additional down- and up-regulated proteins and proteins with changing trends induced by 50 μ M CPF for 16 h compared with an incubation time of 24 h. A total of 48 unique proteins from 68 spots, which includes the same 37 identified unique proteins as those from the samples treated for 24 h, were identified. Out of the altered proteins, 23 were down-regulated and 25 were up-regulated after incubation with 50 μ M CPF for 16 h. These proteins were identified by three trials using mass spectrometry. Figure 2-2-3 displays all of the spots (including the additional proteins identified from the samples treated with 16 h,) corresponding to the identified proteins on the 2D gels of the sample from the control (Figure 2-2-3 A) and the

treated SH-SY5Y samples (Figure 2-2-3 B). These identified proteins can be classified as chaperone proteins, cytoskeletal proteins, enzymes and other proteins.

DISCUSSION

Cell Viability

MTT assay based on the measurement of the reduced product from MTT was applied to examine cell viability for the cytotoxicity assessment caused by CPF. During investigation, cell viability was observed as high as 140% for the cells treated with 25 μ M CPF compared with control cells (Figure 2-2-1). A possible explanation for the high MTT assay value is that CPF promoted enhanced mitochondrial activity producing more formazan from MTT. Since enhanced mitochondrial activity induced by CPF can cause an increase in the abundance of reactive oxygen species in cells, cellular oxidative stress may be a consequence of CPF exposure. The increase of the measured cell viability indicated the increase of oxygen radicals, which is consistent with the result of Crumpton *et al.* (111) who showed that increased reactive oxygen species are associated with CPF in PC12 cells.

Evaluation of 2D Gel Electrophoresis Reproducibility

2D gel electrophoresis is an extremely powerful tool for the analysis of complex protein mixtures. The utility of this technique lies in its enormous resolving power, which allows for the separation of approximately 2,000 proteins in a single electrophoretic run. This technique is powerful for detecting small changes in the levels or properties of proteins in response to changes in cellular conditions. However, several factors can influence the quantification feature of 2D gel electrophoresis, such as solubilization of proteins, rehydration condition of IPG strips, staining, and how PDQuest is used to analyze gel images. The reproducibility of 2D gels can be improved by keeping the practical parameters constant or running all samples at the same time. Even so, there is still another question about the quantification property of this technique. Does the OD value really reflect the real amount of protein in mixtures? The hypothesis of the quantification by 2D gel electrophoresis is that the same percentage of protein in the sample should have the same normalized optical density (OD) on the 2D gel using PDQuest software.

Table 2-2-6. Summary of the additional down-regulated proteins following treatment of SH-SY5Y cells with 50 μ M CPF for 16 h compared with control samples

Protein	Accession # (Sprot)	Molecular mass (KDa)	Spot #	Score	Cov(%)
Chapterone proteins					
Stress-induced-phosphoprotein 1	P31948	63	26, 27	146	26
Enzymes					
Ubiquitin carboxyl-terminal hydrolase					
isozyme L1	P09936	25	28	59	30
Cytoskeletal Protein					
Stathmin	P16949	17	29	120	53
Lamin B2	Q03252	63	30	68	7
Other Proteins					
Elongation factor 1-beta	P24534	25	31	58	13
GTP-binding protein GEM	P55040	34	32	90	16
Rho GDP-dissociation inhibitor 1	P52565	23	33	104	50

Table 2-2-7. Summary of the additional up-regulated proteins following treatment of SH-SY5Y cells with 50 μ M CPF for 16 h compared with control samples.

Protein	Accession #(Spot)	Molecular mass (KDa)	Spot #	Score	Cov(%)
Enzymes					
ATP synthase chain, mitochondrial precursor	P06576	57	31	77	18
Carbonic anhydrase-related protein 10	Q9NS85	38	32	53	10
Cytoskeletal Proteins					
Stathmin 3 (SCG10-like protein)	Q9NZ72	21	34	68	17
Other Proteins					
RAS-related protein Rab-25	P57735	23	33	58	14

The reproducibility of 2D gel electrophoresis was investigated using four proteins as standards in this chapter. Two sets of experiments were performed. Results showed that the experimental data were consistent with the expected data (Table 2-2-2 and 2-2-3), which indicated that 2D-PAGE was a reliable technique for protein quantification.

Evaluation of Protein Identification with Combination of 2DE and MALDI

Protein identifications were also investigated using proteins, BSA, Ova, CA and STI, as standards in this chapter. In the validation experiments, 0.1 µg of each protein was used to do small format 2D gel experiments and three replicate experiments were performed. Proteins were identified by comparing the experimental MALDI mass spectra of the tryptic digests with those from ‘*in silico* digestion’. Results clearly demonstrated the identities of proteins with significant match. The highest MOWSE scores (n=3) for BSA, Ova, CA and STI were 1280, 1050, 980 and 550, respectively.

Proteome Analysis of SH-SY5Y Cells Exposed to 50 µM CPF for 24h

Previous studies of the effects of CPF on neuron development have focused on specific protein alterations, especially Ca²⁺/cAMP response element binding protein (CREB) and adenylyl cyclase (95, 96) using Western-blot and activity assays. There have been no simultaneous, quantitative proteomic studies of changes in protein expression from SH-SY5Y cell cultures treated with CPF at low exposure levels.

This is the first study to investigate proteome analysis of SH-SY5Y cells treated with 50 µM CPF for 24 h. A total of 37 unique, altered proteins were identified in three parallel experiments. These proteins can be classified as chaperone proteins, cytoskeletal proteins, enzymes and other proteins based on their functions. Characterization of proteins identified in these experiments showed that they were from diverse pathways, including ATP energy production, neuritogenesis, protein synthesis, DNA transcription, cell signaling cascades, and antioxidant defense systems.

ATP Energy Production

ATP synthase was detected as a down-regulated protein in CPF-treated samples. This protein plays important roles in the synthesis of ATP from ADP and P_i in the presence of a proton gradient across the membrane. The detected ATP synthase is responsible for proton transportation into the matrix to form ATP. We also observed that one isoform of

enolase 1 (spot 15 in Figure 2-3-3 A) and glyceraldehyde-3-phosphate dehydrogenase were down-regulated. Meanwhile, another isoform of enolase 1 (spot 21 in Figure 2-2-3 B) was up-regulated in CPF-treated neurons. Enolase is important for the ninth step in glycolysis, and glyceraldehydes-3-phosphate dehydrogenase is responsible for the sixth step. Because our study quantified different isoforms of the protein on 2D gels, it was a challenge to determine the total change of enolase represented by different isoforms. Down-regulation of proteins associated with ATP production suggests that ATP levels decreased following exposure to CPF at subcytotoxic doses. These results were consistent with those of Song et al.(95), who showed that adenylyl cyclase, which catalyzes the formation of cyclic AMP from ATP, decreased after exposed to CPF at low levels.

Neuritogenesis

Actin is the most abundant cytoskeletal protein in the neuronal proteome. The state of actin polymerization determines the status of cytoskeleton, neurite (baby axon) and growth cone mobility (101), as well as neurite maintenance and extension. Actin polymerization can make axons extend within the growth cone, a highly dynamic structure at the tip of the axon. In this study, several isoforms of actin (spots marked as 7, 14, 23 in Figure 2-2-3 A and Table 2-2-4) were detected as down-regulated proteins induced by CPF. Changes in actin reported here indicate changes in actin polymerization, which is very important in neuritogenesis and the spiny outgrowths on dendrites. Dendritic spines are known to change shape, to the extension of appearing and disappearing entirely. It has long been hypothesized that such changes may be the basis of memory itself (102) (103). Actin is thought to mediate these changes in dendritic spine shape (104). Therefore, actin changes can eventually lead to long term irreversible learning damage.

Several detected altered proteins play important roles in the regulation of actin polymerization. Rho GDI, which is a small G protein and regulates the reorganization of the actin cytoskeleton, was detected as up-regulated in CPF-treated samples. The role of Rho GDI in pathways is displayed in Figure 2-2-4. The up-regulation of Rho GDI suggests decrease in actin levels and indeed three isoforms of which were detected as down-regulated. Cofilin, which is critical in the control of polymerization/depolymerization of actin, increased in the CPF-treated cultures. Levels of annexin V,

which was reported as a γ -actin binding protein and influences actin polymerization in neuritogenesis (75), were also increased. The elevation of annexin V observed here may be a compensatory response of cells to increase levels of functional protein necessary for the maintenance of actin levels. Profilin another actin-binding protein, which regulates actin polymerization, was detected as an up-regulated protein in CPF-treated neurons. The addition of profilin usually inhibits the assembly of actin filaments, thereby resulting in the decrease of actin. Results suggest that the neuritogenesis may be damaged due to decreased actin.

Actin is not the only important protein in neuritogenesis; vimentin and tubulin also play important roles. Three main cytoskeletal systems (including microtubules, intermediate filaments, and microfilaments composed of tubulin, vimentin and actin) regulate the growth of neurites (axons and dendrites) and their subsequent maintenance, stability and functionality. These cytoskeletal proteins are important in generating and maintaining the morphology of differentiating neurons, motility and leading the pathway of growth cones as well as helping to transport cytoplasmic constituents (105). Although these skeletal proteins share some common functions, they also have some unique functions as described in the next several paragraphs.

The expressions of three isoforms of vimentin (Vm) were altered after exposure to CPF. Vm at spots 13 and 24 in Figure 2-2-3 A were detected as down-regulated; however, Vm at spots 13 and 14 in Figure 2-2-3 B were up-regulated. Vm from the native source has several isoforms due to differential phosphorylations (106). These identified Vm isoforms suggested that the cross-linked infrastructure of an axon may be altered by CPF, resulting in neuritogenesis alteration. The reason is that vimentin is an intermediate filament species which is gradually replaced by neurofilaments during the development of axonal stability (23). In addition, vimentin plays an important role in neurite initiation in the neuroblastoma and hippocampal neurons in culture (22).

Tubulins were identified as altered proteins in this study with many different isoforms resulting from posttranslational modifications. Three posttranslational modifications of α -tubulin are described in the literature (106), and β -tubulin has significantly more complicated and undetermined modifications (106). Here, tubulin at spots 8, 16, and 21 in Figure 2-2-3 A was detected as down-regulated proteins, but tubulin

at spots 19 and 26 in Figure 2-2-3 B was up-regulated. Since all the isoforms of tubulin are structural units for microtubules, the different developing trends of tubulin isoforms must result in different adverse consequence based on their specific functions in neurons. Thus, the changes in tubulin expressions induced by CPF exposure indicated that the developmental neuritogenesis would be damaged.

All the above information suggested that neuritogenesis in neuron cells was impaired after treated with 50 μ M CPF for 24 h. During brain development, neurite grows toward other regions of the nerve system or other organisms such as muscle to form connections. Since the proper functioning like memory/learning of the nervous system depends on the proper formation of proper connections, any disturbance on the neurogenesis could cause dysfunction of neurons.

Protein Synthesis

Studies (107) (108) in a variety of species have shown that the consolidation of newly acquired memories into stable long-term memories depends on the synthesis of new proteins and gene transcription in neurons. One can say that the influence of protein synthesis pathway in neurons could cause memory/learning damage. Eukaryotic translation initiation factor 3 (eIf) was been detected as an up-regulated protein in CPF-treated samples. Translation initiation factors associated with ribosomes are required for the initiation phase of protein synthesis. The observation of the increased levels of eIF, which is involved in the synthetic pathway of other proteins, suggests a compensatory increase by cells exposed to CPF to maintain protein levels. These results are consistent with previous studies, which showed that CPF significantly reduced protein synthesis (95). Heterogeneous nuclear ribonucleoprotein C, which modulates translation of c-myc mRNA (61), was detected as a down-regulated protein in CPF-treated cultures. The decrease of this protein suggests the responding decrease of the translation of mRNA, thus the decrease of protein synthesis.

DNA Transcription

Because histones bind DNA to form nucleosomes, histone proteins regulate the chromatin structure and function related to transcriptional activity and other nuclear functions (109). The posttranslational modifications of the histones are very important for

the regulation of transcription and chromatin condensation. The detected histone proteins showed a similar pattern as a row of spots, some of which (spots at 18, 19, 20, 22 in Figure 2-2-3 A) were identified as down-regulated, some of which (spot at 28 in Figure 2-2-3 B) were up-regulated in cells treated with 50 μ M CPF for 24 h. This phenomenon implies that the changed modifications of the histones may result in transcriptional changes, which may induce memory damage. As known, long-term memory requires new gene expression or gene transcription, which involves the formation of new synaptic connections.

Proteome Analysis of SH-SY5Y Cells Exposed to 50 μ M CPF for 16 h

In the proteome analysis of SH-SY5Y cells from experiments treated with vehicle alone (control) or 50 μ M CPF for 16 h, 48 unique altered proteins were identified. Comparing these identified proteins with those from the samples incubated with CPF for 24 h, 37 unique proteins were observed to be identical. However, 11 additional unique proteins were identified from the samples with incubation time of 16 h. Most of the identified common proteins demonstrated the same trend including glyceraldehyde 3-phosphate dehydrogenase (G-3-PD), which was detected as down-regulated in both 16 h and 24 h samples. However, some protein isoforms were detected as down-regulated in this work, but up-regulated in a former work, such as Rho GDP-dissociation inhibitor (Rho GDI). Proteins identified in these experiments, which play an important role in diverse pathways including ATP energy production, DNA synthesis, cell signaling cascades, axonogenesis and oxidative stress, showed different response trends with time-dependent incubation with CPF. Here, only altered proteins with different trends and the newly identified proteins will be discussed.

One isoform of ATP synthase was detected as an up-regulated protein after incubation with CPF for 16 h. However, a down-regulation of the enzyme was observed in the sample treated with CPF for 24 h. As described before, ATP synthase regulates the synthesis of ATP in mitochondria. Elevation of this protein suggests a compensatory response of CPF-treated cells for a short time period (16 h) to try to maintain ATP levels. However, after incubation for longer time (24 h), cells responded to this stimulation by showing the depletion of ATP synthase, which agrees with that of Braber *et al.* (112) who showed that CPF inhibited Ca-stimulated ATP synthase activity.

One isoform of Rho GDI was detected as a down-regulated protein in cells treated with CPF for 16 h and another isoform was up-regulated in samples treated for 24 h. This protein functions as an inhibitor of the dissociation of GDP from Rho proteins and then inhibits their GDP/GTP exchange reaction, which regulates the formation of cAMP from ATP. Down-regulated Rho GDI suggests increased cAMP production from ATP, resulting in low levels of ATP. This is consistent with the other proteins associated with ATP production, such as ATP synthase. The elevation of Rho GDI at 24 h suggests that longer incubation provides enough time for SY5Ys to adjust to the low levels of ATP in the system. Furthermore, Rho GDI is important in the mediation of cytoskeletal organization. GTP-binding protein GEM, another G-protein, was detected as down-regulated protein in the cells after incubation for 16 h with CPF. The GEM protein interfaces with the Rho pathway and eventually leads to alterations in cellular neurite growth (113). The decrease in GEM suggests a compensatory response of cells to increase the levels of actin, which was detected as down-regulated in this study.

Eukaryotic elongation factor 1-beta (elf), which plays a critical role in the elongation phase of protein synthesis, was detected as a down-regulated protein in cells after incubation with CPF for 16 h. The decrease of this protein suggests a decrease of protein synthesis, which is consistent with previous studies that CPF significantly reduces protein synthesis (95).

Ubiquitin carboxyl-terminal hydrolase isozyme L1 (UCH-L1), a neuronal de-ubiquitinating enzyme whose mutation has been linked to an early-onset familial Parkinson's disease (PD), was detected as a down-regulated protein. This result is consistent with the findings of Choi *et al* (114), who reported that UCH-L1 was down-regulated in idiopathic PD as well as in Alzheimer's disease (AD) brains. The down-regulated UCH-L1 suggests a direct link between damage to neurons and neurodegenerative diseases.

Actions of these altered proteins caused by CPF are summarized in Figure 2-2-4. These detected proteins play important roles in energy production, protein synthesis, DNA transcription, antioxidant defense system, and cell signaling cascades, all of which interact with each other through energy transfer or signal transductions. In brief, cells must be ready to respond to essential signals in their environment. Signaling molecules are often

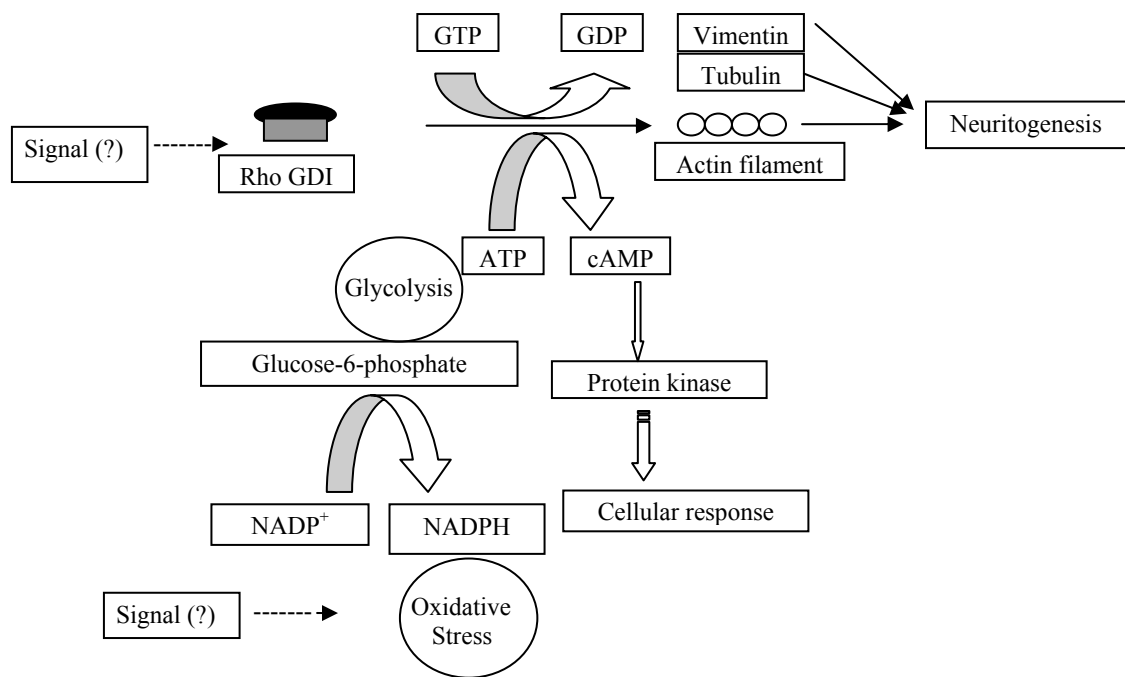


Figure 2-2-4. Summary for the modes of action of CPF-induced altered proteins in the energy production cycle, antioxidant defense systems and cell signaling cascades.

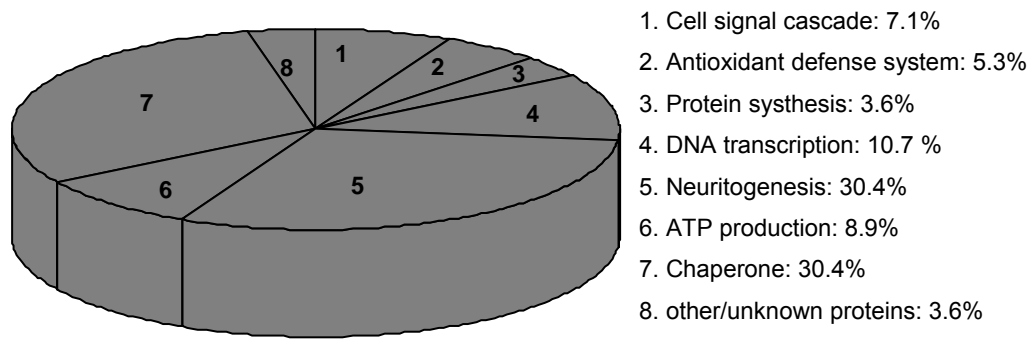


Figure 2-2-5. Distribution of the identified proteins including the down- and up-regulated proteins according to their functions.

chemicals such as hormones, cytokines, or CPF in this study. Some signal proteins, such as Rho GDI (a G-protein), can receive the signals and further transmit it by regulating GDP/GTP exchange and eventually modulating axonogenesis development. The inhibition of GDP/GTP exchange reactions catalyzes the formation of cAMP from ATP, which further causes changes in all metabolism (e.g. glycogenolysis). The changes in metabolism lead to changes in protein synthesis and changes in the antioxidant defense system. Furthermore, these signal molecules can trigger changes in DNA transcription and electric potential across the plasma membrane. It is evident that all cellular responses are related to one other.

The detected proteins were categorized by their functions, as shown in Figure 2-2-5. The largest percentage of detected proteins was neural structural proteins and chaperone proteins. This is understandable, as a range of physiological stresses can induce the expression of heat shock proteins (115). Furthermore, neuron structural proteins are the most abundant proteins and play important roles during neuron development.

CONCLUSIONS

We have successfully investigated the proteome of SY5Y cells treated with 50 μ M CPF for 24 h and 16 h with the combination of 2D gel electrophoresis with MALDI-TOF-MS. Using this approach, we simultaneously, quantitatively identified the CPF- induced altered proteins (both up- and down- regulated). A total of 37 common unique proteins from 56 spots were identified, out of which 16 proteins from 26 ± 4 spots were down-regulated, and 21 proteins from 30 ± 3 spots were up-regulated (mean \pm SD of three experiments). These identified proteins play important roles in ATP production, neuritogenesis, protein synthesis, DNA transcription, signaling cascades and antioxidant defense systems. These detected proteins support the hypothesis that alterations in protein expressions underlie the impairment of energy production, protein synthesis, and neuritogenesis. All these studies show that cells need time to respond to the ‘stimulations’ caused by CPF. In order to respond to these stimulations from CPF, the cells have evolved a response system that induces cell cycle to allow sufficient time to repair or follow the cascades of the damage.

It is still unclear how these protein changes were initiated by CPF. We suggest that some signal proteins, such as Rho GDI, first receive the signal or insult from the cell environment, and further transmit the signal to the whole cell through energy production, or protein synthesis pathways. Based on the protein functions, several altered proteins, such as ATP synthase, vimentin, and Rho GDI, will be further investigated in the next step of experiments using bio-techniques. Mutation studies and metabolic experiments on animals, such as mice, will be the future experiments. It is very promising to understand the mechanism in biochemical pathways leading to neurodegeneration associated with cognitive damage after exposure to CPF at subtoxic levels.

CHAPTER THREE

CONCLUSIONS

There is an increasing concern about exposure of pregnant women, infants and children to chlorpyrifos (CPF), an organophosphate insecticide. This concern is based on the *in vitro* and *in vivo* studies, which indicate that CPF is a developmental neurotoxin. Previous studies suggest that CPF, at concentrations below the threshold for symptoms of systemic toxicity, disrupts brain development and damages cognitive function. Studies both *in vivo* and *in vitro* confirmed that CPF at levels that do not cause cytotoxicity can compromise cellular processes in brain development. However, the actual mechanism for CPF perturbation in neuron development at the subcellular level remains unclear and complicated. This was the first study to systematically investigate CPF neurotoxicity at the subcellular level using SH-SY5Y as a model system. We tested the hypothesis that changes in protein expression underlie neuronal anomalies associated with CPF exposure.

We successfully investigated differential protein expression in SY5Y cells treated with 50 μ M CPF using 2D-PAGE with MALDI-TOF-MS. The time-dependent proteome changes of SH-SY5Y cells resulting from CPF exposure were also successfully examined. This was based on the comparison of the proteome changes of the neuroblastoma cells treated with CPF for 24 h and 16 h. A total of 37 common unique proteins from 56 spots were identified as altered proteins. However, 11 additional unique proteins were detected as altered proteins in samples treated with CPF for 16h. These identified proteins play important roles in ATP production, neuritogenesis, protein synthesis, DNA transcription, signaling cascades and antioxidant defense systems. The changes in protein expression suggested that the alterations were due to cellular responses to CPF stimulation. It is evident that cells need time to respond to the ‘stimulation’ caused from CPF by evolving a response system, which induces cell cycle to allow for sufficient time to repair or follow the cascades of the damage.

2D gel electrophoresis has been a core technology of proteome analysis since the 1980s. The technique offers high-throughput and relatively high reproducibility in combination with either MALDI-TOF-MS or LC/MS. 2D gel electrophoresis is an extremely powerful tool for the analysis of complex protein mixtures. The utility of this

technique lies in its enormous resolving power, which allows for the separation of approximately 2,000 proteins in a single electrophoretic run. The technique is powerful for detecting small changes in the levels or properties of proteins in response to changes in cellular conditions. However, 2D-PAGE is not the only method for proteome analysis. Many research groups are beginning to realize that “MudPIT” (Multidimensional Protein Identification Technology) is an alternate powerful tool. The rapid development of the technique relies on reduced sample preparation and manual labor compared to 2D gel electrophoresis.

Thirty seven common unique proteins were detected as altered proteins in this study. Based on their functions, ATP synthase, vimentin, Rho GDI, and eukaryotic translation initiation factor (eif) will be chosen for further experiments using bio-techniques. The proteins of interest play important roles in ATP production, neuritogenesis, signal cascade protein, and protein synthesis, respectively. Once we systematically understand the altered proteins of the entire SH-SY5Y cells treated by CPF, mutation studies and metabolic experiments on animals, such as mouse, will be followed. These investigations can allow us to clearly understand the actual mechanism for CPF perturbations in neuron development at the subcellular level.

GENERAL CONCLUSION

Some bizarre and puzzling problems, such as altered behaviors of animals in mating, parenting, and nesting, have been discovered all over the world since the 1950s. Many of the disturbing wildlife reports involved behavioral abnormalities and malfunctioning sexual organs, leading to damaged fertility. The loss of young, or the sudden disappearance of entire animal populations indicated that wildlives are disturbed. Most of these incidents seemed associated somehow to chemical pollution, especially man-made pesticides. Through the creation and release of billions of pounds of these man-made chemicals over the past half century, we have been instigating large-scale changes to the Earth's atmosphere and even in chemistry of our own bodies. The magnitude of the damage is frightening. Most disturbing of all, many of us already carry contamination levels that may put us and our children at considerable risk.

In the most extreme circumstances, chemicals were intentionally used as weapons for mass destruction. Associated with military operations, chemical warfare (CW) agents are designed with a high ability to kill, injure or incapacitate the enemy (including military and civilians). Chemical warfare was revolutionized, during World War II, by the discovery by Nazi Germany of nerve agents such as tabun, sarin and soman. Fortunately, the CW agents were not extensively applied during that time. The threat of CW became foremost during the Cold War. Both the Soviet and Western governments poured enormous resources into developing chemical and biological weapons. After the Cold War, mass destructions involving CW reagents occurred on several occasions. Implementation and use of these CW weapons have often led to tragic memories and terrible costs to human lives. About 100,000 Iranian soldiers were victims of Iraqi chemical attacks in 1980. Approximately 5000 Iraqi Kurdish civilians were slaughtered in a few hours by chemical bombs with multiple chemical agents. Things became worse, when CW agents were used as tools by many terrorist organizations. Several events involving the notorious use of CW agents in non-combat settings happened for several occasions lately. The most recent one was the Tokyo subway attack with sarin in 1995.

Defending ourselves from the hazard requires actions on several fronts involving scientific researches. As bioanalytical scientists, we have been conducting research driven by the need to answer several crucial questions:

- What are the chemicals exposed to people?
- What are the exposure levels?
- How is the human body really responding to these chemicals?

The ultimate goal of pesticide exposure research should be recovery of victims. However, efforts are still required for the early detection of pesticide exposure and knowledge of pesticide effects on human before recovery comes to be true. As such, reliable, sensitive and accurate clinical diagnostics are critical in saving human lives and increasing public health.

The concern of public health is increasing because of the extensive use of pesticides and occasional applications of CW agents in local conflicts or terrorism. Public health demands more sensitive and reliable programs for monitoring pesticide exposure. In the first part of this dissertation, a methodology was designed to solve the first two crucial questions mentioned before. This was achieved based on a full understanding of the chemistry, mode of action and toxicity of OPs and CBs, along with careful experimental design in mass spectrometry. The new methodology was based on the analysis of inhibited BChE by pesticides, particularly based on the detection of modified active site peptides generated from trypsin digests of the enzyme. The methodology employed proteomic approaches and much more sensitive, selective, accurate mass spectrometry techniques. Although the MALDI method was proven as a powerful tool for the analysis of single pesticide exposure, the lower ionization efficiency of phosphorylated peptides in MALDI and the suppression of the modified peptides in a complex peptide mixture make this method limited for the analysis of multiple pesticide exposure. However, LC/MS/MS can particularly analyze the precursor ions of interest in the ion trap with the presence of other abundant peptides. LC/MS/MS techniques were successfully applied to analyze a mixture of the phosphorylated peptides *in vitro*, and the precursor ions were monitored by a common fragment ion.

Application of the developed LC/MS/MS methodology for measuring pesticide exposure *in vitro* and in serum samples clearly demonstrated the power of MS-based

method development in pesticide analysis. Results clearly displayed critical evidence of the exposure to OPs and CBs as low as 5 % human BChE inhibition in serum, which the traditional Ellman method can not detect. To design a reliable monitoring methodology and effect a treatment for victims, it is imperative that research focuses on the identification and quantification of exposure to OPs and CBs at early exposure times and at low levels. LC/MS/MS techniques can be broadly applied for the other possible pesticide analysis, such as CW agents, due to the large varieties of LC/MS parameters. For instance, many fragmentation techniques in MS and many types of LC columns can be adjusted to the analyte of interest. The technique of packing columns in laboratory makes it more attractive by customizing columns with the analyte of interest with numerous types of stationary phase available. As such, it is very promising to apply LC/MS-based methods for the analysis of other man-made chemicals. Metabolic studies in other body fluids, such as urine, coupled LC/MS/MS with the other techniques can further provide an indication of pesticide or CW agent exposure.

The two critical questions, ‘what are the chemicals’ and ‘What are the exposure levels’, were successfully answered in the first part of this dissertation. To answer the third crucial question, a comprehensive research program is needed to determine the effects of synthetic chemicals on human health. Probing such questions will require a sophisticated integration of epidemiology on human populations, animal studies, and laboratory investigations of how these chemicals act at the cellular and molecular level. Epidemiological studies are never easy, and particularly difficult in the following instances. First, researchers confront the lack of an uncontaminated population for comparison. All young persons in our society are more or less exposed to synthetic chemicals. Second of all, there is a long time between exposure to these chemicals and the emergence of ill effects. Scientists find that the good opportunities for testing human health effects are cell culture, tissue culture, and organ culture. The diversities of cultures make it more appealing to achieve the different goals of various research subjects, as well as avoiding the long time period needed.

The second part of this dissertation focused on the proteome analysis of SH-SY5Y cells, a neuroblastoma cell line, in an effort to obtain a clear understanding of protein expression in a CPF-treated sample. The protein expression indicated how the cells

respond to essential stimulation resulting from 50 μ M chlorpyrifos (CPF), an organophosphate pesticide. The concerns of CPF exposure to pregnant women, infants and children are increasing due to its developmental neurotoxic effects. The main hypothesis of part two of this dissertation was that changes in protein expression underlie neuronal anomalies associated with CPF exposure. In this dissertation, we investigated the whole proteome alteration induced by CPF at the concentration levels below the threshold for symptoms of systemic toxicity using SH-SY5Y cell line as a model system. Two-dimensional gel electrophoresis (2DE) was applied with MALDI-TOF-MS to analyze differential protein expression. A total of 37 common unique altered proteins were identified, which play important roles in energy production, protein synthesis, DNA transcription, antioxidant defense system, and cell signaling cascades. The changes in protein expression suggest the changes resulting from cell response. Part II of this dissertation provided a basic insight for understanding how undifferentiated neuroblastoma cells respond to CPF at concentration levels without causing cytotoxicity. Some altered proteins, such as ATP synthase, will be further investigated to clearly understand how CPF influences neuron development. These closer examinations should combine biochemical techniques. A quantitative proteomics method combining multi-dimensional chromatographic separation method (MudPIT) and ICAT will probe the proteome analysis in a more productive way.

In order to thoroughly investigate differential protein expression of neuroblastoma cells, proteome analysis of different organelles, such as proteins extracted from mitochondria, should be examined. A sophisticated integration of epidemiology on human populations, animal studies, and laboratory investigations is required to determine the effects of pesticide on human health at the cellular and molecular level. Once we systematically understand the altered proteins of the entire SH-SY5Y cells treated by CPF, mutation studies and metabolic experiments on animals, such as mouse, will follow. These investigations can allow us to clearly understand the actual mechanism for CPF perturbation in neuron development at the subcellular level. Results from these investigations can definitely enable us to find a way to cure or alleviate symptoms of the memory damage and learning disability caused from CPF.

The world market in pesticides amounted to 5 billion pounds in 1989 and included sixteen hundred chemicals. In this dissertation, we successfully analyzed the detection and quantification of two types pesticide of exposure (Part I), and we also successfully investigated how neuroblastoma cells respond to one kind of OP using a proteomics approach and mass spectrometry (Part II). This dissertation reveals a promising future of the proteomics approach and mass spectrometry for pesticide analysis, because of high sensitivity and high-throughput of this technique. However, this technique does have its shortcomings and will not be able to single-handedly tackle and analyze all pesticides. In addition, some emergent situations like the 1995 Tokyo Subway Attack, required a quick investigation from forensic analysis. How to apply the method in the field is a challenge for mass spectrometry specialists. A portable mass spectrometer with high sensitivity should be invented in the next few years. In addition, a culmination of several techniques, including but not limiting to mass spectrometry, UV, and biosensors, will result in the most productivity of pesticide analysis. The next several years should be very exciting as researchers apply mass spectrometry techniques and combine this with the other techniques for the purpose of answering the three crucial questions about pesticides and the other man-made chemicals.

REFERENCES

1. Pandey, A., and Mann, M. (2000) *Nature* **405**, 837-846.
2. Wilkins, M. R., Sanchez, J.C., Gooley, A.A., Appel, R.D., Humphery-Smith, I., Hochstrasser, D.F., and Williams, K.L. (1996) *Eng. Rev.* **13**, 19-50.
3. Yates, J. R. (2000) *3rd J. Mass Spectrom* **16**, 5-8.
4. Yates, J. R. (1998) *3rd J. Mass Spectrom* **33**, 1-19.
5. Zhao, Y., Zhang, W., and White, M.A. (2003) *Anal. Chem.* **75**, 3751-3757.
6. Romijn, E. P., Krijgsveld, J., and Heck, A.J. (2003) *J. Chromatogr. A* **1000**, 589-608.
7. Jaroniec, M. (1993) *J. Chromatogr. A* **656**, 37-50.
8. Marczewski, A. W., Derylo-Marczewska, A., and Jaroniec, M. (1988) *Chemica Scripta* **28**, 173-184.
9. van Deemter, J. J., Zuiderweg, F.J., and Klinkenberg, A. (1956) *Chem. Eng. Aci.* **5**, 271.
10. Dihazi, G. H., Sinz, A. (2003) *Rapid Commun. Mass Spectrom.* **17**, 2005-2014.
11. Bjellqvist, B., EK, K., Rightetti, P., Gianazza, E., Gorg, A., Westermeier, R., and Postel, W. (1982) *J.Biochem. Biophys. Methods* **6**, 317-339.
12. Stephens, W. (1946) *Phys. Rev.* **69**, 691.
13. Wiley, W. C., and McLauren, J.B. (1955) *Rev. Sci.Instrum.* **16**, 1150.
14. Mamyrin, B. A., Karataev, V.I., Schmikk, D.V., and et al. (1973) *Sov. Phys.JETP*, 374.
15. Fenn, J. B., Mann, M., and Meng, C.K. (1989) *Science* **246**, 64.

16. Synder, A. P. (1996) *in* ACS symposium series 619, American Chemical Society., Washington DC.
17. Cole, R. B. (1997) *Electrospray ionization mass spectrometry.*, wiley, Chichester.
18. de la Mora, J. F., Van Berkel, G.J., and Enke, C.G. (2000) *J. Mass. Spectrom.* **35**, 939.
19. Yamashita, M., and Fenn, J.B. (1988) *Phys. Chem.* **88**, 4451.
20. Yamashita, M., and Fenn, J.B. (1988) *Phys. Chem.* **1**, 46.
21. Loo, J. A., Udseth, H.R., and Smith, R.D. (1989) *Anal. Biochem.* **179**, 404.
22. Shea, T. B., and Beermann, M. L. (1993) *Neurosci. Res. Commun.* **11**, 163-169.
23. Cochard, P., and Paulin, D. (1984) *J. Neurosci.* **4**, 2080-2094.
24. Todd, J. F. J. (1991) *Mass Spectrom. Rev.* **10**, 3.
25. Stafford, G. C., Kelley, P.E., and Syka, J.E. (1984) *Int. J. Mass Spectrom. Ion Process* **60**, 85.
26. Jonscher, K. R., and Yates, J. R. I. (1996)
<http://www.abrf.org/abrfnews/1996/september1996/sep96iontrap.html> **The whys and wherefores of quadrupole ion trap mass spectrometry.**
27. Litovitz, T., Smilstein, M., Felberg, L., Klein-Schwartz, W., Berlin, R., and Morgan, J.L. (1997) **15**, 447-500.
28. Stedman, E., and Easson, L.H. (1932) *Biochem. J.* **26**, 2056-2066.
29. Lockridge, O., Adkins, S., LaDu, B.N. (1987a) *J. Biol. Chem.* **262**, 12945-12952.
30. Lockridge, O., Bartel, C.F. , Vaughan, T.A. , Wong, C.K., Norton, S.E. , and Johnson, L.L. (1987) *J. Biol. Chem.* **262**, 549-557.
31. Whittaker, G. N. (1986) *Monographs in Human Genetics* **II**.

32. Burritt, M. F. (1986) *Mayo. Clin. Proc.* **61**, 750-755.
33. Neville, L. F., Gnat, A., Loewenstein, Y., and Soreq, H. (1990a) *J. Neurosci. Res.* **27**.
34. Jbilo, O., Bartel, C.F., Chatonnet, A., Toutant, J-P., and Lockridge, O. (1994) *Toxicol.* **32**, 1445-1457.
35. Gage, J. C. (1967) *Residue Rev.* **18**, 159-173.
36. Broomfield, C. A., Maxwell, D.M., Solana, R.P., Castro, C.A., Finger, A.V., and Lenz, D.E. (1991) *J. Pharmacol. Exp. Ther.* **259**, 633-638.
37. Hart, G. J., and O'Brien, R.D. (1973) *Biochem.* **12**, 2940-2945.
38. Pallilla, S., and Hooper, M. J. (1992) *Proceedings, US EPA workshop on cholinesterase methodologies, Washington, DC.*, 63-81.
39. Winteringham, F. P. W., and Fowler, K. S. (1966) *Biochem. J.* **101**, 127-134.
40. Lockridge, O., Bartel, C.F., Vaughan, T.A., Wong, C.K., Norton, S.E., and Johnson, L.L. (1986) *J. Biol. Chem.* **262**, 549-557.
41. Svensmark, O. (1965) *Acta. Physiol. Scand.* **64, Supplementum, 245**, 10.
42. Tucci, A. F., and Seifter, S. (1969) *J. Biol. Chem.* **244**, 841.
43. Mendel, B., and Mundell, D.B. (1943) *Biochem. J.* **37**, 64.
44. Svensmark, O. (1963) *Acta. Physiol. Scand.* **59**, 378.
45. Strelitz, F. (1944) *Biochem. J.* **38**, 86.
46. Barone, S. J., Das, K.P., Lassiter, T.L., and White, L.D. (2000) *Neurotoxicology.* **21**, 15-36.
47. Connel, G. E., and Shaw, R.W. (1961) *Can. J. Biochem. Physiol.* **39**, 1013.
48. Kalderon, N., Silman, I., Blumberg, S., and Dudai, Y. (1970) *Biochem. Biophys. Acta.* **207**, 560.

49. Dudai, Y., Silman, I., Shinitzky, M., and Bloumberg, S. (1972) *PNAS* **69**, 2400.
50. Blanchet, D., Picard, J., and Morelis, P. (1977) *J. Chromatog.* **135**, 477.
51. Lockridge, O., La Du, B.N. (1978) *J. Biol. Chem.* **253**, 361.
52. Ralston, J. S., Main, A.R., Kilpatrick, B.F., and Chasson, A.L. (1983) *Biochem. J.* **211**, 243.
53. http://www.shianews.com/hi/middle_east/news_id/0000866.php.
54. http://www.factnet.org/cults/aum_shin_rikyo/nerve_gas_victims.htm.
55. Nigg, N., and Knaa, J. B. (2000) *Rev. Environ. Contam. Toxicol.* **163**, 29-112.
56. Ellman, G., Courtney, K. D., Andres, V., and Jr. Featherstone, R. M. (1961) *Biochem. Pharmacol.* **7**, 88-95.
57. Polhuijs, M., Langenberg, J. P., and Benschop, H. P. (1997) *Toxicol. Appl. Pharmacol.* **146**, 156-161.
58. Doorn, J. A., Gage, D. A., Schall, M., Talley, T. T., Thompson, C. M., and Richardson, R. J. (2000) *Chem. Res. Toxicol.* **13**, 1313-1320.
59. Doorn, J. A., Schall, M., Gage, D. A., Talley, T. T., Thompson, C. M., and Richardson, R. J. (2001) *Toxicol. Appl. Pharmacol.* **176**, 73-80.
60. Fidler, A., Hulst, A. G., Noort, D., Ruiter, R. d., Schans, M. J. v. d., Benschop, H. P., and Langenberg, J. P. (2002) *Chem. Res. Toxicol.* **15**, 582-590.
61. Kim, Y. A., Lee, H. S., Park, Y. C., and Lee, Y. T. (2000) *Environmental Research* **84**, 303-309.
62. Inagami, T., and Sturtevant, J. M. (1960) *Biochim. Biophys. Acta* **38**, 64-79.
63. Aldridge, W. N., and Reiner, E. (1972) *North-Holland Publishing Co., Amsterdam, The Netherlands.*

64. Mason, H. J., Waine, E., Stevenson, A., and Wilson, H.K. (1993) *Human & Experimental Toxicology* **12**, 497-503.
65. O'Brien, R. C. (1967) *New York, Academic Press. Insecticides: action and metabolism.*, 32-54.
66. Asara, J. M., and Allison, J. (1999) *J. Am. Soc. Mass. Spectrom.* **10**, 35-44.
67. Annan, R. S., and Carr, S. A. (1996) *Anal. Chem.* **68**, 3413-3421.
68. Resing, K. A., Johnson, R. S., and Walsh, K. A. (1995) *Biochem.* **34**, 9477-9487.
69. Ruse, C. I., Willard, B., Jin, J. P., Haas, T., Kinte, R. M., and Bond, M. (2002) *Anal. Chem.* **74**, 1658-1664.
70. Liao, P.-C., Leykam, J., Andrews, P. C., Gage, D. A., and Allison, J. (1994) *Anal. Biochem.* **219**, 9-20.
71. Rao, P. S., Robert, G. H., Pope, C. N., and Ferguson, P. W. (1994) *Pesticide Biochemistry and Physiology* **48**, 79-84.
72. Alberini, C. M. (1999) *J. Exp. Biol.* **202**, 2887-2891.
73. Groten, J. P., Cassee, F. R., Bladeren, P. J. V., Derosa, C., and Feron, V. J. (1999) *Mixtures, in toxicology.*, Academic Press.NY.
74. Payne, M. D., Rossomando, A.J., Martino, P., Erickson, A.K., Her, J.H., and Shabanowitz, J. (1991) *EMBO J.* **10**, 885-892.
75. Tzima, E., Trotter, P.J., Orchard, M.A., and Walker, J.H. (1999) *Exp. Cell Res.* **251**, 185-193.
76. Stedman, E., Stedman, E., and Easson, L.H. (1932) *Biochem. J.* **26**, 2056-2066.
77. Kalderson, N., Silman, I., Blumberg, S., and Dudai, Y. (1970) *Biochim. Biophys. Acta* **207**, 560.

78. Cuatrecasas, P., and Anfinsen, C.B. (1971) *Methods Enzymol.* **22**, 345-378.
79. Damer, C. K., and Creutz, C.E. (1994) *Prog. Neurobiol.* **43**, 511-536.
80. Raveh, L., Grunwald, J., Marcus, D., Papier, Y., Cohen, E., and Ashani, Y. (1993) *Biochem Pharmacol* **45**, 2465-74.
81. Petroianu, G., Kuhn, F., Thyges, C., Ewald, V., and Missler, A. (2003) *Journal of Applied Toxicology* **23**, 75-79.
82. Pla, A., and Johnson, M. K. (1989) *Biochem Pharmacol* **38**, 1527-1533.
83. <http://www.epa.gov/pesticides/announcement6800.htm> (2002) (U.S., E. P. A., Administrator's Announcement. , Ed.).
84. Perez-polo, J. R., Werrbach-Perez, K., Tiffany-Castiglioni, E. (1979) *Dev. Biol.* **71**, 341.
85. Landrigan, P. J., Claudio, L., Markowitz, S.B., Berkowitz, G.S., Brenner, B.L., Romero, H., Wetmur, J.G., Gore, A.C., Godbold, J.H., Wolff, M.S. (1999) *Environ. Health Perspect.* **107 (Suppl. 3)**, 431-437.
86. Davis, D. L., and Ahmed, Karim. (1998) *Environ. Health Perspect.* **106**, 299.
87. Roy, T. S., Andrew, J.E., Seidler, F.J., Dlotkin, T.A. (1998a) *Teratology* **58**, 62-68.
88. Enrique, M. O., Morales, V., Ngoumgna, E., Prescilla, R., Tan, E., Hernandez, E., Ramirez, G.B., Cifra, H.L., Manlapaz, M.L. (2002) *Neurotoxicology* **23**, 329-339.
89. Garcia, S. J., Seidler, F.J., and Slotkin, T.A. (2003) *Environmental Health Perspectives* **111**, 297-303.
90. Levin, E. D., Addy, N., Baruah, A., Elias, A., Christopher, N.C., Seidler, F.J., and Slotkin, T.A. (2002) *Neurotoxicology and Teratology* **24**, 733-741.

91. Whitney, K. D., Seidler, F.J., Slotkin, T.A. (1995) *Toxicol. Appl. Pharmacol.* **134**, 53-62.
92. Campbell, C. G., Seidler, F.J., Slotkin, T.A. (1997) *Brain Res. Bull.* **43**, 179-189.
93. Janson, A. M., Fuxe, K., Agnati, L.F., Kitayama, I., Harfstrand, A., Anderson, K., Goldstein, M. (1988) *Brain Res.* **455**, 332-345.
94. Levin, E. D., Addy, N., Nakajima, A., Elias, A., Christopher, N.C., Seidler, F.J., and Slotkin, T.A. (2001) *Developmental Brain Research* **130**, 83-89.
95. Song, X., Seidler, F.J., Saleh, J.L., Zhang, J., Padilla, S., Slotkin, T.A. (1997) *Toxicol. Appl. Pharmacol.* **151**, 182-191.
96. Schuh, R. A., Lein, P.J., Beckles, R.A., Jett, D.A. (2002) *Toxicol. Appl. Pharmacol.* **182**, 176-185.
97. O'Farrell, P. H. (1975) *J. Biol. Chem.* **250**, 4007-4021.
98. Perkins, D. N., Pappin, D.J., Creasy, D.M., and Cottrell, J.S. (1999) *Electrophoresis* **20**, 3551-3567.
99. Pappin, D. J. C., Hojrup, P., and Bleasby, A.J. (1993) *Curr. Biol.* **3**, 327-332.
100. Slotkin, T. A. (1999) *Environ. Health Perspect. Suppl. 1.* **107**, 71-81.
101. Hall, A. (1998) *Science* **279**, 509-514.
102. Engert, F., and Bonhoeffer, T. (1999) *Nature* **399**, 66-70.
103. Bailey, C. H., and Kandel, E. R. (1993) *Annu.Rev.Physiol.* **55**, 397-426.
104. Fifková, E., and Morales, M. (1992) *Int.Rev.Cytol.* **139**, 267-307.
105. Hanendel, M. A., Bolinger, K.E., and Baas, P.W. (1996) *J. Neurocytol.* **25**, 289-301.
106. <http://www.cytoskeleton.com/aif.htm>.

107. Nader, K., Schafe, G. E., and Le Doux, J. E. (2000) *Nature* **406**, 722-726.
108. Hernandez, P. J., and Kelley, A. E. (2004) *Learning & Memory* **11**, 748-754.
109. Georgel, P. T., and Hansen, J. C. (2001) *Biochemistry & Cell Biology* **79**, 313.
110. Bebe, F., Panemangalore, Myna. (2003) *Journal of Environmental Science & Health, Part B -- Pesticides, Food Contaminants, & Agricultural Wastes* **38**, 349-363.
111. Crumpton, T. L., Seidler, F.J., and Slotkin, T.A. (2000) *Dev. Brain Res.* **121**, 189-195.
112. Barber, D., Hunt, J., and Ehrich, M. (2001) *Journal of Toxicology and Environmental Health, Part A.* **63**, 101-113.
113. Ward, Y., Yap, S., Ravichandran, V., Matsumura, F., Ito, M., Spinelli, B., and Kelly, K. (2002) *Journal of Cell Biology* **157**, 291-302.
114. Choi, J., Levey, A. I., Weintraub, S. T., Rees, H. D., Gearing||, M., Chin, L.-S., and Li, L. (2004) *J. Biol. Chem.* **279**, 13256-13264.
115. Benjamin, I. J., and McMillan, D.R. (1998) *Circulation research* **83**, 117-132.

VITA

Jinchun Sun was born April 23, 1972 in Shandong Province, China.

Jinchun spent her childhood in a small village isolated by high mountains, where she finished her elementary and high school education. Upon graduating high school in 1992, Jinchun enrolled at Lanzhou University, one of the nation's leading higher-education institutions, as a result of her high scores in the National University Entrance Examinations. In July of 1996, she graduated from Lanzhou University with a B.A. in analytical chemistry. Following graduation, Jinchun was offered to continue her higher education by her alma mater with an exemption from the usually mandatory examinations for graduate school. This offer was based on her excellent undergraduate academic record, ranking among the top 5% of the department. During her three years in graduate school at Lanzhou University, Jinchun received four publications. With an impeccable academic record and distinguished publications, she received the Outstanding Graduate Student Honor in 1998. In July of 1999, Jinchun obtained her Master's Degree as a result of her hard work in physical chemistry. Upon graduation, Jinchun accepted her first job as an assistant professor in the Northwest Normal University, where she gave lectures about molecular structure to junior undergraduate students. In August of 2000, Jinchun continued to pursue her "dream" (Ph.D degree), and this time she came to Mississippi State University. She joined in the research group of Dr. Bert Lynn in the Fall of 2000 and followed him to the University of Kentucky in the summer of 2001. Jinchun started her proteomics "journey" through her involvement in mass spectrometry projects. During her residence at the University of Kentucky, Jinchun was the recipient of a Research Challenge Trust Fund Fellowship. She is also a member of the American Chemical Society and American Society of Mass Spectrometry.

Publications:

1. Jinchun Sun, Bert Lynn, "Mass spectrometry-based analysis of human butyrylcholinesterase inhibition from pesticides in serum" (in process).
2. Jinchun Sun, Bert C. Lynn, "Detection and quantification of butyrylcholinesterase inhibition after exposed to multiple pesticides using LC/MS/MS" (in process).

3. Jinchun Sun, Bert C. Lynn, "Detection of butyrylcholinesterase adducts after inhibition with organophosphates and carbamates at different concentration by using MALDI-TOF-MS", (in process).
4. Jinchun Sun, Mark A. Lovell, Bert C. Lynn, "Chlorpyrifos (CPF) induced protein alterations in the SH-SY5Y cell line", (in process).

Presentations:

1. Jinchun Sun, Bert C. Lynn, "Detection of butyrylcholinesterase adducts after inhibition with organophosphates and carbamates at different concentration by using MALDI-TOF-MS", 2005 ASMS conference (San Antonio, TX). (in process).
2. Jinchun Sun, Mark A. Lovell, Bert C. Lynn, "Chlorpyrifos (CPF) induced protein alterations in the SH-SY5Y cell line", 2004 ASMS conference (Nashville, TN). (in process).